EFFECTS OF STRESS-INDUCED OPTICAL ACTIVITY AND DETERMINATION OF OPTICALLY EQUIVALENT MODEL IN THREE-DIMENSIONAL PHOTOELASTICITY

ME
1972
D
SAR
EFF

BY
A. V. S. S. S. R. SARMA

Th
ME/1972/D
Sa23 e

DEPARTMENT OF MECHANICAL ENGINEERING
INDIAN INSTITUTE OF TECHNOLOGY KANPUR
JULY, 1972

EFFECTS OF STRESS-INDUCED OPTICAL ACTIVITY AND DETERMINATION OF OPTICALLY EQUIVALENT MODEL IN THREE-DIMENSIONAL PHOTOELASTICITY

A Thesis Submitted
In Partial Fulfilment of the Requirements
for the Degree of
DOCTOR OF PHILOSOPHY

[illegible]

BY
A. V. S. S. S. R. SARMA

to the

DEPARTMENT OF MECHANICAL ENGINEERING
INDIAN INSTITUTE OF TECHNOLOGY KANPUR
JULY, 1972

I. I. T. KANPUR
CENTRAL LIBRARY
Acc. No. A 23674

ME-1972-D-SAR-EFF

POST GRADUATE OFFICE
This thesis has been approved
for the award of the Degree of
Doctor of Philosophy (Ph.D.)
in accordance with the
regulations of the Indian
Institute of Technology Kanpur
Dated: 29/3/73

POST GRADUATE OFFICE
Submitted on 26/8/72

CERTIFICATE

This is to certify that this work on "Effects of Stress-Induced Optical Activity and Determination of Optically Equivalent Models in Three-Dimensional Photoelasticity" has been carried out under my supervision and that this has not been submitted elsewhere for a degree.

LSrinath

L.S. SRINATH
Professor
Department of Mechanical Engineering
Indian Institute of Technology, Kanpur
At present on leave to I.I.Sc., Bangalore
as Visiting Professor in Mechanical Sciences.

ACKNOWLEDGEMENT

I am deeply grateful to my thesis supervisor, Prof. L.S. Srinath for his valuable, patient and inspiring guidance during this work.

I am grateful to Prof. G. Srikantiah for his encouragement during my doctoral programme.

My thanks are due to Mr. Bhave for his valuable discussions, to Mr. D.K. Sarkar for his valuable help and advice during the experimentation and to Mr. S.L. Srivastava for valuable assistance rendered by him during my work.

My thanks are also due to Mr. M. Veerabhadra Rao for his unreserved help and assistance during the preparation of this thesis and to Mr. Saini for his diligent typing.

A.V.S.S.S.R.SARMA

TABLE OF CONTENTS

Chapter Page

LIST OF TABLES

LIST OF FIGURES

NOMENCLATURE

SYNOPSIS

1. INTRODUCTION

Stress-Optic Law in Two and Three-Dimensions 2

Stress-Optic Law in Three-Dimensions 3

Three-Dimensional Photoelastic Techniques and Rotational Effects 4

Present Investigation 8

2. THE LIGHT ELLIPSE AND OPTICAL EQUATIONS IN TERMS OF STOKES PARAMETERS

Introduction 14

Light Ellipse 14

Stokes Vector 18

Transformations of Stokes Vector 22

Intensity Calibration Method to Determine Ellipticity 23

Optical Equations of Three-Dimensional Photoelasticity 27

Chapter Page

Equations Using Stokes Parameters 32

Jones Vector 37

3. CHARACTERISTIC PARAMETERS IN THREE-DIMENSIONAL PHOTOELASTICITY AND THEIR EXPERIMENTAL DETERMINATION

Poincare's Sphere Representation 40

Combined Effect of a Series of Retarders 46

Effect of a Series of Retarders Using Stokes Vector 47

Optically Equivalent System for a Continuous Body 52

Some Special Cases 56

Case (a) Pure Rotator 56

Case (b) Reversal of Light Path 58

Case (c) Reflection Polariscope 60

Case (d) Axi-Symmetric Case 62

Case (e) Anti-Symmetric Case 64

Experimental Determination of Characteristic Parameters 70

Method 1 70

Method 2 71

4. SCATTERED LIGHT METHODS IN THREE-DIMENSIONAL PHOTOELASTICITY

Directions of the Secondary Principal-Stresses

Approximate Methods 84

(a) Displacement Pattern Method 85

(b) Sharpest Contrast Method 85

Chapter Page

(c) Minimum Intensity Method 85

Exact Methods

i) The Constant Intensity Method 86

ii) The Zero Intensity or Line Ellipse Method 86

iii) Absolute Intensity Method 88

Critical Analysis 95

Analysis as Applied to a Model Under Combined Tension and Torsion 103

New Methods 115

1) Scattered Light Technique Where the Model Acts as an Analyser

Method (a) 120

Method (b) 124

2) Scattered Light Technique Where the Model Acts as a Polarizer 127

5. MISCELLANEOUS TOPICS

Introduction 131

A: GRAPHICAL METHODS IN PHOTOELASTICITY

(a) Mapping of Light Ellipses of Constant Orientation (α = constant) and Varying Ellipticity 136

(b) Mapping of Light Vibrations of Constant Ellipticity e and Varying Azimuth α 138

Kuske's J Circle Method 140

Chapter Page

Schweiger's Analysis 144

a) Parallel Projection 147

b) Wulff's Grid 149

Determination of Parameters of the Equivalent Optical System for A Combination of Two Linear Retarders 150

Graphical Methods Using Quaternions 156

The Characteristic Quantities of a General System of Retarders 159

The New Approach 165

First Graphical Method 168

Procedure to Use the Graphical Method 171

Passage of Light Through Elements of a Polariscope 173

i) Plane Polariscope 173

ii) Circular Polariscope 176

iii) Tardy's Method 182

Determination of Characteristic Parameters 184

Second Graphical Method 185

Tardy's Method 193

Examples 198

B: THEORY OF COMPENSATION

Combination of Two Linear Retarders of Equal Retardance? 204

Combination of Two Quarter-Wave Plates 208

A Half-Wave Plate Between Two Quarter-Wave Plates 215

Chapter Page

C: DETERMINATION OF INTEGRAL FRINGE ORDERS IN PHOTOELASTICITY

Construction of Nomogram 226

Multiple Values for n_1 and n_2 229

All Possible Values for ϵ and Associated n_2 n_1 Values (Construction' of Ready Reckoner Table) 230

Example and Experimental Results 240

Conclusions 246

6 EXPERIMENTAL RESULTS

(1) Experimental Determination of Characteristic Parameters for Various Loadings

Experimental Procedure

Method 1 254

Method 2 254

(2) Experimental Determination of Characteristic Parameters for Various Wavelengths of Light

Experimental Procedure 258

(3) Tests in Support of the Existence of an Optically Equivalent System 261

(4) Experimental Check for the Validity of Assumptions Involved in the Previous Scattered Light Methods 269

7 CONCLUSIONS 283

APPENDIX A 290

REFERENCES 297

LIST OF PUBLICATIONS

LIST OF TABLES

Table		Page
5.1	Possible Values of ϵ And Associated n_2 And n_1	235
5.2	Experimental Values of Material Fringe Constants for Three Wavelengths of Light	241
5.3	Comparison of Experimental And Theoretical Values of Total Fringe Orders	242
5.4	Computed Values of ϵ (Using z) (The Ready-Reckoner Table)	243
5.5	Computed Values of ϵ^* (Using z^*) (The Ready-Reckoner Table)	244
5.5	Comparison of the Intengral Fringe Orders (Experimental, Values Computed from ϵ and Values Computed from ϵ^*)	245
6.1	Characteristic Parameters for Various Loadings (Theoretical And Experimental)	257
6.2	Characteristic Parameters for Different Wavelengths of Light	260
6.3	Variation of Intensity And Retardation Along the Secondary Characteristic Directions When the Retardation Along the Primary Characteristic Directions is Varied (P = 109 lb. T = 19 lb.in.)	265
6.4	Variation of Intensity And Retardation Along the Secondary Characteristic Directions when the Retardation Along the Primary Characteristic Directions is Varied (P = 96 lb. T = 16 lb. in.)	266

Table Page

6.5 Parameters of Light Ellipse at Exit Using the Optically Equivalent Model 267

Exit Light Ellipse Parameters by Tardy's Method (Change in the Azimuth)

6.6 P = 90 lb. T = 15 lb.in. 273
6.7 P = 96 lb. T ± 12 lb.in. 273
6.8 P = 96 lb. T = 8 lb.in. 274
6.9 P = 96 lb. T = 16 lb.in. 274
6.10 P = 96 lb. T = 24 lb.in. 275

Exit Light Ellipse Parameters by Tardy's Method (Phase Difference and Ellipticity). Experimental and Calculated Values

6.11 P = 90 lb. T = 15 lb.in. 275
6.12 P = 96 lb. T = 12 lb.in. 276
6.13 P = 96 lb. T = 8 lb.in. 276
6.14 P = 96 lb. T = 16 lb.in. 277
6.15 P = 96 lb. T = 24 lb.in. 277

Exit Light Ellipse Parameters (Intensity and Amplitude Ratio)Experimental and Calculated Values

6.16 P = 90 lb. T = 15 lb.in. 278
6.17 P = 96 lb. T = 12 lb.in. 278
6.18 P = 96 lb. T = 8 lb.in. 279
6.19 P = 96 lb. T = 16 lb.in. 279
6.20 P = 96 lb. T = 24 lb.in. 280

LIST OF FIGURES

Figure		Page
1	Light Ellipse and Reference Axes	13
2	Right and Left Handed Light Ellipses	16
3	Rotation of Axes	21
4	Optical Set Up for Two-Dimensional Stress Analysis	25
5	Rotation of Secondary Principal-Stress Axes Along the Optical Path	33
6	Poincare's Sphere Representation of Polarized Light Forms	41
7(a)	Rotation of the Reference Axes	43
7(b)	Addition of Retardation	43
8	Construction for Composition of Two Rotations	45
9	Representation of the Axes of the Birefringent Plates in the Equivalent Systems	50
10	Distribution of Shear Stress τ and Isoclinic Parameter Ø along the Chord A B C in an Axi-Symmetric Case	61
11	Distribution of the Direction Ø and the Difference (p' - q') of the Secondary Principal-Stress along the Optical Path A B C	63
12	Equivalent System for the Optical Path A B C	65

Figure Page

13 Directions of Scattered Light Observation at the Point O 78

14 The Zero Intensity or Line Ellipse Method 87

15 Scattered Light Technique Using the Model as a Polarizer 90

16 Variation of R Along the Optical Path in the Model 104

17 Variation of the Quantity $(\partial R/\partial \epsilon)$ Along the Wave Normal 105

18 Variation of the Amplitude Along the Optical Path 106

19 Variation of Phase-Difference Along the Optical Path (P = 96 lb, T = 8 lb. in.) 107

20 Variation of Phase-Difference Along the Optical Path (P = 100 lb, T = 18 lb. in.) 108

21 Variation of Phase-Difference Along the Optical Path (P = 90 lb., T = 15 lb.in) 109

22 Variation of Amplitude with Retardation 110

23 Phase Difference at the Exit Vs. Phase Difference at the Entrance 111

24 Variation of Sec. Pr. Str. Axes Orientation Ø Along the Optical Path in the Model 113

25 $(p' - q')$ Vs Z 114

26 The Scattered Light Technique with the Model Acting as an Analyser 119

27 Scattered Light Observation Along Two Sets of Axes 45° Apart 123

Figure Page

28 Scattered Light Technique Where the Model Acts as a Polarizer 126

29 Representation of Polarized Light Forms in a Complex Plane 133

30 Constant Ellipticity (e) and Constant Amplitude Ratio Circles in the Conformal Mapping 137

31 Kuske's J Circle Method 139

32 Kuske's J Circle 142

33 Sphere of Polarization (Poincare's Sphere) 145

34 Parallel Projection of the Sphere of Polarization (J Circle) 146

35 **Stereographic** Projection of the Sphere of Polarization (Wuff's Grid) 148

36 Determination of the Angle ρ Active of the Active Plate of an Equivalent System for Two Plane Models 151

37 Finding the Parameters of the Optically Equivalent System 152

38 Representation of Axes of the Two Retarders 153

39 Finding the Parameters of the Optically Equivalent System 154

40 Co-ordinate Set Used for the Description of the General Equation 157

Figure Page

41 Transformation of a Co-ordinate Set at the Point of Emergence, - Azimuth of the Old and New Reference Coordinate System 161
42 The Addition of the Retarder at the Point of Emergence 162
43. The Characteristic Quantities of a General System of Retarders 163
44 The First Graphical Method 167
45 Orientation of the Axes of the Two Retarders 169
46 Effect of Combination of Two Retarders 170
47 Variation of Light Ellipse Parameters in a Plane Polariscope 172
48 Circular Polariscope Set Up 174
49 Transformation of Light Ellipse in a Circular Polariscope 175
50 Optical Set Up in Tardy's Method 180
51 Transformations of Light Ellipse in Tardy's Method 181
52 The Second Graphical Method 186
53 Construction of Constant Phase Difference Lines 187
54 Construction of Constant Azimuth Lines 188
55 Analysis of Tardy's Method Using the Second Graphical Method 192
56 Polar Co-ordinates for J Circle Method 195
57 First Graphical Method ($0 < \alpha < 2\pi$, $0 < \epsilon < 2\pi$) 197

Figure		Page
58(a)	Example (a), First Graphical Method	198
58(b)	Example (a), Second Graphical Method	198
59	Example (b) Second Graphical Method	199
60(a)	Orientations of Axes of Various Elements	209
60(b)	Orientation of Axes of the Two Quarter-Wave Plates and Analyser	209
61	Orientations of the Axes of the Four Retarders	211
62	Orientations of the Retarders in Two Types of Combinations So as to Form Quarter-Wave Plates	218
63	Nomogram for the Determination of Integral Fringe Orders	225
64	Nomogram Showing Discrete Values for ϵ	231
65(a)	Wavelength Vs. Absorption (Filter No. 2938)	236
65(b)	Wavelength Vs. Absorption (Filter No. 3187)	237
65(c)	Wavelength Vs. Absorption (Filter No. 3214)	238
66	Experimental Values of the Material Fringe Constants for Three Wavelengths of Light	239
67	Optical Path in the Model	249
68	Loading Device for Combined Tension & Torsion	250
69	Polariscope Set Up (Plate)	251
70	Loading Arrangement (Plate)	252
71	Residual Stress Pattern (Plate)

NOMENCLATURE

$\bar{\omega}$ = Angular frequency of vibration of the light vector

λ = Wavelength of light used

ϕ = Orientation of the (secondary) principal-stress axes with respect to the reference axes

ρ = Retardation added along the secondary principal-stress axes due to the stresses alone

$\tan\omega$ = Ellipticity of the light ellipse

$= \frac{\text{length of semi-minor axis}}{\text{length of semi-major axis}}$

$= \frac{b}{a}$

a_X , a_Y = Amplitudes of the components of light vector along the X,Y axes

α = Azimuth

= Orientation of the major axis of the light ellipse with respect to the reference axes

$\tan\theta = \frac{a_Y}{a_X}$

= Amplitude ratio

ϵ_X = Phase angle of the component of light vector along the Y axis - Phase angle of the component of light vector along X axis, (The axes X and Y are mutually perpendicular)

Z = Co-ordinate axis along the optical path

t = Time

h = Thickness of the model

δ = Characteristic retardation

ψ_1 = Rotatory power of the optically equivalent system

β_1 = Orientation of the primary characteristic directions with respect to the reference axes

β_2 = Orientation of the secondary characteristic directions with respect to the reference axes

S = Source of light

P = Polarizer

$(\lambda/4)_1$ plate = First quarter-wave plate in the polariscope which is placed before the model (i.e. on the source side of the model)

$(\lambda/4)_2$ plate = Second quarter-wave plate which is placed after the model (i.e. on the analyser side of the model)

$(\lambda/2)$ plate = Half-wave plate

F = Fast axis

S = Slow axis

p, q = Magnitudes of principal-stresses

p', q' = Magnitudes of secondary principal-stresses

F = Material fringe constant

f = Model fringe constant

C = Stress-optic coefficient

n_1, n_2 = Refractive indeces along the principal-stress axes.

SYNOPSIS

EFFECTS OF STRESS-INDUCED OPTICAL ACTIVITY AND DETERMINATION OF OPTICALLY EQUIVALENT MODELS IN THREE-DIMENSIONAL PHOTOELASTICITY

A Thesis Submitted
In Partial Fulfilment of the Requirements
for the Degree of

Ph.D.

by
A.V.S.S.S.R.SARMA
to the
DEPARTMENT OF MECHANICAL ENGINEERING
INDIAN INSTITUTE OF TECHNOLOGY, KANPUR
JULY 1972

Among the methods available to determine the complete state of stress at any point in a three-dimensional body, photoelasticity ranks very high. In photoelasticity, there are essentially two methods, (a) using transmitted light, and (b) using scattered light. The transmitted light technique presently needs a frozen stress model which has to be cut into slices and sub-slices to obtain the required data. Hence, the method is destructive in nature. The scattered light technique however is nondestructive and has certain other advantages in the sense that no frozen stress model is necessary. The models can be subjected to live loads at room temperatures and analysed.

In scattered light technique there are essentially two methods, one developed by Frocht and Srinath, and the other developed by Robert and Guillemet. The method developed by Frocht and Srinath is limited to cases where the effects of stress-induced optical activity is not high. This is equivalent to saying that the rate of rotation of the secondary principal-stresses along the light path is small compared to the rate of retardation. The method developed by Robert and Guillemet does not involve any assumption regarding optical activity, but requires certain characteristic parameters which are indirectly related to the secondary principal-stresses and their directions.

The present investigation is concerned with the following topics:

1) Development of relevant optical equations using Stokes parameters for the analysis of problems involving optical activity;

2) Experimental techniques to determine the characteristic parameters, that is the primary and secondary characteristic directions and the characteristic retardation;

3) Reduction of a three-dimensional photoelastic model to an optically equivalent system;

4) New methods for scattered light analysis without involving assumptions regarding stress-induced optical activity;

5) Development of new graphical methods to determine the integrated effect in problems involving optical activity;

6) Development of a large-field compensator using a few plates of arbitrary but equal retardation-an extension of Pancharatnam's and Tuzi's work;

7) Determination of integral fringe orders using different wavelengths of light;

8) Experimental verification of the above methods using a model under combined torsion and tension;

A short write-up on the above topics is giveb below:

The usual photoelastic analysis consists of trigonometrical resolutions of the light vector at various stages, as it passes through the model. However, the study of light ellipse and its properties as it passes through the various optical elements provides a better and elegant method of analysis. This concept has been used throughout this investigation. To start with, various previous systems of equations of three-dimensional photoelasticity are studied. Then these optical equations are kinematically derived in terms of Stokes parameters. Since the transformations of these parameters when the light ellipse passes through a retarder are linear in these parameters, the resulting optical equations derived in terms of Stokes parameters turn out to be a set of ordinary linear differential equations which are very convenient for analysis and application. Using these equations, the analytical solution for the case where the ratio of the rate of rotation to the rate of retardation is a constant, is obtained (The rate of rotation itself can be any arbitrary function). This case is more general compared to the case investigated by Drucker and Mindlin where each of these rates is a constant.

From these equations, the equivalence of any optical path in a three-dimensional photoelastic model to a system consisting of a retarder and a pure rotator follows directly. Two new direct methods of finding these characteristic parameters experimentally in a transmission polariscope are presented. Extension of these methods to the scattered light technique is described. These methods of scattered light analysis do not involve any assumptions regarding optical activity. Also these do not require the rotation of the analyser at a particular speed as is required in the method of Robert and Guillemet. A direct and whole field method which is derived from the optical equations in terms of Stokes parameters is presented. This method again is general and it does not involve any assumptions.

Further some investigations are carried out on a few related topics. The graphical methods are very convenient to find the integrated optical effect when the secondary principal-stress difference and their directions are given. The existing graphical methods are essentially based on stereographic or parallel projection of the Poincare sphere or the quaternions.

A brief review of these methods is presented. A more direct and simpler approach to develop the graphical methods which is based on the properties of the light ellipse, is then presented. Two simple graphical methods which have certain advantages over the previous methods are described.

The compensator is an indispensable optical element in the photoelastic work. Construction of a large field compensator using a few plates of arbitary but same retardation is described. This is essentially an extension of the works of Pancharatnam and Tuzi. An extension of Pant's method to find the integral fringe order using the fractional fringe order for different wavelengths of light, is presented.

Some experimental results obtained from a rectangular photoelastic model under combined tension and torsion in a transmission polariscope are presented as supporting evidence for the existence of an optically equivalent system, the two methods of determining these parameters experimentally, limitations of the previous scattered light methods and the determination of the integral fringe orders.

CHAPTER 1

INTRODUCTION

Photoelasticity and Electromagnetic Theory of Light

Photoelasticity deals with the study of propagation of light through elastic bodies under load in order to determine the stress distribution inside these bodies. Photoplasticity, photoviscoelasticity, dynamic photoelasticity etc. are immediate extensions of the basic principles of photoelasticity. The basic phenomenon of double refraction on which photoelasticity stands was discovered in 1816 by David Brewster. Neumann formulated the stress-optic law in terms of strain in 1841. Later after ten years, the same law was formulated in terms of stress by Maxwell. The first engineering applications were tried by French engineer Mesnager and the British scientists Coker and Filon in the beginning of the present century.

The electromagnetic theory of light explains all the photoelastic phenomena. According to this theory[1], it is assumed that the transmission of all forms of radiant energy (including light) through space takes place in the form of electromagnetic disturbances. The radiant energy of light is equally divided between electric energy and magnetic energy. At any instant, these electric and magnetic fields at a given point in a ray of light may be represented by two equal and mutually perpendicular vectors called electric and magnetic vectors in a plane perpendicular to the ray of light. Because of the interdependence of these two vectors, we can for all practical purposes in the photoelastic analysis, consider only one vector say, the electric vector. The electromagnetic spectrum of radiant energy covers in addition to the visible light rays, the heat rays, X-rays, radio waves and the shorter gamma rays. In ordinary or unpolarized light, the light vector (electric vector) has no directional preference and its changes are chaotic. When the electric vector changes its azimuth (orientation with respect to some fixed axes) and magnitude according to a certain law, we have polarized light. When the tip of the electric vector traces out an ellipse or a circle, it is elliptically polarized light or circularly polarized light respectively. When the azimuth of light vector does not change, that is, the electric vector stays in a particular plane, it is plane polarized light. This phenomenon of polarization is observed throughout the electromagnetic spectrum.

Stress-Optic Law in Two and Three-Dimensions

In a transparent isotropic plate, in which the stresses are two-dimensional, and within the elastic limit, the phase difference or relative retardation ρ in wavelengths between the rectangular wave components of light travelling through it and produced by temporary birefringence is given by

$$\rho = C_\lambda \, h \, (p - q) \tag{1.1}$$

in which C_λ is a constant known as the stress-optic coefficient for the particular material for wavelength λ, h is the thickness of the plate and p and q the principal-stresses. This temporary retardation or phase diffe-rence (this vanishes when the loads are removed) is introduced along the principal-stress axes.

Stress-Optic Law in Three-Dimensions

In a three-dimensional photoelastic model, a retardation (in wavelengths or fringes) equal to

$$dn = C_\lambda \, dh \, (p' - q') \tag{1.2}$$

will be added along the secondary principal-stress axes to the phase of the components of light vector along these directions. C_λ is the stress-optic coefficient as in two-dimensional case. dh is the actual length of light path (dh is so small that the rotation of the secondary principal-stress axes over this distance is negligible), p', q' are the secondary principal-stresses for the direction of the given ray. The secondary principal-stresses for a given direction of light propagation are defined as the principal-stresses resulting from the stress components which lie in a plane normal to the direction of light ray. In both the above cases, the stress-optic coefficient may also depend upon the temperature of the model material.

Thus, the photoelastic analysis essentially involves the measurement of retardation introduced in the model and finding the directions along which this retardation is introduced. A photoelastic model under an isotropic state of stress will not introduce any retardation and a general state of stress can be broken into two parts, the isotropic part and the deviatoric part. So, the photoelastic analysis will yield five stress components at a point out of the total six components[2]. The other unknown can be found by using either the shear difference method[3], oblique incidence[4], electric analogy or by an interferometric method[2.5.6]. The photoelastic technique in the two dimensional case is almost perfected. In this case, the model making and the simulation of the loading of the prototype take much of the time while the experiment is direct and simple. The birefringent coating method and photoelastic study with a reflection polariscope eliminate model making without loosing the advantages of the transmission method[7].

Three-Dimensional Photoelastic Techniques and Rotational Effects:

In the general three-dimensional cases of stress distribution, the secondary principal-stresses vary continuously along the wavenormal and this makes the analysis difficult. The three-dimensional photoelastic techniques in vogue are essentially two, (i) the stress freezing technique [8,9] where the stresses are frozen into the model and the model is carefully cut into very thin slices without disturbing the frozen stress pattern, so that in each slice the rotational effect is negligible (to freeze the stresses into it, the model is made to undergo a special thermal cycle) and (ii) the scattered light methods [10-16] where measurements on light scattered in a plane perpendicular to the light path are made.

In 1939 Weller[17] made use of the scattered light phenomenon in his analysis of three-dimensional state of stress in a photoelastic model. Using the ether theory of light Drucker and Mindlin[18] investigated the effect of rotation of secondary principal-stress axes along the wave normal, on the retardation in a photoelastic model. They solved the problem where the principal-stress magnitude remains constant and their directions change linearly along the wavenormal. They concluded that (i) the rotation increased the relative retardation by a factor $S = (1 + 4R^2)^{\frac{1}{2}}$ where R is the ratio of the rate of rotation to the rate of retardation and that (ii) at high stress the light vector rotated with the principal-stress directions, plane polarized light entering along a direction of principal-stress remained practically plane polarized in the direction of stress through the entire model.

Mindlin and Goodman [19] derived optical equations of three-dimensional photoelasticity from Maxwell's electromagnetic equations by neglecting the inplane (plane perpendicular to the wavenormal) variations of the indeces of refraction and the displacements and some other quantities of very low magnitude. They derived Maxwell-Neumann equations[20] and showed the order of magnitudes of necessary approximations involved. They also showed that the parameter R was the essential one controlling optical wave propagation in three-dimensional photoelasticity.

Ginsburg[21] derived yet another system of differential equations governing the propagation of electromagnetic waves in an anisotropic, inhomogeneous medium. Aben[22] simplified these equations by neglecting certain quantities and assuming a particular form for the solution. His equations are finally reduced to two first order ordinary differential equations with variable coefficients. He proved the equivalence of any length of optical path in the model to a system containing three parameters called the characteristic parameters in analogy with the parameters for a system of birefringent plates.[23] He suggested that the experimental data of these parameters for various wavelengths of light would yield additional information regarding the stress distribution inside the photoelastic model.

Frocht and Srinath[10,11,12] developed a scattered light method in which they assumed that: when the amplitudes of light vibration along the secondary principal-stress axes at the entrance were equal, with the addition of retardation along these axes at the entrance (i) the amplitudes along the secondary principal-stress axes at any point on the light path did not vary and (2) whatever retardation was added at the entrance, the same amount appeared as an additional retardation along the secondary principal-stress axes at any point on the optical path. This is equivalent to assuming that the retardation vs. distance (along the wavenormal) curve shifts parallel to itself when a certain amount of retardation is added at the entrance. These assumptions however are valid for the cases where the rate of rotation is not high, and these are based on the findings of Drucker and Mindlin[18] .

Aderholdt, Mckinney, Ranson and Swinson[13] in their scattered light method treated the light components to be following the secondary principal-stress axes in cases where the rotation to retardation ratio is small. This was also based on the findings of Drucker and Mindlin[18] .

Robert and Guillemet[14,15,16] followed an altogether different approach to overcome the rotational effect. They used the ellipticity measurement technique that was common in crystallographic investigations[23] . In this technique, the analyser is rotated at a particular speed and the ratio of the amplitudes of alternating and direct components of light from the analyser is measured with suitable electronic instrumentation. The analysis in this method is not direct but through the characteristic parameters. This method however, does not involve any assumptions as in the above methods.

Present Investigation

The objective of the present investigation is

(i) to develop the necessary equations describing optical phenomena in a photoelastic medium in the presence of rotation of the secondary principal-stress axes, in terms of Stokes parameters [23],

(ii) to solve these equations analytically or numerically for various cases and study the validity of assumptions of previous investigations,

(iii) to use these equations for proving the existence of an optically equivalent system consisting of a retarder and a rotator,

(iv) to devise methods (both with transmitted and scattered light) for the determination of the parameters of the optically equivalent system (characteristic parameters) experimentally,

(v) to devise new graphical methods to describe passage of light through a photoelastic model in which the rotation of secondary principal-stress axes is present and to apply these graphical methods for the determination of the integrated optical effect and the characteristic parameters,

(vi) to develop new techniques of compensation

(vii) to develop methods for the determination of integral fringe orders (upto any value, when there is no stress free corner to count from),

(viii) to devise and perform experiments to check the validity of (a) the governing optical equations (b) the existence of an optically equivalent system and the techniques for the determination of the parameters of this equivalent system (c) the assumptions of the previous scattered light methods and (d) to find the variation of characteristic parameters with the wavelength of light.

A brief outline of the contents of each chapter is presented below.

In Chapter 2, a discussion on the available systems of optical equations in three-dimensional photoelasticity is presented. A new set of ordinary, linear simultaneous equations are derived kinematically in terms of Stokes parameters . These are very convenient for analysis and application. Using these equations, the analytical solution for the case where the ratio R of the rate of rotation (ϕ') to the rate of retardation ρ' is a constant (ϕ' can be any arbitrary function) is derived. Also presented is a discussion on the concept and properties of light ellipse.

In Chapter 3, the existence of an optically equivalent model for any length of light path in the photoelastic model is proved. The importance of the concept of an optically equivalent system is appraised. Some special cases in which there exists some relation between the parameters of the optically equivalent system (called characteristic parameters) are discussed. Two direct and simple methods of determining these parameters experimentally are described.

In Chapter 4, a discussion on the previous methods of scattered light analysis is presented. The validity of the assumptions involved in these methods is investigated using the analytical solution derived in Chapter 2, the numerical solutions for some cases of loading (of a rectangular bar under combined tension and torsion) and the concept of 'optically equivalent system'. Modifications of the methods of determining the characteristic parameters with transmitted light (described in Chapter 3) for use with scattered light are suggested.

Chapter 5 on Miscellaneous Topics deals with the following:

(A) 'Discussion on various graphical methods in three-dimensional photoelasticity' - In this section a brief discussion of various existing graphical methods developed by Jerrard[24], Robert and Guillemet[14], Kuske[25], Schwieger[26], Cernosek[27], is presented. A new, direct approach based on the concept of light ellipse with two graphical methods is described. Use of these graphical methods in finding the characteristic parameters is demonstrated.

(B) 'Discussion of the existing methods of compensation and development of a large field compensator' - In this section use of (a) a system of four retarders each having the same retardation, with the polarizer or analyser and (b) a system of eight retarders each having the same retardation, as a compensator is described. This is essentially an extension of the works of Pancharatman [28] and Tuzi [29].

(C) 'Determination of integral fringe orders in photoelasticity' - In this section the construction of a nomogram and a ready reckoner table which can be used to determine the integral fringe order (virtually upto any value) from the fractional fringe orders for two wavelengths of light, is described. This method is essentially an extension of the method developed by Pant [30]. Some experimental values (for a circular disc under diametral compression) are presented to demonstrate the value of these methods.

In Chapter 6 are presented results from experiments conducted on a rectangular bar under combined tension and torsion. These form the supporting evidence for the validity of the governing optical equations and the existence of an optically equivalent system. The techniques described in Chapter 3 are successfully employed to determine the characteristic parameters experimentally for various values of tension and torsion. These experimental values are compared with the values obtained by numerically integrating the governing optical equations derived in Chapter 2. The agreement between these two sets of values is found to be good. The characteristic parameters are also found experimentally for three wavelengths of light for the same loading.

The change in the characteristic directions is 34° when the wavelength is changed from 5004°A to 5950°A (the corresponding change in the material fringe constant is from 128 - 158 psi. in./fringe). For the particular values of tensile and torsional loads considered, the assumptions of the previous scattered light methods are not found to be valid.

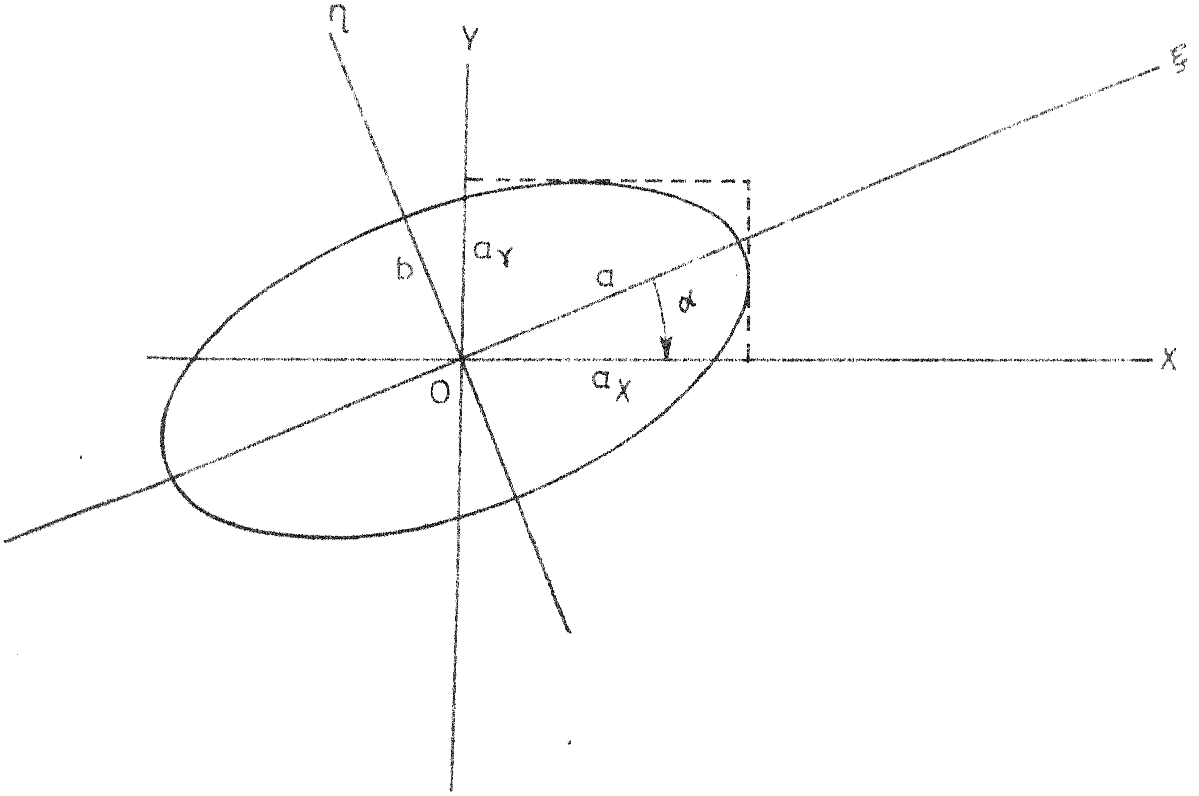

FIG. 1. LIGHT ELLIPSE AND REFERENCE AXES AZIMUTH α IS MEASURED FROM THE MAJOR AXIS TO X-AXIS IN THE CLOCK WISE DIRECTION.

CHAPTER 2

THE LIGHT ELLIPSE AND OPTICAL EQUATIONS IN TERMS OF STOKES PARAMETERS

Introduction :

The photoelastic analysis consists of observing the changes in the properties of the polarized light in the photoelastic model experimentally and relating these to the (secondary) principal-stresses and their directions using the stress-optic law. This is usually done by resolving trigonometrically the light vector along different directions and examining the amplitudes and phase angles of each component. A simpler and more convenient way is to study the properties of the light ellipse and its transformations as the light passes through a model or a series of optical elements and then to use this information in the photoelastic analysis.[31]

Light Ellipse

The most general type of polarized light is the elliptically polarized light which can be represented by an ellipse called the light ellipse. This can be represented by two simple harmonic vibrations along two orthogonal reference axes OX and OY, Fig. 1., as:

$$E_X = a_X \cos \bar{\omega} t$$

and (2.1)

$$E_Y = a_Y \cos(\bar{\omega} t + \epsilon)$$

where ϵ is the relative phase difference between the two vibrations, and a_X, a_Y are the amplitudes along these two axes.

In the case of a stressed photoelastic medium, it is conventional to make the reference axes coincide with the secondary principal-stress axes.

Eliminating $\bar{\omega} t$ between the above two equations, the equation of the light ellipse is obtained as

$$\left[\frac{E_X}{a_X}\right]^2 + \left[\frac{E_Y}{a_Y}\right]^2 - \frac{2 E_X E_Y}{a_X a_Y} \cos\epsilon = \sin^2\epsilon \qquad (2.2)$$

The major axis of the light ellipse makes an angle with the X-axis such that

$$\tan 2\alpha = \frac{2 a_X a_Y}{a_X^2 - a_Y^2} \cos\epsilon$$

$$= \tan 2\theta \cos\epsilon \qquad (2.3)$$

where $\tan\theta = \frac{a_Y}{a_X}$ = amplitude ratio (2.4)

α is called the azimuth of the light ellipse with respect to the reference axis-OX.

If a and b are the lengths of the semi-major and semi-minor axes of the light ellipse, their values are given by

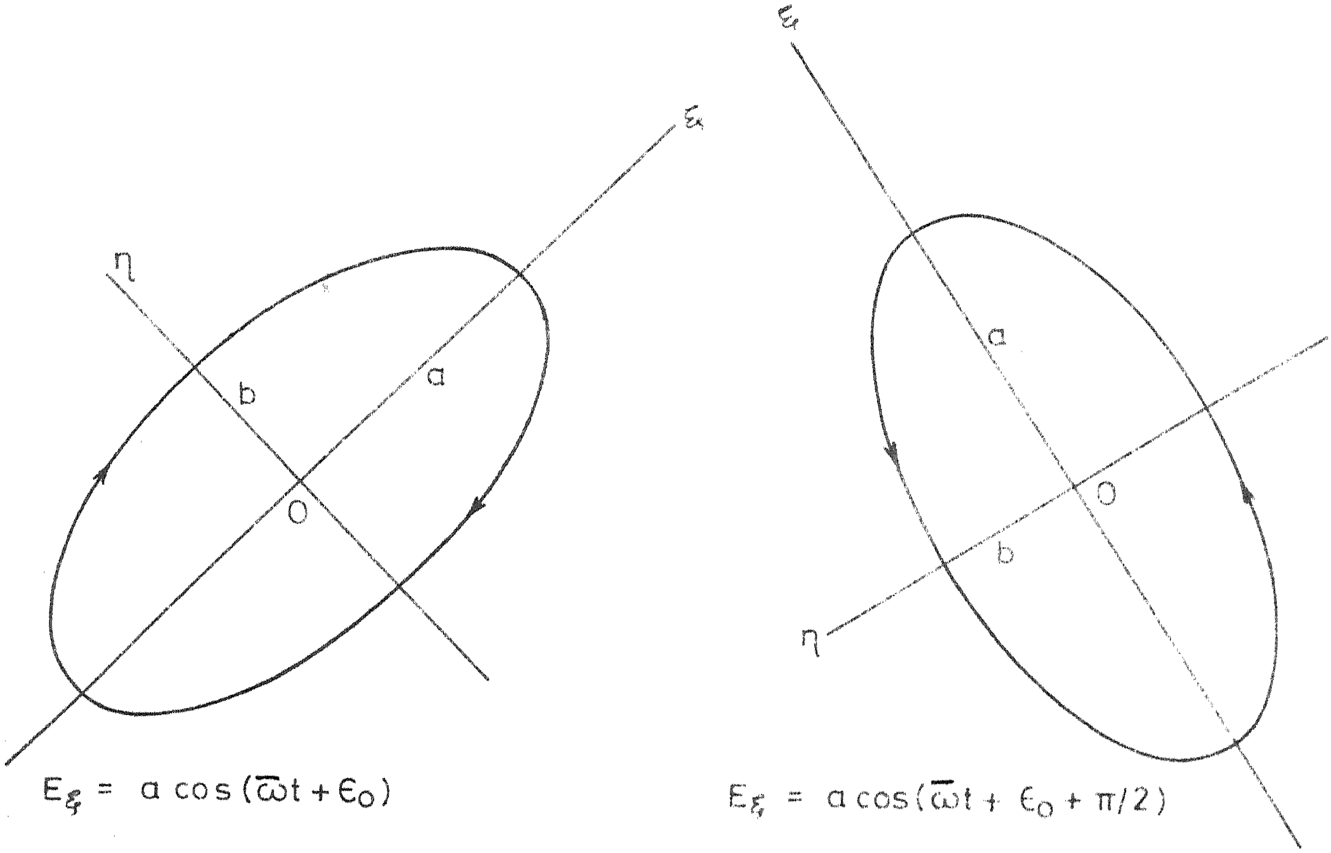

$$E_\xi = a\cos(\overline{\omega}t + \epsilon_0)$$

$$E_\eta = b\cos(\overline{\omega}t + \epsilon_0 + \pi/2)$$

$$E_\xi = a\cos(\overline{\omega}t + \epsilon_0 + \pi/2)$$

$$E_\eta = b\cos(\overline{\omega}t + \epsilon_0)$$

FIG. 2. RIGHT AND LELT-HANDED LIGHT ELLIPSES

$$\begin{aligned} a^2 &= a_X^2 \,\mathrm{Cos}^2\alpha + a_Y^2 \,\mathrm{Sin}^2\alpha + 2a_X\, a_Y \,\mathrm{Cos}\alpha \,\mathrm{Sin}\alpha \,\mathrm{Cos}\epsilon \\ b^2 &= a_X^2 \,\mathrm{Sin}^2\alpha + a_Y^2 \,\mathrm{Cos}^2\alpha - 2a_X\, a_Y \,\mathrm{Cos}\alpha \,\mathrm{Sin}\alpha \,\mathrm{Cos}\epsilon \end{aligned} \qquad (2.5)$$

so that $a^2 + b^2 = a_X^2 + a_Y^2$ (2.6)

The ratio :

$$\tan\omega = \frac{b}{a} = e \qquad (2.7)$$

e is called the ellipticity.

The light ellipse can also be referred to its own major and minor axes ξ and η - giving

$$\begin{aligned} E_\xi &= a \,\mathrm{Cos}(\overline{\omega} t + \epsilon_o) \\ E_\eta &= b \,\mathrm{Cos}(\overline{\omega} t + \epsilon_o \pm \pi/2) \\ &= \pm b \,\mathrm{Sin}(\overline{\omega} t + \epsilon_o) \end{aligned} \qquad (2.8)$$

$$\text{Where } \tan\epsilon_o = \frac{a_Y \,\mathrm{Sin}\epsilon \,\mathrm{Sin}\alpha}{a_X \,\mathrm{Cos}\alpha + a_Y \,\mathrm{Sin}\alpha \,\mathrm{Cos}\epsilon} \qquad (2.9)$$

The plus or minus sign indicates left handedness or right handedness of the light ellipse.

The following points are observed and used in the subsequent analysis.

1) When the light ellipse is referred to its own axes, the relative phase difference is $\pm\pi/2$.

2) If E_η is ahead of E_ξ by $\pi/2$, the light ellipse is right handed. If E_ξ is ahead of E_η by $\pi/2$, the ellipse is left handed, Fig. 2.

3) If a phase difference of $\pm\pi/2$ is added along the major or minor axis of the light ellipse, it becomes a line ellipse

(linearly polarized), oriented at an angle ω such that $\tan\omega = \pm b/a$.

4) If the amplitudes a_X and a_Y along the reference axes are equal, then $\tan 2\alpha = \infty$, which means, that the axis of the ellipse will be at 45° to the X-axis.

5) If $a_X = a_Y$ and $\epsilon = \pi/2$, the light ellipse becomes a circle and $a = b$ (circularly polarized - from Eq. (2.5)).

The state of polarization as represented by Eqs. (2.5) and (2.6) can be expressed in terms of the azimuth α and the ellipticity b/a. These two quantities are sufficient to express completely the state of polarization if one disregards the absolute intensity (as is the case in most of photoelastic work).

Stokes Vector

The components of light vibration along the reference axes OX and OY, Fig. 1, are given by E_X and E_Y in Eq. (2.1). The components of this vibration along a set of new axes OX' and OY', Fig.3, inclined at an angle of α' to the OX, OY axes are given by

$$E_{X'} = a_X \mathrm{Cos}\,\bar{\omega}t\ \mathrm{Cos}\,\alpha' + a_Y \mathrm{Sin}\,\alpha'\,(\mathrm{Cos}\,\bar{\omega}t\ \mathrm{Cos}\,\epsilon - \mathrm{Sin}\,\bar{\omega}t\ \mathrm{Sin}\,\epsilon) \qquad (2.10)$$

$$E_{Y'} = -\,a_X \mathrm{Cos}\,\bar{\omega}t\ \mathrm{Sin}\,\alpha' + a_Y \mathrm{Cos}\,\alpha'\,(\mathrm{Cos}\,\bar{\omega}t\ \mathrm{Cos}\,\epsilon - \mathrm{Sin}\,\bar{\omega}t\ \mathrm{Sin}\,\epsilon)$$

The amplitudes along the new axes are given by

$$a^2_{X'} = (a_X \mathrm{Cos}\,\alpha' + a_Y \mathrm{Sin}\,\alpha'\ \mathrm{Cos}\,\epsilon)^2 + (a_Y \mathrm{Sin}\,\alpha'\ \mathrm{Sin}\,\epsilon)^2$$

$$a^2_{Y'} = (-\,a_X \mathrm{Sin}\,\alpha' + a_Y \mathrm{Cos}\,\alpha'\ \mathrm{Cos}\,\epsilon)^2 + (a_Y \mathrm{Cos}\,\alpha'\ \mathrm{Sin}\,\epsilon)^2 \qquad (2.11)$$

$\therefore a_{X'}^2 + a_{Y'}^2 = a_X^2 + a_Y^2$ since the total intensity will not change with the rotation of the reference axes.

From Eqs. (2.5) and using Eq. (2.3),

$$a^2 - b^2 = (a_X^2 - a_Y^2)\, \text{Cos}2\alpha + 2a_X a_Y\, \text{Sin}2\alpha\, \text{Cos}\epsilon$$

$$= (a_X^2 - a_Y^2)\, \text{Cos}2\alpha + (a_X^2 - a_Y^2)\, \tan 2\alpha\, \text{Sin}2\alpha$$

$$= \frac{a_X^2 - a_Y^2}{\text{Cos}2\alpha}$$

But, from Eqs. (2.4) and (2.7)

$$\frac{a^2 - b^2}{a_X^2 - a_Y^2} = \frac{\text{Cos}2\omega}{\text{Cos}2\theta}$$

$$\therefore \text{Cos}2\omega\, \text{Cos}2\alpha = \text{Cos}2\theta \qquad (2.12)$$

Multiplying this by Eq. (2.3), we obtain:

$$\text{Cos}2\omega\, \text{Sin}2\alpha = \text{Sin}2\theta\, \text{Cos}\epsilon \qquad (2.13)$$

Squaring and adding the above two Eqs.,

$$\text{Cos}^2 2\omega = \text{Cos}^2 2\theta + \text{Sin}^2 2\theta\, \text{Cos}^2\epsilon$$

$$\text{or} \quad \text{Sin}^2 2\omega = \text{Sin}^2 2\theta\, \text{Sin}^2\epsilon$$

Taking the positive square root on both sides,

$$\text{Sin}2\omega = \text{Sin}2\theta\, \text{Sin}\epsilon \qquad (2.14)$$

The four quantities $(a_X^2 + a_Y^2)$, $(a_X^2 - a_Y^2)$, $2a_X a_Y \text{ Cos } \epsilon$ and $2a_X\, a_Y \text{ Sin}\epsilon$ are referred to as Stokes parameters[32, 33, 34, 23] which were introduced by the British physicist G.G. Stokes in 1852. The first quantity $(a_X^2 + a_Y^2)$ corresponds to the total intensity of light vibration. The variations of this total intensity due to absorption in the medium are not of any consequence in most of the photoelastic investigations. For convenience, we set this quantity equal to unity. We shall represent the Stokes vector by $V = (S_0, S_1, S_2, S_3)$.

Throughout this discussion only the last three parameters will be used ignoring the first one as it will not affect the present analysis. The Stokes vector will either be written in the form of a column vector $\begin{bmatrix} S_1 \\ S_2 \\ S_3 \end{bmatrix}$ or in the form of a row vector (S_1, S_2, S_3) depending on the convenience.

Now, we have the following equivalent forms for the Stokes vector (with $a_X^2 + a_Y^2 \equiv 1$),

$$\begin{bmatrix} S_1 \\ S_2 \\ S_3 \end{bmatrix} \equiv \begin{bmatrix} a_X^2 - a_Y^2 \\ 2a_X\ a_Y \operatorname{Cos}\epsilon \\ 2a_X\ a_Y \operatorname{Sin}\epsilon \end{bmatrix} \equiv \begin{bmatrix} \operatorname{Cos}2\theta \\ \operatorname{Sin}2\theta \operatorname{Cos}\epsilon \\ \operatorname{Sin}2\theta \operatorname{Sin}\epsilon \end{bmatrix} \equiv \begin{bmatrix} \operatorname{Cos}2\omega \operatorname{Cos}2\alpha \\ \operatorname{Cos}2\omega \operatorname{Sin}2\alpha \\ \operatorname{Sin}2\omega \end{bmatrix} \quad (2.15)$$

It may now be noted that these parameters are with reference to a set of perpendicular axes which make an angle of α with the major and minor axes of the light ellipse. If these reference axes are rotated, the quantities ϵ, α, θ, a_X and a_Y change and so the Stokes parameters will also change correspondingly.

Also $$S_1^2 + S_2^2 + S_3^2 = 1 \quad (2.16)$$

Since $S_1 = a_X^2 - a_Y^2$, the first Stokes parameter S_1

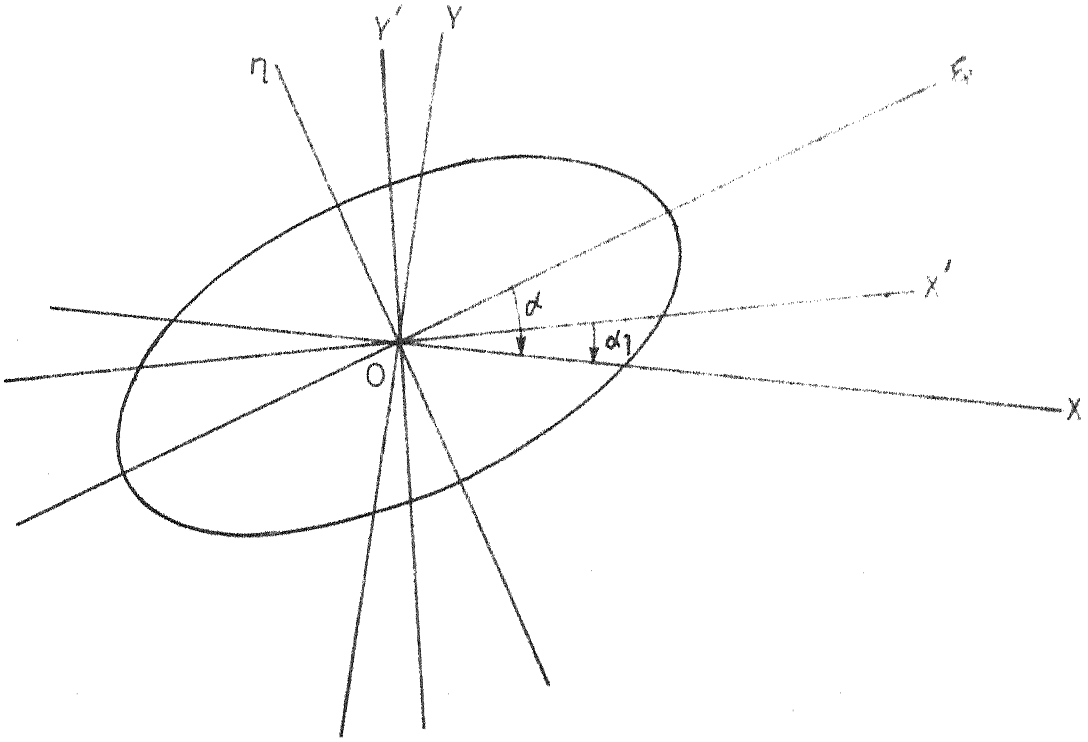

FIG. 3. ROTATION OF AXES.

depends only on the amplitudes of components along the reference axes. Also, $S_3 = \mathrm{Sin}2\omega$ and the third Stokes parameter S_3 depends only on the ellipticity of the light ellipse.

Transformations of Stokes Vector

When a certain amount of retardation ϵ_1 is added along one of the reference axes, say, OY-axis, Fig.3, the phase difference ϵ , becomes $(\epsilon + \epsilon_1)$, and the amplitudes a_X and a_Y remain unaltered (i.e. θ remains unaltered). i.e. the parameter $S_2 = \mathrm{Sin}2\,\theta\mathrm{Cos}\,\epsilon$ becomes $\bar{S}_2 = \mathrm{Sin}2\,\theta\mathrm{Cos}(\epsilon + \epsilon_1)$ and $S_3 = \mathrm{Sin}2\,\theta\mathrm{Sin}\,\epsilon$ becomes $\bar{S}_3 = \mathrm{Sin}2\,\theta\mathrm{Sin}(\epsilon + \epsilon_1)$

i.e. the vector $\begin{bmatrix} S_1 \\ S_2 \\ S_3 \end{bmatrix}$ becomes $\begin{bmatrix} \bar{S}_1 \\ \bar{S}_2 \\ \bar{S}_3 \end{bmatrix} = \begin{bmatrix} S_1 \\ S_2\ \mathrm{Cos}\,\epsilon_1 - S_3\ \mathrm{Sin}\,\epsilon_1 \\ S_3\ \mathrm{Cos}\,\epsilon_1 + S_2\ \mathrm{Sin}\,\epsilon_1 \end{bmatrix}$

(2.17)

If the reference axes are rotated in the anti--clockwise direction through an angle α_1, Fig.3, the azimuth α becomes $(\alpha - \alpha_1)$ and the ellipticity remains unaltered, so that $S_1 = \mathrm{Cos}2\,\omega\,\mathrm{Cos}2\,\alpha$ becomes $\bar{S}_1 = \mathrm{Cos}2\omega\ \mathrm{Cos}2(\alpha - \alpha_1)$ and $S_2 = \mathrm{Cos}2\omega\ \mathrm{Sin}2\alpha$ becomes $\bar{S}_2 = \mathrm{Cos}2\,\omega\,\mathrm{Sin}2(\alpha - \alpha_1)$.

i.e. the vector

$$\begin{bmatrix} S_1 \\ S_2 \\ S_3 \end{bmatrix} \text{ becomes } \begin{bmatrix} S_1\ \mathrm{Cos}2\alpha_1 + S_2\ \mathrm{Sin}2\alpha_1 \\ S_2\ \mathrm{Cos}2\alpha_1 - S_1\ \mathrm{Sin}2\alpha_1 \\ S_3 \end{bmatrix} = \begin{bmatrix} \bar{S}_1 \\ \bar{S}_2 \\ \bar{S}_3 \end{bmatrix} \qquad (2.18)$$

Now, consider the addition of a retardation of ϵ_1 along the set of axes OX', OY', Fig.3, which make an angle of α_1 with the original reference axes. For this process, the transformation is obtained by first decreasing the azimuth α by an amount α_1 without altering the ellipticity, and then increasing the phase difference ϵ_1 by an amount ϵ_1 without altering the amplitudes. This is equivalent to the successive application of the above two transformations. In this case, the vector (S_1, S_2, S_3) becomes,

$$\begin{bmatrix} S_1 \cos 2\alpha_1 + S_2 \sin 2\alpha_1 \\ (S_2 \cos 2\alpha_1 - S_1 \sin 2\alpha_1)\cos\epsilon_1 - S_3 \sin\epsilon_1 \\ S_3 \cos\epsilon_1 + \sin\epsilon_1 (S_2 \cos 2\alpha_1 - S_1 \sin 2\alpha_1) \end{bmatrix} = \begin{bmatrix} \bar{S}_1 \\ \bar{S}_2 \\ \bar{S}_3 \end{bmatrix} \qquad (2.19)$$

Here, the vector $(\bar{S}_1, \bar{S}_2, \bar{S}_3)$ is with respect to the new set of axes OX', OY'. If this vector is again referred to OX, OY axes, we will have

$$\begin{bmatrix} \bar{S}_1 \\ \\ \bar{S}_2 \\ \\ \bar{S}_3 \end{bmatrix} = \left[\begin{array}{l} (S_1 \cos 2\alpha_1 + S_2 \sin 2\alpha_1)\cos 2\alpha_1 - \sin 2\alpha_1 [(S_2 \cos 2\alpha_1 \\ \quad - S_1 \sin 2\alpha_1)\cos\epsilon_1 - S_3 \sin\epsilon_1] \\ [(S_2 \cos 2\alpha_1 - S_1 \sin 2\alpha_1)\cos\epsilon_1 - S_3 \sin\epsilon_1]\cos 2\alpha_1 \\ \quad + \sin 2\alpha_1 (S_1 \cos 2\alpha_1 + S_2 \sin 2\alpha_1) \\ S_3 \cos\epsilon_1 + \sin\epsilon_1 (S_2 \cos 2\alpha_1 - S_1 \sin 2\alpha_1) \end{array}\right] \qquad (2.20)$$

Intensity Calibration Method To Determine Ellipticity

Consider a system consisting of a $\lambda/4$ plate and an analyser, the angle between their axes being 45°. Let the Stokes vector for the light ellipse before this system with respect to the axes of the $\lambda/4$ plate be $A_1 = (S_1, S_2, S_3)$.

Let B_1 be the Stokes vector for the light ellipse after the $\lambda/4$ plate referred to the $(\lambda/4)$ plate axes and C_1, the Stokes vector of the light ellipse after the $(\lambda/4)$ plate referred to the axes of the analyser. Then the transformation through this system is given by

$$\begin{array}{cccc} \underline{A_1} & \underline{B_1} & \underline{C_1} & \\ \begin{bmatrix} S_1 \\ S_2 \\ S_3 \end{bmatrix} & \begin{bmatrix} S_1 \\ -S_3 \\ S_2 \end{bmatrix} & \begin{bmatrix} -S_3 \\ -S_1 \\ S_2 \end{bmatrix} & \equiv \begin{bmatrix} \overline{S}_1 \\ \overline{S}_2 \\ \overline{S}_3 \end{bmatrix} \end{array} \qquad (2.21)$$

Using the transformation laws given by Eqs. (2.17) and (2.18). If

$$\begin{array}{c} \underline{A_1} \\ \begin{bmatrix} S_1 \\ S_2 \\ S_3 \end{bmatrix} \end{array} = \begin{bmatrix} \mathrm{Cos}2\omega\ \mathrm{Cos}2\alpha \\ \mathrm{Cos}2\omega\ \mathrm{Sin}2\alpha \\ \mathrm{Sin}2\omega \end{bmatrix} \quad \text{and} \quad \overline{S}_1 = a_X^2 - a_Y^2$$

then, $\overline{S}_1 = -\mathrm{Sin}2\omega = 2a_X^2 - 1$ since $a_X^2 + a_Y^2 = 1$

$$\text{or} \quad a_X^2 = \frac{1 - \mathrm{Sin}2\omega}{2}$$

Also, the intensity along the OX-axis is given by (OX, OY now refer to the analyser axes)

$$I = K\, a_X^2 = \frac{K}{2}\,(1 - \mathrm{Sin}2\omega) \qquad (2.22)$$

where K is the constant of proportionality.

So, we have the following theorem:

Theorem 1 : Consider a system consisting of a $(\lambda/4)$ plate and an analyser, the angle between their axes being 45°. The intensity of light I from the analyser is dependent only on the ellipticity of the light incident on the

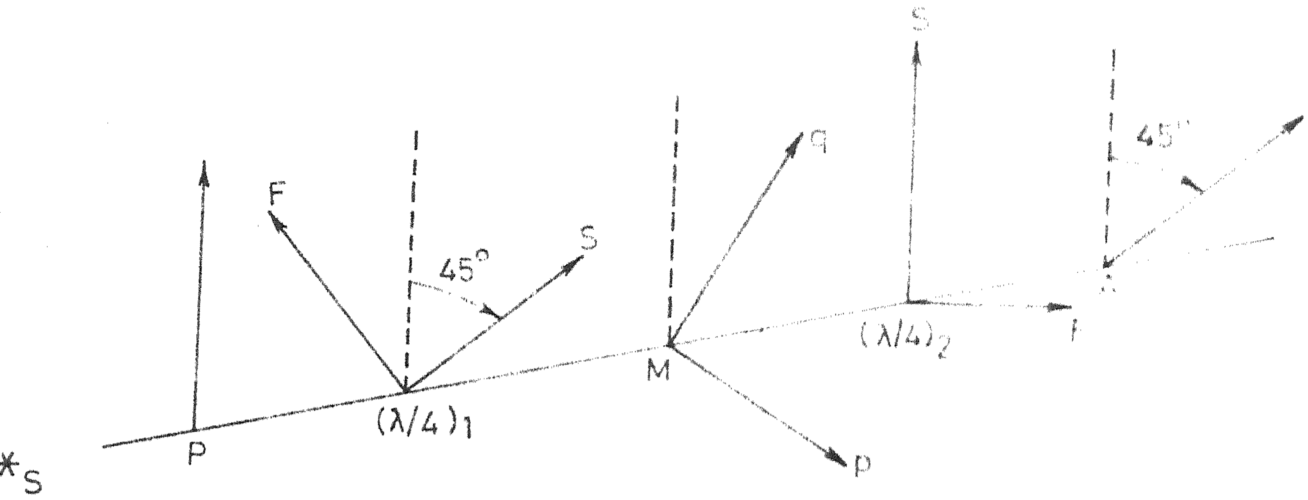

S – Source of light

P – Polarizer

$(\lambda/4)_1, (\lambda/4)_2$ – First and second quarter-wave plates.

M – Model

F – Fast axis

S – Slow axis

p,q – Principal - stress directions

A – Analyser

FIG. 4. OPTICAL SET-UP FOR TWO-DIMENSIONAL STRESS ANALYSIS.

$(\lambda/4)$ plate and is given by Eq. (2.22). This theorem can be used with advantage in two-dimensional stress analysis. Consider the optical set up shown in Fig. 4. The light after the $(\lambda/4)_1$ plate is circularly polarized so that the amplitudes along the p,q-axes are equal. Along p,q-axes the phase difference is $\pi/2$ before the model and $(\pi/2 + \rho)$ after the model, if the amount of retardation added in the model is ρ. From the property of light ellipse, the ellipticity of light after the model is $\tan(\pi/4 + \rho/2)$. Using Theorem 1, the intensity I from the analyser is given by Eq. (2.22), where $\tan\omega$ is the ellipticity.

So,

$$I = \frac{K}{2}(1 - \text{Sin}(\pi/2 + \rho) = \frac{K}{2}(1 - \text{Cos}\,\rho) \qquad (2.23)$$

This equation relates the retardation introduced in the model which is proportional to the principal-stress difference $(p - q)$ to the intensity I from the analyser. To find the constant of proportionality K, Tardy's method can be used. For this, remove the $(\lambda/4)_2$ plate and rotate the analyser for minimum intensity, thus obtaining the directions of the major and minor axes of the light ellipse after the model. Now set the axes of the $(\lambda/4)_2$ plate parallel to these major and minor axes so that the light after the $(\lambda/4)_2$ plate is plane polarized. Rotate the analyser for minimum intensity, thus finding the direction of plane polarization. The angle between this direction and the major axis will be ω where $\tan\omega$ is ellipticity of the light ellipse after the model and $\omega = (\rho + \pi/2)/2$. Now arrange the $(\lambda/4)_2$ plate and analyser as shown in Fig. 4, and note the intensity I. Since the quantities I and ρ are known, the constant K can be evaluated using Eq. (2.23). Once the value of K is known, the principal-stress difference can be computed using Eq. (2.23) from the value of ± for any other point on the model. A calibration graph showing the relation between I and (p - q) can be drawn for convenience.

Optical Equations of Three-Dimensional Photoelasticity

Several systems of equations have been put forth to describe the optical phenomena in the presence of the rotation of secondary principal-stress axes. We shall give a brief account of some of these derivations. The first of these are the Maxwell-Neumann equations:

$$d\,a = -\,a\ \mathrm{Cos}\ d\phi;\ d\,a = -\,a\ \mathrm{Cos}\ d\phi \qquad (2.24)$$

$$\text{and}\quad d = \left(\frac{a_X}{a_Y} - \frac{a_Y}{a_X}\right)\mathrm{Sin}\ d\phi + d\rho \qquad (2.25)$$

where $d\phi$ is the change in the orientation of the secondary principal-stresses and $d\rho$ is the retardation introduced (due to stresses only) in an infinitesimal length dz of the optical path in the model. Coker and Filon[20] derived these equations kinematically. They assumed the components of the light vector in the trigonometrical form. Also, in this derivation, after a distance dz along the optical path in the model, the reference axes were first rotated to coincide with the directions of the new principal-stress axes and then the retardation caused due to stresses alone was added to obtain the components of the new light vector.

Drucker and Mindlin[18] formulated the problem in terms of the elastic ether theory of light. The ether theory is based upon the ideas of stress, strain and displacement and upon the equations of motion. The governing differential equations are exactly the same as those obtained from the electromagnetic theory of light if the symbols representing displacement, density and shear modulus are interpreted as magnetic force, magnetic permiability and reciprocal of dielectric coefficient respectively. They obtained the analytical solution for the case where the secondary principal-stress difference remained constant and their orientation varied linearly along the light path. They concluded the following : (1) Rotation increases the relative phase retardation by a factor $S = \left[1 + (\frac{2\phi}{\Delta})^2\right]^{\frac{1}{2}}$ which at times may be quite large. (ϕ is the orientation of the secondary principal-stresses for the case under consideration. Δ is the relative retardation caused by the magnitude of stress alone). If the ratio $\frac{2\phi}{\Delta}$ is not constant, the ratio of the increment in 2ϕ to the increment in Δ between fringes can be used in regions of high stress. (2) At high stress, the light vector rotates with the principal-stress directions, plane polarized light entering along a direction of principal-stress will remain practically plane polarized in the direction of the stress through the entire model.

Mindlin and Goodman[19] derived a set of dynamical equations of three-dimensional photoelasticity using the Electromagnetic theory, with the purpose of revealing the approximations involved in the kinematical derivation. For this they made an analysis of the orders of magnitudes of the quantities involved in the equations. The orders of magnitude of these quantities are presented below.

(i) $$\frac{b^2}{\omega^2}\frac{\partial^2\phi}{\partial s^2} = 0\left[\lambda^2\frac{\partial^2\phi}{\partial s^2}\right]$$

(ii) $$\left[\frac{b}{\omega}\frac{\partial\phi}{\partial s}\right]^2 = 0\left[\lambda\frac{\partial\phi}{\partial s}\right]^2$$

(iii) $$\left[\frac{b}{\omega}\frac{\partial\phi}{\partial s}\right]\left[bz\frac{\partial b^{-1}}{\partial s}\right] = 0\left[\lambda\, z\frac{\partial\phi}{\partial s}\frac{\partial n}{\partial s}\right]$$

(iv) $$\frac{b}{\omega}\, bz\frac{\partial^2 b^{-1}}{\partial s^2} = 0\left[\lambda\, z\frac{\partial^2 n}{\partial s^2}\right] \qquad (2\text{-}26)$$

(v) $$\frac{1}{\omega^2}\frac{\partial\phi}{\partial s}\frac{\partial c^2}{\partial s} = 0\left[\lambda^2\frac{\partial n}{\partial s}\frac{\partial\phi}{\partial s}\right]$$

(vi) $$\frac{z}{\omega}\frac{\partial c^2}{\partial s}\frac{\partial b^{-1}}{\partial s} = 0\left[\lambda z\left(\frac{\partial n}{\partial s}\right)^2\right]$$

S, n and b are representative lenghts in the X,Y plane (the plane of the wave front), index of refraction and wave velocity respectively. λ is the wavelength of light in vacuum and $0\left[\;\right]$ stands for "order of magnitude of". To estimate the order of magnitude of these ratios, consider a wavelength of $6\text{x}10^{-4}$mm, a stress gradient of

10^8 dynes/cm^2($\cong$ 1500 lb/in.^{2}) per mm. and a stress-optical coefficient of 100 Brewsters. Under these extreme conditions, $\lambda \frac{\partial n}{\partial s} = 0\left[10^{-7}\right]$ and, for a model 5 mm. thick, $z \frac{\partial n}{\partial s} = 0\left[10^{-3}\right]$. With regards to terms involving ϕ, if the rotation of the principal axes were 2π radians in one millimeter, $\lambda \frac{\partial \phi}{\partial s} = 0\left[10^{-3}\right]$. Since the ratios involve squares or products of terms not exceeding $0\left[10^{-3}\right]$ the ratios themselves donot exceed $0\left[10^{-6}\right]$. It is true that in the neighbourhood of an isotropic piont, $\frac{\partial \phi}{\partial s}$ becomes very large. However, $\frac{\partial \phi}{\partial s}$ may be expressed in terms of $\frac{\partial n}{\partial s}$ and the principal-stress difference through the use of the stress equations of equilibrium and the stress-optic law, following which it may be shown, by a limiting process, that the ratios involving $\frac{\partial \phi}{\partial s}$ are, again, small. Also, the order of magnitude of $(n_1 - n_2)/n$ and $\lambda \frac{\partial \phi}{\partial z}$ (n_1, n_2 are the refractive indeces) is $\left[10^{-3}\right]$. It is not impossible for $\frac{d\phi}{dz}$ to become very large. An example is the case of combined tension and torsion of a cylindrical bar. For a wavenormal intersecting the axis of the bar $\frac{d\phi}{dz}$ approaches infinity as the tension approaches zero and the product of the two has a zero limit in the neighbourhood of the axis of the bar. They simplified the governing equations by neglecting these quantities. They obtained the Maxwell-Neumann equations by assuming the solutions in the trigonometric form. By changing the independent variables, they obtained the following simplified form of the optical equations.

$$R\ u' = \frac{\partial v'}{\partial \tau} \tag{2.27}$$

$$R\ v' = -\frac{\partial u'}{\partial \sigma} \tag{2.28}$$

$$\text{where} \qquad R = \frac{d\phi/dz}{(2\pi/\lambda)\ (n_2 - n_1)} \tag{2.29}$$

$$\sigma = \overline{\omega}\,(t - \int K_1^{-1} dz) \tag{2.30}$$

$$\tau = \overline{\omega}(t - \int K_2^{-1} dz) \tag{2.31}$$

$$K_1^2 = \mu^{-1}\ n_1^{-2}, \quad K_2^2 = \mu^{-1}\ n_2^{-2} \tag{2.32}$$

In the electrostatic system of units $\mu = v_o^{-2}$ where v_o is the velocity of light in vacuum. u' and v' are the components of the light vector along the secondary principal-stress directions.

Eqs. (2.27) and (2.28) show that R is the essential parameter controlling optical wave propagation in three-dimensional photoelasticity. Thus, we see that the kinematical equations for all practical purposes are accurate enough as can be observed from the assumptions involved in the dynamical derivations.

Aben[22] derived yet another system of differential equations governing the optical phenomena in three-dimensional photoelasticity. He used, the system of equations for the propagation of electromagnetic waves in an anisotropic inhomogeneous medium obtained by Ginsburg[21]. Using the fact that the photoelastic medium is only weakly anisotropic, he obtained the following system of ordinary linear differential equations.

$$\frac{dB_1'}{dz} = -\frac{i}{2} C' (\sigma_1 - \sigma_2) B_1' + \frac{d\phi}{dz} B_2' \qquad (2.33)$$

and

$$\frac{dB_2'}{dz} = -\frac{d\phi}{dz} B_1' + \frac{i}{2} C' (\sigma_1 - \sigma_2) B_2' \qquad (2.34)$$

where $C' = CC_o$ (2.35)

C is the velocity of light in vacuum and C_o is the photo-elastic constant. σ_1 σ_2 are the secondary principal-stresses and B_1', B_2' are the components of light vector along the directions of the secondary principal-stresses.

Equations Using Stokes Parameters:

We shall now obtain a kinematical derivation of the governing optical equations in the presence of the rotation of the secondary principal-stress axes to facilitate a better understanding of the optical phenomena.

An observation of the transformation Eq. (2.19), shows that it is linear (i.e. no products, squares or trigonometric functions of the Stokes parameters are involved). This prompts us to use the Stokes parameters directly as the variables in the kinematic derivation.

Let the Stokes vector referred to the secondary principal-stress axes at points O and O' be (S_1, S_2, S_3) and $(\bar{S}_1, \bar{S}_2, \bar{S}_3)$ respectively. The point O is at a

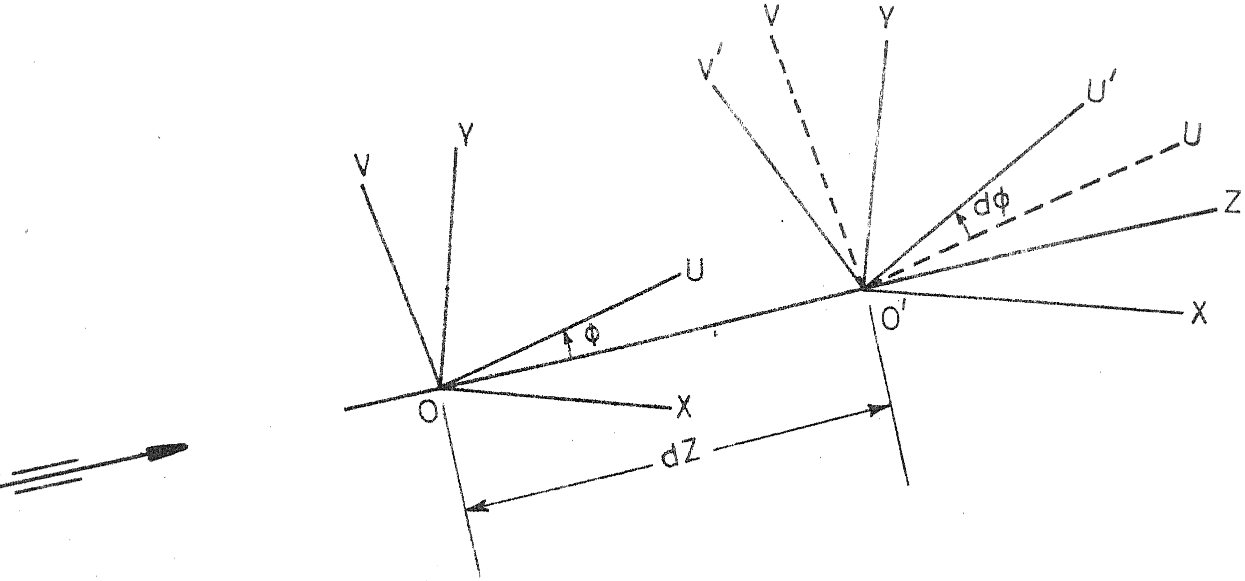

FIG. 5. ROTATION OF SECONDARY PRINCIPAL STRESS AXES ALONG THE OPTICAL PATH.

distance z from the origin which is at the point of entrance to the model, Fig. 5. Let the change in the orientation of the secondary principal-stress axes over the distance dz be $d\phi$ and the retardation introduced due to stresses alone be $d\rho$. Then using the transformation represented by Eqs. (2.19), and noting that for sufficiently small distance dz, the quantities $d\phi$ and $d\rho$ will be very small so that $\sin 2\phi \cong 2d\phi$, $\sin d\rho \cong d\rho$, $\cos 2d\phi \cong 1$, $\cos d\rho \cong 1$, $d\phi\, d\rho \cong 0$, we obtain

$$\begin{bmatrix} \bar{S}_1 \\ \bar{S}_2 \\ \bar{S}_3 \end{bmatrix} = \begin{bmatrix} S_1 + dS_1 \\ S_2 + dS_2 \\ S_3 + dS_3 \end{bmatrix} = \begin{bmatrix} S_1 + 2S_2\, d\phi \\ S_2 - 2S_1\, d\phi - S_3\, d\rho \\ S_3 + S_2\, d\rho \end{bmatrix} \tag{2.36}$$

Dividing each of the above equations by dz and taking the limit as $dz \to 0$, we obtain,

$$S_1' = \frac{dS_1}{dz} = 2S_2 \frac{d\phi}{dz} = 2S_2\phi \tag{2.37}$$

$$S_2' = \frac{dS_2}{dz} = -2S_1 \frac{d\phi}{dz} - S_3 \frac{d\rho}{dz} = -2S_1\phi' - S_3\rho' \tag{2.38}$$

and

$$S_3' = \frac{dS_3}{dz} = S_2 \frac{d\rho}{dz} = S_2\rho' \tag{2.39}$$

If the Stokes vector $(\bar{S}_1, \bar{S}_2, \bar{S}_3)$ is referred to the fixed axes OX, OY, we have from Eqs. (2.20) (replace α_1 by $\phi + d\phi$ and ε_1 by ρ)

$$\begin{bmatrix} \bar{S}_1 \\ \bar{S}_2 \\ \bar{S}_3 \end{bmatrix} = \begin{bmatrix} S_1 + dS_1 \\ S_2 + dS_2 \\ S_3 + dS_3 \end{bmatrix}$$

$$= \begin{bmatrix} (S_1 \cos 2(\phi + d\phi) + S_2 \sin 2(d\phi + \phi)) \cos 2(\phi + d\phi) \\ - \sin 2(\phi + d\phi) \{(S_2 \cos 2(\phi + d\phi) - S_1 \sin 2(\phi + d\phi)) \cos d\rho \\ - S_3 \sin d\rho\} \\ \\ \cos 2(\phi + d\phi) \{(S_2 \cos 2(\phi + d\phi) - S_1 \sin 2(\phi + d\phi) \cos d\rho \\ - S_3 \sin d\rho\} + \sin 2(\phi + d\phi) (S_1 \cos 2(\phi + d\phi) \\ + S_2 \sin 2(\phi + d\phi) \\ \\ S_3 \cos d\rho + \sin d\rho (S_2 \cos 2(\phi + d\phi) - S_1 \sin 2(\phi + d\phi) \end{bmatrix} \qquad (2.40)$$

As above, for sufficiently small distance dz, $d\phi$ and $d\rho$ are very small so that $\sin d\rho \cong d$, $\cos 2d\phi \cong 1$, $\cos d\rho \cong 1$, $d\phi\, d\rho \cong 0$, $\cos 2(\phi + d\phi)\phi \ \cos 2\phi - \cong 2d\phi \sin 2\phi$; $\sin 2(d\phi + \phi) \cong 2d\phi \cos 2\phi + \sin 2\phi$ so that

$$\begin{bmatrix} \bar{S}_1 \\ \bar{S}_2 \\ \bar{S}_3 \end{bmatrix} = \begin{bmatrix} S_1 + dS_1 \\ S_2 + dS_2 \\ S_3 + dS_3 \end{bmatrix} = \begin{bmatrix} S_1 + S_3\, d\rho \ \sin 2\phi \\ S_2 - S_3\, d\rho \ \cos 2\phi \\ S_3 + S_2\, d\rho \cos 2\phi - S_1\, d\rho \ \sin 2\phi \end{bmatrix} \qquad (2.41)$$

Dividing each of the above equations by dz and taking the limit as dz ⟶ 0, we obtain

$$S_1' = \frac{dS_1}{dz} = S_3\, \rho' \sin 2\phi \qquad (2.42)$$

$$S_2' = \frac{dS_2}{dz} = - S_3 \rho' \cos 2\phi \qquad (2.43)$$

and

$$S_3' = \frac{dS_3}{dz} = - S_2\, \rho' \cos 2\phi - S_1\, \rho' \ \sin 2\phi \qquad (2.44)$$

These equations can also be obtained from Maxwell-Neumann equations by converting the dependent variables into Stokes parameters.

Eqs. (2.42) - (2.44) will be particularly suitable for scattered light analysis. This will be discussed in a later chapter. The above sets of equations are linear, ordinary simultaneous first order differential equations which are very convenient for analysis and application. Using the Eqs. (2.37) - (2.39), we shall obtain the analytical solution for the case where the rate of rotation ϕ' can be any arbitrary function, but the ratio $R = \frac{\phi'}{\rho'}$ is a constant. (The case studied by Drucker and Mindlin where both ϕ' and ρ' are separately constants is a particular case of this).

$$\text{Let} \quad K^2 = \frac{4R^2 + 1}{4R^2} \tag{2.45}$$

from Eqs. (2.37) and (2.39)

$$S_3' = \frac{S_1'}{2R}$$

Integrating both sides,

$$S_3 = \frac{S_1}{2R} + A_1$$

where A_1 is an arbitrary constant.

Substituting this expression for S_3 into the equation

$$S_1^2 + S_2^2 + S_3^2 = 1$$

(instead of using Eq. (2.38))

we obtain an expression for S_2 in terms of S_1.

Substituting this expression in Eq. (2.37) and integrating, we obtain

$$S_1 = \frac{A_1}{2RK^2} + \frac{1}{K}\left(1 - \frac{A_1^2}{K^2}\right)^{\frac{1}{2}} \mathrm{Sin}(2K\phi + A_2) \qquad (2.46)$$

where A_2 is an arbitrary constant.

Using Eq. (2.37) again, we obtain

$$S_2 = \frac{S_1'}{2\phi'} = \left(1 - \frac{A_1'}{K^2}\right)^{\frac{1}{2}} \mathrm{Cos}\ (2K\phi + A_2) \qquad (2.47)$$

and

$$S_3 = \frac{S_1}{2R} + A_1 = \frac{A_1}{k^2} + \frac{\left(1 - \frac{A_1}{K^2}\right)^{\frac{1}{2}}}{2RK} \mathrm{Sin}\ (2K\phi + A_2) \qquad (2.48)$$

The arbitrary constants A_1 and A_2 are to be evaluated from the initial conditions.

Jones Vector

It is sometimes more convenient to use Jones vector[32] in photoelastic analysis. This vector has two elements

$$P = a_X\, e^{i(\epsilon_X + \bar{\omega} t)} \qquad (2.49)$$

and

$$Q = a_Y\, e^{i(\epsilon_Y + \bar{\omega} t)} \qquad (2.50)$$

The quantities a_X, a_Y are the amplitudes along two reference axes OX, OY; and ϵ_X, ϵ_Y are the phase angles of the instantaneous components along these axes.

Since $e^{i(\epsilon_X + \bar{\omega} t)} = e^{i\bar{\omega} t}\, e^{i\epsilon_X}$ and the term $e^{i\bar{\omega} t}$ occurs in the expressions for both P and Q this can be ignored in the photoelastic analysis where the variation with time is of no consequence. So, we have

$$P = a_X\, e^{i\varepsilon_X} \tag{2.51}$$

$$Q = a_Y\, e^{i\varepsilon_Y} \tag{2.52}$$

It can be noted that the transformations corresponding to the rotation of the reference axes will be linear in P and Q. So, if we derive the optical equations of three-dimensional photoelasticity in terms of the elements of the Jones vector, we should obtain ordinary linear differential equations in P and Q.

Now, referring to Fig. 5, let (P,Q) be the Jones vector with respect to the axes OU, OV at the point O. If this vector is referred to the axes OU', OV', its elements become

$$P' = P\,\mathrm{Cos}\,\Delta\phi + Q\,\mathrm{Sin}\,\Delta\phi$$

$$Q' = -\,P\,\mathrm{Sin}\,\Delta\phi + Q\,\mathrm{Cos}\,\Delta\phi$$

Now, if a retardation of $\Delta\rho$ is added to the P' component, the elements of the new vector are given by

$$P'' = P' e^{i\Delta\rho} = P\, e^{i\Delta\rho}\,\mathrm{Cos}\Delta\phi + Q\, e^{i\Delta\rho}\,\mathrm{Sin}\,\Delta\phi$$

and $Q'' = Q'$

For sufficiently small distance Δz, $\Delta\rho$ and $\Delta\phi$ are very small so that $\mathrm{Sin}\,\Delta\rho \cong \Delta\rho$, $\mathrm{Sin}\,\Delta\phi \cong \phi$, $\mathrm{Cos}\,\Delta\rho \cong 1$, $\mathrm{Cos}\,\Delta\phi \cong 1$, $\Delta\rho\ \ \Delta\phi \cong 0$, $e^{i\Delta\rho} \cong 1 + i\Delta\rho$. We, then have

$$P'' = P + \Delta P = P(1 + i\Delta\rho\quad) + Q$$

and $Q'' = Q + \Delta Q = -\,P\ \Delta\phi + Q$

Dividing these equations by Δz and taking the limit as $z \rightarrow 0$, we obtain

$$\frac{dP}{dz} = P' = i \frac{d\rho}{dz} P + Q \frac{d\phi}{dz} = i P\rho' + Q \phi' \qquad (2.53)$$

and

$$\frac{dQ}{dz} = Q' = - \frac{d\phi}{dz} P = - P \phi' \qquad (2.54)$$

Instead of adding a retardation of $\Delta\rho$ to one component only, if we add retardations $\frac{\Delta\rho}{2}$ and $-\Delta\rho/2$ to the two components (i.e. $P'' = P' e^{i\Delta\rho/2}$, $Q'' = Q' e^{-i\Delta\rho/2}$), we obtain

$$P' = - \frac{i}{2} \rho' P + \phi' Q \qquad (2.55)$$

and

$$Q' = - \phi' P + \frac{i}{2} \rho' Q \qquad (2.56)$$

These equations are same as those derived by Aben.

In this chapter, we have introduced the concept of light ellipse as an elegant tool in photoelastic analysis. We have given a brief review of some of the previous derivations of the optical equations of three-dimensional photoelasticity to show that, for all practical purposes, the kinematically derived equations are sufficiently accurate. We have also derived two new sets of equations for three-dimensional photoelasticity, which are convenient for analysis and application. Using these equations we obtained the analytical solution for the case where the rate of rotation ϕ' can be any arbitrary function, but the ratio $R = \phi'/\rho'$ is a constant. The contents of this chapter form the basis for subsequent chapters.

CHAPTER 3

CHARACTERISTIC PARAMETERS IN THREE-DIMENSIONAL PHOTOELASTICITY AND THEIR EXPERIMENTAL DETERMINATION

Poincare' Sphere Representation :

In this chapter, we shall discuss the existence of an optically equivalent system, its theoretical and experimental determination and its importance in three-dimensional photoelastic analysis. In crystallography, it is established that a series of retarders is equivalent to a system consisting of a single retarder (an optical element which adds a certain amount of retardation to the components of the incident light along a particular set of axes) and a pure rotator (an optical element which rotates the incident light ellipse through a certain angle known as the rotatory power). This has been proved geometrically by using the Poincare' sphere representation of polarized forms. We shall present this proof below.

An elliptically polarized light can be characterised by two quantities (1) the azimuth and (ii) the ellipticity tan ω. This can be represented by a point P on the surface of a sphere of unit radius called the Poincare'

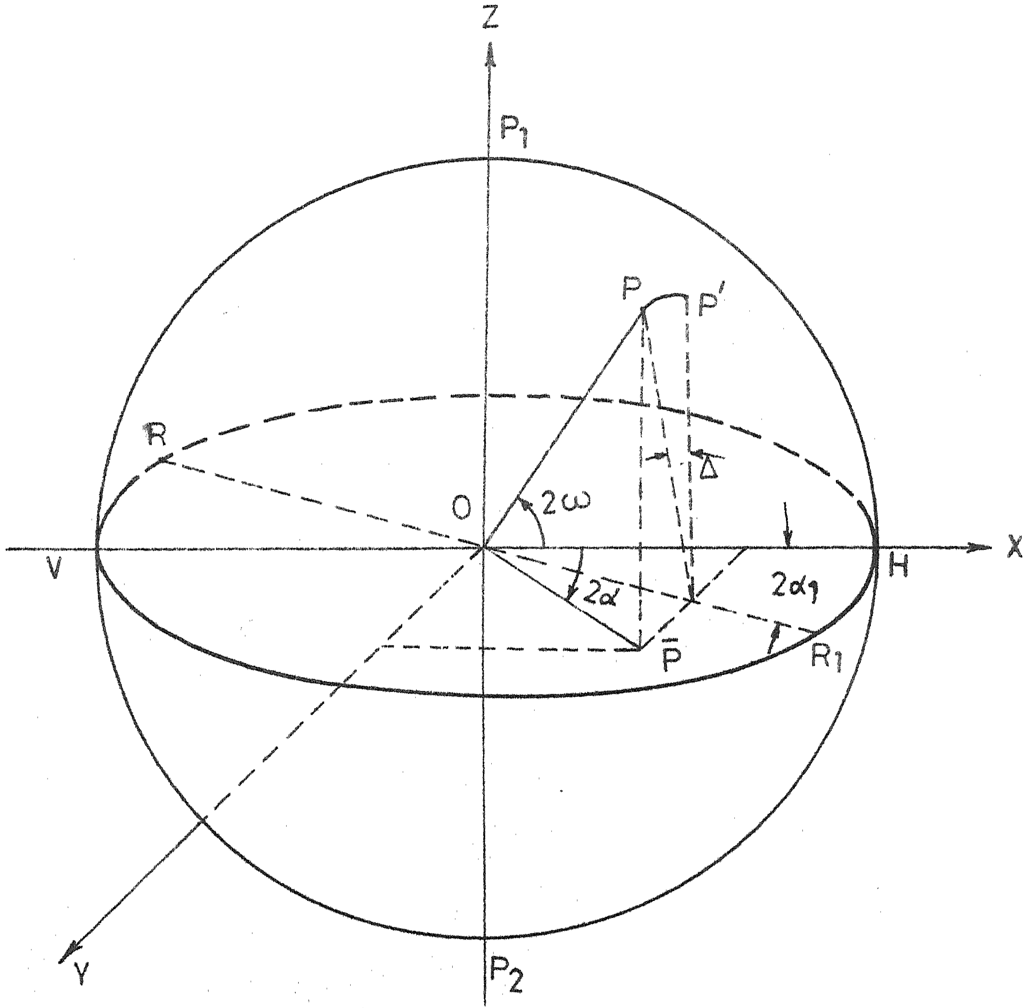

FIG. 6. POINCARE SPHERE REPRESENTATION OF POLARIZED LIGHT FORMS.

sphere with co-ordinates : $x = \text{Cos}2\omega\ \text{Cos}2\alpha$, $y = \text{Cos}2\omega\ \text{Sin}2\alpha$, and $z = \text{Sin}2\omega$(these three correspond to the three Stokes parameters S_1 , S_2 and S_3 of the light ellipse), as shown in Fig. 6. (Let us recall that the first Stokes parameter $S_1 = \text{Cos}2\omega\ \text{Cos}2\alpha$ corresponds to the light intensity along one of the reference axes. If the amplitude of light vibration along X-axis is a_X and the intensity is I, then $I = K\ a_X^2 = \frac{K(1 + S_1)}{2}$). The angle 2α is measured clockwise from H. The angle 2ω is measured upward from the equator. The upper and lower poles P_1 and P_2 represent left and right circularly polarized light ($2\omega = 90^\circ$, $\tan\omega = 1$). Points on the equator indicate polarized light (plane, $2\omega = 0$ $\tan\omega = 0$). The action of a linear retarder can be conveniently represented on Poincare' sphere. Consider an elliptically polarized light represented by the point P, Fig. 8. with ellipticity $\tan\omega$ and azimuth α, to be incident on a linear retarder with retardance Δ and azimuth α_1 . Its axes are represented by line RR_1 in the figure. The x co-ordinate of the point P corresponds to the intensity of this light vibration along one of the reference axes. The projected length of the radius vector OP along the axis ROR_1 corresponds to the light intensity along one of the retarder axes. (This can be proved as follows: X - Y plane is shown in Fig. 7(a). OX', OY' are the new reference axes with $XOX' = 2\bar{\alpha}$. $\bar{P}$ is the projection of P on the X - Y plane. The projection of $\bar{P}$ on OX' is given by,

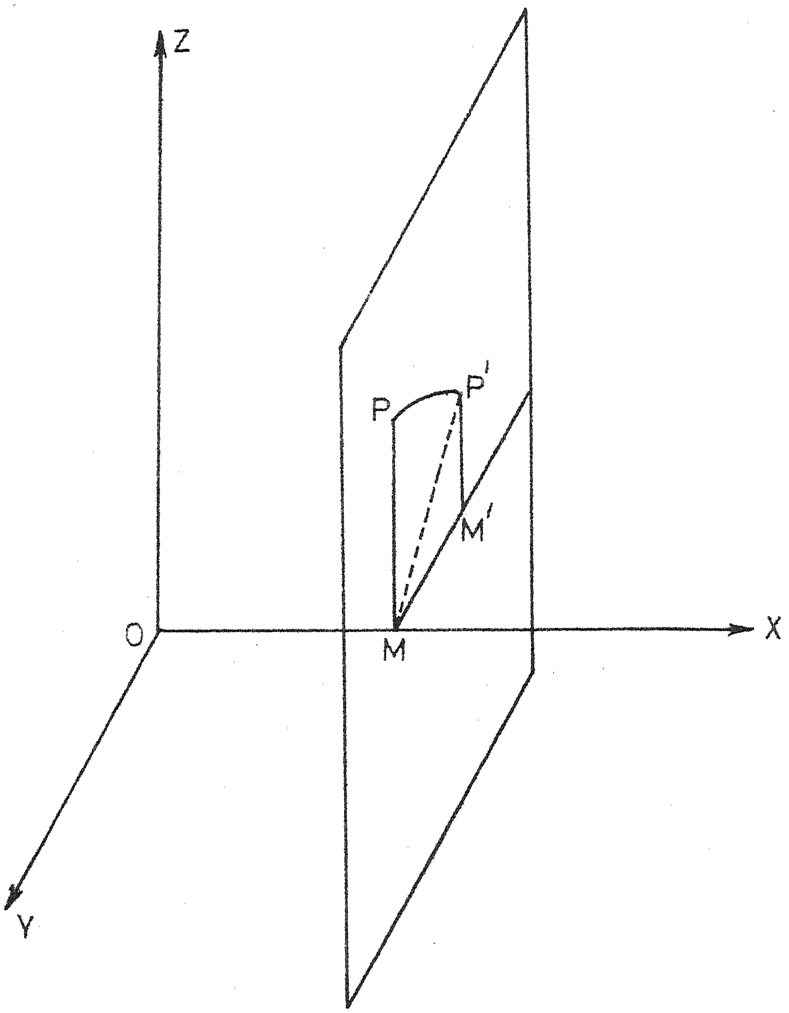

FIG. 7(b). ADDITION OF RETARDATION.

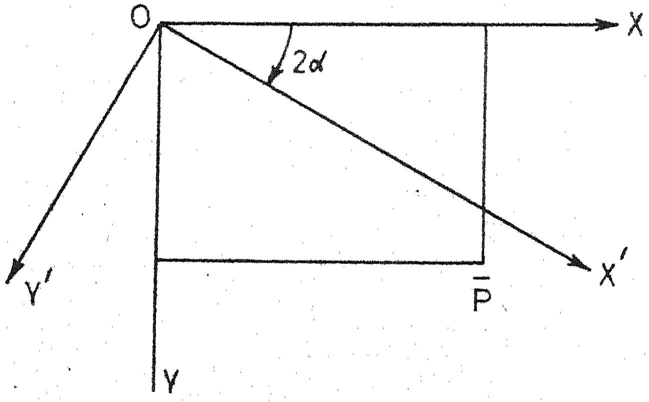

FIG. 7(a). ROTATION OF THE REFERENCE AXES.

$x' = x \, Cos2\bar{\alpha} + y \, Sin2\bar{\alpha} = S_1 \, Cos2\bar{\alpha} + S_2 \, Sin2\bar{\alpha} = \bar{S}_1$ (say). But, $\bar{S}_1$ is also the first Stokes parameter obtained after rotation of the reference axes through an angle $\bar{\alpha}$. i.e. the projection of the point $\bar{P}$ (which again is the projection of P on X - Y plane) on any axis OX' in the X - Y plane corresponds to the light intensity (of light vibration represented by P) along the same axis OX').

Since this intensity remains constant during the addition of retardation, the process of addition of retardation in the retarder is represented by an arc from the point P to P' about the axis ROR_1. This arc PP' on the sphere makes an angle of Δ on the axis ROR_1. Rotation of the reference axes through an angle $d\alpha$ corresponds to rotation about the Z-axis through an angle $2d\alpha$ on the Poincare' sphere. During this rotation, the z-coordinate and so the ellipticity remains unaltered.

The process of addition of retardation along the reference axes can be explained as follows. For this, consider Fig. 7(b). Point P represents a certain elliptically polarized light referred to axes OX, OY in the figure. For point P, x = OM, y = 0, z = MP. Now rotate MP about axis OX through an angle Δ so that its new position is MP'. Now, for point P', the co-ordinates are $x' = OM' = OM$, $y' = - MM' = - MP' \, Sin \Delta = - z \, Sin \Delta$, $z' = MP' Cos \Delta = z \, Cos \Delta$. Now consider the three Stokes parameters S_1, S_2, S_3 of the polarized light represented by the point P. These are $S_1 = OM$

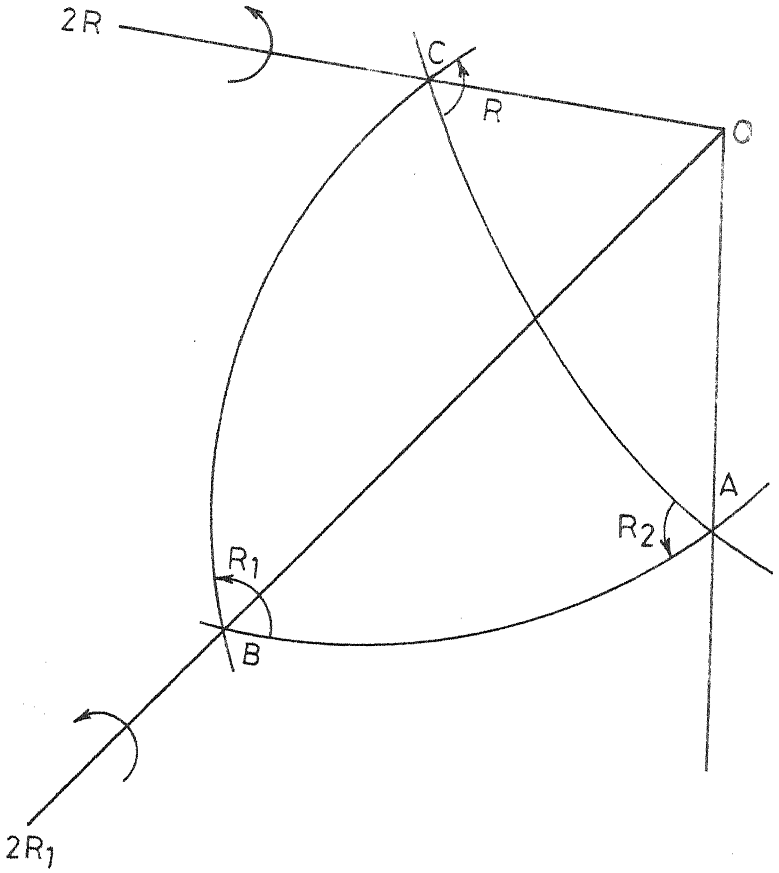

FIG. 8. CONSTRUCTION FOR COMPOSITION OF TWO ROTATIONS.

= x, S_2 = 0, S_3 = MP = z. Consider the polarized light P' obtained by the addition of a retardation of Δ along the reference axes. The Stokes parameters for this are given by S'_1 = x, S'_2 = - z Sin Δ and S'_3 = z Cos Δ. The same values are obtained by rotation about the OX-axis. Thus, the effect of a single retarder of retardation Δ can be represented on the Poincare' sphere by a rotation through an angle Δ (upwards) about the corresponding axis in the equitorial plane.

Combined Effect of a Series of Retarders:

The combined effect of a series of retarders can be represented by successive rotations of the Poincare' sphere about the corresponding axes in the equitorial plane. This in turn can be replaced by a single rotation about some general axis in Poincaré sphere. Alternatively, this resultant single rotation of the sphere can be resolved into two rotations about perpendicular axes - the first may be about the Z-axis and the other will then be about some axis in the equitorial plane which may be determined by the construction[23] of Fig. 8. A rotation about AO through twice the internal angle at A followed by a rotation about BO through twice the internal angle at B is equivalent to a rotation about CO through twice the external angle at C.

Thus the combination of a series of linear retarders is equivalent to a system containing two elements, one a rotator and the other a retardation plate. Since finite rotations about nonparallel axes are noncommutative operations, it is necessary to specify the exact sequence of the various elements. Interchanging any two of them would in general lead to a change in the final state of polarization.

The above result has also been proved by the matrix method by Hurwitz and Jones [35].

Effect of a Series of Retarders Using Stokes Vector :

The above result will now be proved in detail using the Stokes vector ignoring the variation in the total intensity. The transformation that the Stokes vector undergoes when a given elliptically polarized light traverses through a two-dimensional photoelastic model can be obtained from Eq. (2.20) as:

$$\bar{V} = M_1 V$$

where

$$V = \begin{bmatrix} S_1 \\ S_2 \\ S_3 \end{bmatrix} \quad ; \quad \bar{V} = \begin{bmatrix} \bar{S}_1 \\ \bar{S}_2 \\ \bar{S}_3 \end{bmatrix}$$

are the initial and final Stokes vectors and M_1 is given by

$$\begin{bmatrix} (\mathrm{Cos}^2 2\alpha_1 + \mathrm{Sin}^2 2\alpha_1 \,\mathrm{Cos}\,\epsilon_1) & \mathrm{Sin}2\alpha_1 \,\mathrm{Cos}2\alpha_1 \,(1 - \mathrm{Cos}\,\epsilon_1) & \mathrm{Sin}\,\epsilon_1 \,\mathrm{Sin}2\alpha_1 \\ \mathrm{Sin}2\alpha_1 \,\mathrm{Cos}2\alpha_1 (1 - \mathrm{Cos}\,\epsilon_1) & \mathrm{Cos}^2 2\alpha_1 \,\mathrm{Cos}\,\epsilon_1 + \mathrm{Sin}^2 2\alpha_1 & -\,\mathrm{Sin}\,\epsilon_1 \,\mathrm{Cos}2\alpha_1 \\ -\,\mathrm{Sin}2\alpha_1 \,\mathrm{Sin}\,\epsilon_1 & \mathrm{Cos}2\alpha_1 \,\mathrm{Sin}\,\epsilon_1 & \mathrm{Cos}\,\epsilon_1 \end{bmatrix}$$

In the above matrix α_1 and ϵ_1 are the azimuth and retardance of the retarder respectively.

This means, that the effect of **a** two-dimensional model at a particular point can be represented by a 3 x 3 matrix. If the light represented by the vector V is incident on n successive models, the outcoming light vector is given by

$$\bar{V} = (M_n \cdots M_3 M_2 M_1)\, V = MV \tag{3.1}$$

where $M = M_n \cdots M_3 M_2 M_1$

This means that the effect of a series of two-dimensional photoelastic models can also be represented by a 3 x 3 matrix.

Now consider the relation (3.1)

Let

$$M = \begin{bmatrix} m_{11} & m_{12} & m_{13} \\ m_{21} & m_{22} & m_{23} \\ m_{31} & m_{32} & m_{33} \end{bmatrix} \; ; \; M^T = \begin{bmatrix} m_{11} & m_{21} & m_{31} \\ m_{12} & m_{22} & m_{32} \\ m_{13} & m_{23} & m_{33} \end{bmatrix} \tag{3.2}$$

$$\text{Now } V = (M_n \cdots M_3 M_2 M_1)^{-1} (\bar{V})$$

$$= (M_1^{-1} \; M_2^{-1} \cdots) \; (\bar{V})$$

One can show from the M_1 matrix that $M_1^{-1} = M_1^T$.

Similarly $M_2^{-1} = M_2^T$; $M_3^{-1} = M_3^T$ etc. Hence

$$V = (M_1^T \; M_2^T \cdots) \; (\bar{V})$$

$$= (M_n \; M_{n-1} \cdots M_2 M_1)^T \; (\bar{V})$$

$$\text{i.e. } V = M^T \bar{V} \tag{3.3}$$

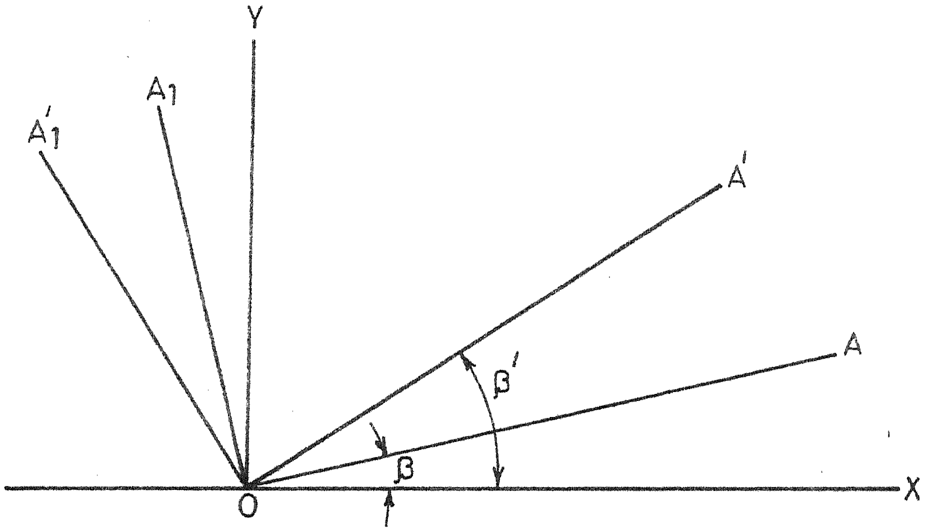

FIG. 9. REPRESENTATION OF THE AXES OF THE BIREFRINGENT PLATES IN THE TWO EQUIVALENT SYSTEMS.

$$\bar{S}_1 = \bar{S}_3 = 0, \ \bar{S}_2 = 1; \ m_{21}^2 + m_{22}^2 + m_{23}^2 = 1 \qquad (3.16)$$

$$\bar{S}_1 = \bar{S}_2 = 0, \ \bar{S}_3 = 1; \ m_{31}^2 + m_{32}^2 + m_{33}^2 = 1 \qquad (3.17)$$

Thus, we have six relations connecting the nine quantities m_{ij}, $i,j = 1,2,3$ so that the matrix M has only three independent quantities. So, a series of two-dimensional photoelastic models (for a particular light path) or birefringent plates, in general is equivalent to an optically equivalent system with three independent parameters. A single birefringent plate has two parameters namely, its azimuth α and its retardation ρ. A pure rotator which rotates the incident light ellipse has one parameter ψ_1 namely its rotatory power. The most simple optical systems consisting of only birefringent plates and pure rotators and having three parameters are (i) a system with a birefringent plate and a pure rotator in that order and (ii) a system with a pure rotator and a birefringent plate in that order.

If the systems (i) and (ii) are to be equivalent, the pure rotatory power in both systems must be same, the angle between the axes of the birefringent plates in the systems (i) and (ii), Fig. 9. must be equal to this rotatory power and the retardations of the plates in both systems must be equal. This can be proved as follows. For the first system, let the rotatory power be ψ_1, the azimuth of the birefringent plate be β and its birefringence be δ. For the second system, let these quantities be ψ_1', β' amd δ'

I. I. T. KANPUR
CENTRAL LIBRARY
Acc. No. A 23674

respectively. Now consider polarized light to be incident along one of the axes of the birefringent plate in the first system, so that after this plate, it still remains plane polarized along the same direction. The pure rotator rotates it through an angle of ψ_1 so that at the exit of the first system we have plane polarized light at an azimuth of $(\beta + \psi_1)$. In the second system also, let the incident light be polarized at an azimuth of β. The pure rotator makes its azimuth $(\beta + \psi_1')$. This light should be polarized along one of the axes of the birefringent plate in the second system so that we have plane polarized light at the exit of the second system also with the same azimuth as in the first system. Therefore, $\beta + \psi_1' = \beta + \psi_1$ or $\psi_1 = \psi_1'$. That is, the rotatory powers in both the systems are same and the difference between the azimuths of the birefringent plates in the two systems is equal to the rotatory power of either system. Now consider circularly polarized light at the entrance of both the systems. For the ellipticities of the light ellipses at the exit of these systems to be equal, the birefringence of the plates in both the systems must be equal. That is, $\delta = \delta'$

Optically Equivalent System for a Cintinuous Body:

Now, we shall discuss the existence of an optically equivalent system for continuous systems. Aben[22] proved the existence of an optically equivalent system (consisting of a retarder and a rotator) for an optical path in a three-

-dimensional photoelastic model along which the secondary principal-stresses and their directions vary continuously. Since the governing differential Eqs. (2.34),(2.35) are linear, ordinary simultaneous differential equations, the light propagation is governed again by equations of the form (3.4)-(3.6). The rest of the proof is similar to the one presented by Hurwitz and Jones [35]. Aben called the two axes of the retarder as primary characteristic directions and its retardation as the characteristic retardation. He also called the mutually perpendicular directions which made an angle equal to the pure rotatory power with these axes as the secondary characteristic directions. These three quantities namely, the primary characteristic directions, the secondary characteristic directions and the characteristic retardation, are referred to as the characteristic parameters. His proof for the existence of these parameters is based on the theory of unitary matrices. It may now be noted that, plane polarized light entering a photoelastic model along one of the primary characteristic directions at the entrance comes out as plane polarized light at the exit along one of the secondary characteristic directions. The corresponding primary and secondary characteristic directions are termed the conjugate characteristic directions. The existence of these characteristic parameters in the case of continuous systems will now be proved in detail using the optical equations in terms of Stokes parameters. Consider Eqs. (2.37) and (2.38), we have:

$$\left[\frac{S_1'}{2\phi'}\right]' = S_2' = -2S_1\phi' - S_3\rho'$$

The primes denote differentiation with respect to the distance co-ordinate z.

$$\left[\frac{\left[\frac{S_1'}{2\phi'}\right]' + 2S_1\phi'}{\rho'}\right]' = -S_3' = -S_2\rho' = -\frac{S_1'\rho'}{2\phi'}$$

using Eqs. (2.39) and (2.37).

On rearranging various terms and simplifying, we obtain

$$S_1'' - S_1''\left[\frac{2\phi''}{\phi'} + \frac{\rho''}{\rho'}\right] + S_1'\left[\frac{2\phi''^2}{\phi'^2} - \frac{\phi'''}{\phi'} + 4\phi'^2 - \rho'^2 + \frac{\rho''\phi''}{\phi'}\right]$$
$$+ 4S_1\left[\phi''\phi' - \frac{\phi'^2\rho''}{\rho'}\right] = 0 \qquad (3.18)$$

This is a third order ordinary linear differential equation in S_1 with variable coefficients. The initial conditions are:

For a given initial set of (S_1, S_2, S_3) i.e. for a known type of incident light, the following quantities can be determined at $z = 0$ since the values ϕ and ρ are also assumed to be known:

$$S_1' = 2S_2\phi' \text{ and } S_1'' = 2S_2\phi'' + 2\phi' S_2' = 2S_2\phi'' - 2\phi'(2S_1\phi' - S_3\rho') \qquad (3.19)$$

are also known.

The solution for this initial value problem exists and is unique over the closed interval in which the coefficients in Eq. (3.18) are continuous. The solution will be of the form

$$\overline{S}_1 = A_1 f_1(z) + A_2 f_2(z) + A_3 f_3(z) \qquad (3.20)$$

where A_1, A_2 and A_3 are arbitrary constants which are to be determined from the initial conditions given by Eqs.(3.19).

i.e. $\bar{S}_1\Big|_{z=0} = A_1 f_1(z)\Big|_{z=0} + A_2 f_2(z)\Big|_{z=0} + A_3 f_3(z)\Big|_{z=0} = S_1$

$$\bar{S}_1'\Big|_{z=0} = A_1 f_1'(z)\Big|_{z=0} + A_2 f_2'(z)\Big|_{z=0} + A_3 f_3'(z)\Big|_{z=0} = 2S_2\phi'\Big|_{z=0}$$

$$\bar{S}_1''\Big|_{z=0} = A_1 f_1''(z)\Big|_{z=0} + A_2 f_2''(z)\Big|_{z=0} + A_3 f_3''(z)\Big|_{z=0}$$

$$= 2S_2\phi''\Big|_{z=0} + \Big[2\phi'(-2S_1\phi - S_3\rho')\Big]_{z=0}$$

From these relations, the constants A_1 , A_2 and A_3 can be obtained as linear functions of the initial Stokes parameters. Aslo at exit, we have

$$\bar{S}_2 = \frac{\bar{S}_1'}{2\phi'}$$

and $\bar{S}_3 = -\dfrac{(2\bar{S}_1\phi' + \bar{S}_2)}{\rho'}$ from Eqs. (2.81) and (2.82)

where ϕ', ρ', are the values at exit.

Hence, $\bar{S}_1$, $\bar{S}_2$ and $\bar{S}_3$ are linear functions of the initial Stokes parameters so that we can write

$$\begin{bmatrix}\bar{S}_1\\ \bar{S}_2\\ \bar{S}_3\end{bmatrix} = M \begin{bmatrix}S_1\\ S_2\\ S_3\end{bmatrix} \qquad (3.21)$$

where M is a 3x3 matrix.

The elements of the matrix M are not functions of the initial Stokes parameters S_1, S_2 and S_3. They are however functions of ϕ' and ρ' and also of the wavelength of the light that is used. Since Eq. (3.21) is of the same form as Eqs. (3.4) - (3.6), all the conclusions regarding the existence of an optically equivalent system and the characteristic parameters follow as derived in the previous section. We also note that these parameters are dependent on the wavelength of light that is used since the elements of the matrix M depend upon the wavelength of light.

Some Special Cases:

For some particular cases of stress distribution in the photoelastic model, there exist some relations between the characteristic parameters. In such cases, the experimental determination of these parameters is direct and simple.

Case (a), Pure Rotator:

We shall now show that a system of two half-wave plates with the angle between their axes being constitutes a pure rotator. If V is the Stokes vector at the entrance of this system referred to the axes of the first half-wave plate, the transformations through this system are given by

$$V = \begin{bmatrix} \text{Cos}2\omega\ \text{Cos}2\alpha \\ \text{Cos}2\omega\ \text{Sin}2\alpha \\ \text{Sin}2\omega \end{bmatrix} \text{ becomes } \overset{V_1}{\begin{bmatrix} \text{Cos}2\omega\ \text{Cos}2\alpha \\ -\text{Cos}2\omega\ \text{Sin}2\alpha \\ -\text{Sin}2\omega \end{bmatrix}} = \begin{bmatrix} \text{Cos}2\omega\ \text{Cos}(-2\alpha) \\ \text{Cos}2\omega\ \text{Sin}(-2\alpha) \\ -\text{Sin}2\omega \end{bmatrix}$$

$$\longrightarrow \overset{V_2}{\begin{bmatrix} \mathrm{Cos}2\omega\,\mathrm{Cos}2\,(-\alpha_1\ -\alpha) \\ \mathrm{Cos}2\omega\,\mathrm{Sin}2\,(-\alpha_1\ -\alpha) \\ -\ \mathrm{Sin}2\omega \end{bmatrix}} \longrightarrow \overset{V_3}{\begin{bmatrix} \mathrm{Cos}2\omega\,\mathrm{Cos}2\,(\alpha + \alpha_1) \\ \mathrm{Cos}2\omega\,\mathrm{Sin}2\,(\alpha + \alpha_1) \\ \mathrm{Sin}2\omega \end{bmatrix}}$$

$$\longrightarrow \overset{V_4}{\begin{bmatrix} \mathrm{Cos}2\omega\ \mathrm{Cos}2\,(\alpha + 2\alpha_1) \\ \mathrm{Cos}2\omega\ \mathrm{Sin}2\,(\alpha + 2\alpha_1) \\ \mathrm{Sin}2\omega \end{bmatrix}}$$

Where V_1 is the Stokes vector after the first half-wave plate with respect to its axes, tan ω is the ellipticity and α is the azimuth with respect to the axes of the first plate, of the incident light ellipse, V_2 is the Stokes vector of light after the first half-wave plate with respect to the axes of the second half-wave plate, V_3 is the Stokes vector of light after the second half-wave plate referred to its axes and V_4 is the Stokes vector after the second half-wave plate referred to the axes of the first half-wave plate.

This shows that the effect of the combination of two half-wave plates is to rotate the light ellipse through twice the angle between the corresponding axes of the half-wave plates and in the same direction as the angle through which the first half-wave plate is to be rotated so that its axes become parallel to the axes of the second half-wave plate.

Case (b), Reversal of Light Path:

For studying the optical phenomena when the light path is reversed, the Jones vector[32] is more convenient since it contains only two elements.

The Jones vector V is given by $V = \begin{bmatrix} x \\ y \end{bmatrix} = \begin{bmatrix} E_x\, e^{i\phi_x} \\ E_y \end{bmatrix}$

The phase angle for the Y component is taken to be zero since we are only concerned with the relative phase difference and not the absolute phase angle in our present investigation. The transformation of the Jones vector through a retarder with retardation ϵ_1 and azimuth α_1 is given by

$$\overline{V} = \begin{bmatrix} \cos\alpha & -\sin\alpha \\ \sin\alpha & \cos\alpha \end{bmatrix} \begin{bmatrix} e^{i\epsilon_1} & 0 \\ 0 & 1 \end{bmatrix} \begin{bmatrix} \cos\alpha & \sin\alpha \\ -\sin\alpha & \cos\alpha \end{bmatrix} \begin{bmatrix} V \end{bmatrix}$$

$$= \begin{bmatrix} e^{i\epsilon_1}\cos^2\alpha_1 + \sin^2\alpha_1 & \frac{\sin 2\alpha_1}{2}\,(e^{i\epsilon_1} - 1) \\ \frac{\sin 2\alpha_1}{2}\,(e^{i\epsilon_1} - 1) & \frac{\sin 2\alpha_1}{2}\,(e^{i\epsilon_1} + 1) \end{bmatrix} \begin{bmatrix} V \end{bmatrix} = M_1 V$$

(Both the Jones vectors V and $\overline{V}$ are referred to the same reference axes).

So, M_1 is a symmetric matrix. (i.e. $M_1 = M_1^T$)

It is of the form:

$$M_1 = \begin{bmatrix} a_1 & b_1 \\ b_1 & c_1 \end{bmatrix}$$

Let the matrix M_2 corresponding to another retarder be given by

$$M_2 = \begin{bmatrix} a_2 & b_2 \\ b_2 & c_2 \end{bmatrix}$$

So, $M_2 M_1 = M_2^T M_1^T = (M_1 M_2)^T$

Let M_3 be the matrix representing a third retarder.

$M_3^T = M_3$

Now, $M_1 M_2 M_3 = M_1^T M_2^T M_3^T = (M_3 M_2 M_1)^T$

For n retarders, we have

$$M_1 M_2 M_3 \ldots M_n = M_1^T M_2^T M_3^T \ldots M_n^T = (M_n \ldots M_3 M_2 M_1)^T$$

Thus, the reversal of the light path is equivalent to transposing the matrix of the series of retarders.

It is proved earlier, that a system of linear retarders is equivalent to a system containing a single retarder (of retardation ϵ and azimuth α) and a pure rotator (of rotatory power ψ_1). The transformation matrix for such a system is given by

$$\overline{M}_1 = \begin{bmatrix} \text{Cos}\alpha_1 & -\text{Sin}\alpha_1 \\ \text{Sin}\alpha_1 & \text{Cos}\alpha_1 \end{bmatrix} \begin{bmatrix} e^{i\epsilon} & 0 \\ 0 & 1 \end{bmatrix} \begin{bmatrix} \text{Cos}\alpha & \text{Sin}\alpha \\ -\text{Sin}\alpha & \text{Cos}\alpha \end{bmatrix}$$

where $\alpha_1 = \alpha + \psi_1$

$$= \begin{bmatrix} e^{i\epsilon}\ \text{Cos}\alpha\ \text{Cos}\alpha_1 + \text{Sin}\alpha\ \text{Sin}\alpha_1 & e^{i\epsilon}\ \text{Sin}\alpha\ \text{Cos}\alpha_1 - \text{Sin}\alpha_1\ \text{Cos}\alpha \\ e^{i\epsilon}\ \text{Cos}\alpha\ \text{Sin}\alpha_1 - \text{Sin}\alpha\ \text{Cos}\alpha_1 & e^{i\epsilon}\ \text{Sin}\alpha\ \text{Sin}\alpha_1 + \text{Cos}\alpha\ \text{Cos}\alpha_1 \end{bmatrix}$$

The rotatory power ψ_1 for this system is given by

$\psi_1 = \alpha_1 - \alpha$

For a system consisting of a pure rotator (rotatory power ψ_1) and a linear retarder (azimuth α_1, retardation ϵ) in that order, the transformation matrix is again $\overline{M}_1$. That is, the transformation matrix can represent either one of the above two systems. Now, the series of retarders M_1, M_2, M_3, ...M_n is equivalent to an optically equivalent system with a retarder and a rotator. Let this be represented by the matrix $\overline{M}_1$. If the light path is reversed, the transformation matrix of the equivalent system will be the transpose of the matrix $\overline{M}_1$ i.e. M_1^T. Now, $\overline{M}_1^T$ represents a system with a pure rotator of rotatory power $-\psi_1 = \alpha - \alpha_1$ and a retarder of retardation ϵ_1 and azimuth α.

Case (c), Reflection Polariscope:

In a reflection polariscope, the characteristic retardation ρ is added along the primary characteristic directions and the light ellipse is rotated through an angle ψ for the forward ray of light. When this is reflected, it is rotated in the opposite direction through the same angle ψ and a retardation of ρ is again added along the same directions. Thus the combined optical path (forward and backward) is equivalent to a single retarder. (In this case, if the forward optical path is equivalent to a system represented by matrix M, the backward optical path will be equivalent to a system represented by the matrix M^T.)

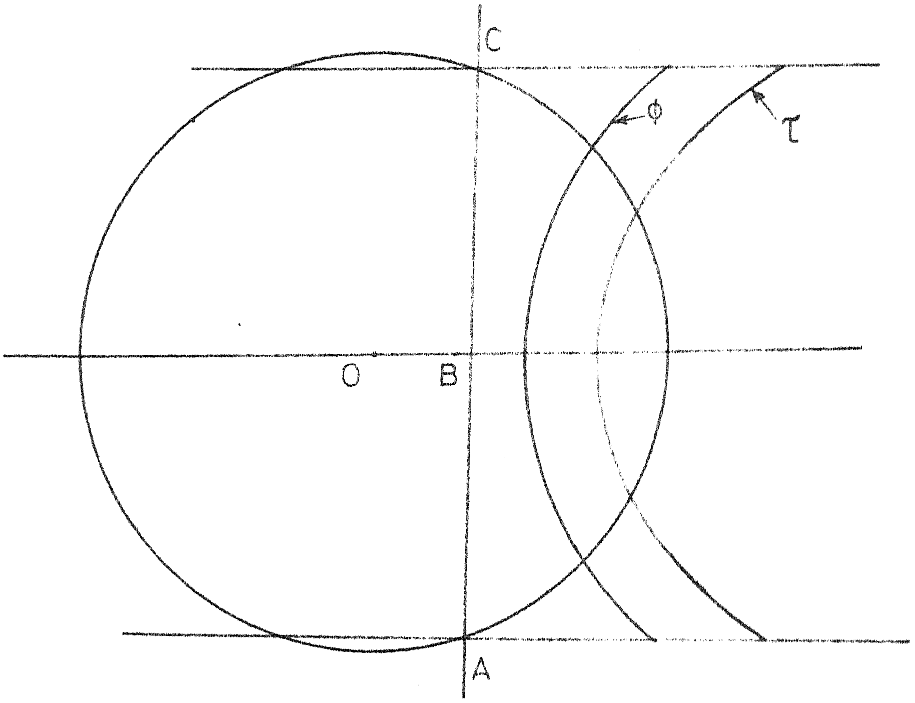

FIG. 10. DISTRIBUTION OF SHEAR STRESS τ AND ISOCLINIC PARAMETER φ ALONG THE CHORD ABC IN AN AXI-SYMMETRIC CASE.

Case (d), Axi-symmetric Case:

In this case, the magnitude and directions of the secondary principal-stresses are symmetrical about the middle point of the optical path in a transverse plane. (example: the optical path along a chord in a plane perpendicular to the loading axis of a sphere under diametral compression.) If the total optical path is divided into two equal parts, and if the first part is equivalent to a retarder (azimuth α, retardation ρ) and a pure rotator (rotatory power ψ), then the second half is equivalent to a pure rotator (rotatory power $-\psi$) and a retarder (retardation ρ and azimuth α).

Now observe Fig. 10. The optically equivalent systems for both the light paths AB and CB will be same. Let the corresponding matrix for these optically equivalent systems be M. Then for the optical path BC, the matrix representing the optically equivalent system will be M^T. So, for the total optical path ABC the matrix representing the optically equivalent system will be $M^T M$. So this total optical path ABC is equivalent to a single retarder with azimuth α and retardation 2ρ. The quantities α and 2ρ however depend upon the rate of rotation of the secondary principal-stresses and the rate of retardation along the optical path ABC.

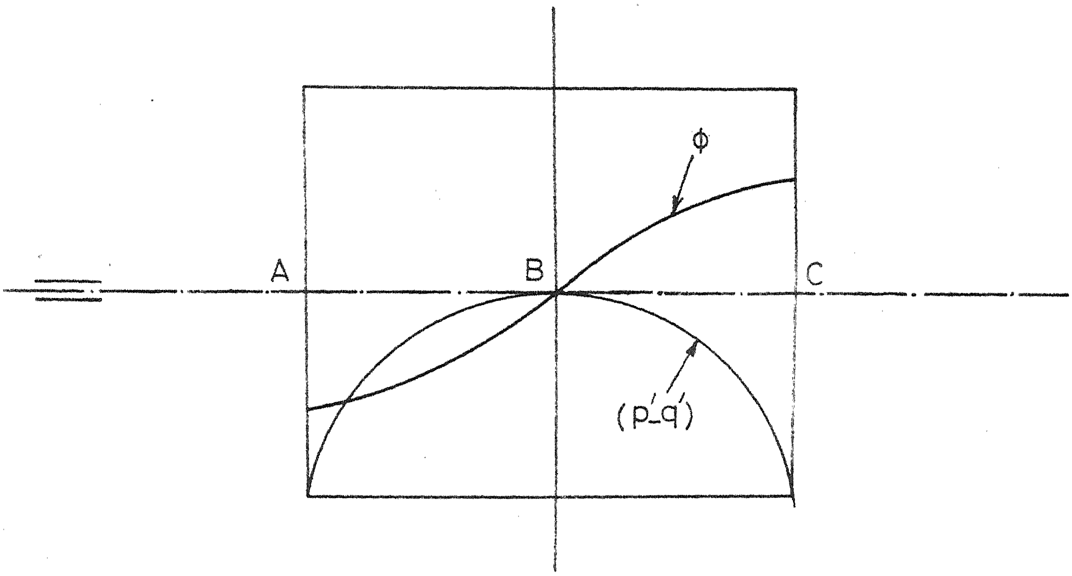

FIG.11. DISTRIBUTION OF THE DIRECTION ϕ AND THE DIFFERENCE $(p'-q')$ OF THE SECONDARY PRINCIPAL-STRESS ALONG THE OPTICAL PATH ABC. FIGURE SHOWS THE CROSS SECTION OF A RECTANGULAR BAR UNDER COMBINED TENSION AND TORSION

Case (e), Anti-symmetric Case:

In this case the secondary principal-stress directions are anti-symmetrical and the secondary principal-stress difference is symmetrical about the middle point o the optical path (example: the optical path in a plane perp dicular to the direction of tensile loading in a rectangul model under combined tension and torsion.)

In Fig. 11. let the optical path AB be equivalent to a system with a retarder (of retardation ρ and azimuth $\bar{\alpha}$) and a rotator (rotatory power ψ). Then the optical path CB is equivalent to a system with a retarder (retardation ρ and azimuth $-\bar{\alpha}$) and a rotator (rotatory power $-\psi$). The optical path BC is equivalent to a rotator (rotatory power ψ) and a retarder (azimuth $\bar{\alpha}$- and retardation ρ). So the total optical path ABC is equivalent to a retarder (retardation ρ and azimuth $\bar{\alpha}$), a rotator (rotatory power $- 2\psi$) and another retarder (retardation ρ and azimuth $-\bar{\alpha}$). This system is again equivalent to a single retarder and a pure rotator. The primary and secondary characteristic directions will be inclined equally, but in opposite directions to the axes of the first and second retarders or to the secondary principal-stress axes at the points A and C. This can be proved as follows;

From Eqs. (2.15)

$$\tan 2\omega = \tan\epsilon \ \mathrm{Sin} 2\alpha$$

$$= \tan (180 - \epsilon) \ \mathrm{Sin} (- 2\alpha) \text{ and } \mathrm{Cos} 2\theta = \mathrm{Cos} 2\omega \ \mathrm{Cos} 2\alpha$$

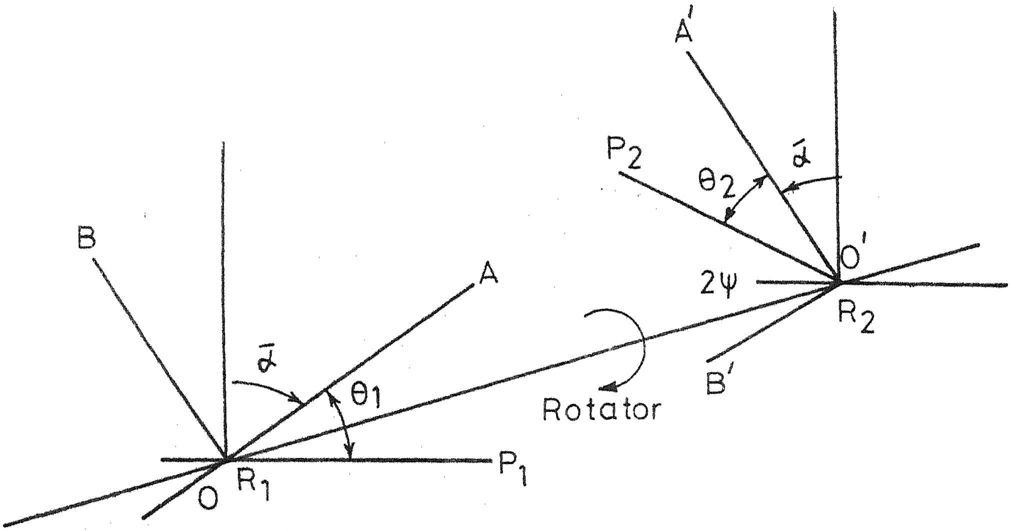

FIG.12. EQUIVALENT SYSTEM FOR THE OPTICAL PATH ABC. OA,OB ARE THE AXES OF THE RETARDER R_1. 2ψ IS THE ROTATORY POWER OF THE ROTATOR. OA',OB' ARE THE AXES OF THE RETARDER R_2. OP_1,$O'P_2$ ARE THE PRIMARY AND SECONDARY CHARACTERISTIC DIRECTIONS OF THE SYSTEM RESPECTIVELY.

$= \cos 2\omega \cos(-2\alpha)$ i.e. along axes inclined equally but in opposite directions (α, $-\alpha$), to the major axis of a particular light ellipse of ellipticity $\tan\omega$, the phase differences will be ϵ and $180 - \epsilon$ respectively. Also, the amptitudes of light vibration are equal along these axes. In Fig. 12. OA, OB are the axes of the retarder R_1, 2ψ is the rotatory power of the rotator, OA$'$, OB$'$ are the axes of the retarder R_2 and OP_1, $O'P_2$ are the primary and secondary characteristic directions of the system respectively. Now, let the incident light on this system be plane polarized along the primary characteristic direction OP_1. Then at the exit of the system, the light will be plane polarized along the secondary characteristic direction $O'P_2$. The changes in the properties of the light ellipse as it passes through the two retarders will be as follows:

The phase difference and the amplitude ratio after the first retarder along its axes will be ρ and $\tan\theta_1$ respectively. The light ellipse is then rotated through an angle 2ψ by the pure rotator after which a retardation of ρ is added along the axes of the second retarder.

Also, the light is plane polarized at the exit of the system along $O'P_2$, one of the secondary characteristic directions. So, the phase difference and the amplitude ratio of the light vibration before the second retarder along its axes should be $(\pi - \rho)$ and $\tan(-\theta_2)$ respectively. The same light ellipse has a phase difference of ρ and an amplitude ratio of $\tan\theta_1$ when referred to the axes of the first retarder.

So,

$$\tan\theta_1 = \tan(-\theta_2)$$
$$\text{or } \theta_1 = -\theta_2$$

Also, the angle between the axis of the first retarder and the major axis of this light ellipse is $\frac{(2\psi + 2\bar{\alpha})}{2} = (\psi + \bar{\alpha})$. (Because along two sets of axes equally inclined, but in opposite directions to the major axis of the light ellipse, the amplitude ratios are equal and the phase differences differ by π. The effective (taking into account the rotatory power 2ψ) angle between the axes of the two retarders is $(2\psi + 2\bar{\alpha})$.

If $\psi + \bar{\alpha} = \alpha_1$

$\tan 2\alpha_1 = \tan 2\theta_1 \text{ Cos } \rho$ - using Eqs. (2.15)

or $\tan 2(\psi + \bar{\alpha}) = \tan 2\theta_1 \text{ Cos } \rho$

This relation connects the angle θ_1 (the angle between the primary characteristic directions and the axes of the first retarder) and ψ, $\bar{\alpha}$ and ρ.

Thus, in the anti-symmetric cases, the primary and secondary characteristic directions are inclined equally but in opposite directions to the secondary principal-stress axes at the entrance and exit respectively. (Because, the axes of the two retarders are inclined equally but in the opposite directions to the secondary principal-stress directions at the entrance and the exit respectively).

Theoretical Determination of Characteristic Parameters:

The matrix M in Eqs. (3.21) in the most general case will have three independent quantities namely the three characteristic parameters. In these equations, only two are independent since $S_1^2 + S_2^2 + S_3^2 = \overline{S}_1^2 + \overline{S}_2^2 + \overline{S}_3^2 = 1$. These are linear equations in S_1, S_2, S_3, $\overline{S}_1$, $\overline{S}_2$ and $\overline{S}_3$. To determine these three characteristic parameters we need the exit light ellipse parameters $\overline{S}_1$, $\overline{S}_2$ and $\overline{S}_3$ for atleast two sets of independent initial Stokes parameters S_1, S_2 and S_3 so that we have four equations in the three unknowns. One of these three equations can be used for checking. The exit light ellipse parameters for two types of incident light ellipse can be found theoretically by integrating numerically the governing differential equations when the functions ϕ' and ρ' are known. From these values, the three characteristic parameters can be calculated.

Experimental Determination of the Characteristic Parameters:

The exit light ellipse parameters for two types of incident light can be found experimentally and the characteristic parameters can be calculated from this data. If a reflection polariscope is used, the primary characteristic direction and the characteristic retardation can be found directly as the combination of the forward and (reflected) backward optical paths is equivalent to a single retarder. However, this can be used only for comparatively thin models.

These quantities can be found directly in a transmission polariscope for axi-symmetric bodies for, in this case also the optical path is equivalent to a single retarder.

It will be very useful,if there exist direct and simple experimental methods to find these parameters in the general case without any calculations or iterations. Robert and Guillemet[14,15,16] presented a method of finding these parameters experimentally in a direct way. The principle of this method is the same as the one suggested by Kent and Lawson[36] for the ellipticity measurement. In this method, the ellipticity of light from the analyser is calibrated in terms of the ratio of the constant and alternating components of light intensity, when the analyser is rotated at a particular angular frequency $\tilde{\omega}$. In this case, the intensity of light from the analyser is given by $I = K_2 (1 + \cos 2\omega \cos 2\tilde{\omega} t)$ where K_2 is a constant, Eqs. (2.15). This method however requires additional instrumentation for measuring the alternating and constant components of voltage. To find the primary characteristic direction using this method, the polarizer at the entrance of the model is rotated until the ellipticity at the exit is zero.

We shall now describe two direct and simple methods to determine these characteristic parameters experimentally, which donot involve the rotation of the analyser at a particular speed or any additional instrumentation.

Method 1:

If the light at entrance to the model is circularly polarized, the light ellipse at exit will have its major axis at an angle of 45° to the secondary characteristic directions. This is so since the amplitudes along the primary and secondary characteristic directions will be equal in this case (if the absorption of light along the optical path is neglected). If the light path is considered to be equivalent to a pure rotator and a retarder, the pure rotator will not have any effect on the incident circularly polarized light while the retarder increases the phase difference along its axes from 90° to (90 +δ) where δ is the characteristic retardation. Along these axes the amplitudes will be equal even after the addition of retardation. These axes correspond to the secondary characteristic directions. This angle of (90 +δ) can be measured by using Tardy's method. One of the primary characteristic directions is found by rotating the polarizer until the intensity along one of the secondary characteristic directions is minimum. The final position of the polarizer axes are the primary characteristic directions.

Experimental Procedure:

Keep the first quarter-wave plate axes at 45° to the polarizer axis so that we have a circularly polarized light at entrance to the model. With the second quarter-

-wave plate out of the field, rotate the analyser for minimum intensity and note this direction D_1. This direction corresponds to the minor axis of the light ellipse. Along the directions $D_1 \pm 45^\circ$ the amplitudes of the components of the light vector are equal and these directions correspond to the secondary characteristic directions.

Now, introduce the second quarter-wave plate so that its axes are parallel to the D_1 and $D_1 \pm 90^\circ$ directions. Rotate the analyser for minimum intensity which will be absolute minimum. Let the minimum intensity position be D_2. The $2\ (D_2 - D_1) = (90 + \delta)$. Now remove both the quarter-wave plates and keep the analyser axes along one of the secondary characteristic directions. Rotate the polarizer for absolute minimum intensity. The final orientation of the polarizer axis corresponds to one of the primary characteristic directions.

Method 2:

The principle of this method is the same as that of the intensity calibration method described in chapter 2.

Procedure:

Let the optical set up consist of the polarizer (at arbitrary orientation), the stressed model, the quarter-wave plate (at arbitrary orientation) and the analyser. Rotate the analyser for minimum intensity thus finding the orientation of the major and minor axes of the light ellipse.

Rotate the analyser through 45° in either direction and note the intensity I_{45} with a photometer. All ellipses (of different orientations and ellipticities) will have an intensity equal to I_{45} along directions which make an angle of 45° with their major or minor axis. Now keep the angle between the axes of the second quarter-wave plate and analyser equal to 45° and rotate the polarizer until the intensity from the analyser is equal to the previously found value of I_{45}. The final orientation of the axis of the polarizer corresponds to one of the primary characteristic directions. The reasoning for this is as follows. When the intensity of light from the analyser is equal to I_{45}, it means that the axes of the light ellipse are at 45° to the analyser axes. That is, they are along the axes of the second quarter-wave plate. Since the phase difference along the major and minor axes is 90°, the phase difference along the same axes but before the second quarter-wave plate must have been zero which corresponds to the case of plane polarized light. The orientations of the polarizer axes which produces plane polarized light after the model correspond to those of the primary characteristic directions.

Now remove the second quarter-wave plate and rotate the analyser for absolute minimum intensity. The final orientations of the analyser axes correspond to the secondary characteristic directions. The characteristic retardation can be found as in the first method or by any other method.

With minor modifications, the first method can be used in the scattered light technique where the model acts as an analyser and the second method in the technique where the model acts as a polarizer. These will be described in the next chapter.

It may be noted now that in a transmission polariscope only the fractional part of the characteristic retardation can be found directly while in general, it is difficult to find the integral part of the characteristic retardation. The usual method of using the Babinet-Soleil compensator with white light, as in two-dimensional problems can not be used here since the characteristic retardation in general, is a function of not only the wavelength of light, but also the orientation and magnitude of the secondary principal-stresses along the optical path. The importance of the concept of optically equivalent system and the characteristic parameters lies in the fact that in a three-dimensional model, in general, the preferential directions (directions which can be directly found by experiment) are the characteristic directions and not the secondary principal-stress directions.

In this chapter, the proof for the existence of an optically equivalent model is presented in detail. The behaviour of light when the light path is reversed is discussed. The relationship between the two optically equivalent systems one with the retarder followed by a pure rotator and the other with a pure rotator followed by a retarder, is derived. Using this information, the optical phenomenon for each of the following three cases are discussed.

(a) Reflection Polariscope

(b) Model having axi-symmetric stress distribution

(c) Model having anti-symmetric stress distribution

Two direct and simple methods to determine experimentally the characteristic parameters are presented. These methods can be extended for use in a scattered light polariscope also. This will be discussed in detail in Chapter 4.

CHAPTER 4

SCATTERED LIGHT METHODS IN THREE-DIMENSIONAL PHOTOELASTICITY

Unlike the stress-freezing technique, the scattered light method is non-destructive for analysis of stresses in three-dimensional photoelasticity. In the scattered light technique, the models can be subjected to live loads at room temperatures and analysed, and no frozen stress model is necessary. In this chapter, we shall first make a brief survey of the existing techniques in scattered light photoelasticity, investigate their limitations, and then suggest refined techniques.

It was first suggested by Weller[17] that the three-dimensional photoelastic analysis could be done by measuring the intensities of the scattered light components. His suggestion was based on the theory of absorption and re-emission of light by vibrating particles.

According to this theory,(i) the light that is scattered at right angles to the direction of propagation is always linearly polarized (ii) the intensity of this scattered light is proportional to the square of its apparent amplitude when viewed from that direction. By 'apparent amplitude' is meant, the component of amplitude normal to the line of sight. His method in the three-dimensional case consists of computing the secondary principal-stress difference from the minimum spacing of the scattered light fringes. That is, the model is rotated about the light path under consideration until the spacing of the fringes becomes minimum. If 'd' is the fringe spacing, the secondary principal-stress difference $(p' - q')$ is given by

$$(p' - q') = \frac{F}{d} \text{ where F is the material fringe constant (Psi.in/fringe)} \qquad (4.1)$$

The directions of the secondary principal-stresses are found by rotating the model until the fringe system vanishes. This method doesnot take into account the effect of rotation of the secondary principal-stress axes.

Drucker and Mindlin[18] investigated the effect of rotation of the secondary principal-stress axes along the wavenormal on the retardation in a photoelastic model. **They** obtained an analytical solution for the case where the principal-stress magnitude remains constant and their directions vary linearly along the wavenormal. They concluded that (i) the rotation increased the relative retardation by a factor $S = (1 + 4R^2)^{\frac{1}{2}}$ where R is the ratio of the rate of rotation to the rate of retardation and that (ii) at high stress, the light vector rotated with the secondary principal-stress directions; plane polarized light entering along a direction of one of the secondary principal-stresses remained practically plane polarized in the direction of the stress through the entire model. They suggested that the factor 'S' be incorporated in the scattered light analysis so that we have

$$(p' - q') = \frac{F}{Sd} \qquad (4.2)$$

Saleme[37] suggested a method of analysis which involves the measurement of absolute intensities in two sets of mutually perpendicular directions, the angle between which is 45°. His analysis is as follows:

Let $V_1 = (S_1, S_2, S_3)$ be the Stokes vector of light referred to the secondary principal-stress axes at a particular point in the model.

$$V_1 = \begin{matrix} S_1 \\ S_2 \\ S_3 \end{matrix} = \begin{matrix} \mathrm{Cos}2\theta \\ \mathrm{Sin}2\theta\ \mathrm{Cos}\epsilon \\ \mathrm{Sin}2\theta\ \mathrm{Sin}\epsilon \end{matrix} \qquad (4.3)(a)$$

When the same light ellipse is referred to OXY making an angle α with Opq, we get

$$V_2 = \begin{matrix} \bar{S}_1 \\ \bar{S}_2 \\ \bar{S}_3 \end{matrix} = \begin{matrix} \mathrm{Cos}2\theta\ \mathrm{Cos}2\alpha + \mathrm{Sin}2\theta\ \mathrm{Cos}\epsilon\ \mathrm{Sin}2\alpha \\ \mathrm{Sin}2\theta\ \mathrm{Cos}\epsilon\ \mathrm{Cos}2\alpha - \mathrm{Cos}2\theta\ \mathrm{Sin}2\alpha \\ \mathrm{Sin}2\theta\ \mathrm{Sin}\epsilon \end{matrix} = \begin{matrix} \mathrm{Cos}2\theta_1 \\ \mathrm{Sin}2\theta_1\ \mathrm{Cos}\epsilon_1 \\ \mathrm{Sin}2\theta_1\ \mathrm{Sin}\epsilon_1 \end{matrix}$$

$$(4.3)(b)$$

Let the amplitudes of light vector components along X,Y-axes be a_X and a_Y. $\tan\theta_1 = \frac{a_Y}{a_X}$, ϵ_1 is the phase difference corresponding to Stokes vector V_2. $a_X^2 - a_Y^2 = \bar{S}_1 = 2a_X^2 - 1$ $= 1 - 2a_Y^2$ $\therefore$ $a_X^2 + a_Y^2 = 1$

The intensities I_X and I_Y along these axes are given by

$$I_X = Ka_X^2 = K\left(\frac{1 + \bar{S}_1}{2}\right) \qquad (4.4)$$

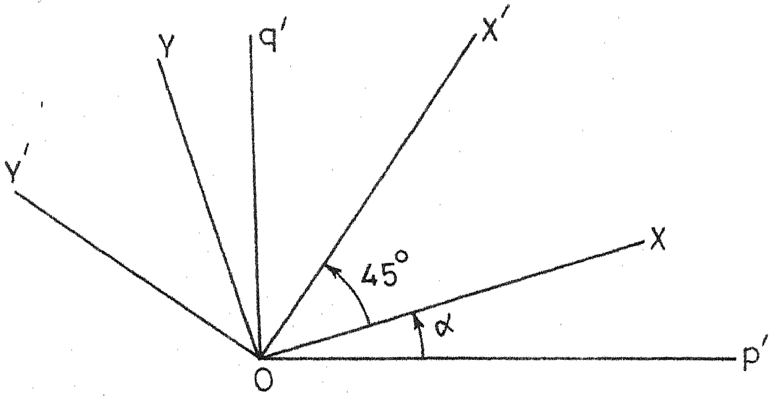

FIG. 13. DIRECTIONS OF SCATTERED LIGHT OBSERVATION AT THE POINT O

$$I_Y = Ka_Y^2 = K\left(\frac{1 + \bar{S}_1}{2}\right) \qquad (4.5)$$

where K is a constant.

Now consider the intensities I_X' and I_Y' along the axes which are inclined at an angle of 45° to the X,Y-axes, Fig. 13. These are obtained by substituting $(\alpha + 45^\circ)$ for α in the expression for $\bar{S}_1$ in the above equations.

So, $$I_X' = \frac{K}{2}\left(1 - \mathrm{Cos}2\theta\,\mathrm{Sin}2\alpha + \mathrm{Sin}2\theta\,\mathrm{Cos}\epsilon\,\mathrm{Cos}2\alpha\right) \qquad (4.6)$$

$$I_Y' = \frac{K}{2}\left(1 + \mathrm{Cos}2\theta\,\mathrm{Sin}2\alpha - \mathrm{Sin}2\theta\,\mathrm{Cos}\epsilon\,\mathrm{Cos}2\alpha\right) \qquad (4.7)$$

Let z denote the distance along the wavenormal. Neglecting the rotation of the secondary principal-stress axes, i.e. θ_1 and α are independent of z, we have

$$\frac{dI_X}{dz} = -\frac{K}{2}\,\mathrm{Sin}2\theta\,\mathrm{Sin}2\alpha\,\mathrm{Sin}\epsilon\,\frac{d\epsilon}{dz} \qquad (4.8)$$

$$\frac{dI_Y}{dz} = \frac{K}{2}\,\mathrm{Sin}2\theta\,\mathrm{Sin}2\alpha\,\mathrm{Sin}\epsilon\,\frac{d\epsilon}{dz} \qquad (4.9)$$

$$\frac{dI_X'}{dz} = -\frac{K}{2}\,\mathrm{Sin}2\theta\,\mathrm{Cos}2\alpha\,\mathrm{Sin}\epsilon\,\frac{d\epsilon}{dz} \qquad (4.10)$$

$$\frac{dI_Y'}{dz} \doteq \frac{K}{2}\,\mathrm{Sin}2\theta\,\mathrm{Cos}2\alpha\,\mathrm{Sin}\epsilon\,\frac{d\epsilon}{dz} \qquad (4.11)$$

$$I_X + I_Y = K \qquad (4.12)$$

from Eqs. (4.4) and (4.5)

$$\frac{\dfrac{dI_X}{dz}}{\dfrac{dI_X'}{dz}} = \frac{\dfrac{dI_Y}{dz}}{\dfrac{dI_X'}{dz}} = \tan2\alpha \qquad (4.13)$$

from Eqs. (4.8) - (4.11)

$$I_X - I_Y = K\overline{S}_1 = K\cos 2\theta_1 \qquad (4.14)$$

$$I_{X'} - I_{Y'} = \sin 2\theta_1 \cos\varepsilon_1 \qquad (4.15)$$

From the above Eqs. (4.12) - (4.15), the quantities K, α, θ_1 and ε_1 can be computed from the values of the intensities I_X, I_Y, $I_{X'}$ and $I_{Y'}$.

Since $(p' - q') = F\frac{d\varepsilon}{dz}$ (4.16)

The quantity $(p' - q')$ can be calculated if the rotational effect is neglected.

Jessop[38] attempted to arrive at a qualitative estimate of the magnitude of the rotational effect and deduced certain conditions under which this effect will be small enough to be neglected. He considered the Maxwell-Neumann equations

$$\frac{d\varepsilon}{dz} = \frac{d\rho}{dz}\left[1 + \left(\frac{a_X}{a_Y} - \frac{a_Y}{a_X}\right)\sin\varepsilon\,\frac{d\phi}{d\rho}\right] \qquad (4.17)$$

$$\frac{da_X}{d\rho} = a_Y\cos\varepsilon\,\frac{d\phi}{d\rho} \quad\text{and}\quad \frac{da_Y}{d\rho} = -\,a_Y\cos\,\frac{d\phi}{d\rho} \qquad (4.18)$$

Now, a relation connecting the quantity $\frac{d\rho}{dz}$ (to be determined) and the quantity ε (that can be observed experimentally) is to be arrived.

The quantity $\frac{d\rho}{dz}$ is equal to $\frac{d\varepsilon}{dz}$ at points where either $a_X = a_Y$ or $\sin\varepsilon = 0$. The first condition can be satisfied at the point of entry of the beam into the model, by orienting the model so that the secondary principal-stresses at this point are inclined at 45° to the direction of vibration of the incident light, but it is not in general satisfied elsewhere. The second condition is satisfied at points where whole or half-fringes appear but the value of $\frac{d\epsilon}{dz}$ at these points cannot be obtained from a smooth curve plotted through the observed values. Also, in the absence of rotation, the quantity $\frac{d\epsilon}{dz}$ will be equal to $\frac{d\rho}{dz}$. To find the effect of neglecting the second term in Eq. (4.17) which represents the rotational effect, we consider,

$$\frac{d}{d\rho}\left(\frac{a_X}{a_Y} - \frac{a_Y}{a_X}\right) = \left(2 + \frac{a_X^2}{a_Y^2} + \frac{a_Y^2}{a_X^2}\right) \operatorname{Cos}\epsilon \frac{d\phi}{d\rho} \qquad (4.19)$$

from Eq. (4.18)

$$\simeq 4 \operatorname{Cos}\epsilon \frac{d\phi}{d\rho},$$ if a_X and a_Y are initially equal.

If both $\frac{d\phi}{d\rho}$ and its derivatives are small

$$4 \operatorname{Cos}\epsilon \frac{d\phi}{d\rho} = 4 \left[\frac{d}{d\rho}\left(\operatorname{Sin}\epsilon \frac{d\phi}{d\epsilon}\right) - \operatorname{Sin}\epsilon \frac{d^2\phi}{d\epsilon d\rho}\right]$$

$$\simeq 4 \frac{d}{d\rho}\left(\operatorname{Sin}\epsilon \frac{d\phi}{d\epsilon}\right)$$

so that $\left(\frac{a_X}{a_Y}\right) - \frac{a_Y}{a_X}. \simeq \operatorname{Sin}\epsilon \frac{d\phi}{d\epsilon}$ frp, Eq. (4.19)

$$\left[\frac{a_X}{a_Y} - \frac{a_Y}{a_X}\right] \operatorname{Sin}\epsilon \frac{d\phi}{d\rho} \simeq \frac{d\phi}{d\epsilon} \cdot \frac{d\phi}{d\rho} \operatorname{Sin}^2\epsilon = \mu \operatorname{Sin}^2\epsilon$$

where $\mu = \frac{d\phi}{d\epsilon} \cdot \frac{d\phi}{d\rho}$

So, μ is a small variable coefficient of the order $(\frac{d\emptyset}{d\rho})^2$. An estimate of the magnitude of $\frac{d\emptyset}{d\rho}$ in any particular case can be made by observing the dimunition of the sharpness of the fringes in the model after rotating about the light path. If the total change in the orientation of the secondary principal-stress axes over the light path in the model is 30° and the relative retardation introduced (due to stresses only) is n wavelengths, the value of $\frac{d\emptyset}{d\rho}$ can not exceed (1/12n). If the fringes are sharply defined over a range of two or more wavelengths, the error introduced in $\frac{d\epsilon}{dz}$ by drawing the , z graph as a smooth curve through the points obtained by measurements of the positions of the fringes will not exceed something of the order of 1% and this will generally be less than the possible error of measurement.

Based on the above findings, Frocht and Srinath[10,11,12] developed methods for measuring the secondary principal-stress difference and their orientation. An account of these methods will now be presented.

Consider Eqs. (2.1) - (2.5) of chapter 2. Let X-and Y-axes represent the directions of the secondary principal-stresses. The intensity I_α for a direction of observation making an angle α with the X-axis is given by the expression

$$I_\alpha = a_X^2 \operatorname{Sin}^2\alpha + a_Y^2 \operatorname{Cos}^2\alpha - 2a_X a_Y \operatorname{Cos}\alpha \operatorname{Sin}\alpha \operatorname{Cos}\epsilon \qquad (2.5)$$

if the proportionality constant is assumed to be unity.

This light intensity will be maximum when the direction of observation is along the minor axis of the light ellipse and is a minimum when the direction of observation is along the major axis. That is, the intensity is a maximum or minimum when the angle α satisfies Eq. (2.3)

$$\tan 2\alpha = \frac{2a_X a_Y}{a_X^2 - a_Y^2} \cos \epsilon = \tan 2\theta \cos \epsilon \qquad (2.3)$$

From Eq. (2.5), we note that for any fixed direction of observation α and for fixed values of a_X and a_Y, the intensity of scattered light varies from a maximum to a minimum depending upon the value of ϵ. When α is less than $\pi/2$, the intensity is a minimum (although not necessarily zero) when $\epsilon = 2m\pi$ and becomes a maximum when $\epsilon = (2m - 1)\pi$. When α is greater than $\pi/2$, the condition for maximum and minimum will be reversed. Except for special cases, ϵ will vary from point to point along the axis of propagation and in general, will assume the values necessary for a maximum and a minimum light intensity. This gives rise to a sequence of bright and dark regions which forms the scattered light pattern. Also for approximately equal amplitudes a_X and a_Y, the axes of the light ellipse are at 45° to the directions of the secondary principal-stresses and therefore this direction gives a pattern of sharpest contrast.

If the directions of the secondary principal-stress axes donot vary along the optical path and the amplitudes of the light components along these axes at the entrance to the model are equal, (i) these remain equal all along the optical path and (ii) whatever retardation is added along these axes at the entrance, the same will appear as an additional retardation at all points on the optical path in the model. We then have,

$$(p' - q') = F\frac{dn}{dz} \qquad (4.20)$$

A compensator can be placed at the entrance to the model with its axes parallel to the secondary principal-stress axes. If the axes of the polarizer, which is kept before the compensator make an angle of 45° with the axes of the compensator, the amplitudes along the secondary principal-stress axes in the model will be equal. The compensator then acts as a continuation of the model. Along directions making an angle of 45° with the secondary principal-stress axes, the scattered light fringes will have the sharpest contrast. This is so since, the major and minor axes of the light ellipse at any point on the optical path in the model will be along these axes. From these fringes, the n-z curve can be plotted from which the slope $\frac{dn}{dz}$ can be computed.

Even in the presence of rotation of the secondary principal-stress axes, the above method of plotting the n-z curve and thus calculating the secondary principal-stress can be used provided that the conditions mentioned by Jessop [38] are satisfied.

Directions of the Secondary Principal-Stresses:

Approximate Methods:

The approximate locations of the secondary principal-stress axes can be readily found by visual observation without a compensator or a photometer.

(a) Displacement Pattern Method:

When looking along either one of the two secondary principal-stress axes, the center of the local scattered light pattern is of uniform brightness, and the fringes on opposite sides of this region become displaced relative to each other by half a fringe. The discontinuity in the fringes arises because, for a direction of observation on one side of the uniform region α is less than $\pi/2$ and on the other side it is greater than $\pi/2$. Therefore, the same retardation $2m\pi$ will produce dark fringes on one side and bright fringes on the other as can be seen from Eq. (2.5). The stress pattern resembles the picture of an X-ray of the spiral column with emanating ribs.

(b) Sharpest Contrast Method:

The model is rotated until the scattered light stress pattern appears of sharpest contrast to the naked eye when viewed along the line of vision of the photometer. In this position, the secondary principal axes are approximately at $\pm 45^\circ$ to the line of vision of the photometer.

(c) Minimum Intensity Method:

If the light is circularly polarized at the entrance, the axes of the light ellipse at any point are independent of the birefringence and are always inclined at 45°, approximately to the directions of the secondary principal-stresses. Hence, the determination of one of the axes of the ellipse also determines the directions of the secondary principal--stresses. The direction of the major axis of the ellipse can be readily and accurately located with a photometer since, the intensity of the light is a minimum for observations along the major axis.

(d) Exact Methods:

(i) The Constant Intensity Method:

When $\frac{d\emptyset}{dz}$ is small, the changes in the amplitudes a_X and a_Y, when retardation in the compensator (whose axes are set parallel to the directions of the secondary principal-stresses) is varied, are negligible. So, from Eq. (2.5), when $\alpha = 0$, the intensity I_α is independent of the birefringence and it remains constant even though the retardation at that point is changed.

(ii) The Zero Intensity or Line Ellipse Method:

From Eq. (2.5), it can be observed that for a fixed value of α ($<\pi/2$), the intensity is a maximum when $\epsilon = (2m - 1)\pi$ and a minimum when $\epsilon = 2m\pi$. In both these cases, the light ellipse degenerates into a straight line. When $\epsilon = 2m\pi$, the line is inclined at an angle $\alpha_1 = \tan^{-1}(\frac{a_Y}{a_X})$ and when $\epsilon = (2m - 1)_\pi$, the line is inclined at an angle

$\alpha_1 = \tan^{-1}(\frac{-a_Y}{a_X})$ to the X-axis. The intensities of scattered light for observations along these lines will be zero. To determine the directions of the secondary principal-stresses, the retardation in the compensator is adjusted to make the intensity at a point minimum for an arbitrary direction of observation say OM, Fig. 14. Assuming α to be less than $\pi/2$, ϵ will then have assumed a value of $2m\pi$ and the light ellipse will have become a straight line CO, Fig. 14. making an angle $\alpha = \tan^{-1}(\frac{a_Y}{a_X})$ with the X-axis, which can be located with a photometer. Next, keeping approximately the same direction of observation OM, the retardation in the compensator is adjusted to give the maximum light intensity. When this occurs, the light ellipse will have become once again a straight line, only this time it will be DO inclined at an angle $\alpha_1 = \tan^{-1}(\frac{-a_Y}{a_X})$ to the X-axis. This line is also located with a photometer. The directions CO and DO, are equally inclined with respect to the direction OX which is one of the secondary principal-stress axes.

(iii) Absolute Intensity Method:

This method which involves the measurement of the absolute intensity has been suggested by Menges[39] and Salame[37]. This has been described earlier. The main disadvantage with this method is that it involves the measurement of absolute intensity which will depend upon the absorption along the varying optical paths.

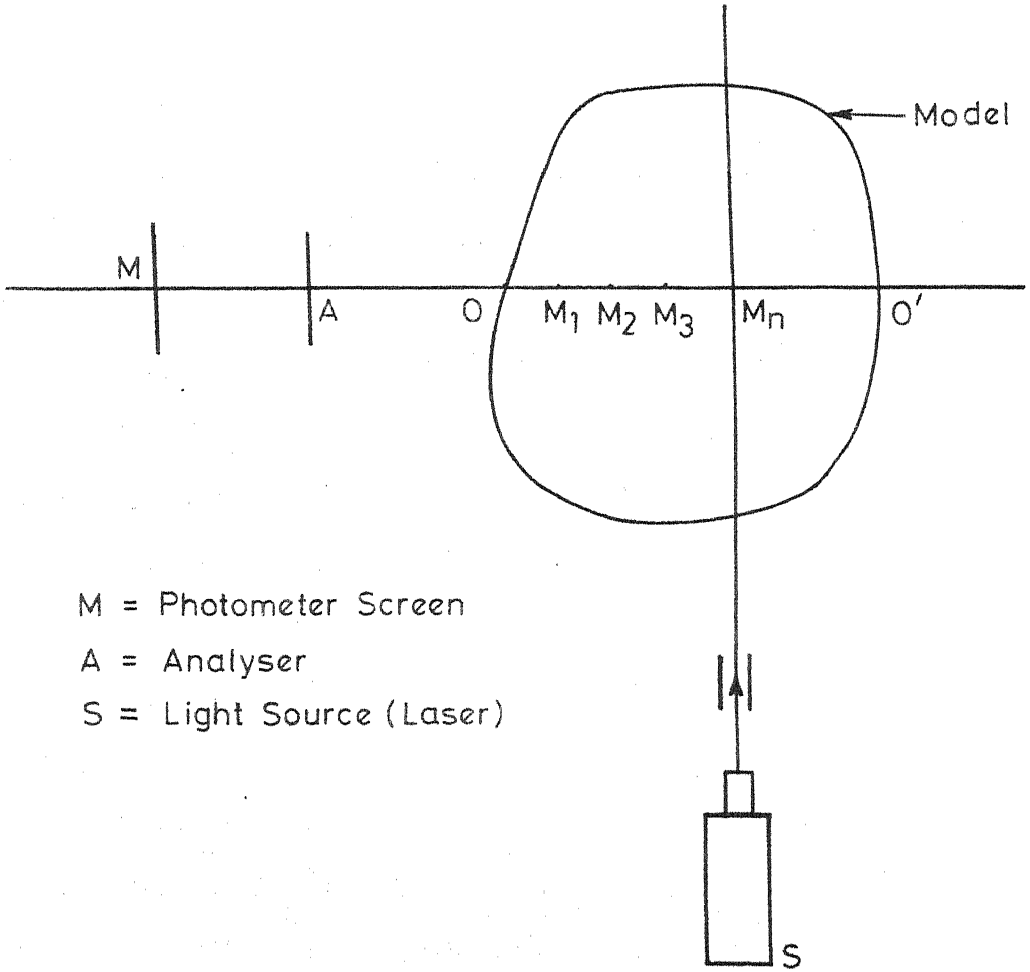

FIG. 15. SCATTERED LIGHT TECHNIQUE USING THE MODEL AS A POLARIZER.

Cheng [40] described a new method which records simultaneously the intensities of scattered light along two directions of observation 45° apart in a plane normal to the beam of light. The theory of this method is the same as the one described by Salame [37] except that the effect of varying lengths of light path is eliminated by recording the intensities before the loading of the model. He made use of Drucker and Mindlin's conclusion that for cases where the parameter R is small, plane polarized light entering the model along one of the secondary principal-stress axes at the entrance follows that axis throughout the model. The polarizer axis is set along this direction and both the polarizer and the model are rotated in unision until the light intensity is minimum at the particular point under consideration. When the minimum occurs, the direction of observation is along one of the principal-stress axes.

Robert and Guillemet [14,15,16] adopted an altogether different approach towards scattered light analysis in the three-dimensional cases. Since any length of light path in a photoelastic model under load can be replaced by the combination of a linear retarder and a pure rotator, the characteristic parameters of this equivalent system can be found at each point on the optical path with respect to the point at the entrance to the model, Fig. 15. After knowing these parameters, the secondary principal-stress difference and orientations can be found by using the governing optical equations. To find these parameters, they adopted the method that is popular in crystal physics, of rotating the analyser at a particular speed and then measuring the ratio of alternating and constant components of light from the analyser. This ratio is dependent only upon the ellipticity of light from the analyser (see Chapter 3). The light incident on the model in this method is unpolarized and the model acts as a polarizer. The intensity from the analyser is given by

$$I = K\left(\frac{1 - S_1}{2}\right)$$

where S_1 is the first Stokes parameter of the light ellipse and K is a constant.

or $$I = \frac{K}{2}(1 - \operatorname{Cos}2\omega \operatorname{Cos}2\alpha)$$

Tan ω is the ellipticity and α is the azimuth (with respect to the analyser axes) of the light ellipse incident on the analyser. If the analyser is rotated at an angular velocity of $\tilde{\omega}$, $\alpha = \tilde{\omega}\, t$ (t is the time.) The ratio of the alternating to the constant components of this intensity is obviously

$$\operatorname{Cos}2\omega = \frac{1 - e^2}{1 + e^2} \qquad \text{where } e = \tan\omega$$

$$\text{Also } \operatorname{Cos}2\omega = \sqrt{1 - S_3^2} = \sqrt{1 - \operatorname{Sin}^2 2\theta \operatorname{Sin}^2 \epsilon}$$

$$= Y \text{ (say)}$$

$$\text{then } \operatorname{Cos}\epsilon = \frac{Y\big|_{\theta = 45^\circ}}{Y\big|_{\theta = 0}}$$

To find the primary characteristic directions the model is rotated with respect to the incident light vibration until the value of Y observed is zero, which corresponds to plane polarized light ($e = 0$) before the analyser. The position of the incident light beam with respect to the model axes will be the primary characteristic direction. Now this beam is rotated through an angle of 45° and the value of Y is noted. Then $Y = \text{Cos}^{\epsilon}$ where ϵ corresponds to the characteristic retardation. The direction of the major axis of the light ellipse before the analyser when the incident light beam is along one of the primary characteristic directions corresponds to one of the secondary characteristic directions. For finding these parameters the model is rotated about the axis $00'$, Fig. 15. These parameters are found for the optical paths OM_1, OM_2, ... OM_n,...., $00'$.

Aderholdt, Mckinney, Ranson and Swinson[13] in their scattered light method assumed that for problems where the rotation to retardation ratio is small, the light waves follow the secondary principal-stress axes. That is, the amplitudes of the components of light along these axes remain constant along the light path. This assumption is again based on the findings of Drucker and Mindlin[18]. Keeping the light at the entrance to the model circularly polarized, the directions at each point of the optical path in the model along which the fringes appear to be fading (or the intensity is constant) are noted which give the directions of secondary principal-stresses. The fringes are counted by moving along the light path and at the same time, rotating the observation angle such that the angle of observation at any point is 45° from one of the secondary principal-stress axes.

Srinath[41] made an analysis of some of the previous scattered light techniques. He suggested a method called mini-max method, which is a combination of the zero and absolute intensity methods, to find the directions of the secondary principal-stresses. In this method, the orientation $\emptyset$ of these directions is found from the formula

$$\tan\alpha = \frac{\mu_1 + \mu_2}{\mu_3 + \mu_4}$$

where

$$\mu_1^2 = K\,(a \,\mathrm{Sin}\alpha + b \,\mathrm{Cos}\alpha)^2 = (I\alpha)_{max}$$

$$\mu_2^2 = K\,(a \,\mathrm{Sin}\alpha - b \,\mathrm{Cos}\alpha)^2 = (I\alpha)_{min}$$

$$\mu_3^2 = K\,(a \,\mathrm{Cos}\alpha + b \,\mathrm{Sin}\alpha)^2 = (I\beta)_{max}$$

$$\mu_4^2 = K\,(a \,\mathrm{Cos}\alpha - b \,\mathrm{Sin}\alpha)^2 = (I\beta)_{min}$$

$$\beta = \alpha + \frac{\pi}{2}$$

and the retardation ρ is obtained from the equation

$$\mathrm{Cos}\,\rho = \frac{-\,2\,I_\alpha + (\mu_1 + \mu_2)}{(\mu_1 - \mu_2)}$$

where

$$I_\alpha = K\,(a^2 \,\mathrm{Sin}^2\alpha + b^2 \,\mathrm{Cos}^2\alpha - 2ab \,\mathrm{Sin}\alpha \,\mathrm{Cos}\alpha \,\mathrm{Cos}\,\rho)$$

- obtained from Eq. (2.5)

Critical Analysis:

A critical analysis of the above described scattered light methods will now be made. Except the method described by Robert and Guillemet, all the methods are connected with the findings of Drucker and Mindlin[18]. These findings in turn are based on the analytical solution for the case where the secondary principal-stress difference is constant and their orientation varies linearly along the optical path. These results are confined to the cases where the parameter R is small.

We shall now examine the validity of the assumptions involved in the previous scattered light methods for the case where the rate of rotation ϕ' can be any arbitrary function, but the ratio $R = \frac{\phi'}{\rho'}$ is a constant.

The analytical solution for this case is given by Eqs. (2.46) - - (2.48). These are:

$$S_1 = \frac{A_1}{2RK^2} + \frac{1}{K}\left(1 - \frac{A_1^2}{K^2}\right)^{\frac{1}{2}} \text{Sin}(2K\phi + A_2) \qquad (4.21)$$

$$S_2 = \left(1 - \frac{A_1^2}{K^2}\right)^{\frac{1}{2}} \text{Cos}(2K\phi + A_2) \qquad (4.22)$$

and

$$S_3 = \frac{S_1}{2R} + A_1 = \frac{A_1}{K^2} + \frac{(1 - \frac{A_1^2}{K^2}}{2RK} \text{Sin}\ (2K\phi + A_2) \qquad (4.23)$$

where A_1 , A_2 are arbitrary constants which are to be determined from the initial conditions.

Let us now examine this solution for two types of incident light, (i) plane polarized light along one of the secondary principal-stress axes at the entrance and (ii) circularly polarized light.

Case (i) : Incident Light is Plane Polarized Along one of the Secondary Principal-Stress axes At the Entrance

At $Z = 0$, $\phi = 0$ (say), $S_1 = 1$, $S_2 = S_3 = 0$

From Eq. (4.23)

$$A_1 = -1/2R$$

and from Eq. (4.21)

$$1 = \frac{1}{4R^2+1} + \frac{1}{K}\left(1 - \frac{1}{4R^2+1}\right)^{\frac{1}{2}} \operatorname{Sin} A_2$$

i.e $\operatorname{Sin} A_2 = 1$

or $A_2 = \pi/2$.

So, at any point on the optical path we have

$$S_3 = -\frac{1}{2RK^2} + \frac{1}{2RK}\left(1 - \frac{1}{4R^2+1}\right)^{\frac{1}{2}} \operatorname{Sin}\left(2K\phi + \frac{\pi}{2}\right)$$

$$= \frac{1}{2RK^2}(\operatorname{Cos} 2K\phi - 1)$$

The light is plane polarized at points where

$S_3 = 0$

$$\text{i.e. when } 2K\phi = 2n\pi \qquad (4.24)$$

At these points

$$S_1 = \frac{1}{4R^2K^2} + \frac{1}{K}\left(1 - \frac{1}{4R^2K^2}\right)^{\frac{1}{2}}$$

$$= 1$$

i.e. the intensity attains its absolute maximum value. So, the light vector will be along the direction of one of the secondary principal-stresses.

The change in the orientation of the secondary principal-stress axes between two fringes is given by Eq. (4.24) as

$$
\begin{aligned}
d\phi &= \pi/K = R\,d\rho \\
\text{i.e.}\quad d\rho &= \pi/KR
\end{aligned}
\qquad (4.25)
$$

i.e. between two fringes, the change in the retardation $d\rho$ introduced due to the stresses only is given by Eq. (4.25). If the effect of the rotation of the secondary principal-stress axes is neglected, this is given by

$$d\rho = 2\pi$$

So, the effect of rotation is to decrease the fringe spacing by a factor $\frac{1}{2KR}$ or $\frac{1}{(4R^2 + 1)^{\frac{1}{2}}}$

Case (ii): Incident Light is Circularly Polarized.

At $Z = 0$, $S_1 = S_2 = 0$, $S_3 = 1$, $\phi = 0$

From Eq. (4.23)

$$A_1 = 1$$

and from Eq. (4.21)

$$0 = -\frac{1}{2RK^2} + \frac{1}{K}\left(1 - \frac{1}{K^2}\right)^{\frac{1}{2}} \operatorname{Sin}A_2$$

i.e. $\operatorname{Sin}A_2 = 1$ or $A_2 = \pi/2$

At any point on the optical path,

$$S_3 = \frac{4R^2}{4R^2 + 1} + \frac{\operatorname{Cos}2K\phi}{4R^2 + 1}$$

$=$ [illegible]

$$\text{if } \cos 2K\phi = -4R^2 \tag{4.26}$$

If $4R^2 \ll 1$

$$\text{i.e. } 2K\phi = (2n + 1)\frac{\pi}{2} \tag{4.27}$$

At these points,

$$S_1 = -\frac{1}{2RK^2} + \frac{1}{K^2}(K^2-1)^{1/2}\cos 2K\phi$$

$$= -\frac{1}{2RK^2} + \frac{1}{2RK^2}\cos 2K\phi$$

$$= -\frac{1}{2RK^2}(1 - \cos 2K\phi)$$

$$= -\frac{2R\ (1 + 4R^2)}{(4R^2 + 1)}$$

$$\simeq 0.$$

$$S_2 = -\left(1 - \frac{1}{K^2}\right)^{\frac{1}{2}}\sin 2K\phi$$

$$= -\frac{1}{(4R^2 + 1)^{\frac{1}{2}}}\sin 2K\phi$$

$$\simeq -\sin\frac{(2n + 1)\pi}{2} \tag{4.28}$$

The second Stokes parameter S_2 gives us the intensity along axes making an angle of 45° with the reference axes (in this case, the secondary principal-stress axes).

From Eqs. (4.27) and (4.28) we observe that between two successive fringes,

$$d\phi = R\,d\rho = \frac{\pi}{K} \tag{4.29}$$

So, in this case also, the effect of the rotation of the secondary principal-stress axes is to decrease the fringe spacing by a factor $\frac{1}{(4R^2+1)^{\frac{1}{2}}}$. The same conclusions were drawn by Drucker and Mindlin[18] for the case where **both** of the functions ϕ' and ρ' are constants.

Now, we shall examine the above analytical solution in light of the assumptions of the previous scattered light methods. In the scattered light method developed by Frocht and Srinath[10,11,12], the following assumptions are made: With the addition of a certain amount of retardation $\Delta\epsilon_0$ at the entrance along the secondary principal-stress axes when the amplitudes of light vector components along these directions are equal, (1) a retardation of $\Delta\epsilon_0$ appears as an additional retardation at every point on the optical path along the secondary principal-stress axes and (2) the amplitudes (or the intensities) along the secondary principal-stress axes at any point on the optical path do not change with the change in the retardation ϵ_0 added at the entrance. At $Z = 0$ let $S_1 = 0$ (i.e. the amplitudes are equal along the secondary principal-stress axes at the entrance).

$S_3 = \mathrm{Sin}\epsilon_0$, $\phi = \phi_i$, $S_2 = \mathrm{Cos}\epsilon_0$

The light intensity $I = \overline{K}\, a_x^2$

$$= \overline{K}\left(\frac{1+S_1}{2}\right)$$

where K is a constant.

$$\frac{dI}{d\epsilon_0} = \frac{K}{2}\,\frac{dS_1}{d\epsilon_0} \qquad (4.30)$$

Let us evaluate the constants A_1 and A_2 of the solution for these initial conditions.

From Eq. (4.23)

$$S_3 = \mathrm{Sin}\epsilon_0 = A_1 \qquad (4.31)$$

From Eq. (4.22)

$$S_2 = \mathrm{Cos}\epsilon_0 = (1 - \frac{\mathrm{Sin}^2\epsilon_0}{K^2})^{\frac{1}{2}} \mathrm{Cos}(2K\phi_i + A_2)$$

or

$$\mathrm{Cos}(2K\phi_i + A_2) = \frac{\mathrm{Cos}\epsilon_0}{(1 - \frac{\mathrm{Sin}^2\epsilon_0}{K^2})^{1/2}} \qquad (4.32)$$

and from Eq. (4.21)

$$\mathrm{Sin}(2K\phi_i + A_2) = \frac{\mathrm{Sin}\epsilon_0}{2RK(1 - \frac{\mathrm{Sin}^2\epsilon_0}{K^2})^{\frac{1}{2}}} \qquad (4.33)$$

Substituting these expressions in Eqs. (4.21) - (4.23) so that the constants A_1 and A_2 are eliminated, we obtain the following expressions for S_1, S_2 and S_3 at any point.

$$S_1 = -\frac{\mathrm{Sin}\epsilon_0}{2RK^2} + \frac{1}{K}(\mathrm{Sin}K_2\ \mathrm{Cos}\epsilon_0 + \frac{\mathrm{Cos}K_2\ \mathrm{Sin}\epsilon_0}{2RK}) \qquad (4.34)$$

$$S_2 = \mathrm{Cos}K_2\ \mathrm{Cos}\epsilon_0 - \frac{\mathrm{Sin}K_2\ \mathrm{Sin}\epsilon_0}{2RK} \qquad (4.35)$$

and

$$S_3 = \frac{\mathrm{Sin}\epsilon_0}{K^2} + \frac{1}{2RK}(\mathrm{Sin}K_2\ \mathrm{Cos}\epsilon_0 + \frac{\mathrm{Cos}K_2\ \mathrm{Sin}\epsilon_0}{2RK}) \qquad (4.36)$$

where $K_2 = 2K(\phi - \phi_i)$ (4.37)

$$\therefore \quad \frac{dI}{d\epsilon_0} = -\frac{KR}{(1+4R^2)}\left[\mathrm{Cos}\epsilon_0 + \mathrm{Sin}K_2\ \mathrm{Sin}\epsilon_0\ (1+4R^2)^{\frac{1}{2}} - \mathrm{Cos}K_2\ \mathrm{Cos}\epsilon_0\right]$$

$$= 0$$

for all values of ϵ_0

when $K_2 = 2n\pi = 2K(\emptyset - \emptyset_i)$ (4.38)

Also

$$\frac{dI}{d\epsilon_0} \simeq 0$$

for all values of ϵ_0

when $R \ll 1$ (4.39)

The phase difference ϵ along the secondary principal-stress axes is given by

$$\tan\epsilon = \frac{S_3}{S_2} = \frac{\dfrac{\mathrm{Sin}\epsilon_0}{K^2} + \dfrac{\mathrm{Sin}K_2\ \mathrm{Cos}\epsilon_0}{2RK} + \dfrac{\mathrm{Cos}K_2\ \mathrm{Sin}\epsilon_0}{4R^2K^2}}{\mathrm{Cos}K_2\ \mathrm{Cos}\epsilon_0 - \dfrac{\mathrm{Sin}K_2\ \mathrm{Sin}\epsilon_0}{2RK}}$$

$$= \frac{4R^2\ \mathrm{Sin}\epsilon_0 + (4R^2+1)^{\frac{1}{2}}\ \mathrm{Sin}K_2\ \mathrm{Cos}\epsilon_0 + \mathrm{Cos}K_2\ \mathrm{Sin}\epsilon_0}{(1+4R^2)\ \mathrm{Cos}K_2\ \mathrm{Cos}\epsilon_0 - (1+4R^2)^{\frac{1}{2}}\ \mathrm{Sin}K_2\ \mathrm{Sin}\epsilon_0}$$

$$= \tan\epsilon_0$$

if $K_2 = 2n\pi$ (4.40)

$$\tan\epsilon \simeq \tan(\epsilon_0 + K_2) \qquad (4.41)$$

if $4R^2 \ll 1$

The quantity $4R^2$ may be neglected when compared to unity if it is less than 0.01 i.e. for $R<0.05$.

So, the assumptions in the above scattered light method may be considered valid for the cases where the parameter R is less than 0.05.

Aderholdt, Mckinney, Ranson and Swinson[13], in their scattered light method assume that the intensity along the secondary principal-stress axes remains almost constant (for certain class of problems where the rate of rotation is not high) along the optical path.

Also from the above solution, i.e. Eq. (4.34),

$$\frac{da_Y^2}{dz} = -\frac{S_1'}{2} = \phi'\left(\frac{\mathrm{Sin}K_2\ \mathrm{Sin}\epsilon_0}{2RK}\right) - \mathrm{Cos}K_2\ \mathrm{Cos}\epsilon_0)$$

$$< 2\phi'$$

i.e. $da_y^2 < 2d\phi$ (4.42)

(where $S_1 = a_X^2 - a_Y^2$ and $a_X^2 + a_Y^2 = 1$.)

i.e. the intensity variation along the secondary principal--stress axes depends upon the rate of rotation and not on the parameter R. The change in the square of the amplitude (and so the intensity) will be less than 0.1 if the rate of rotation is less than 0.05 radians per one tenth of a millimeter. The above scattered light method may be taken to be valid for rates of rotation lesser than this value. Even if these assumptions are satisfied at each point, the errors involved may be cumulative and prove to be disastrous over long light paths. This sets a serious restriction on these methods. Although the above remarks are based on the solution for a special case where the ratio R is a constant, this solution holds over a length of light path even in a very general case. This makes the above remarks relevant.

Jessop[38] from his analysis concludes that the error introduced by drawing the ϵ , z graph as a smooth curve through the points obtained by measurements of the positions of the fringes will be μ $\sin^2\epsilon$ where μ is a small variable coefficient of the order $(\frac{d\phi}{d\rho})^2$. In his derivation he assumes that both the quantities $\frac{d\phi}{d\rho}$ and its derivatives are small so that

$$\cos \frac{d\phi}{d\rho} = \frac{d}{d\rho}\left(\sin\epsilon \frac{d\phi}{d\epsilon}\right) - \sin\epsilon \frac{d^2\phi}{d\epsilon d\rho}$$

$$\simeq \frac{d}{d\rho}\left(\sin\epsilon \frac{d\phi}{d\rho}\right)$$

Analysis as Applied to a Model Under Combined Tension and Torsion:

Figs. 16-25 show the plots of various quantities for the case of a model under combined tension and torsion. The model material is paraplex. The material fringe constant is 139 Psi.in./fringe. The values of shear stress are computed from the series solution, Timoshenko[42]. The integrated optical effects are computed by numerically integrating the governing optical equations in terms of Stokes parameters. Runge-Kutta-Gill method of numerical integration is used. It was found that the results didnot vary when the number of steps is increased from 50 to 100. At each step the values of the three Stokes parameters S_1 , S_2 and S_3 were found to satisfy the equation $S_1^2 + S_2^2 + S_3^2 = 1$.

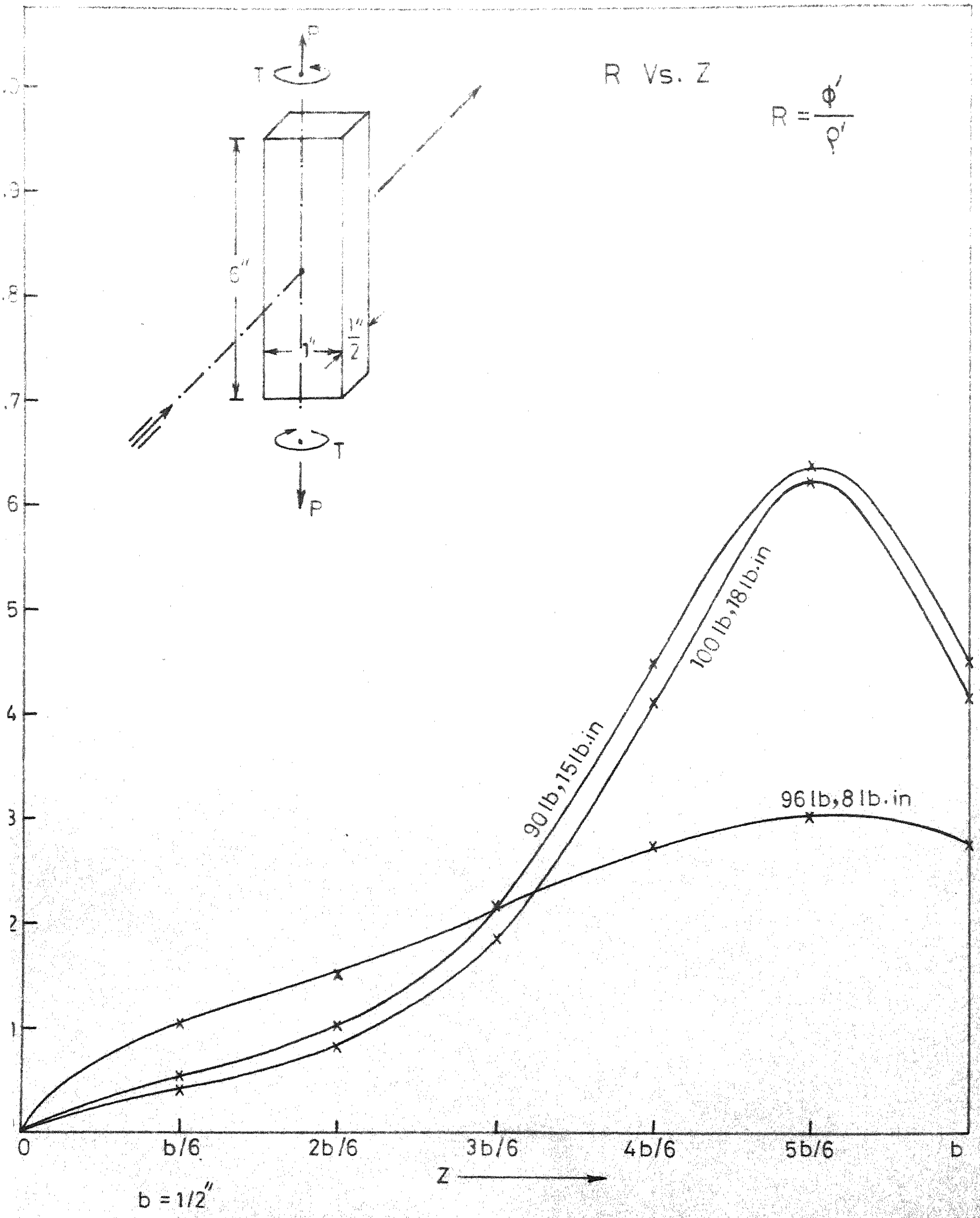

FIG. 16. VARIATION OF R ALONG THE OPTICAL PATH IN THE MODEL.

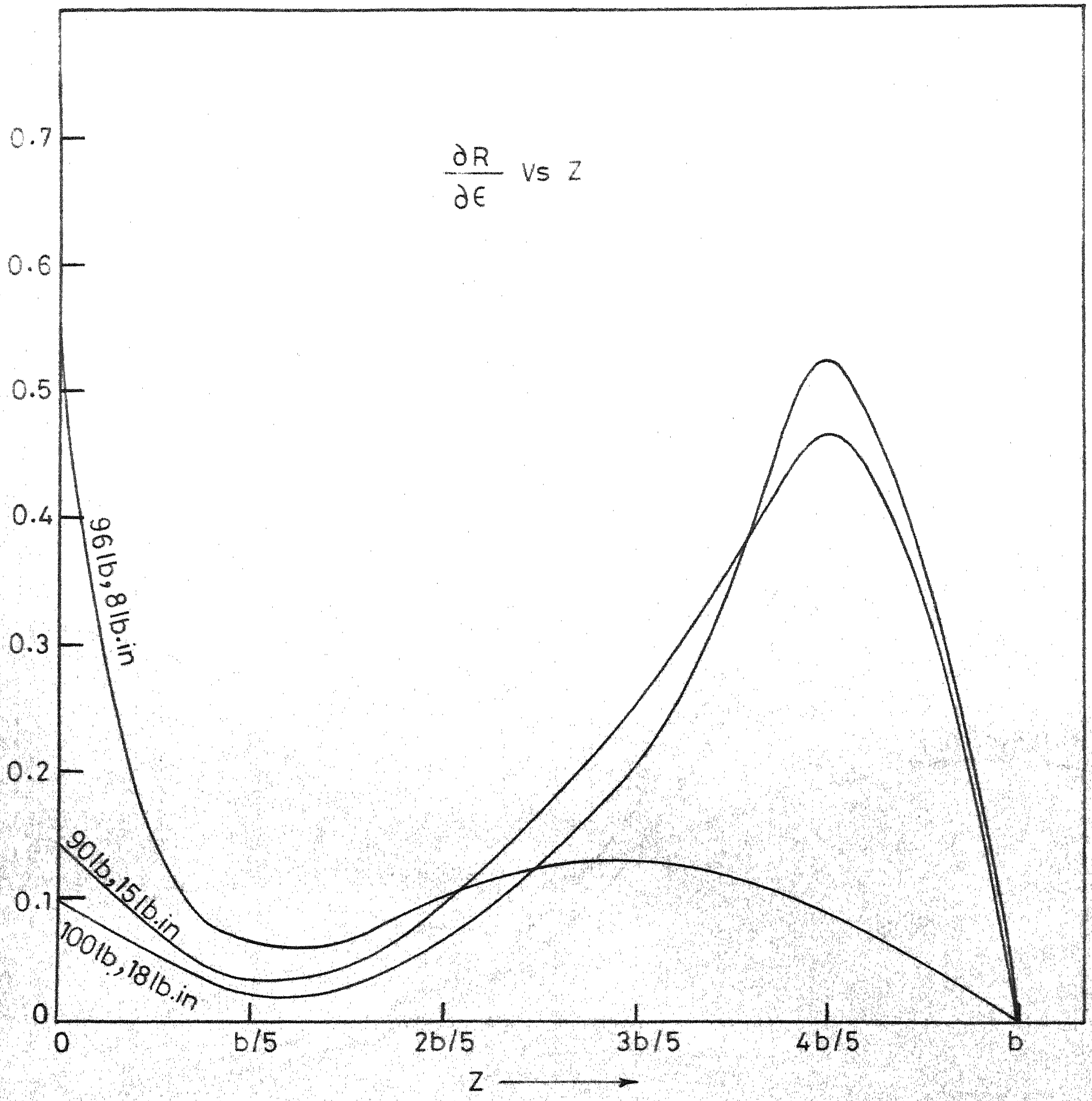

FIG.17. VARIATION OF THE QUANTITY ALONG THE WAVE NORMAL. $\left(\frac{\partial R}{\partial \epsilon}\right)$

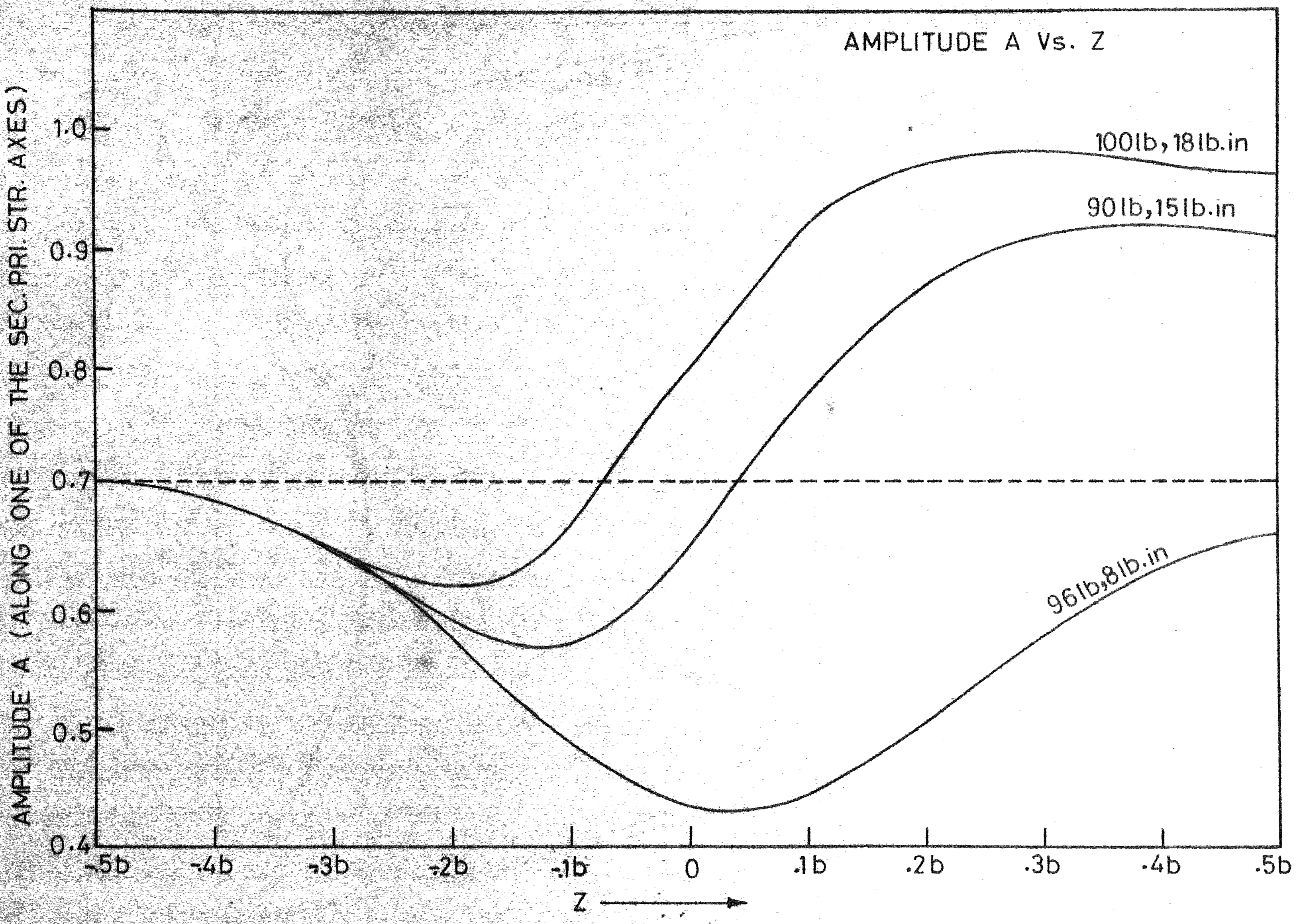

FIG. 18. VARIATION OF AMPLITUDE ALONG THE OPTICAL PATH

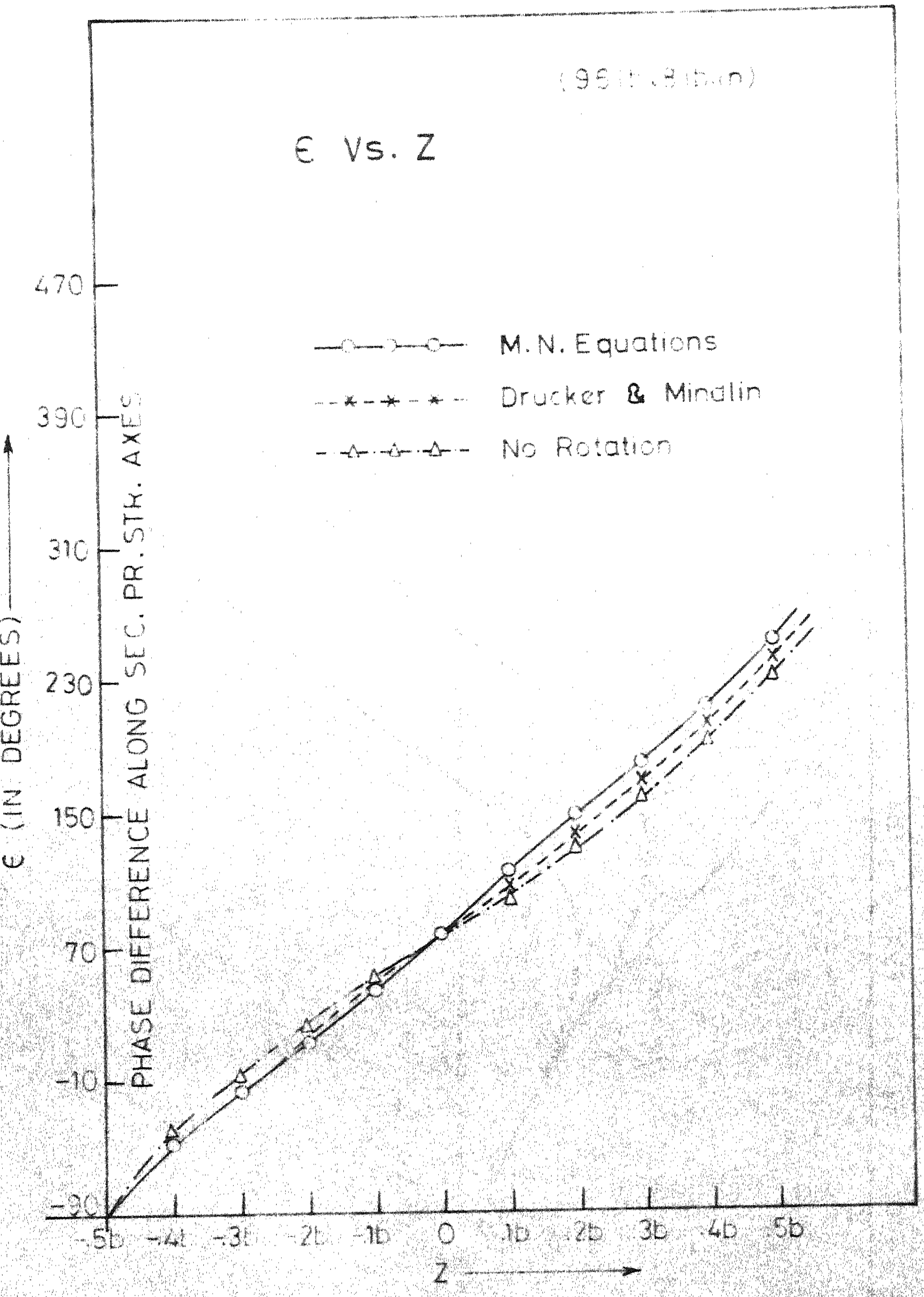

FIG.19. VARIATION OF PHASE DIFFERENCE ALONG THE OPTICAL PATH.

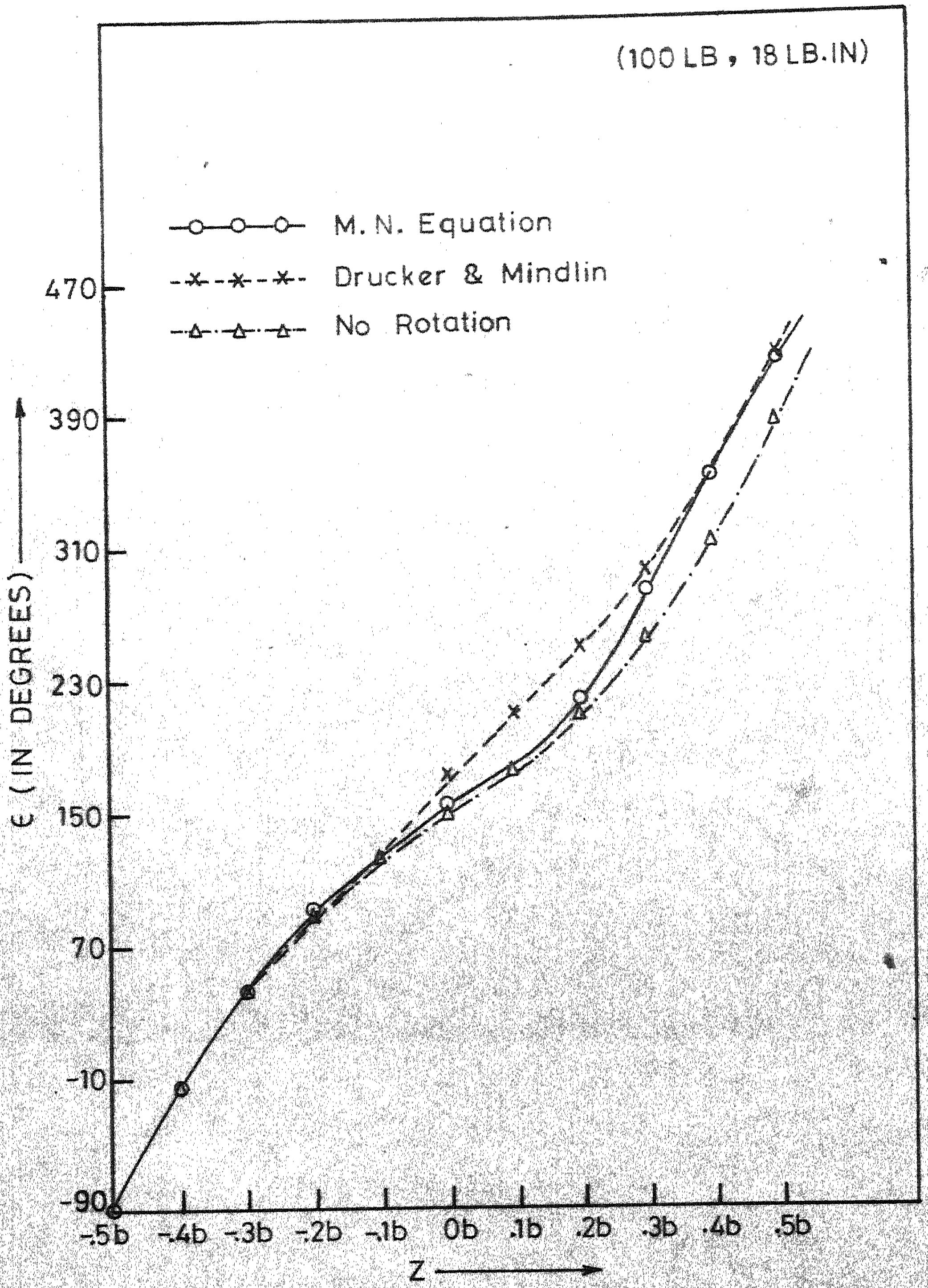

FIG. 20. VARIATION OF PHASE DIFFERENCE ϵ ALONG THE OPTICAL PATH.

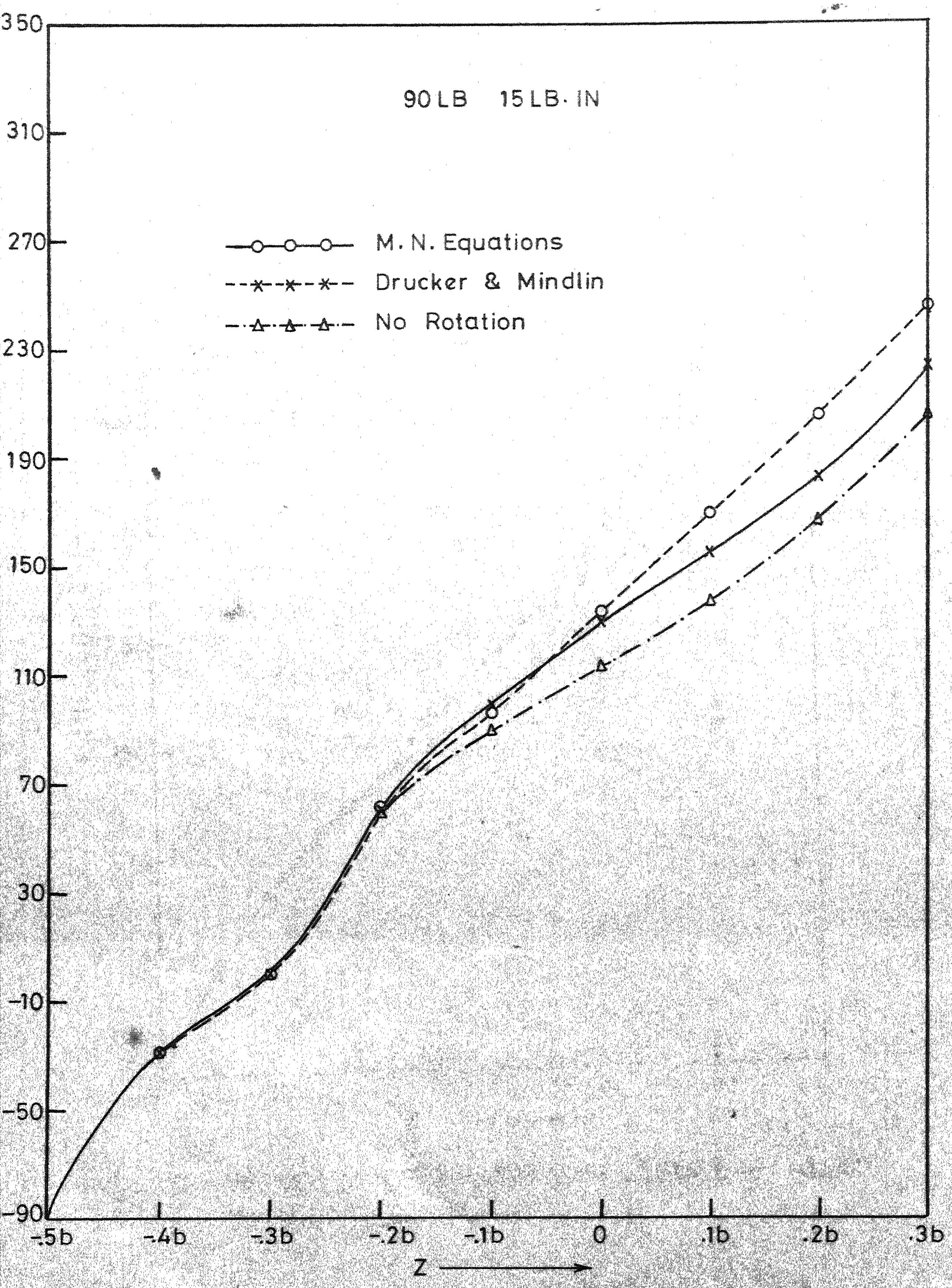

G·21. VARIATION OF PHASE DIFFERENCE ϵ ALONG OPTICAL PATH.

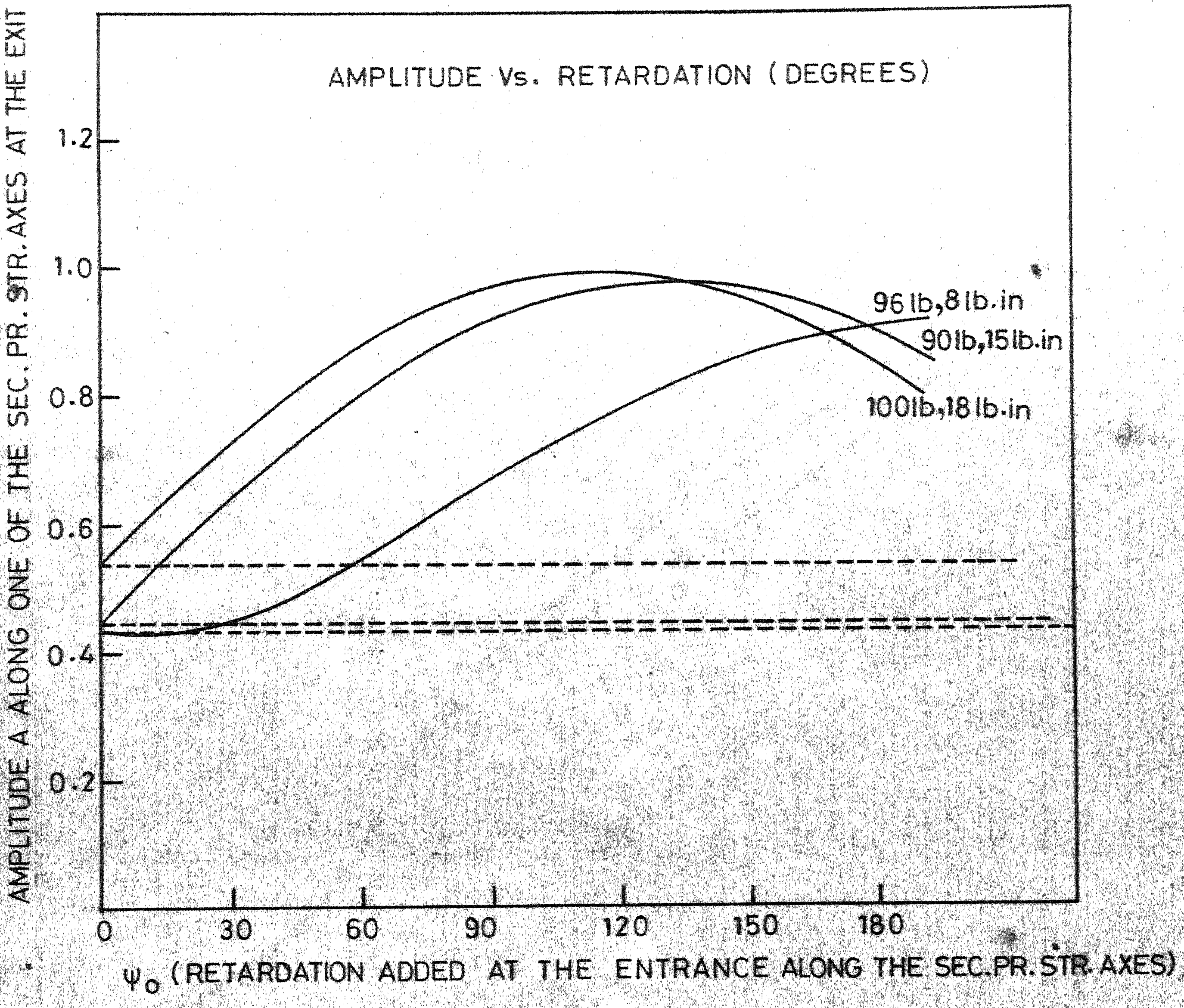

FIG. 22. VARIATION OF AMPLITUDE A WITH RETARDATION ψ_o.

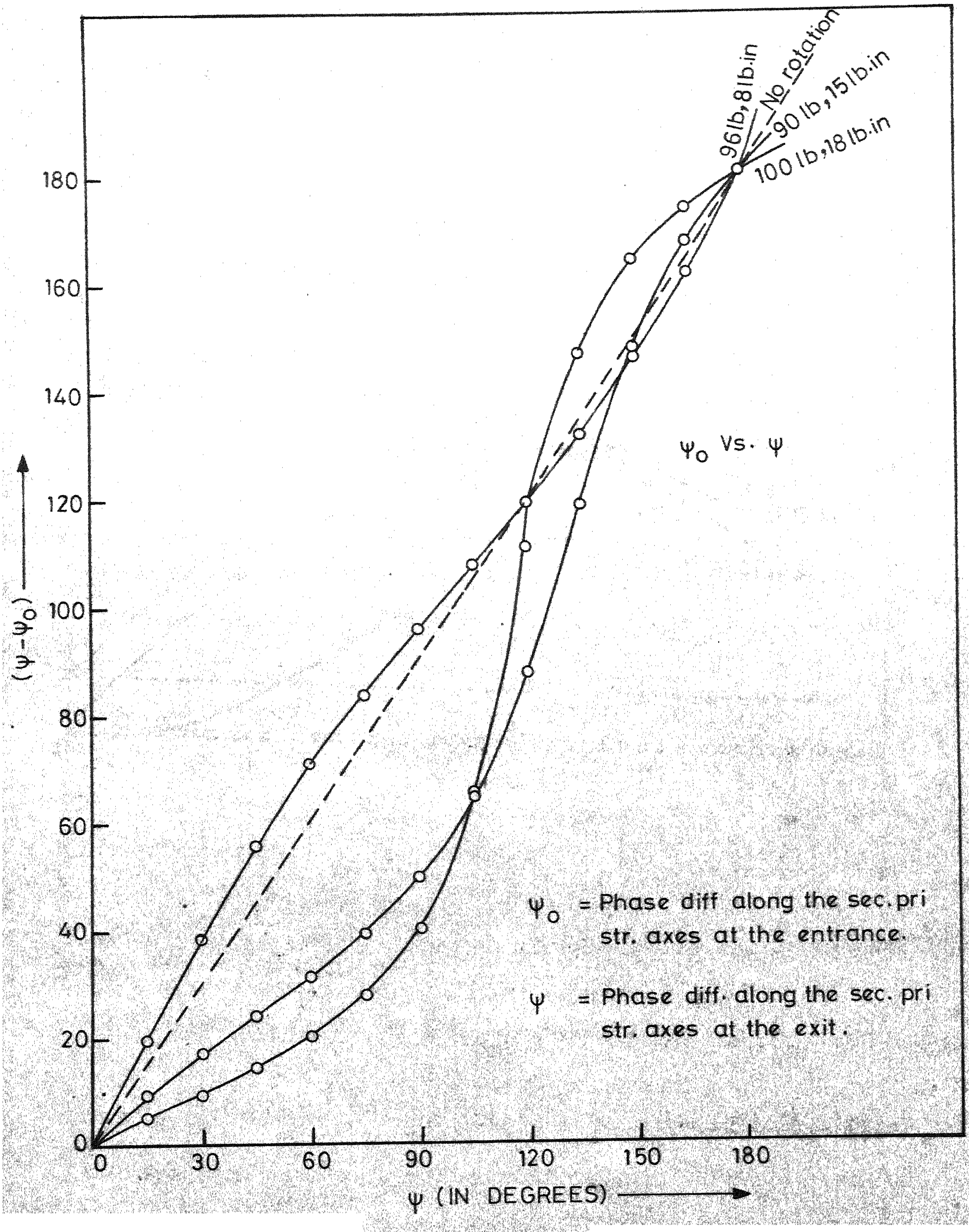
180
160
140
120
100
80
60
40
20
0
$(\psi-\psi_o)$
0
30
60
90
120
150
180
ψ (IN DEGREES)
96 lb, 8 lb.in
No rotation
90 lb, 15 lb.in
100 lb, 18 lb.in
ψ_o Vs. ψ
ψ_o = Phase diff along the sec. pri str. axes at the entrance.
ψ = Phase diff. along the sec. pri str. axes at the exit.

FIG. 23

From Figs. 16 and 17 we observe that the quantities R and $\frac{\partial R}{\partial \varepsilon}$ are of the same order of magnitude along most of the length of the light path in the model. Hence Jessop's[38] assumption of neglecting the term $\sin\varepsilon \frac{\partial R}{\partial \varepsilon}$ compared to the term $R\cos\varepsilon$ is not justified in these cases. It can be said that in general, the quantity $\frac{\partial R}{\partial \varepsilon}$ need not be small and negligible.

The conclusions of Drucker and Mindlin[18] are based on the solution for the case where ϕ' and ρ' are constants and their ratio is a small quantity. However, these conclusions cannot be extended to the general case as can be seen from Figs. 19 - 21. Fig. 19. shows that the phase difference along the secondary principal-stress axes calculating without considering the rotation is greater than that calculated with rotational effect, along some part of the optical path. This is contrary to the prediction by Drucker and Mindlin[18].

Now consider the assumptions in the methods described by Frocht and Srinath[10,11,12]. These are not satisfied for the particular loadings considered as can be seen from Figs. 22 and 23. The variation of the amplitudes along the secondary principal-stress axes with distance z along the light path is quite marked for these cases, Fig. 18. and the method described by Swinson et. al[13] is not applicable here. So, before using either of these methods, one has to check for the problem under consideration whether the rate of rotation ϕ' or the parameter R is within the limits suggested in

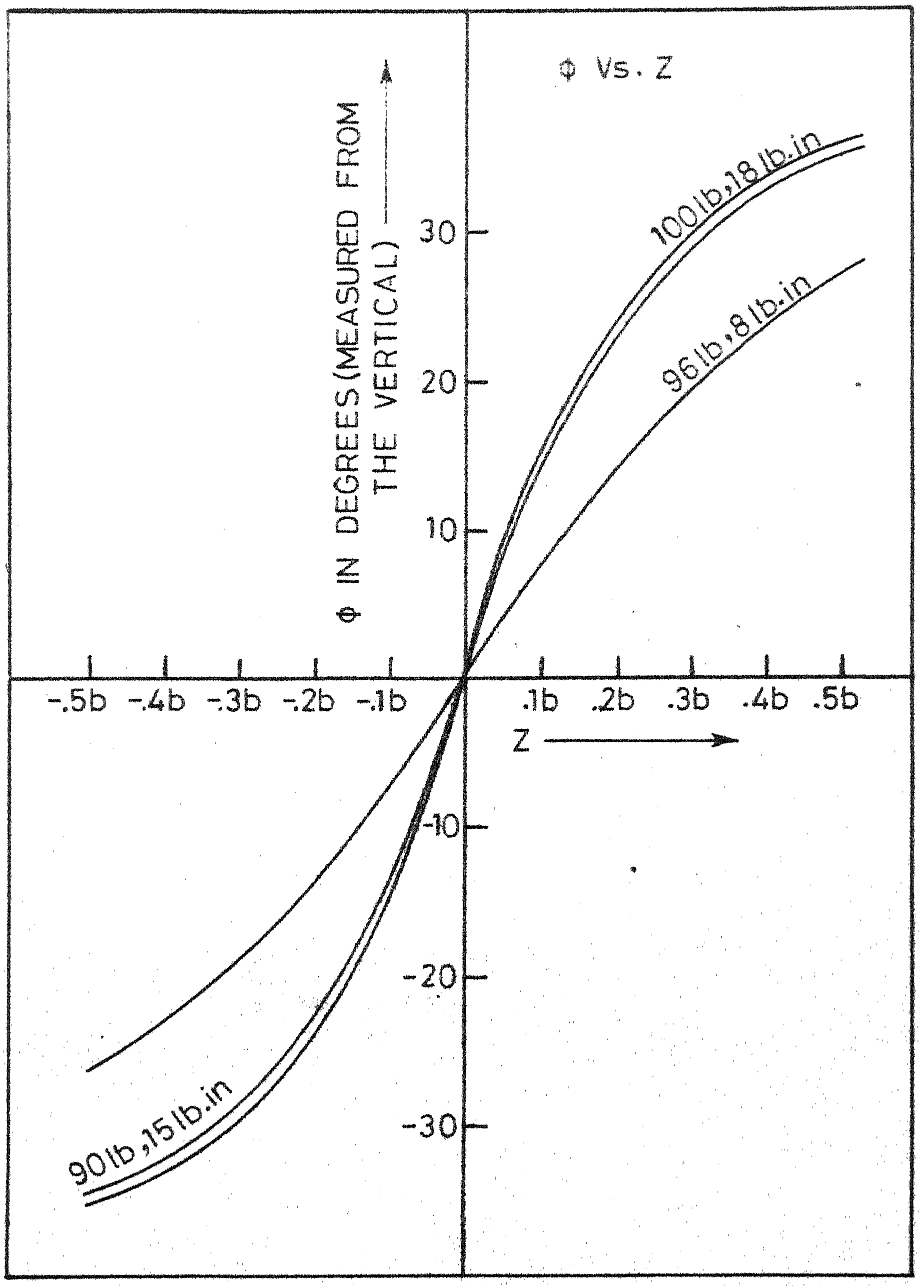

24. VARIATION OF THE SEC. PR. STR. AXES ORIENTATION ϕ ALONG THE OPTICAL PATH IN THE MODEL.

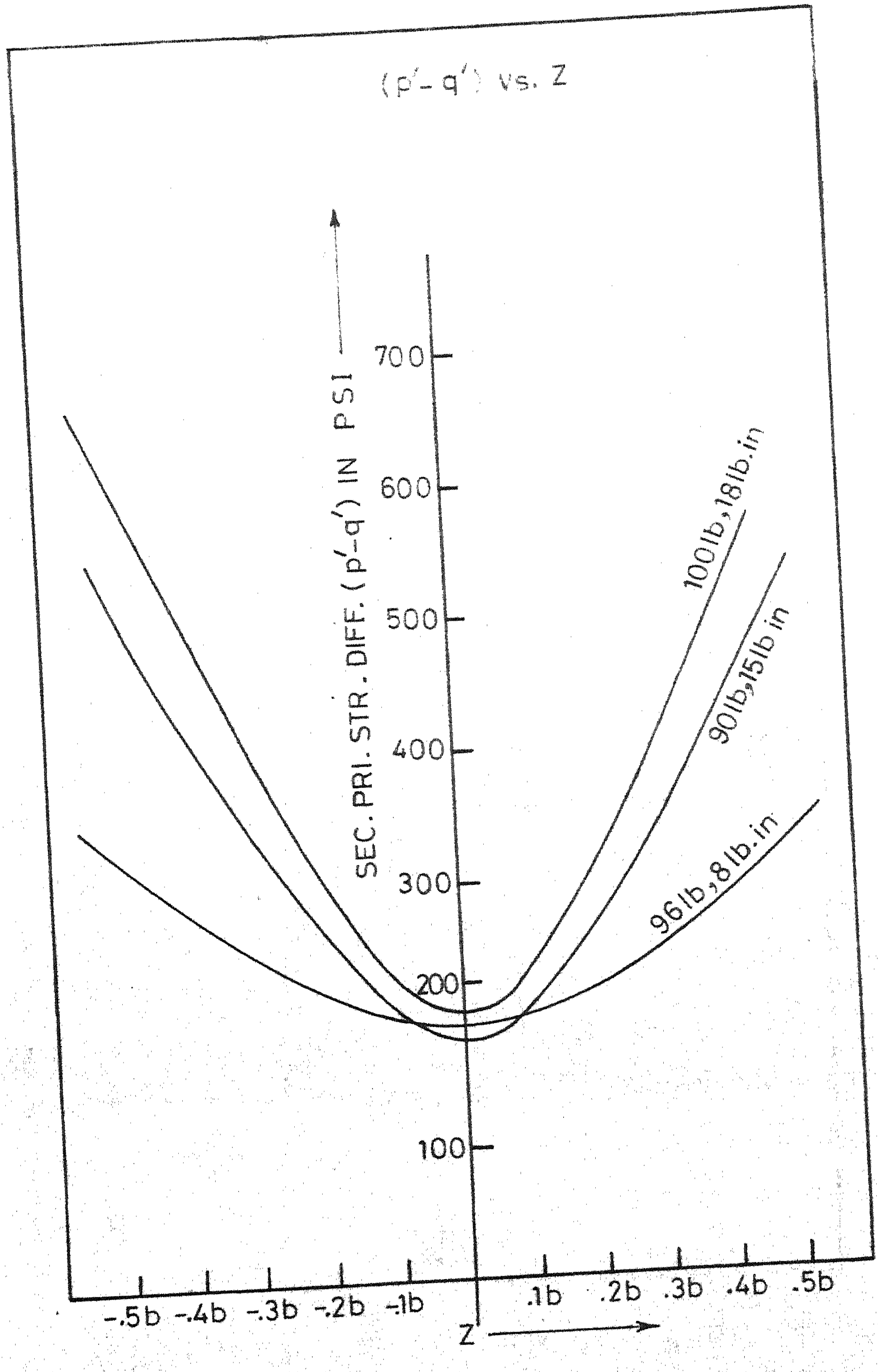
(p'- q') vs. Z
SEC. PRI. STR. DIFF. (p'-q') IN PSI
700
600
500
400
300
200
100
100lb,18lb.in
90lb,15lb.in
96lb,8lb.in
-.5b
-.4b
-.3b
-.2b
-.1b
.1b
.2b
.3b
.4b
.5b
Z

FIG · 25

the previous section. The plot of Ø Vs. z and $(p' - q')$ Vs. z are presented in Figs. 24. and 25. for reference.

The method described by Robert and Guillemet[14,15,16] doesnot involve any of these above mentioned assumptions. But the analysis here is through the characteristic parameters. This method requires the rotation of the analyser at a particular speed and some additional instrumentation.

New Methods:

It is highly desirable and useful to have methods which donot have any of these drawbacks. These methods should essentially be based on the Maxwell-Neumann equations or their equivalent forms since these are the equations available at present which describe the optical phenomena in the presence of the rotation of the secondary principal-stress axes, accurately as shown by various dynamical derivations (Chapter 2). It is now clear that at any point on the optical path in a photoelastic model under three-dimensional state of stress in general, the preferential directions (the directions which can be determined directly by experiment) are the characteristic directions and not the secondary principal-stress directions. So, in general, the secondary principal-stress axes cannot be found directly from the experimental [illegible] at a single point unless it is coupled with the data at the neighbouring points.

The scattered light technique involves the following steps: (1) measurement of scattered light intensity along different directions taking into account, the variation of the lengths of the light path involved, (ii) finding the parameters of the light ellipse and the characteristic parameters at the point under consideration and (iii) evaluating the functions $\emptyset$ and ρ using these values and the governing optical equations.

One of the methods of avoiding the error due to the variations of the length of optical path is to obtain absolute minimum (zero) intensity at the point under consideration along any particular direction (Frocht and Srinath[10,11,12]). Another method is to note the intensities along the required directions before and after the loading of the model (Cheng[40]). The former method has the drawback in that, it would not be possible to obtain the zero intensity in general, using the methods described previously because of the rotational effect. In the method described by Robert and Guillemet[14,15,16] the variation in the length of light path doesnot enter into picture.

Now, let us recall that (i) the amplitudes along directions at 45° inclination to the major axis of a light ellipse on either side are equal and (ii) any part of the light path in the model is equivalent to a system consisting of a linear retarder and a rotator. Now consider the passage of light through a system consisting of a linear retarder (retardance ρ_1, azimuth α_1) and a pure rotator of rotatory power ψ_1. The transformations through this system are given by

$$\begin{bmatrix} S_1 \\ S_2 \\ S_3 \end{bmatrix} \rightarrow \begin{bmatrix} S_1 \\ S_2\text{Cos}\rho_1 - S_3\text{Sin}\rho_1 \\ S_3\text{Cos}\rho_1 + S_2\text{Sin}\rho_1 \end{bmatrix} \rightarrow \begin{bmatrix} S_1\text{Cos}2\psi + \text{Sin}2\psi(S_2\text{Cos}\rho_1 - S_2\text{Sin}\rho_1) \\ (S_2\text{Cos}\rho_1 - S_3\text{Sin}\rho_1)\text{Cos}2\psi - S_1\text{Sin}2\psi \\ S_3\text{Cos}\rho_1 + S_2\text{Sin}\rho_1 \end{bmatrix} = \begin{bmatrix} \bar{S}_1 \\ \bar{S}_2 \\ \bar{S}_3 \end{bmatrix} \qquad (4.42)$$

$V = (S_1, S_2, S_3)$ is the Stokes vector of the incident light referred to the axes of the linear retarder $\bar{V} = (\bar{S}_1, \bar{S}_2, \bar{S}_3)$ is the Stokes vector of the light at the exit of the system referred to some arbitrary set of axes $\psi = (\alpha - \psi_1)$ where α is the angle between the set of arbitrary axes X', Y' chosen and the axes of the linear retarder.

Also ,

$\bar{S}_1 = a^2_{X'} - a^2_{Y'}$ where $a_{X'}$, $a_{Y'}$ are the amplitudes of the components of light along the X', Y' axes.

So,

$$\bar{S}_1 = a^2_{X'} - a^2_{Y'} = S_1\text{Cos}2\psi + (S_2\text{Cos}\rho_1 - S_3\text{Sin}\rho_1)\,\text{Sin}2\psi$$

Consider now, the following cases:

1) (a) $S_1 = S_2 = 0,\ S_3 = 1,\quad \bar{S}_1 = a^2_{X'} - a^2_{Y'} = -\text{Sin}\rho_1\ \text{Sin}2\psi$

(b) $S_1 = S_2 = 0,\ S_3 = -1,\quad \bar{S}_1 = a^2_{X'} - a^2_{Y'} = \text{Sin}\rho_1\ \text{Sin}2\psi$

2) (a) $S_1 = \text{Cos}2\beta,\ S_2 = \text{Sin}2\beta,\ S_3 = 0,\ \bar{S}_1 = (\text{Cos}2\beta\ \text{Cos}2\psi + \text{Sin}2\beta\ \text{Cos}\rho_1\ \text{Sin}2\psi)$

(b) $S_1 = \text{Cos}2(\beta + \frac{\pi}{2})$, $S_2 = \text{Sin}2(\beta + \frac{\pi}{2})$, $S_3 = 0$,

$\overline{S}_1 = - \text{Cos}2\beta\ \text{Cos}2\psi - \text{Sin}2\beta\ \text{Cos}\rho_1\ \text{Sin}2\psi$

3) (a) $S_1 = 0$, $S_2 = \text{Cos}\epsilon$, $S_3 = \text{Sin}\epsilon$, $\overline{S}_1 = \text{Sin}2\psi(\text{Cos}\epsilon_1\ \text{Cos}\rho_1$

$- \text{Sin}\epsilon\ \text{Sin}\rho_1)$

$= \text{Cos}(\epsilon + \rho_1)\ \text{Sin}2\psi$

(b) $S_1 = 0$, $S_2 = \text{Cos}(\epsilon + \pi)$, $S_3 = \text{Sin}(\epsilon + \pi)$

$\overline{S}_1 = - \text{Sin}2\psi\ \text{Cos}(\epsilon + \rho_1)$

We note that by changing the incident Stokes parameters from the case (a) to those of case (b), the sign of the first Stokes parameter of the light at exit is reversed. This means that, if the amplitudes along the X' axis is $a_{X'}$ in case (a), it will become $a_{Y'}$ in case (b). This is true for any direction of observation since the angle α is taken to be arbitrary. We are thus able to obtain the component $a_{Y'}$ along the axis X'. This can be achieved in many more ways. But the above mentioned ways can be said to be representative of the rest. Of these again, the first two cases (1) and (2) are of inportance since these donot require the knowledge of the primary characteristic directions. In case (1), right circularly polarized light is converted into left circularly polarized light at the entrance. This can be achieved by introducing a half-wave plate or by rotating the quarter-wave plate after the polarizer through 90°. In case (2), the polarizer is rotated through 90°. Using these results, we have the following scattered light techniques.

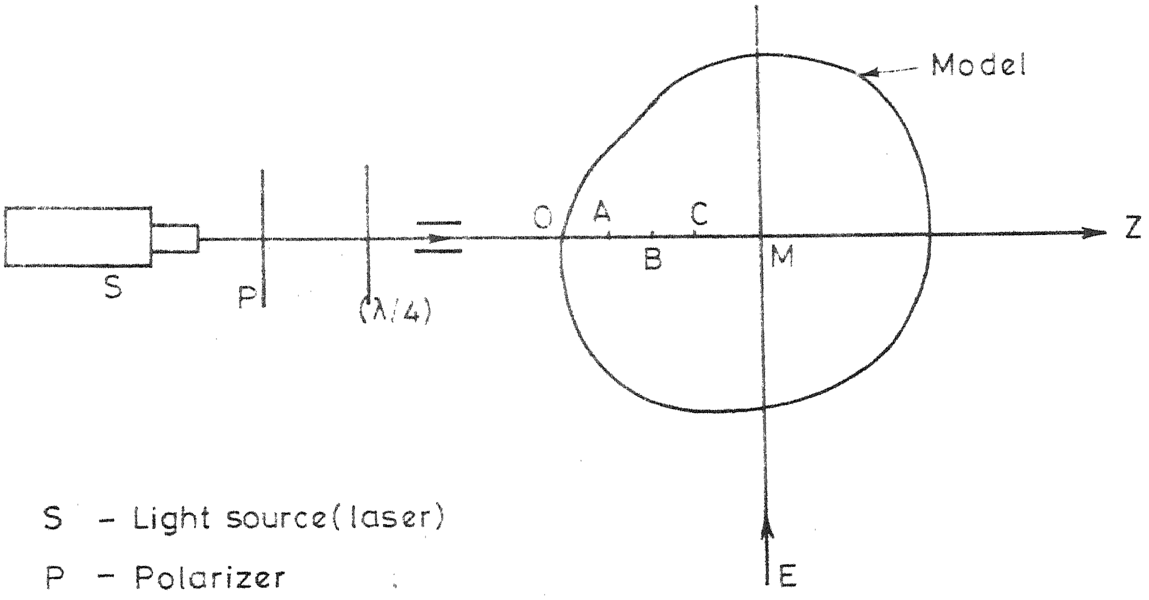

S – Light source(laser)

P – Polarizer

(λ/4)– Quarter-wave plate

EM – Direction of observation

FIG. 26. SCATTERED LIGHT TECHNIQUE WITH THE MODEL ACTING AS AN ANALYSER.

(1) The Model Acts As an Analyser

A schematic diagram of the set up is shown in Fig. 26.

Method (a)

Let the incident light be right circularly polarized. Note the intensity I_1 along the direction of observation EM at the point under consideration M. Now make the incident light left circularly polarized and note the intensity I_2. Now change the direction of observation until $I_1 = I_2$.

If I_1 corresponds to an amplitude of a_X, then I_2 corresponds to a_Y where $a_X^2 + a_Y^2 = 1$. When, the condition $a_X = a_Y$ is obtained, it means that the direction of observation is making an angle of 45° with the major axis of the light ellipse at the point under consideration. So the final position of the direction of observation will then correspond to one of the secondary characteristic directions (for the light path OM). Now keep the direction of observation in this position, rotate the polarizer (after removing the quarter-wave plate) until the intensity of light becomes zero. The final positions of the axes of the polarizer are the primary characteristic directions. Now, keep the axes of the quarter-wave plate 45° to the primary characteristic directions and the direction of observation 45° to one of the secondary characteristic directions. Rotate the polarizer until the intensity observed is zero. Then the characteristic retardation will be equal to 2α where α is the angle between the axes of the polarizer and the quarter-wave plate (inverse Tardy method, Cheng[43]). This is so since the zero intensity (corresponding to plane polarized light) will be obtained at the point under consideration only if the retardation in the linear retarder of the equivalent system is nullified at the entrance.

The total optical path in the model can be broken into small segments so that each segment can be represented by a single linear retarder. The axes of these retarders can be taken to be the directions of the secondary principal-stress axes at the middle points of the corresponding segments. The secondary principal-stress difference can be calculated from the retardance of this linear retarder. Consider the segment AB of the optical path, Fig. 26. First find the characteristic parameters for the optical path OA as described above. Keep the axes of the quarter-wave plate at 45° to the primary characteristic directions. Keep the angle between the axes of the polarizer and quarter-wave plate as $(\pi/4 - \alpha/2)$ so that we have circularly polarized light (say right handed) at the point A. Note the intensity I_1 along any direction at the point B. Now change the light at the point A from right handed to left handed circularly polarized light by rotating the polarizer through 90° and then note the intensity I_2. Change the direction of observation until $I_1 = I_2$. The final direction of observation corresponds to one of the secondary principal-stresses in the region AB. To find the retardation corresponding to the segment AB, nullify the effect of the equivalent system for the optical path OA. Let the characteristic parameters of this equivalent system be θ_1 (primary characteristic direction), ρ (characteristic retardation) and ψ_1 (rotatory power). Now keep a compensator at the entrance with its axes along these primary characteristic directions and with a retardation of $-\rho$. Keep the axes of the quarter-wave plate along a direction making an angle of $(\pi/4 - \psi_1)$ with secondary principal-stress directions of the segment AB. Fix the direction of observation along a direction making an angle of $\pi/4$ with these secondary principal-stress axes. Now rotate the polarizer until the intensity is minimum. If the angle between the axes of the polarizer (in the final position) and the quarter-wave plate is α, then the retardation corresponding to the segment AB is -2α.

The orientation and difference of the secondary principal-stresses can also be found from the characteristic parameters using the governing optical equations referred to some fixed axes, Eqs. (2.42) - (2.44). For a particular incident light the three Stokes parameters S_1, S_2 and S_3 with respect to some fixed axes are found at each point using the characteristic parameters determined experimentally. The derivatives S_1', S_2' and S_3' (with respect to the distance z along the optical path) are also found. Then from Eqs. (2.42) - (2.44)

$$\tan 2\phi = -\frac{S_1'}{S_2'}$$

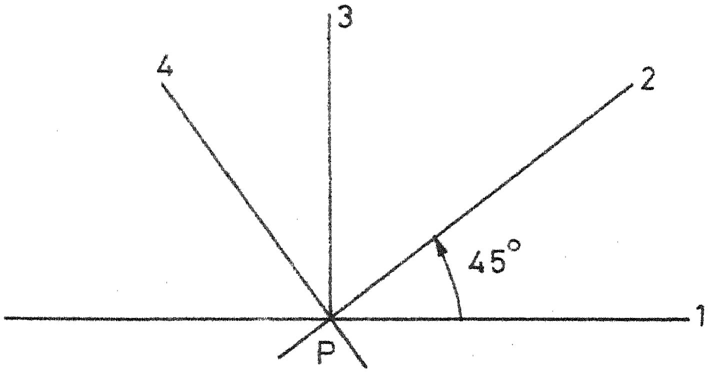

FIG. 27. SCATTERED LIGHT OBSERVATION ALONG TWO SETS OF AXES 45° APART.

and

$$\rho' = \frac{S_1'}{S_3 \mathrm{Sin} 2\phi}$$

(b) Determination of Characteristic Parameters From the Measurement of Intensities Along Two Directions 45° Apart

Consider any point **P** on the optical path in the model. Choose two directions which are 45° apart and denote these by the numbers 1 and 2, Fig. 27. Let the incident light be circularly polarized. Note the intensities I_1 and I_2 along these directions.

We then have

$$I_1 = K_1 \; a_1^2$$

$$I_2 = K_2 \; a_2^2$$

where K_1, K_2 are constants which take into account the absorption through the corresponding lengths of scattered light paths. Now make the incident light left circularly polarized and note the intensities I_1' and I_2' along the directions 1 and 2.

$$I_1' = K_1(1 - a_1^2)$$

$$= K_1 \; a_3^2$$

and

$$I_2' = K_2(1 - a_2^2)$$

$$= K_2 a_4^2$$

So $$I_1 + I_1' = K_1$$

and $$I_2 + I_2' = K_2$$

Now consider the Stokes vector transformation when the reference axes are rotated through 45°.

$$\begin{bmatrix} \cos 2\omega \cos 2\alpha \\ \cos 2\omega \sin 2\alpha \\ \sin 2\omega \end{bmatrix} = \begin{bmatrix} S_1 \\ S_2 \\ S_3 \end{bmatrix} \rightarrow \begin{bmatrix} S_2 \\ -S_1 \\ S_3 \end{bmatrix}$$

i.e. in this transformation the first and second Stokes vectors are interchanged with a sign change.

Also

$$S_1^2 + S_2^2 = \cos^2 2\omega$$

$$S_1 = a_1^2 - a_3^2 = \frac{I_1 - I_1'}{K_1} = \frac{I_1 - I_1'}{I_1 + I_1'}$$

$$S_2 = a_2^2 - a_4^2 = \frac{I_2 - I_2'}{K_2} = \frac{I_2 - I_2'}{I_2 + I_2'}$$

$$S_1^2 + S_2^2 = \left[\frac{I_1 - I_1'}{I_1 + I_1'}\right]^2 + \left[\frac{I_2 - I_2'}{I_2 + I_2'}\right]^2$$

$$= \cos^2 2\omega$$

$$\frac{S_2}{S_1} = \tan 2\alpha = \frac{(I_2 - I_2')(I_1 + I_1')}{(I_2 + I_2')(I_1 - I_1')}$$

The characteristic retardation ρ of the equivalent system (for the optical path from the point of entrance of the beam into the model to the point P) is given by

$$\rho = (2\omega - \pi/2)$$

The orientation of the secondary characteristic direction $= \alpha \pm \pi/4$.

To find the primary characteristic directions rotate the polarizer (with the quarter-wave plate out of field) at the entrance to the model until the condition

$$S_1^2 + S_2^2 = \left[\frac{I_1 - I_1'}{I_1 + I_1'}\right]^2 + \left[\frac{I_2 - I_2'}{I_2 + I_2'}\right]^2 = 1$$

is satisfied.

The final positions of the axes of the polarizer correspond to the primary characteristic directions. Alternatively, keep the angle between the axes of the polarizer and the quarter-wave plate equal to $(\pi/4 - \rho/2)$ and rotate them in unision until $\frac{I_1}{K_1} = \frac{I_2}{K_2}$ (K_1 and K_2 are already known). When this condition is satisfied, the light ellipse at the point P is circularly polarized and so the final directions of the quarter-wave plate axes will be at 45° to the primary characteristic directions.

In Appendix A are described two more scattered light techniques, (i) determination of characteristic parameters when the direction of observation is fixed and (ii) a whole field method.

(2) Scattered Light Technique Where the Model Acts As a Polarizer:

A schematic diagram of the set up is shown in Fig. 28.

The technique to be described is essentially an extension of the intensity calibration method for the determination of characteristic parameters (Chapter 3). Let the angle between the axes of the quarter-wave plate and analyser be 45°, Fig. 28. Note the intensity I_1. Rotate the analyser through 90° and again note the intensity I_2. Rotate the model or the incident light beam about the direction of observation DM_1 until $I_1 = I_2$. The final position of the incident beam corresponds to one of the primary characteristic directions. The reasoning is as follows.

The intensities I_1 and I_2 are the intensities of the components of light vector along two mutually perpendicular directions. If these are equal, this means that the light ellipse before the analyser has its major and minor axes along the axes of the quarter-wave plate so that before this plate the light is plane polarized. The corresponding position of the light beam is one of the primary characteristic directions. To find the secondary characteristic directions remove the quarter-wave plate and rotate the analyser for minimum intensity. In the final position, the axes of the analyser are along the secondary characteristic directions. Now keep the light beam and the quarter-wave plate axes at 45° to the primary and secondary characteristic directions respectively. In this case the amplitudes of light components along the primary characteristic directions are equal and so the amplitudes of light components along the secondary characteristic directions are equal at the exit of the scattered light path in the model. The light ellipse at the exit has its major and minor axes along the axes of the quarter-wave plate. Now rotate the analyser for minimum intensity and let the axes of the analyser in this position make an angle α with the axes of the quarter-wave plate. The ellipticity of the light ellipse before the quarter-wave plate is $\tan\alpha$. The phase angle along the secondary characteristic directions is 2α so that $\rho = 2\alpha$ where ρ is the characteristic retardation of the optical path $M_n M_1$, Fig.28. The characteristic parameters of the equivalent systems for the optical paths $M_2 M_1$, $M_3 M_1$, ...$M_n M_1$, ... etc. are thus found. Using this data and the governing optical equations, the difference and the directions of the secondary principal-stresses are found as described earlier.

In this chapter, we have discussed the assumptions involved in some of the previous scattered light methods. This is done using the analytical solution obtained for the case where the rate of rotation is arbitrary, but the ratio $R = \phi'/\rho'$ is a constant and numerical results for optical phenomena for some loadings of a rectangular model under combined tension and torsion. For the cases shown, the scattered light methods developed by Frocht and Srinath and Swinson et. al. are found to be inadequate. Five methods of scattered light experimentation and analysis are described which neither involve any assumptions nor the rotation of analyser at a particular speed as in the method described by Robert and Guillemet. Of these, method 1(b) which involves the measurement of intensities along axes 45° apart is a very fast method of determining the characteristic parameters at various points, if the computation of the products and quotients of the measured intensities is made automatic. As nondestructive techniques these methods hold high potentiality for three-dimensional stress analysis.

CHAPTER 5

MISCELLANEOUS TOPICS

Introduction:

In the previous chapters methods have been described to determine the characteristic parameters for an optically equivalent system either for a series of retarders or for any optical path in a photoelastic model under a three-dimensional state of stress. Using the concept of light ellipse and Stokes parameters, we shall investigate three additional topics in photoelasticity, namely: A. The Graphical Methods, B. The Theory of Compensation and C. Determination of Integral Fringe Orders In Photoelasticity. These topics are useful in the general three-dimensional photoelastic analysis.

A. Graphical Methods in Photoelasticity

Graphical methods in photoelasticity are essentially pictorial representations of the changes in the parameters of the light ellipse as it passes through a photoelastic model, or the polariscope elements. These are useful (i) in finding the changes in the light ellipse parameters as the polarized light passes through various polariscope elements, without cumbersome calculations, (ii) in finding the characteristic parameters of a particular light path in a three-dimensional photoelastic model or for a series of linear retarders and (iii) in estimating the effects of various errors in the elements of the polariscope (ex: error in the orientation of the axes of the polarizer, deviation of the retardation of the quarter-wave plate from $\pi/2$ etc.). Most of the existing graphical methods are derived from the Poincare'[23] sphere (see Chapter 3) representation of polarized forms. After a brief description of the graphical methods described by Jerrard[24], Robert and Guillemet[14,15,16], Kuske[25], Schwieger[26] and Cernosek[27], we shall describe a new and simpler approach to graphical methods.

Jerrard[24] has given a detailed account of Poincare' sphere representation, its derivation and plane representation of the polarized light by using conformal transformation. Robert and Guillemet[14,15,16] also have discussed these. In the derivation of the Poincare' sphere representation the light vibration is first represented in a complex plane. The most general type of polarized light can be represented by a combination of two simple harmonic motions along the axes OX and OY as:

$$x = a_X \text{ Cos } (\bar{\omega} t + \epsilon_X) = \text{Real } Ae^{i\bar{\omega} t} \qquad (5.1)$$

with $A = a_X e^{i\epsilon_X}$

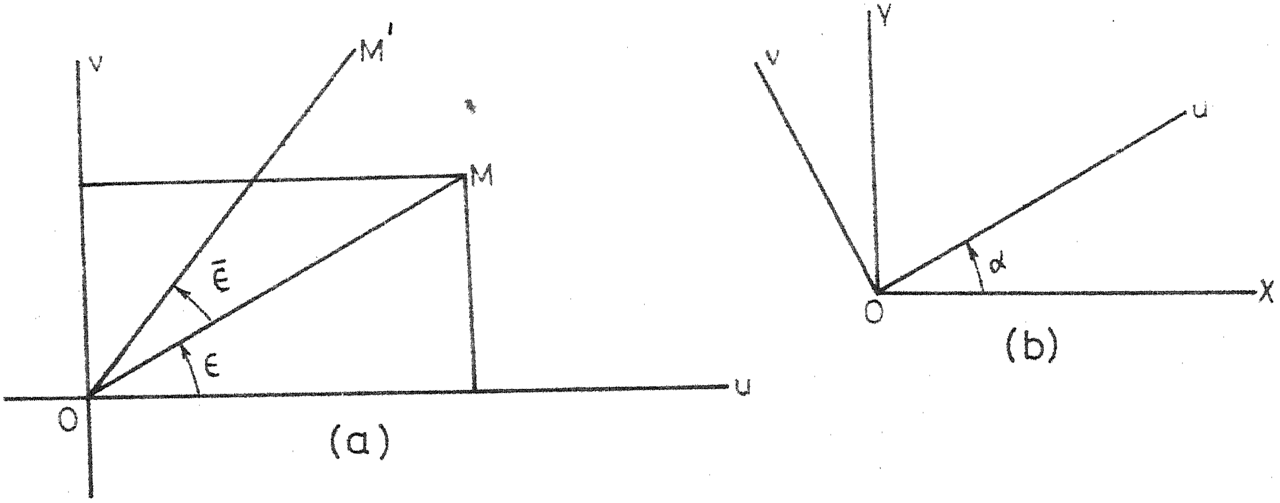

FIG. 29. REPRESENTATION OF POLARIZED LIGHT FORMS IN A COMPLEX PLANE.

$$y = a_Y \cos(\bar{\omega} t + \varepsilon_Y) = \text{Real} \quad B e^{i\bar{\omega} t} \qquad (5.2)$$

$$\text{with } B = a_Y e^{i\varepsilon_Y}$$

where $\bar{\omega}$ is the angular frequency, t is the time and ε_X, ε_Y are the phase angles.

The ratio B/A is in general a complex quantity and can be written as:

$$W = B/A = u + iv = \frac{a_Y}{a_X} e^{-i(\varepsilon_X - \varepsilon_Y)} = \tan\theta(\cos\varepsilon + i \sin\varepsilon) \qquad (5.3)$$

$$\text{where} \quad \tan\theta = \frac{a_Y}{a_X}; \varepsilon = \varepsilon_Y - \varepsilon_X$$

tan θ is the ratio of the amplitudes of the components of vibrations along the reference axes OX and OY, Fig. 29, and ε is the difference between the phase angles of these components. So, any general type of polarized light can be represented by a complex quantity B/A = u + iv as described above. This is represented by point M in the complex plane u - v, Fig. 29(a).

$$OM = \frac{a_Y}{a_X} \quad \text{Amplitude ratio}$$

The inclination ε of OM with the u axis is the relative phase difference. If this phase difference is increased by $\bar{\varepsilon}$, the point M moves to M' where $OM = OM'$ and $MOM' = \bar{\varepsilon}$. In this mapping, all points on the real axis represent linear vibrations since in this case, the phase angle ε (inclination of OM with the u axis when M is on the u axis) is zero. The length of OM again represents the ratio of the amplitudes along the reference axes OX and OY. If B/A is purely imaginary, the representative point M lies on the imaginary axis, the phase difference ϵ is $\pi/2$ and so the major and minor axes coincide with the reference axes OX and OY. (Because, with respect to the major and minor axes the phase difference is $\pi/2$.) Right hand vibrations in which the OY vibration leads the OX vibration, are represented by points above and left handed vibrations by points below the real axis. Thus the amplitude ratio and the phase difference of a particular light ellipse referred to a particular set of axes, can be represented in the complex plane. It will however be useful if the ellipticity and the azimuth of the light ellipse (with respect to a particular set of axes) are also represented in this mapping. For this consider an elliptic vibration with ellipticity b/a and azimuth α (with reference to the axes X,Y), Fig. 29(b). This can be defined in terms of the vibration along the axes u,v (i.e. the major and minor axes are along the u,v axes), so

$$u = a \operatorname{Cos} \bar{\omega} t$$

$$v = b \operatorname{Sin} \bar{\omega} t$$

$$b/a = e = \text{ellipticity}$$

Resolving along the axes OX and OY, we have, component along the OX axis = x

$$= (a \operatorname{Cos} \bar{\omega} t \operatorname{Cos}\alpha - b \operatorname{Sin}\bar{\omega} t \operatorname{Sin}\alpha)$$

$$= \text{Real} \left[(a \operatorname{Cos}\alpha + i\, b \operatorname{Sin}\alpha)\, e^{i\bar{\omega}t} \right] \qquad (5.4)$$

$$\left.\begin{array}{l}\text{Component along}\\ \text{the OY axis}\end{array}\right\} = y\,(a \cos\bar{\omega}t \sin\alpha + b \sin\bar{\omega}t \cos\alpha)$$

$$= \text{Real}\left[(a \sin\alpha - i\, b \cos\alpha)\, e^{i\bar{\omega}t}\right] \qquad (5.5)$$

Comparing these equations with Eqs. (5.1) - (5.3), we obtain,

$$w = \frac{a \sin\alpha - i\, b \cos\alpha}{a \cos\alpha + i\, b \sin\alpha}$$

$$= \frac{\tan\alpha - i\, e}{1 + i\, e \tan\alpha}$$

This equation is a special form of the bilinear transformation

$$w = \frac{a + bt}{c + dt} \qquad (5.6)$$

with $ad \neq bc$ (condition for conformality)

In this conformal transformation circles and straights lines are mapped into circles and straight lines.

(a) Mapping of Light Ellipses of Constant Orientation (α = Constant) and Varying Ellipticity ($-\infty < e < \infty$)

$$w = \frac{\tan\alpha - i\, e}{1 + i\, e \tan\alpha}$$

$$= u + i\, v$$

$$= \frac{\tan\alpha\,(1 - e^2) - i\, e\,(1 + \tan^2\alpha)}{(1 + e^2 \tan^2\alpha)}$$

so that $u = \dfrac{(1 - e^2)\tan\alpha}{1 + e^2 \tan^2\alpha}$

$$u \to 0 \text{ as } \alpha \to 0 \text{ or } \pi/2 \qquad (5.7)$$

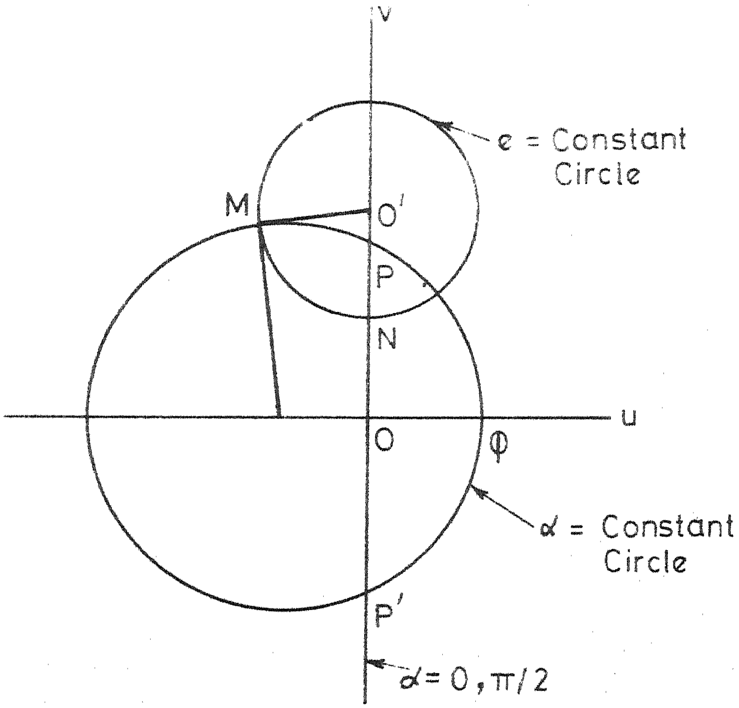

FIG. 30. CONSTANT ELLIPTICITY (e) AND CONSTANT AMPLITUDE RATIO CIRCLES IN THE CONFORMAL MAPPING.

and $$v = \frac{-e(1+\tan^2\alpha)}{(1+e^2\tan^2\alpha)}$$

$$v \rightarrow -e \text{ or} -1/e \quad \text{as} \quad \alpha \rightarrow 0 \quad \text{or} \quad \pi/2$$

Now consider two values of e i.e. $e_1 = e$ and $e_2 = -e$, then for these values (with same α), the values of u are the same where as the values of v are equal in magnitude but opposite in sign. So, the mapping is symmetrical about the u - axis. Also u varies with e so that it can take nonzero values also (if $\alpha \neq 0, \pi/2$). Therefore, the mappings of constant azimuth α light vibrations are circles with centers on the u - axis. (when $\alpha = 0$ or $\pi/2$, this degenerates into a straight lines, the v - axis). Also $u = 0$ and $v = \pm 1$ if $e = \pm 1$ irrespective of the values of α. Therefore, all the circles pass through the points P(0,1) and P'(0, - 1), Fig. 30.

(b) Mapping of Light Vibrations of Constant Ellipticity e and Varying azimuth α

Consider two values for tan α in Eqs. (5.7) i.e. for $\tan\alpha_1 = f$ and $\tan\alpha_2 = -f$ (e is same for both). For mappings of both these vibrations the values of v are the same, but the values of u are equal in magnitude but opposite in sign. Hence these mappings are symmetrical about the v - axis. Also v varies with α if $e \neq 0$ so that it takes nonzero values also. Therefore, these mappings are circles with their centers on the v - axis. When $e = 0$, this degenerates into a straight line, the u axis.

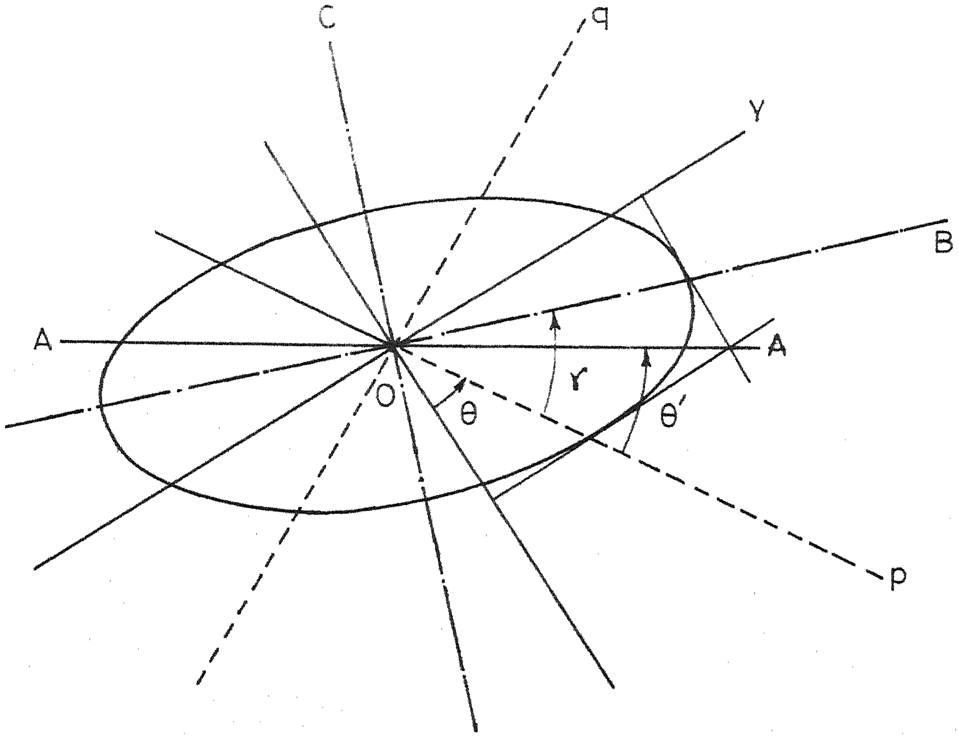

FIG. 31. KUSKE'S J CIRCLE METHOD

These two families of circles are 'orthogonal since $OP.\ OP' = ON.\ ON' = 1$. Thus, if a vibration is represented by a point M the orientation of the ellipse is obtained from the circle through P, P' and M with $OQ = \tan\alpha$, and the ellipticity is obtained from the orthogonal circle through M with $e = ON$.

(ii) Kuske's[25] J Circle Method:

Consider a plane polarized light of unit amplitude represented by the straight line AOA as shown in Fig. 31. The components along the principal-stress axes p, q are $\mathrm{Cos}\,\theta'$ and $\mathrm{Sin}\,\theta'$. If a phase difference of ϵ is added between these two components in the model,

$$\left.\begin{array}{l}\text{Vibration component along}\\ \qquad p \text{ axis}\end{array}\right\} = \mathrm{Cos}\,\theta' \ \mathrm{Cos}\,\bar{\omega} t$$

$$\left.\begin{array}{l}\text{Vibration component along}\\ \qquad q \text{ axis}\end{array}\right\} = \mathrm{Sin}\,\theta' \ \mathrm{Cos}(\bar{\omega} t + \epsilon)$$

Now with respect to the axes OB and OC which are inclined at an angle γ to the p, q axes, the vibration components are given by

$$\begin{aligned}\text{Component along OB} &= \mathrm{Cos}\,\bar{\omega} t\,(\mathrm{Cos}\,\theta'\,\mathrm{Cos}\,\gamma + \mathrm{Sin}\,\theta'\,\mathrm{Cos}\,\epsilon\,\mathrm{Sin}\,\gamma)\\ &\quad - \mathrm{Sin}\,\theta'\,\mathrm{Sin}\,\bar{\omega} t\,\mathrm{Sin}\,\epsilon\,\mathrm{Sin}\,\gamma\\ &= a'\,\mathrm{Cos}\,(\bar{\omega} t + \epsilon_1)\end{aligned}$$

$$\begin{aligned}\text{Component along OC} &= \mathrm{Cos}\,\bar{\omega} t\,(\mathrm{Sin}\,\theta'\,\mathrm{Cos}\,\epsilon\,\mathrm{Cos}\,\gamma\\ &\quad - \mathrm{Cos}\,\theta\ \mathrm{Sin}\,\gamma) - \mathrm{Sin}\,\bar{\omega} t\,\mathrm{Sin}\,\theta'\,\mathrm{Sin}\,\epsilon\,\mathrm{Cos}\,\gamma\\ &= b'\,\mathrm{Cos}\,(\bar{\omega} t + \epsilon_2)\end{aligned}$$

$$\therefore\ a'^2 = \mathrm{Sin}^2\theta'\ \mathrm{Sin}^2\gamma + \mathrm{Cos}^2\theta'\ \mathrm{Cos}^2\gamma + \mathrm{Sin}2\theta'\ \mathrm{Cos}\varepsilon\ \mathrm{Cos}\gamma\ \mathrm{Sin}\gamma \qquad (5.8)$$

and

$$b'^2 = \mathrm{Sin}^2\theta'\ \mathrm{Cos}^2\gamma + \mathrm{Cos}^2\theta'\ \mathrm{Sin}^2\gamma - \mathrm{Sin}2\theta'\ \mathrm{Cos}\varepsilon\ \mathrm{Cos}\gamma\ \mathrm{Sin}\gamma \qquad (5.9)$$

To find the maximum and minimum values of a' and b' (corresponding to the lengths of semi-major and minor axes a and b), we differentiate the above expressions with respect to γ and equate to zero

$$\frac{da'^2}{d\gamma} = \frac{db'^2}{d\gamma} = 0$$

giving $\tan 2\gamma = \mathrm{Cos}\,\varepsilon \tan 2\theta'$ (5.10)

Substituting this expression in terms of γ in Eqs. (5.8) and (5.9), we obtain

$$a^2 = \tfrac{1}{2}\left[1 + (\mathrm{Cos}^2 2\theta' + \mathrm{Cos}^2\varepsilon\ \mathrm{Sin}^2 2\theta')^{\frac{1}{2}}\right] \qquad (5.11)$$

$$= \tfrac{1}{2}\,(1 + J)$$

where $J = (\mathrm{Cos}^2 2\theta' + \mathrm{Cos}^2\varepsilon\ \mathrm{Sin}^2 2\theta')^{\frac{1}{2}}$

and $b^2 = \tfrac{1}{2}\,(1 - J)$ (5.12)

The quantity $(\mathrm{Cos}^2 2\theta' + \mathrm{Sin}^2\theta'\ \mathrm{Cos}^2\varepsilon)^{\frac{1}{2}}$ is called J. The ellipticity and the orientation of the major axis can be represented by an arrow (vector) having length equal to J and oriented at a **chosen** angle. The angle between this direction and a chosen reference direction are doubled and so are all the other angles involved.

$$\text{Now, } J = 2a^2 - 1 = 1 - 2b^2 = \frac{1 - e^2}{1 + e^2} \qquad (5.13)$$

where $e = \frac{b}{a}$ = ellipticity

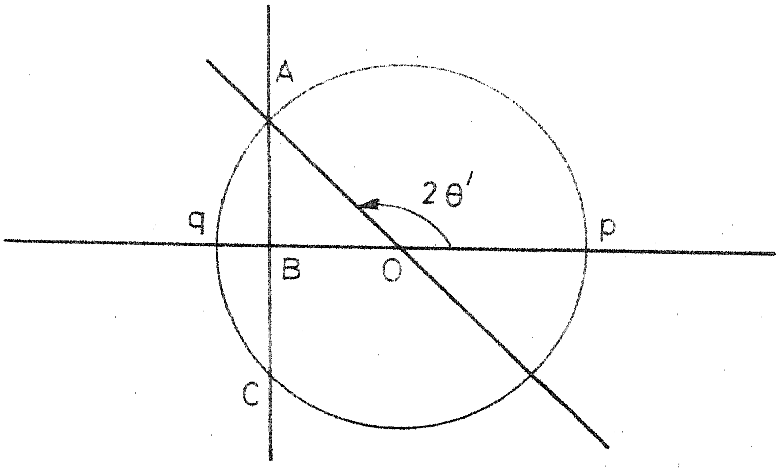

FIG. 32. KUSKE'S J CIRCLE

So, the magnitude of J depends on the ellipticity only. Further,

$$e^2 = \frac{1 - J}{1 + J} \qquad (5.14)$$

So, J = 1 represents plane polarized light and J = 0 represents circularly polarized light. That is in Fig. 32, a tip of the J vector on the circumference of the circle means plane polarized light, a tip in the center corresponds to circularly polarized light while all other positions represent elliptically polarized light. Since all the angles are doubled, the mutually perpendicular principal-stress axes are represented by the straight line qOp, since qOp $= \pi$. If plane polarized light is at an angle θ' to one of the principal-stress axes, the components along the principal-stress axes are Cos θ' and Sin θ'. Consider the plane polarized light represented by the point A on the circumference of the circle. The line AC is perpendicular to line qOp.

Now,

$$q\,B = 1 - \mathrm{Cos}2\theta' = 2\mathrm{Sin}^2\theta'$$

$$\text{and} \quad BP = 2\mathrm{Cos}^2\theta'$$

i.e. q B and BP are proportional to the squares of the amplitudes of components along the principal-stress axes. In order to find the intensities of light components along two mutually perpendicular directions, a perpendicular is to be drawn from the tip of the J vector on the straight line which corresponds to these mutually perpendicular directions.

The intercepts correspond to the required intensities. Since, during the addition of retardation along the principal-stress axes, the intensities of components of light along these axes remain constant, the representative point moves along the straight line AC which is perpendicular to the line qOp. At the point A,

$$J = (\cos^2 2\theta' + \sin^2 2\theta' \cos^2 \epsilon)^{\frac{1}{2}} = 1$$

$$\text{or } \cos^2\epsilon = 1$$

$$\text{i.e. } \epsilon = 0, \pi, \ldots, n\pi$$

At the point B,

$$\begin{aligned} J &= OB \\ &= -\cos 2\theta' \\ &= (\cos^2 2\theta' + \cos^2\epsilon \ \sin^2 2\theta')^{\frac{1}{2}} \end{aligned}$$

$$\text{or } \cos^2\epsilon = 0$$

$$\text{i.e. } \epsilon = \pi/2, 3\pi/2, \ldots, \frac{(2n+1)\pi}{2}$$

This can be interpreted as follows: At the point A, the phase difference is zero. As the phase difference is increased to $\pi/2$, the representative point moves to B along line AB. As the phase difference is further increased to π it moves to the point C along line BC. When it is $3\pi/2$, the representative point comes back to B and so on.

(iii) Schwieger's[26] Analysis:

Schwieger presented some rotation rules to be used with J circle method. He introduced the Wulff's grid method of crystallography into photoelasticity and described methods to find the characteristic parameters for a combination of

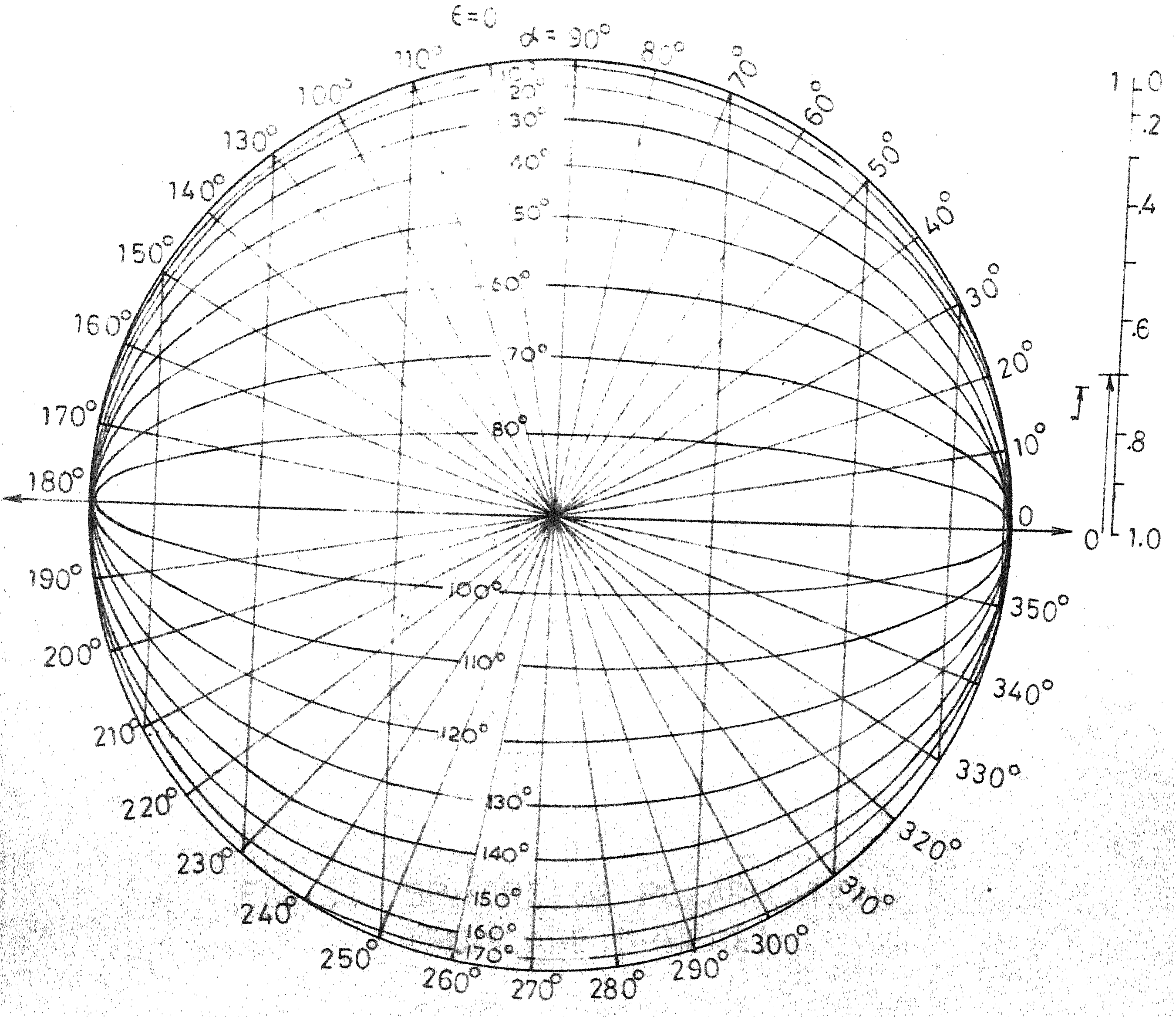

FIG. 34. PARALLEL PROJECTION OF THE SPHERE OF POLARIZATION (J CIRCLE)

linear retarders. A brief summary of his analysis is presented below:

The four parameters of light ellipse, namely, α, the azimuth, the angle θ (or tan θ, the amplitude ratio), the angle ω (or tan ω, the ellipticity) and ϵ the phase difference. From the equations of Chapter 2 we have the following relations connecting these four parameters.

$$\sin\epsilon \ \sin 2\theta = \sin 2\omega \tag{5.15}$$

$$\cos\epsilon \ \tan 2\theta = \tan 2\alpha \tag{5.16}$$

$$\cos 2\alpha \ \cos 2\omega = \cos 2\theta \tag{5.17}$$

The angles of a spherical triangle satisfy these relations and so these parameters can be represented on Poincare' sphere.

(a) Parallel Projection:

In Fig. 33. all points of the upper hemi-sphere represent left elliptically polarized light while points in the lower hemi-sphere represent right elliptically polarized light. The area of the J circle can be obtained by parallel projection on a plane having a normal which is parallel to the axis connecting the poles of the sphere.

The chords drawn in the J circle, Fig. 34. are lines of constant amplitude ratio, the ellipses are loci of points of constant phase difference. The radial lines are lines of constant azimuth. The actual azimuth will be half of the angular inclination of these radial lines with the OX axis. The reference axes are the lines OX and OY. The scale on the right hand side of this plane representation

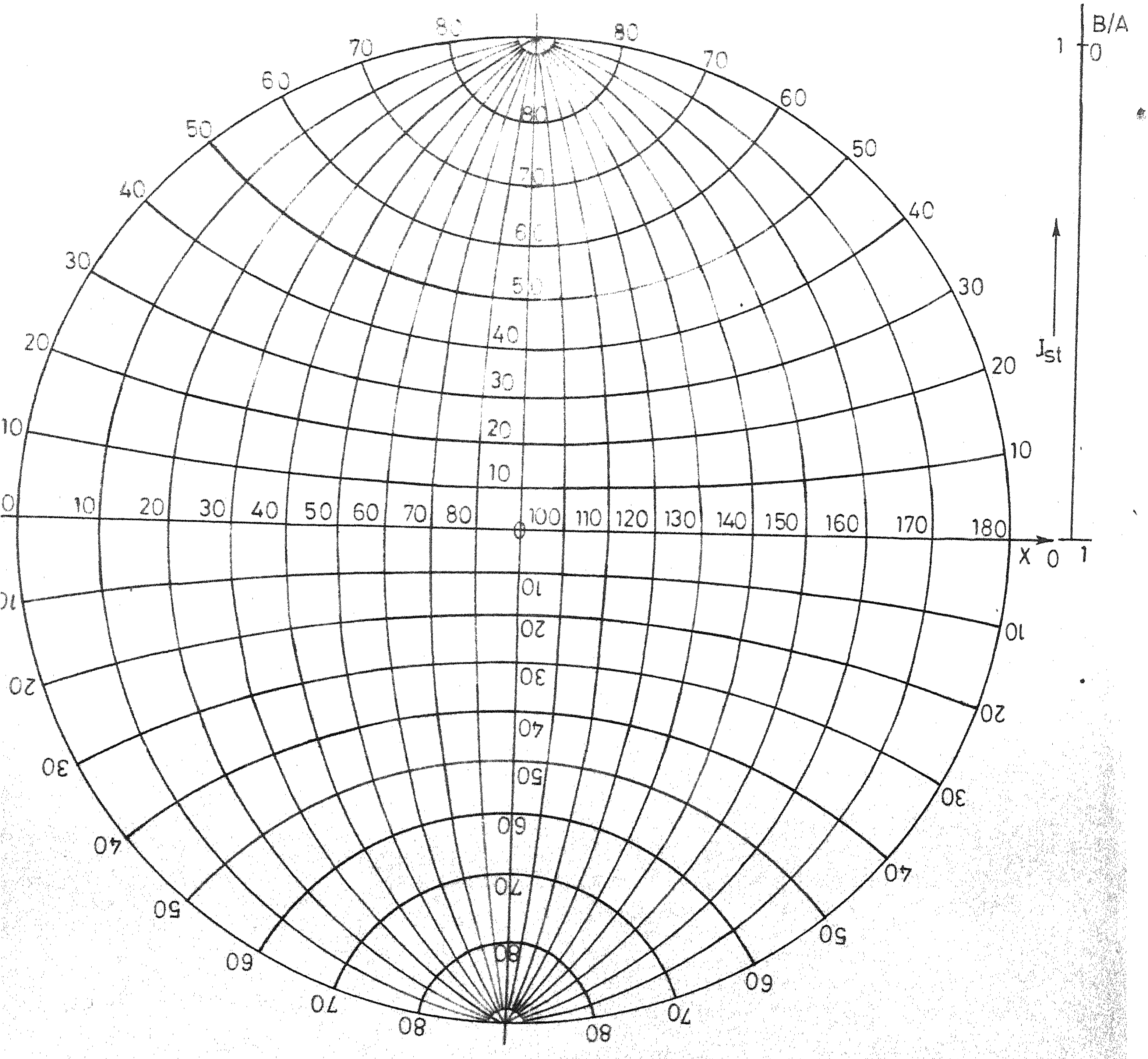

FIG. 35. STEREOGRAPHIC PROJECTION OF THE SPHERE OF POLARIZATION.

is calibrated in terms of ellipticity. This plane representation can be readily used to find the resulting photoelastic effect after the passage through a set of linear retarders. Addition of phase difference corresponds to moving along the chords of constant amplitude ratio, the length of movement corresponding to the value of retardation added. Rotation of reference axes corresponds to moving along a constant ellipticity circle until the angular inclination to OX is increased by double the amount of rotation of reference axes.

(iv) Wulff's Grid:

This is the stereographic projection of Poincare' sphere of polarization.

The stereographic map is the projection of a sphere on the plane of a great circle, Fig. 35, in such a way that the projection of a point A on the sphere is the point in which the line through A and a pole of that great circle intersects the plane of the great circle. This projection is conformal[44].

The chords of constant amplitude ratio in the parallel projection correspond to the curved lines surrounding the YOX axis in the stereographic projection. The radial lines here again represent lines of constant azimuth. The loci of points of constant phase difference are arcs of circles in this projection.

Determination of Parameters of the Equivalent Optical System For A Combination of Two Linear Retarders:

Δ_1 = Retardation introduced in the first plate

Δ_2 = Retardation introduced in the second plate

The optically equivalent system consists of a linear retarder and a pure rotator. If the incident light is plane polarized along the axes of this linear retarder it remains plane polarized after the retarder but is rotated by the pure rotator. That is, it is plane polarized at the exit. To find the rotatory power of this pure rotator and the orientation of this linear retarder draw two lines OX_1 and OX_2 corresponding to the axes of the two plane models. Construct the circular arcs on these lines corresponding to Δ_1 = constant and $180 - \Delta_2$ = constant. From this point of intersection P of these two arcs, proceed to the point Q and R on the circumference of the circle along the constant amplitude ratio curves corresponding to the axes OX_1 and OX_2. The angle ROQ will be twice the rotatory power of the system. Also, $X_1\hat{O}Q = 2\rho_{repl}$, where ρ_{repl} is the angle between the axes of the first plate and the axes of the linear retarder in the optically equivalent system. The procedure can be easily understood from Fig. 37. In this figure $A_1P_1P_2A_2$ represents the passage of light through the two retarders.

$$P_1\hat{O}P_2 = 2\bar{\theta}$$

The actual problem is to locate the points P_1 and

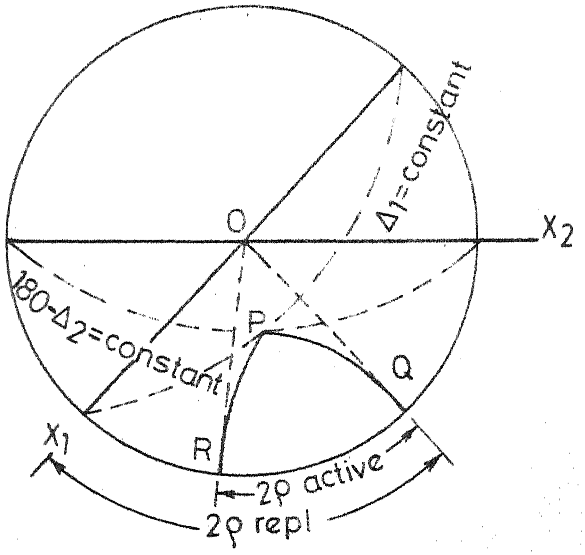

FIG. 36· DETERMINATION OF THE ANGLE ρ ACTIVE OF THE ACTIVE PLATE OF AN EQUIVALENT SYSTEM FOR TWO PLANE MODELS.

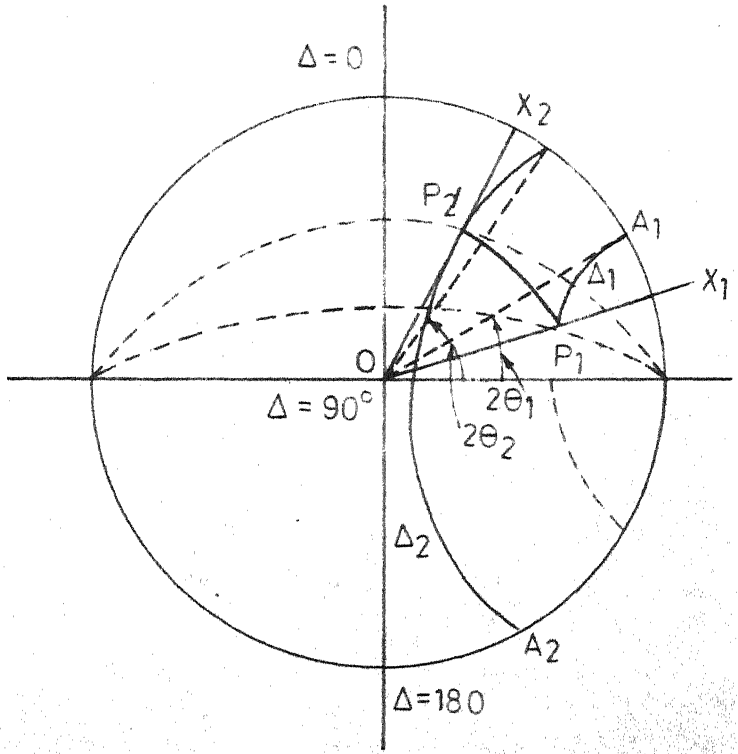

FIG. 37. FINDING THE PARAMETERS OF THE OPTICALLY EQUIVALENT SYSTEM.

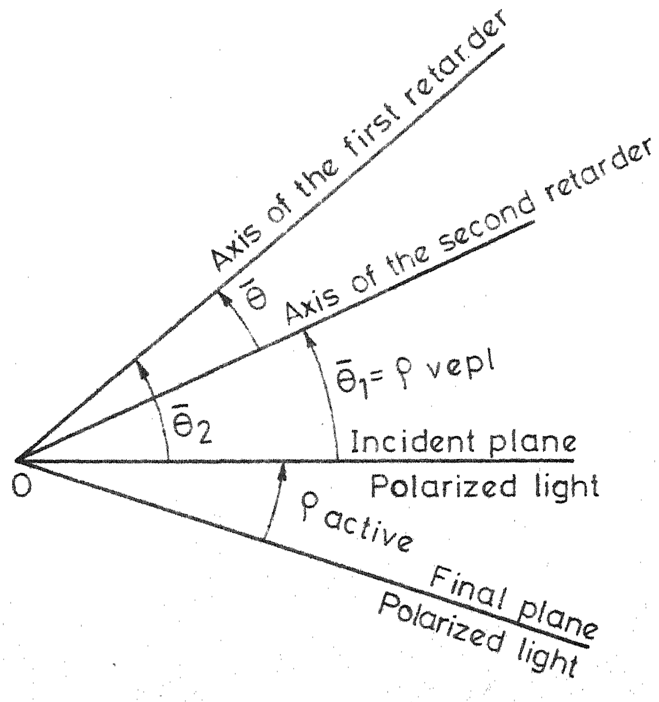

FIG. 38. REPRESENTATION OF AXES OF THE TWO RETARDERS.

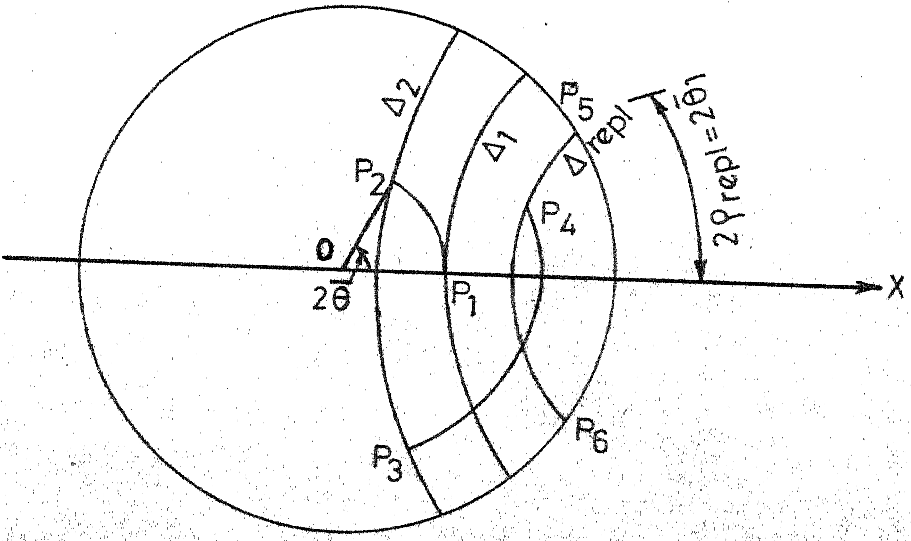

FIG. 39. FINDING THE PARAMETERS OF THE OPTICALLY EQUIVALENT SYSTEM.

P_2 which lie on the constant phase difference curves $\Delta = \Delta_1$ and $\Delta = 180 - \Delta_2$ respectively such that

$$P_1 \hat{O} P_2 = 2\bar{\theta}$$

This is done by rotating one curve with respect to the other by an angle $2\bar{\theta}$ as in Fig. 36. so that their point of intersection P corresponds to the points P_1 and P_2 of Fig. 37. Fig. 38. shows the orientation of the axes of the retarders.

In Fig. 36.,

$$R\hat{O}Q = 2\ (\bar{\theta}_2 - \bar{\theta}_1)$$

$$R\hat{O}Q \neq 2\rho_{active}$$ as mentioned by Schwieger.

To find the retardance Δ_{repl} of the optically equivalent system consider plane polarized light along the axes of the first plate represented by the point P in Fig. 39. Retardation Δ_1 in this plate brings it to P_1. Rotation of the reference axes to make them coincide with the axes of the second plate brings it to the point P_2. Addition of a retardation Δ_2 in the second plate is represented by the path P_2P_3 so that the point P_3 represents the state of polarization at the exit of the two plates when referred to the axes of the second plate. We should arrive at the same point P_3 even if we use the optically equivalent system. Now proceed back to the point P_4 where $P_3\hat{O}P_4 = 2\rho_{active}$ and $OP_4 = OP_3$. Find the point P_5 on the circumference such that $P\hat{O}P_5 = 2\bar{\theta}_1$. That is, the point P_5 represents the state of polarization at the entrance when referred to the axes of the equivalent retarder. The points P_5 and P_4 lie on the same curve of constant amplitude ratio. (This fact can be used to check the values of θ_1 and ρ_{active}.) The path P_5P_4 represents the equivalent retardation Δ_{repl}. In the case of systems with many number of retarders, this method can be used successively. Schwieger, in his example with ten plates, mentions an iterative procedure where the azimuth of the incident plane polarized light is varied until the light at the exit is plane polarized.

(vi) Graphical Method Using Quaternions

Cernosek[27] devised a geometrical method based on the properties of quaternions to find the characteristic parameters of a system of linear retarders. He made use of Jones vector in this derivation. The principle of this method is described below.

Let the Jones vector for a certain elliptically polarized light referred to the X,Y axes be given by

$$\begin{bmatrix} a_X\, e^{i(\epsilon_X + \bar{\omega} t)} \\ a_Y\, e^{i(\epsilon_Y + \bar{\omega} t)} \end{bmatrix}$$

where ϵ_X, ϵ_Y are the phase angles and A_X, A_Y are the amplitudes of the components along the X, Y axes respectively.

$$\text{Let } I = \begin{vmatrix} 1 & 0 \\ 0 & 1 \end{vmatrix}; \; i = \begin{vmatrix} i & 0 \\ 0 & -i \end{vmatrix}; \; j = \begin{vmatrix} 0 & 1 \\ -1 & 0 \end{vmatrix}; \; k = \begin{vmatrix} 0 & i \\ i & o \end{vmatrix} \quad (5.18)$$

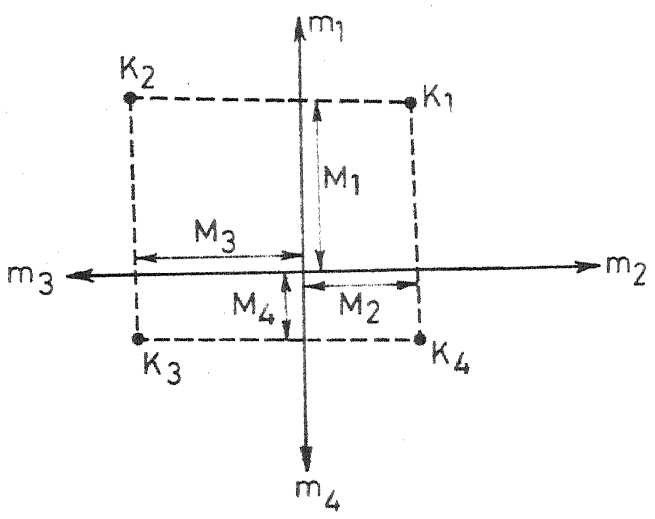

FIG.40. CO-ORDINATE SET USED FOR THE DESCRIPTION OF THE GENERAL QUATERNION M_1, M_2, M_3, M_4 ARE THE COEFFICIENTS OF THE QUATERNION.

The general unitary 2 x 2 matrix, which represents the transformation of polarized light from its entrance through a system of linear retarders to its emergence can be uniquely expressed as a quaternion

$$M = M_1 I + M_2 i + M_3 j + M_4 k \qquad (5.19)$$

The coefficients of the quaternion M are connected by the unitary norm relation

$$M_1^2 + M_2^2 + M_3^2 + M_4^2 = 1 \qquad (5.20)$$

The quaternion can be described graphically as shown in Fig. 40. The co-ordinates of the four points K_1, K_2, K_3 and K_4 in Fig. 40. are the coefficients of the quaternion M defined by Eq. (5.19), M_1, M_2 ; M_3, M_1 ; M_3, M_4 and M_2, M_4 respectively in four different co-ordinate systems (m_1, m_2), (m_3, m_1), (m_3, m_4) and (m_2, m_4) which are in the same plane but have different orientations. The values of M_1, M_2, M_3 and M_4 for a rotator and a retarder placed before or a after the system can be easily found from the transformation relations. Each of these transformations corresponds to a particular type of rotation of some of the four radius vectors OK_1, OK_2 OK_3 and OK_4. Thus, the final positions of the points K_1, K_2, K_3 and K_4 can be found graphically very easily for either a retarder or a rotator when it is placed either before the system or after the system by simple rotation of the radius vectors K_2 and K_4 or K_1 and K_3. Two other points in each step will then be found by drawing lines parallel to the coordinate systems.

The Characteristic Quantities of a General System of Retarders:

Before studying a system of retarders, we shall present the quaternions for simple operations.

Quaternion of rotation:

$$S\ (\alpha_2) = \text{Cos}\alpha_2 \cdot I - \text{Sin}\alpha_2 \cdot J$$

α_2 is the rotation angle.

Quaternion $U\alpha_2 = S\ (\alpha_2)\ M$ when $S\ (\alpha_2)$ is placed after M.

then

$$U = A_{12}I + A_{22}i + A_{32}j + A_{42}k \qquad (5.21)$$

where

$$A_{12} = M_1\ \text{Cos}\alpha_2 + M_3\ \text{Sin}\alpha_2 \qquad (5.22)$$

$$A_{22} = M_2\ \text{Cos}\alpha_2 - M_4\ \text{Sin}\alpha_2 \qquad (5.23)$$

$$A_{32} = M_3\ \text{Cos}\alpha_2 - M_1\ \text{Sin}\alpha_2 \qquad (5.24)$$

$$A_{42} = M_4\ \text{Cos}\alpha_2 + M_2\ \text{Sin}\alpha_2 \qquad (5.25)$$

Quaternion for a linear retarder of retardance Δ_2 is given by

$$G\ (\Delta_2) = \text{Cos}\ \Delta_2 \cdot I + \text{Sin}\ \Delta_2 \cdot i$$

If this retarder is placed after M, the quaternion for the combined system is given by

$$U\ (\Delta_2) = G\ (\Delta_2)\ M = B_{12}I + B_{22}i + B_{32}j + B_{42}k \qquad (5.26)$$

where

$$B_{12} = M_1\ \text{Cos}\Delta_2 - M_2\ \text{Sin}\Delta_2 \qquad (5.27)$$

$$B_{22} = M_2 \operatorname{Cos}\Delta_2 - M_1 \operatorname{Sin}\Delta_2 \qquad (5.28)$$

$$B_{32} = M_3 \operatorname{Cos}\Delta_2 - M_4 \operatorname{Sin}\Delta_2 \qquad (5.29)$$

$$B_{42} = M_4 \operatorname{Cos}\Delta_2 + M_3 \operatorname{Sin}\Delta_2 \qquad (5.30)$$

If the rotator and the retarder are placed before the system M, the corresponding quaternions for the combined systems will be as given below:

$$U\ (\alpha_1) = M\ S\ (\alpha_1) = A_{11}I + A_{21}i + A_{31}j + A_{41}k \qquad (5.31)$$

where

$$A_{11} = M_1 \operatorname{Cos}\alpha_1 + M_3 \operatorname{Sin}\alpha_1 \qquad (5.32)$$

$$A_{21} = M_2 \operatorname{Cos}\alpha_1 + M_4 \operatorname{Sin}\alpha_1 \qquad (5.33)$$

$$A_{31} = M_3 \operatorname{Cos}\alpha_1 - M_1 \operatorname{Sin}\alpha_1 \qquad (5.34)$$

$$A_{41} = M_4 \operatorname{Cos}\alpha_1 - M_2 \operatorname{Sin}\alpha_1 \qquad (5.35)$$

and

$$U_{\Delta_1} (= M\ G\ (\Delta_1) = B_{11}I + B_{21}i + B_{31}j + B_{41}k \qquad (5.36)$$

where

$$B_{11} = M_1 \operatorname{Cos}\Delta_1 - M_2 \operatorname{Sin}\Delta_1 \qquad (5.37)$$

$$B_{21} = M_2 \operatorname{Cos}\Delta_1 + M_1 \operatorname{Sin}\Delta_1 \qquad (5.38)$$

$$B_{31} = M_3 \operatorname{Cos}\Delta_1 + M_4 \operatorname{Sin}\Delta_1 \qquad (5.39)$$

$$B_{41} = M_4 \operatorname{Cos}\Delta_1 - M_3 \operatorname{Sin}\Delta_1 \qquad (5.40)$$

The coefficients of the resulting quaternion U_{α_2} after a rotation through an angle α_2 can be found by

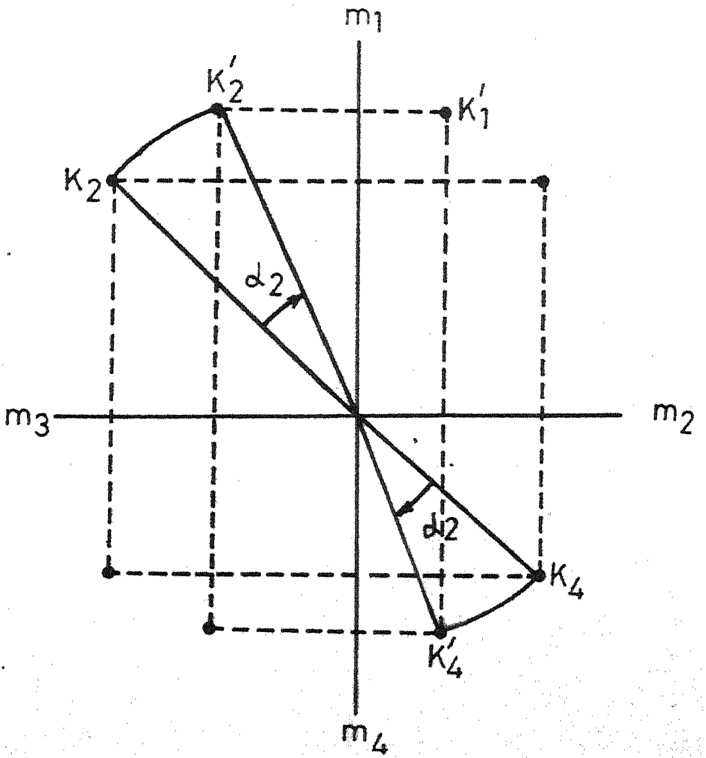

FIG. 41. TRANSFORMATION OF A CO-ORDINATE SET AT THE POINT OF EMERGENCE α_2. AZIMUTH OF THE OLD AND NEW REFERENCE CO-ORDINATE SYSTEM.

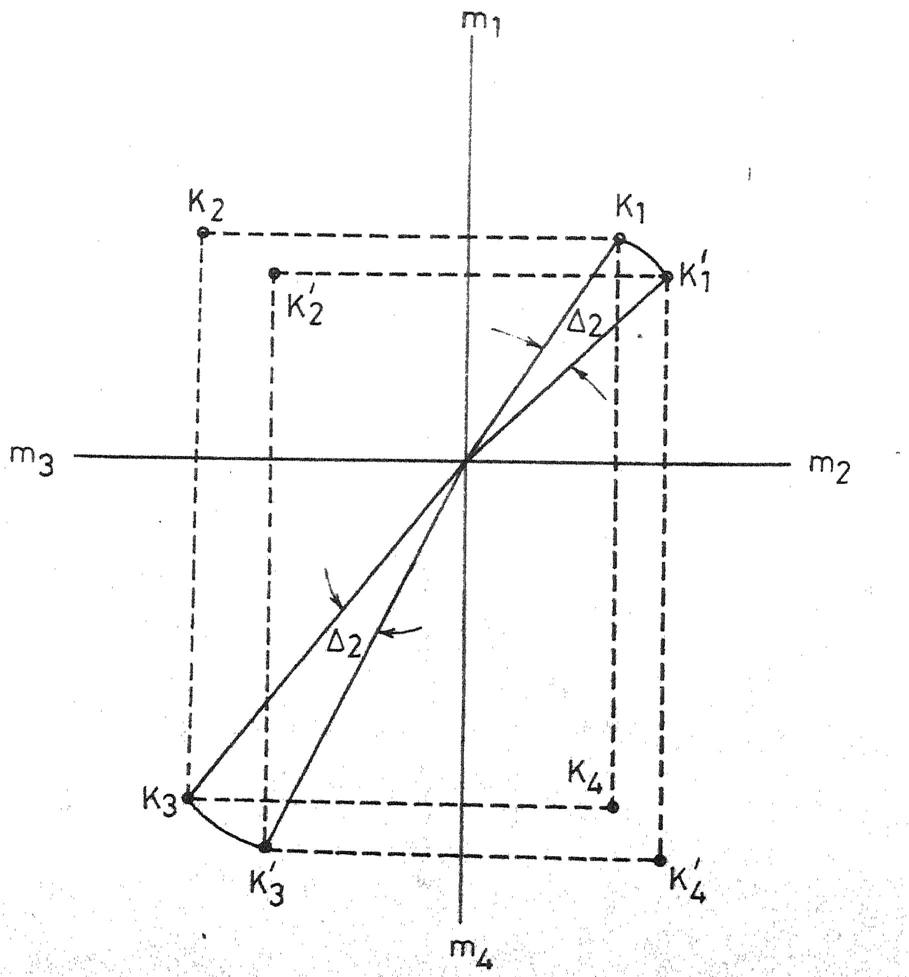

FIG. 42 THE ADDITION OF THE RETARDER AT THE POINT OF EMERGENCE, COORDINATE SETS $m_1 - m_2$ AND $m_3 - m_4$ ROTATED IN OPPOSITE DIRECTIONS, $2\Delta_2$: PHASE RETARDATION OF THE ADDED RETARDER.

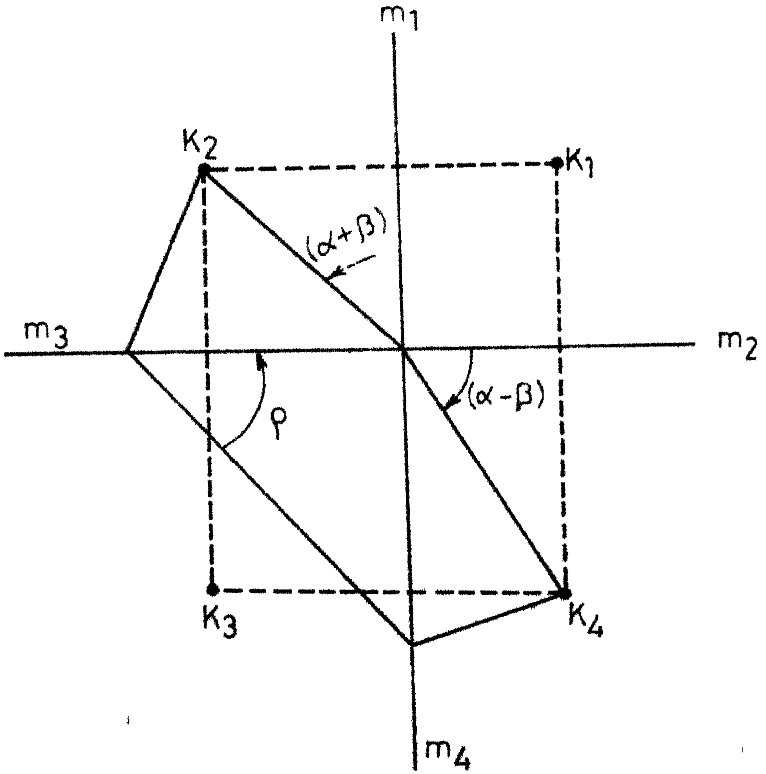

FIG. 43. THE CHARACTERISTIC QUANTITIES OF A GENERAL SYSTEM OF RETARDERS, α, β ARE THE ORIENTATIONS OF THE PRIMARY AND SECONDARY CHARACTERISTIC DIRECTIONS 2ρ IS THE CHARACTERISTIC PHASE RETARDATION.

$$\tan(\alpha+\beta) = \frac{M_3}{M_1}$$

$$\tan(\alpha-\beta) = \frac{M_4}{M_2}$$

$$\tan\rho = \left(\frac{M_1^2 + M_4^2}{M_1^2 + M_3^2}\right)^{1/2}$$

rotating the radius vectors of the points K_2 and K_4 in the clockwise direction, Fig. 41. as can be seen from Eqs.(5.22)-(5.25). In the same way the coefficients of the quaternion for a retarder whose axes are inclined at an angle α, with the reference axes can be found by rotating the radius vectors of K_2 and K_4 (multiplication by the quaternion of rotation) through an angle α_1 in the opposite directions and then rotating the radius vectors of K_1 and K_3 by an angle Δ_1, both in the same direction (for the addition of a retardance of Δ_1 in the linear retarder), Fig. 42.

Similarly, the geometrical procedures corresponding to the equations (5.32) - (5.35) and (5.37) - (5.40) can be established.

Using the above relations, we have the following representation of the quaternion for the combination of a linear retarder and a pure rotator (of the optically equivalent system), Fig. 43. Following the procedures described above, the quaternion for a system of linear retarders can be found graphically. Comparing this with the quaternion for the optically equivalent system, Fig. 43. the characteristic parameters of the system of linear retarders can be found. In Fig. 43. the characteristic quantities of a general system of retarders are given by

$$\epsilon_1 = \alpha + \beta$$

$$\epsilon_2 = \alpha - \beta$$

So, the variation of any two of these parameters with respect to one another can be plotted keeping one of the other two parameters constant. For example, the azimuth α and the phase difference ϵ can be plotted along X and Y axes so that we have constant amplitude ratio curves and constant ellipticity curves. We will have other systems of graphs if other combinations of the parameters are taken with different coordinate systems.

From the above equations, we have

$$\tan\epsilon = \frac{\tan 2\omega}{\mathrm{Sin}\,2\alpha} = \frac{2e}{(1 - e^2)\ \mathrm{Sin}\,2\alpha} \qquad (5.44)$$

and

$$\tan 2\alpha = \frac{2a_X\ a_Y}{a_X^2 - a_Y^2}\ \mathrm{Cos}\,\epsilon = \frac{2e_X}{(1 - e_X^2)} \cdot \mathrm{Cos}\,\epsilon \qquad (5.45)$$

where

$e = b/a = \text{ellipticity} = \tan\omega$

$e_X = a_Y/a_X = \text{amplitude ratio} = \tan\theta$

From these relations, it is clear that for given values of e and α, the values of ϵ is fixed and for given values of e_X and ϵ, the value of α is fixed. The values of these parameters can be tabulated and this table can be used for computing the effect of a series of retarders.

From Eqs. (5.44) and (5.45), we note that for a given value of e the ellipticity (not equal to unity), the phase difference ϵ has a minimum value which occurs at $\alpha = 45^\circ$. For a given value of e_X the amplitude ratio (not equal to unity), the azimuth α has a maximum (or minimum)

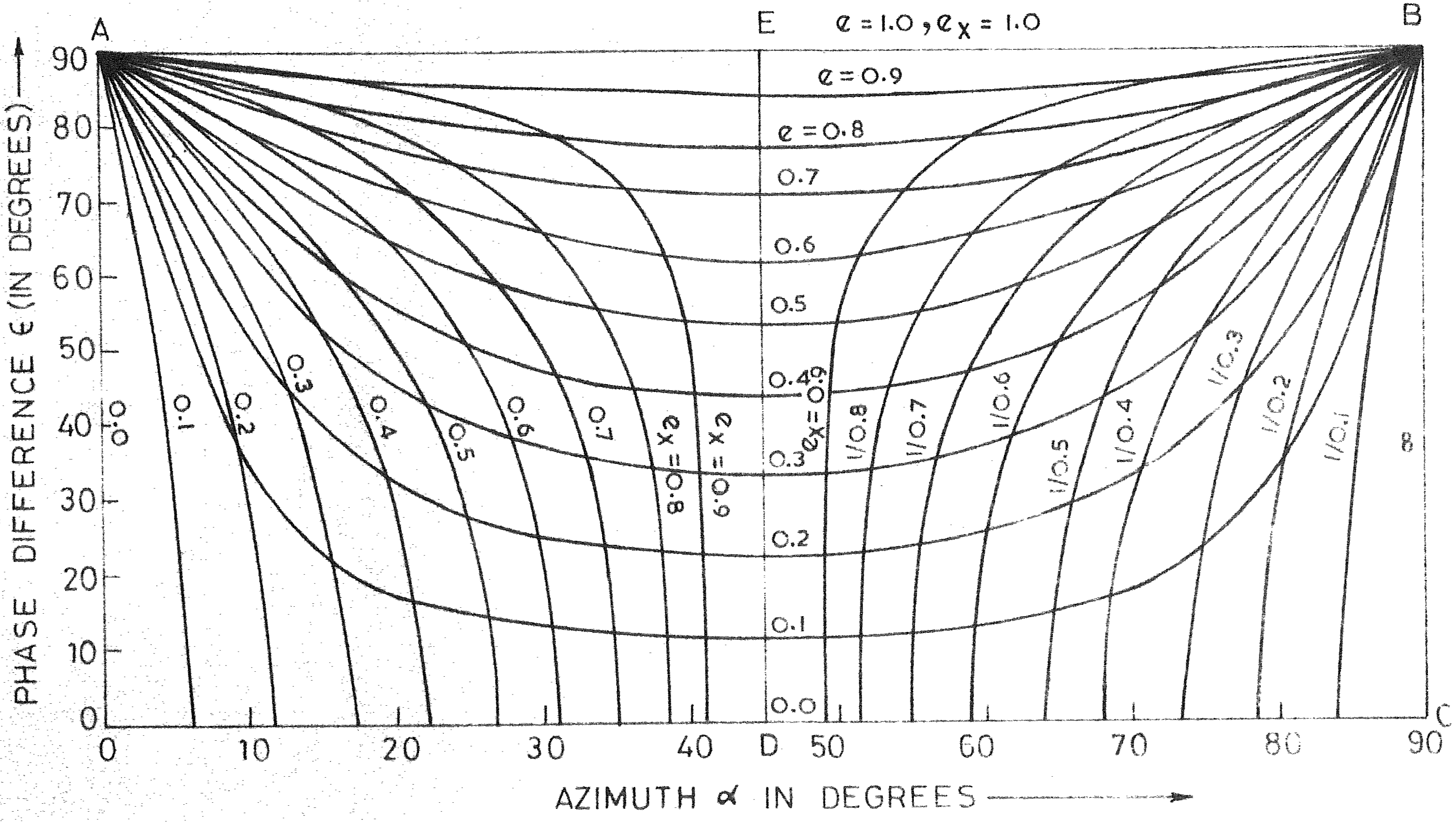

AB – Circularly polarized light

Points A B – light vibrations referred to the major and minor axes of the light ellipse

Path AOCB – Plane polarized light

FIG. 44. THE FIRST GRAPHICAL METHOD

value which occurs at $\epsilon = 0$. When the amplitude ratio equals unity and the phase difference $\epsilon \neq 90^\circ$, the azimuth α equals 45°. When $e_X = 1$ and $\epsilon = 90^\circ$, it is circularly polarized light and α takes all values.

One can plot Eqs. (5.44) and (5.45) as shown in Fig. 44. In this figure, the horizontal axis represents the azimuth α and the vertical axes the phase difference ϵ. Use of Eq. (5.44) gives "Constant Ellipticity" curves. To get these, one plots α vs ϵ; for fixed values of e getting curves like APB, AEB, etc. Use of Eq. (5.45) gives "Constant Amplitude Ratio" curves. These are obtained by plotting α vs ϵ for fixed value of e_X. At points A and B the phase difference ϵ is $\pi/2$ and the azimuths α are 0 and $\pi/2$ respectively. So points A and B represent states of polarization when the reference axes coincide with the major and minor axes of the light ellipse. The line AB represents circularly polarized light and the lines AO, OC and CB represent plane polarized light. This form of graphical representation of light ellipse is very convenient, since in photoelastic analysis, we add a certain amount of retardation along a particular set of axes (during this addition, the amplitude ratio along these axes remains constant and so this process is represented by movement along the constant amplitude ratio curves) and rotation of the reference axes (during this process, the ellipticity remains constant and so it is represented by movement along the constant ellipticity curves). The same graph can be used for ranges

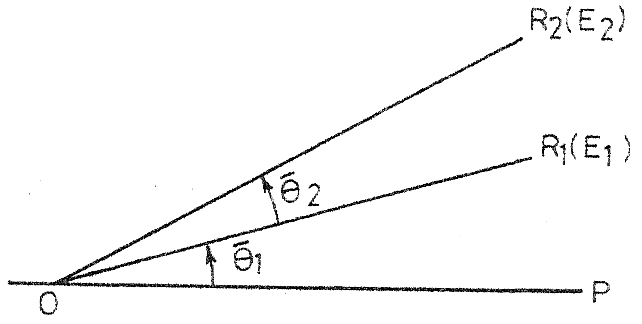

OR- Axis of the first retarder
OR$_2$-Axis of the second retarder
OP -Reference axis

FIG. 45. ORIENTATION OF THE AXES OF THE TWO RETARDERS.

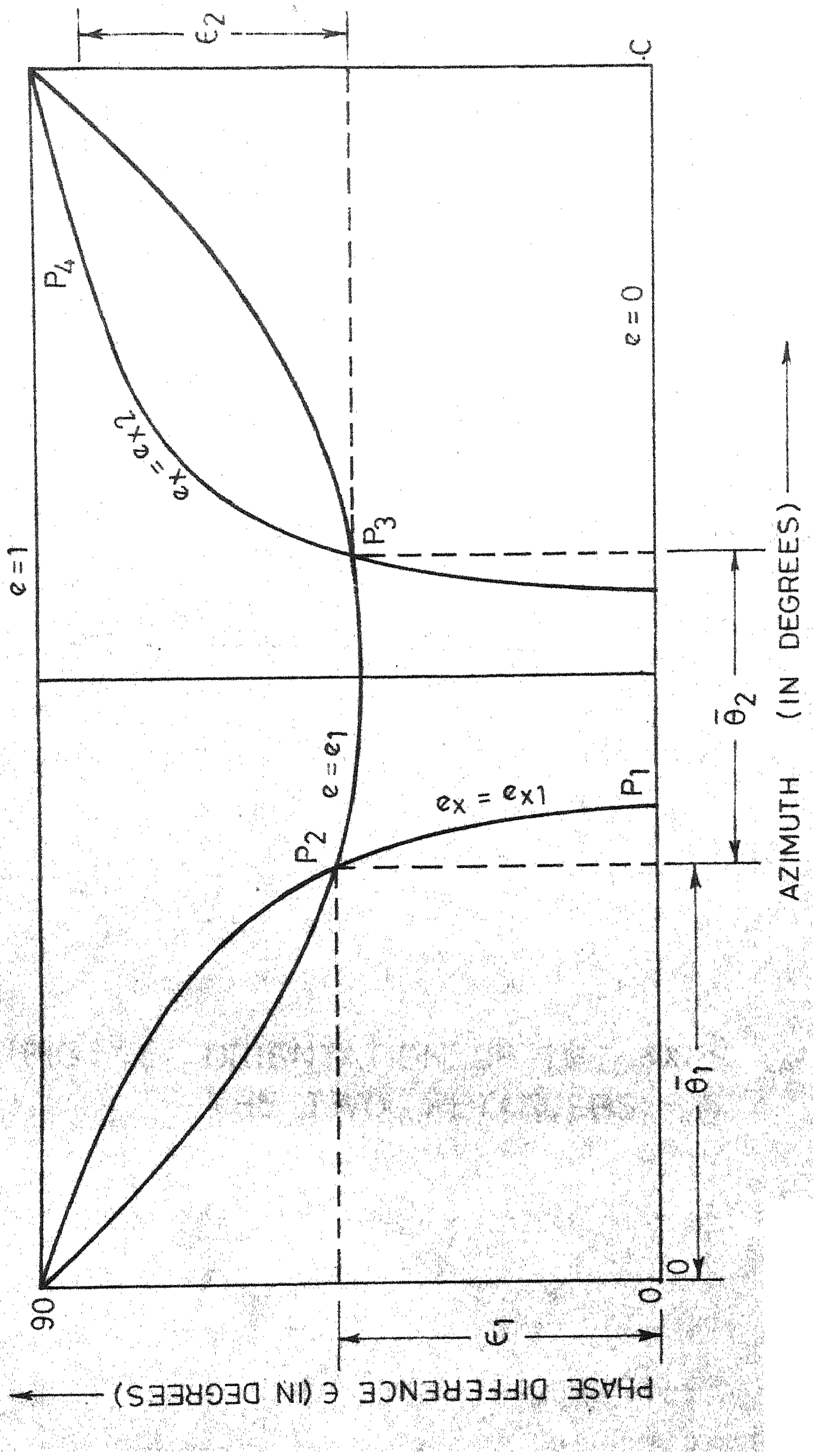

FIG. 46. EFFECT OF COMBINATION OF TWO RETARDERS.

beyond $\pi/2$ radians for the azimuth and the phase difference by taking into account the sign variations and using Eqs. (5.44) and (5.45). This is demonstrated at the end of this section.

Procedure to Use the Graphical Method:

Consider two retarders, R_1 and R_2 whose axes are inclined with respect to each other by an angle $\overline{\theta}_2$ and let the axes of R_1 make angle θ_1 and $\theta_1 + \pi/2$ with respect to a given fixed axis, Fig. 45. Let the initial light be plane polarized along the refering axis. This initial light ellipse is represented by point O (with $\epsilon = 0$ and $\alpha = 0$), Fig. 46. When this is referred to the axes of R_1, the initial light ellipse will be given by point P_1 (with e = 0 and amplitude ratio e_X given by point P_1). Addition of retardation ϵ_1 by R_1 is represented by movement along constant amplitude ratio curve P_1 P_2 up to the point P_2, such that the ordinate (phase difference ϵ) of P_2 is greater than that of the point P_1 by an amount ϵ_1. Now, we refer this light ellipse to the axes of the second retarder by moving to the point P_3 from the point P_2 along the constant ellipticity curve such that the azimuth of the point P_3 is greater than that of the point P_2 by an amount $\overline{\theta}_2$, where $\overline{\theta}_2$ is the angle between the axes of the two retarders. Addition of a phase difference of ϵ_2 in the second retarder is represented by movement along the constant amplitude ratio curve P_3 P_4 from the point

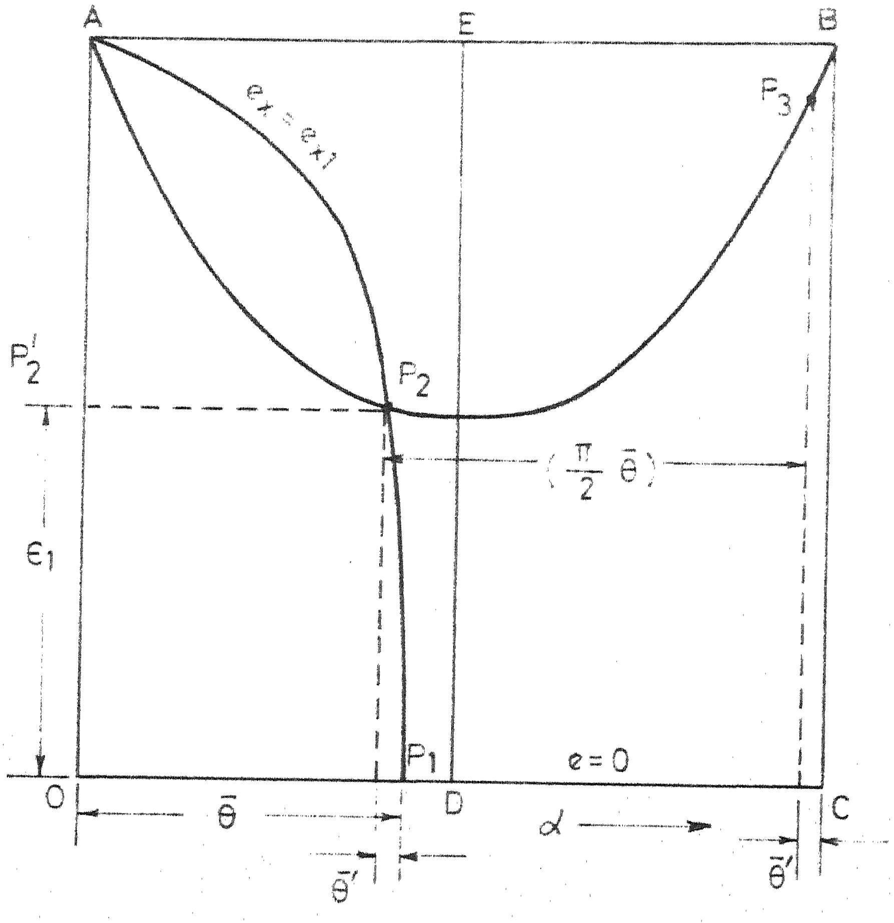

FIG. 47. VARIATION OF LIGHT ELLIPSE PARAMETERS IN A PLANE POLARISCOPE.

P_3 to the point P_4 where the ordinate ϵ of the point P_4 is greater than that of the point P_3 by an amount ϵ_2, where ϵ_2 is the retardation introduced by the second retarder. Finally, the point P_4 in the chart represents the light vibration at the exit of the second retarder with respect to its axes. So, during the representation of the variation of light ellipse as it passes through a system of linear retarders on this graph, the point under consideration always represents light vibration with respect to the axes along which the retardation has just been added or about to be added.

Passage of Light through Elements of a Polariscope:

(i) Plane Polariscope:

In Fig. 47. point O represents the plane polarized light along the axis of the polarizer; point P_1, the plane polarized light referred to the principal-stress axes of the model at its entrance; point P_2, the light at its exit after an addition of ϵ_1 retardation referred to the axes of the model, and P_3, the same light vibration but referred to the axes of the analyser which is kept crossed with respect to the polarizer. If one of the axes of the retarder (i.e. model) coincides with the direction of the initially polarized light, then we move from O to P_2', where $OP_2' = \epsilon_1$. When the analyzer is at $\pi/2$ to polarizer axis, we move along the constant ellipticity line P_2'ODC (e = 0) until we come to the orientation of the analyzer axes, that is, **point** C.

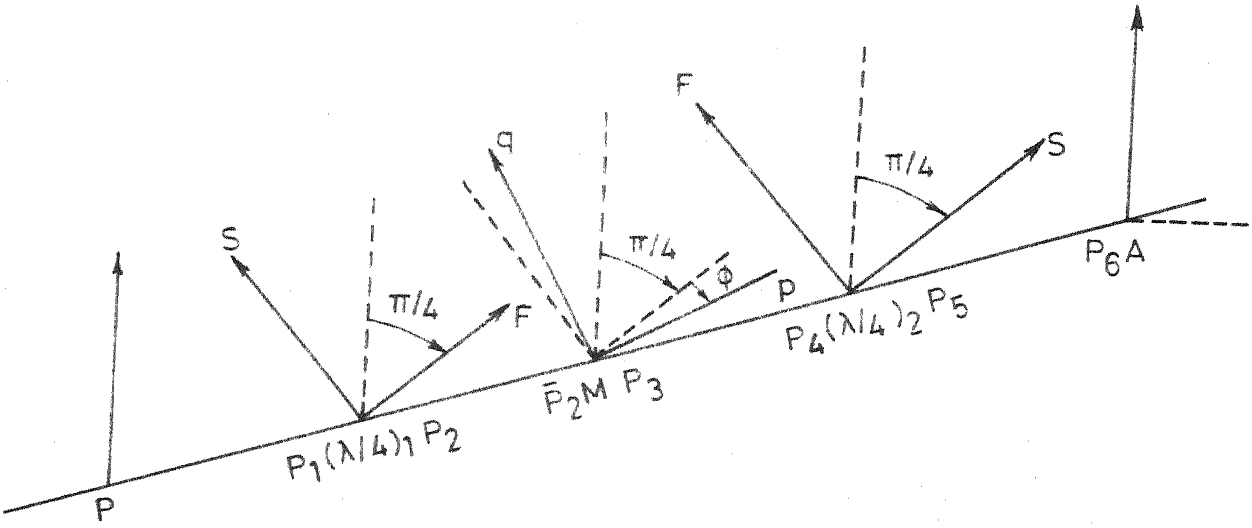

FIG. 48. CIRCULAR POLARISCOPE SET-UP.

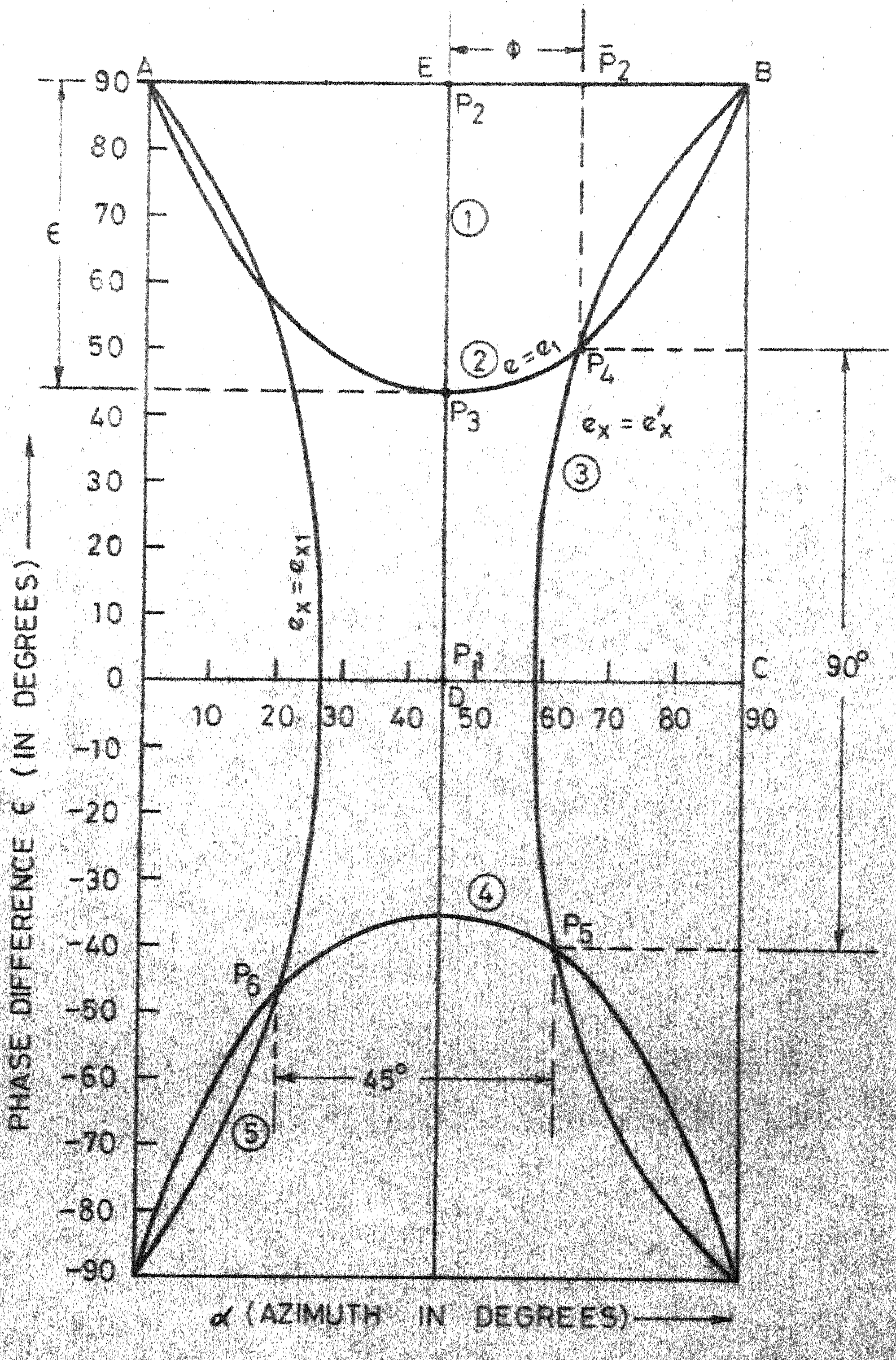

FIG. 49. TRANSFORMATIONS OF LIGHT ELLIPSE IN A CIRCULAR POLARISCOPE.

The amplitude ratio is zero and no light emerges from the analyzer.

(ii) Circular Polariscope:

Fig. 48 shows the elements of the circular polariscope. The points P_1 and P_2 in Fig. 49. represent light vibrations before and after the first quarter-wave plate referred to its axes, the points $\overline{P}_2$, P_3 ,the light vibrations before and after the model referred to its principal--stress axes at the particular point under consideration. The points P_4, P_5 represent the light vibrations before and after the second quarter-wave plate with respect to its axes and the point P_6, the light vibration before the analyser referred to its axes. Now, we have to prove that e_{X_1}, the amplitude ratio corresponding to the point P_6 depends only on the retardation introduced in the model and not on the angle ∅, the orientation of the principal-stress axes with respect to the axes of the quarter-wave plate. In a graph of Fig. 49, which is drawn to scale, point P_6 will always lie on the $e_x = e_{x_1}$ line, irrespective of the value of ∅ used. This can also be shown by Eqs. (5.44) and (5.45) that are used to construct Fig. 49. To show this we proceed as follows:

From Eqs. (5.44) and (5.45), we obtain

$$\tan\epsilon = \frac{\tan 2\omega}{\sin 2\alpha} \qquad (5.46)$$

and

$$\tan 2\alpha = \tan 2\theta \cos \epsilon \qquad (5.47)$$

where $\tan\theta$ is the amplitude ratio.

Let $\epsilon_3, \epsilon_4, \epsilon_5, \epsilon_6$ be the phase differences at the points P_3, P_4, P_5, P_6 respectively.

From Fig. 49

$$\epsilon_3 = \pi/2 - \epsilon^*$$

$$\alpha_3 = \pi/4$$

$$\tan\epsilon_3 = \frac{\tan 2\omega_3}{\sin 2\alpha_3} = \tan 2\omega_3$$

$$\therefore \quad 2\omega_3 = \epsilon_3 = \pi/2 - \epsilon^* \tag{5.48}$$

For the point P_4

$$\tan\epsilon_4 = \frac{\tan 2\omega_3}{\sin 2(\frac{\pi}{4} + \phi)} = \frac{\cot\epsilon^*}{\cos 2\phi} \tag{5.49}$$

$$\epsilon_5 = \epsilon_4 - \pi/2$$

$$\therefore \quad \tan\epsilon_5 = -\cot\epsilon_4 = -\frac{\cos 2\phi}{\cot\epsilon^*} \tag{5.50}$$

from Eq. (5.51)

Also, for points P_4 and P_5

$$\tan 2(\tfrac{\pi}{4} + \phi) = -\cot 2\phi = \tan 2\theta_4 \cos\epsilon_4 \tag{5.52}$$

$$\text{and} \quad \tan 2\alpha_5 = \tan 2\theta_5 \cos\epsilon_5 = \tan 2\theta_4 \sin\epsilon_4 \tag{5.53}$$

$$\therefore \quad \tan 2\alpha_5 = -\cot 2\phi \tan\epsilon_4$$

$$= -\frac{\cot 2\phi \cot\epsilon^*}{\cos 2\phi}$$

from Eq. (5.49)

$$= -\frac{\cot\epsilon^*}{\sin 2\phi} \tag{5-54}$$

Now, for the points P_5 and P_6 we have

$$\tan 2\omega_5 = \tan\epsilon_5 \operatorname{Sin} 2\alpha_5 \tag{5.55}$$

and

$$\tan 2\omega_6 = \tan 2\omega_5$$

$$= \tan\epsilon_6 \operatorname{Sin} 2\alpha_6$$

$$= -\tan\epsilon_6 \operatorname{Cos} 2\alpha_5 \tag{5.56}$$

$$\therefore \quad \tan\epsilon_6 = -\tan\epsilon_5 \tan\alpha 2_5$$

$$\because \quad \alpha_6 = \alpha_5 - \pi/4$$

$$= -\operatorname{Cot} 2\phi$$

from Eqs. (5.50) and (5.54)

$$\therefore \quad \epsilon_6 = \pi/2 + 2\phi \tag{5.57}$$

Now for point P_6

$$\tan 2\theta_6 = \frac{\tan 2\alpha_6}{\operatorname{Cos}\epsilon_6} = \frac{\operatorname{Cot}\alpha 2_5}{\operatorname{Sin} 2\phi}$$

from Eq. (5.57)

$$= -\frac{\operatorname{Sin} 2\phi}{\operatorname{Cot}\epsilon^* \operatorname{Sin} 2\phi}$$

from Eq. (5.54)

$$= \tan(\pi - \epsilon^*)$$

$$\therefore \quad 2\theta_6 = (\pi - \epsilon^*) \tag{5.58}$$

or

$$\theta_6 = \frac{\pi}{2} - \frac{\epsilon^*}{2}$$

So, the amplitude ratio $\tan\theta_6 = \varepsilon_{X6}$ depends only on the retardation ε^* introduced in the model and not on the orientation $\emptyset$ of the principal-stress axes with respect to the axes of the first quarter-wave plate. In the case of light field (the quarter-wave plates are crossed but the polarizer and analyser are parallel) polariscope,

$$\theta_6 = n\pi$$

whenever $\varepsilon^*_1 = (2n+1)\pi$

then

$$\tan\theta_6 = a_Y/a_X = 0$$

i.e. the extinction of light occurs.

In the dark field set up, the analyser and polarizer are crossed and the two quarter-wave plates are crossed. In this case

$$\alpha_6 = \alpha_5 + \pi/4$$

Here Eq. (5.56) becomes

$$\tan 2\omega_6 = \tan\varepsilon_6 \operatorname{Cos} 2\alpha_5$$

and $\tan\varepsilon_6 = \operatorname{Cot} 2\emptyset$

$$= \tan\left(\frac{\pi}{2} - 2\emptyset\right)$$

or $\varepsilon_6 = \pi/2 - 2\emptyset$ (5.57)

becomes

$$\theta_6 = \varepsilon^*/2$$

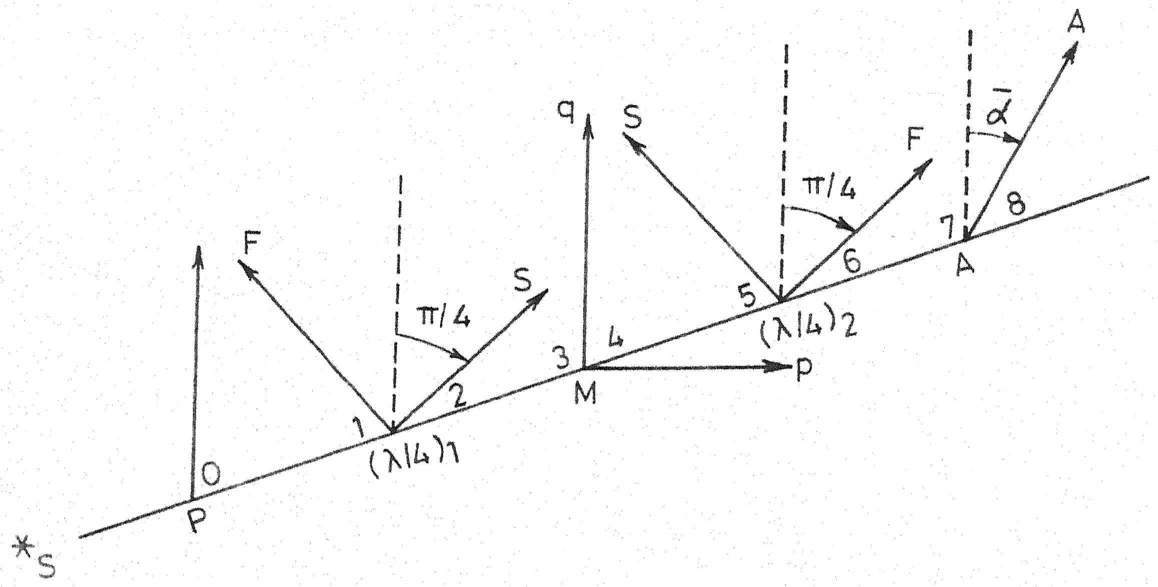

FIG. 50. OPTICAL SET-UP IN TARDY'S METHOD.

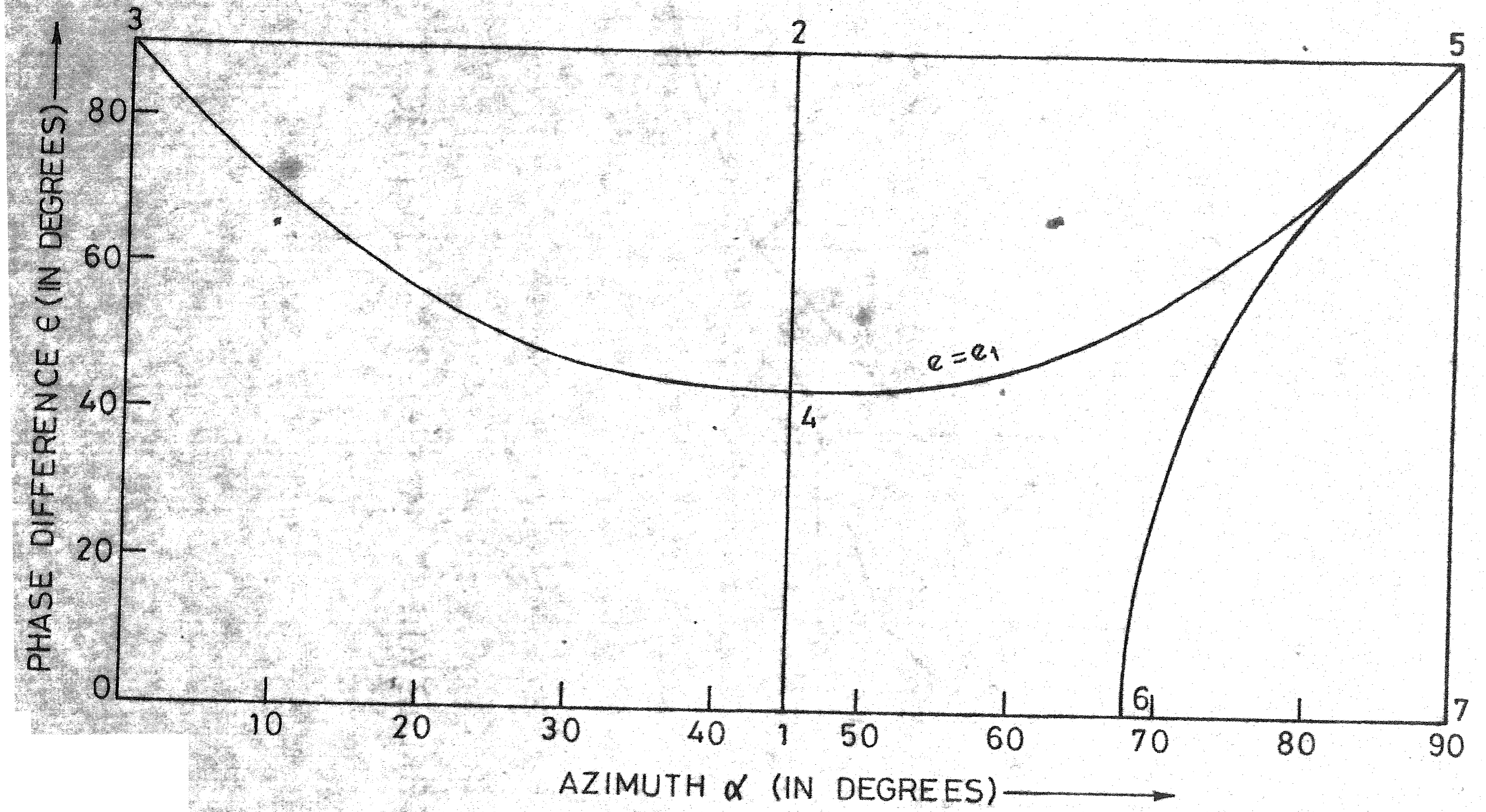

FIG. 51. TRANSFORMATIONS OF LIGHT ELLIPSE IN TARDY'S METHOD.

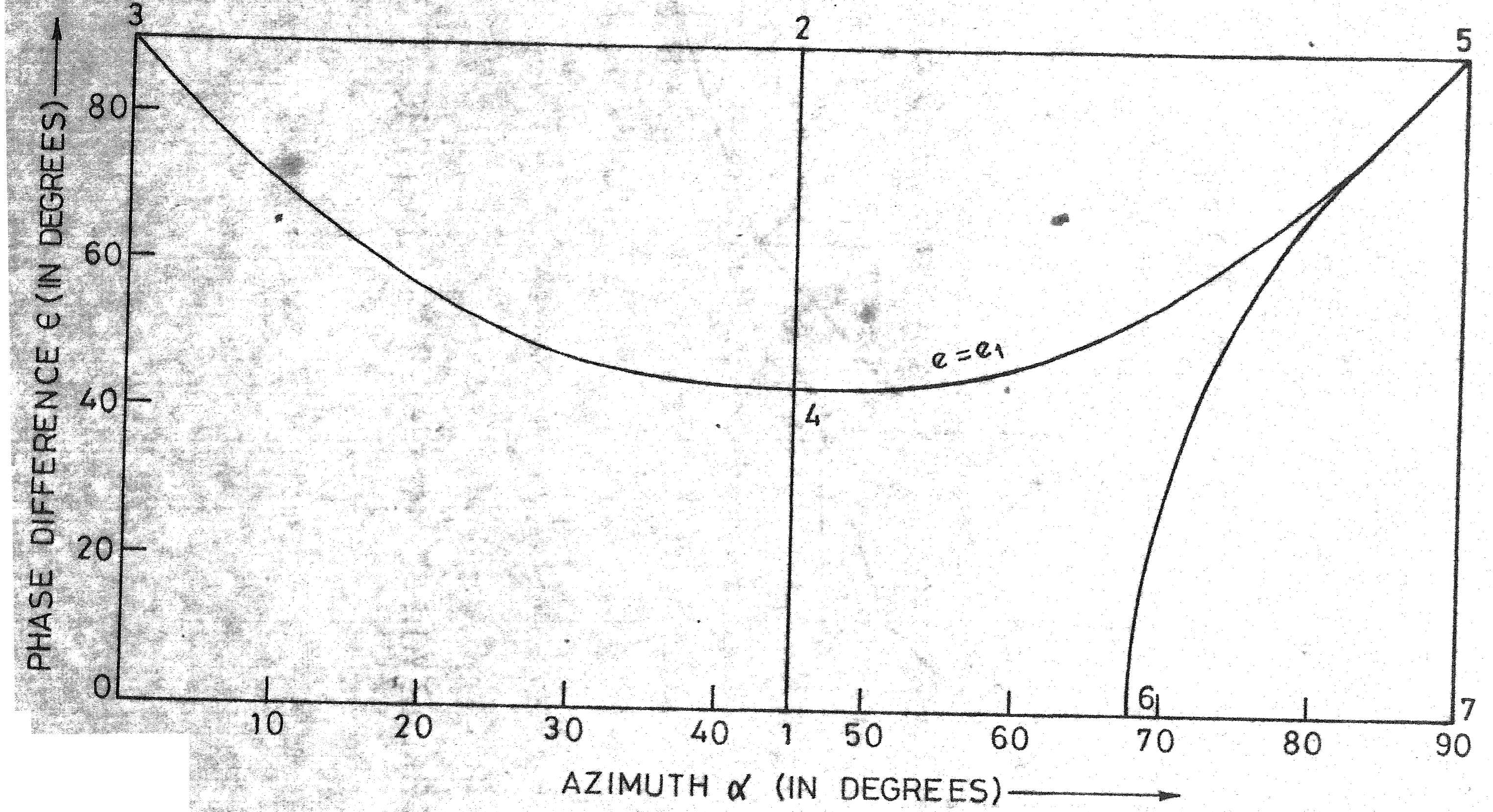

FIG. 51. TRANSFORMATIONS OF LIGHT ELLIPSE IN TARDY'S METHOD.

so that

$$\tan \varepsilon_6 = \tan\varepsilon^*/2$$
$$= 0$$

i.e. extinction of light occurs.

when $\varepsilon_1 = 2m\pi$

These results can be proved in exactly the same way for other alternative set ups of the dark and light field arrangements.

(iii) Tardy's Method:

The set up is shown in Fig. 50. Point 0 in Fig. 51 represents plane polarized light referred to the polarizer axis. Points 1 and 2 represent light before and after the first quarter-wave plate referred to its axes. Points 3 and 4 (path 3-2-4) represent light before and after the model with respect to the principal-stress axes. Points 5 and 6 represent light before and after the second quarter-wave plate. In order to cut off light, the amplitude ratio along the analyser axis must be ∞. This can be achieved by making point 6 come to point 7 along the constant ellipticity line. The orientation of the analyser axis is then $(\alpha_7 - \alpha_6)$ whose value can be found as follows:

From Fig. 51 we note that

$$\varepsilon_4 = \pi/2 - \varepsilon^*$$

$$\alpha_4 = \pi/4$$

$$\therefore \quad \tan 2\omega_4 = \tan\varepsilon_4 \ \text{Sin}\ 2\alpha_4$$

$$= \tan \epsilon_4$$

$$= \tan\left(\frac{\pi}{2} - \epsilon^*\right)$$

or $2\omega_4 = \pi/2 - \epsilon^*$

Also,

$$\epsilon_5 = \pi/2$$

From Eq. (5.43)

$$\sin 2\theta \sin\epsilon = \sin 2\omega$$

when $\epsilon = \pi/2$

$$\theta = \omega$$

$$\therefore \quad \theta_5 = \omega_5 = \theta_6$$

$$\tan 2\alpha_6 = \tan 2\theta_6 \cos\epsilon_6 = \tan 2\omega_5$$

i.e. $\alpha_6 = \omega_5 = \omega_4 = \frac{\pi}{4} - \frac{\epsilon^*}{2}$

The angle between the axes of the second quarte -wave plate and analyser is given by

$$\alpha_7 - \alpha_6 = \pi/2 - \alpha_6$$

$\therefore$ The orientation of analyser axes is given by

$$\bar{\alpha} = (\alpha_7 - \alpha_6) + \pi/4$$

$$= 3\pi/4 - \alpha_6$$

$$= \frac{\pi}{2} + \frac{\epsilon^*}{2}$$

or $\epsilon^* = 2\bar{\alpha} - \pi$

From this graphical representation the essential features of light ellipse can be observed clearly. For any light ellipse, for directions nearly at 45° to its major or minor axis, the variation of phase difference with direction is very small. (Because, the constant ellipticity curves are almost flat for values of α around 45°). This variation is high for directions close to the major or minor axis. Also, we see that as the ellipticity nears unity, the variation of amplitude with direction becomes small. This chart will be very useful in finding the effects of small errors in the retardances of quarter-wave plates readily.

Determination of Characteristic Parameters:

To find the characteristic parameters of a system of linear retarders Schwieger suggested a geometrical construction and an iterative method, and Cernosek presented a method based on quaternions. A much simpler and direct method to find these characteristic parameters will now be described. If the incident light on the equivalent optical system is circularly polarized, the amplitudes of the components of light vibration before and after the linear retarder along its axes (primary characteristic directions) are equal, and these components are just rotated in space by the pure rotator to coincide with the secondary characteristic directions (Because, the angle between the primary and secondary characteristic directions is equal to the rotatory power). So, the mutually perpendicular directions at the exit of the system along which the light components have equal amplitudes are the secondary characteristic directions.

This method can be used with any of the above described graphical methods (except the one using quaternions) and with the second graphical method to be described now. Once the secondary characteristic directions are found, the primary characteristic directions and the characteristic retardation can be found directly by using a different type of incident polarized light other than circularly polarized light. An example of finding the characteristic parameters for a combination of two retarders using this chart will be presented at the end of this section.

The Second Graphical Method:

Squaring and adding Eqs. (5.41) and (5.42), we obtain

$$\mathrm{Sin}^2\, 2\theta\, \mathrm{Cos}^2\epsilon + \mathrm{Cos}^2\, 2\theta = \mathrm{Cos}^2\, 2\omega$$

or

$$\mathrm{Cos}^2\, 2\theta\, \mathrm{Sin}^2\epsilon + \mathrm{Cos}^2\epsilon = \mathrm{Cos}^2\, 2\omega$$

Let $\mathrm{Cos}^2\, 2\omega = x$ and $\mathrm{Cos}^2\, 2\theta = y$

then

$$y = \frac{x}{\mathrm{Sin}^2\epsilon} - \mathrm{Cot}^2\epsilon \qquad (5.59)$$

For a given value of ϵ, this equation represents a straight line.

Since the set of values $x = 1$, $y = 1$ satisfies Eq. (5.59) irrespective of the value of ϵ, Eq. (5.59) represents a family of straight lines all passing through the point $x = 1$, $y = 1$. Also,

if $\epsilon = 0$, $x = 1$; and if $\epsilon = \pi/2$, then $x = y$

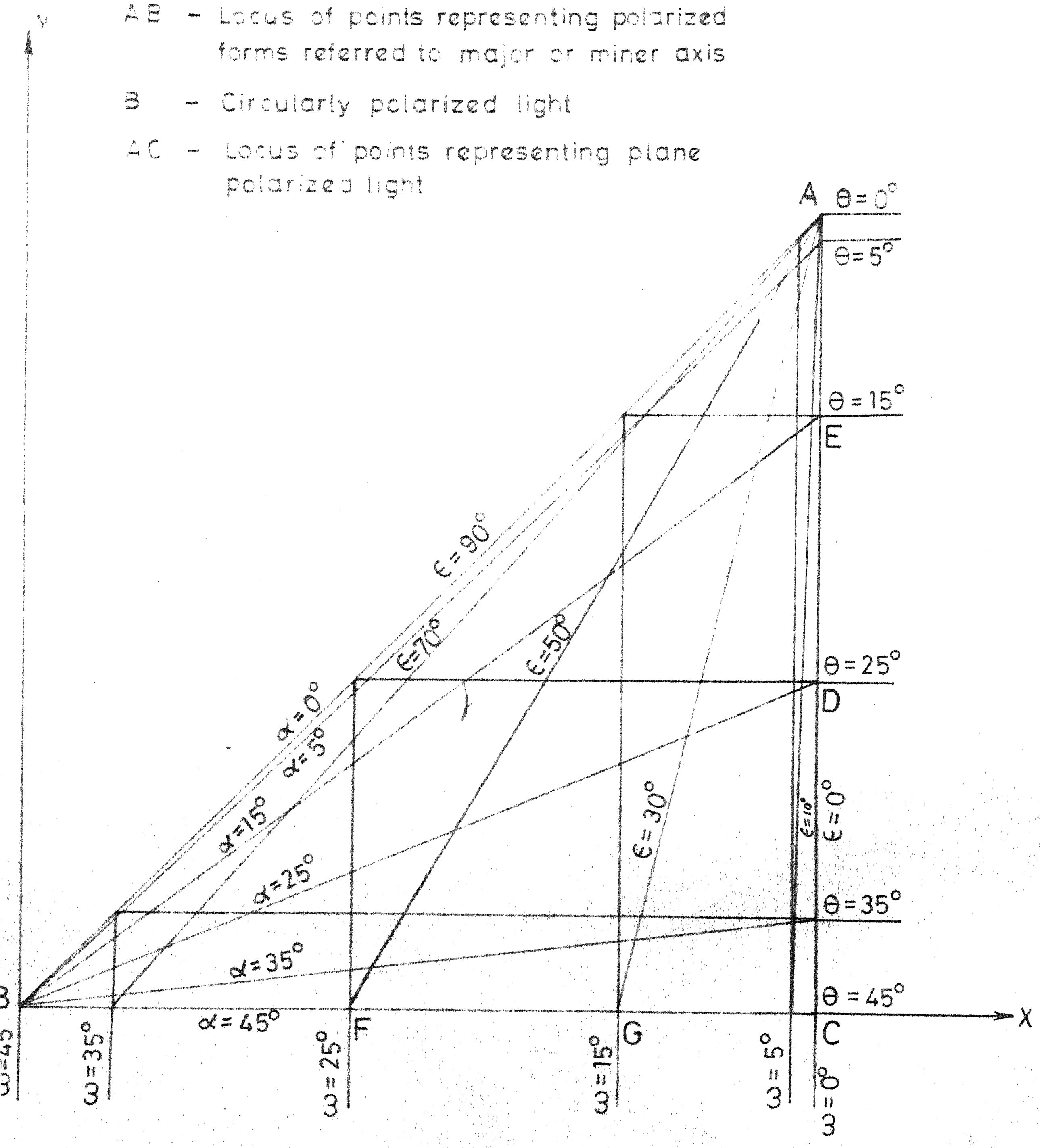
y
AB - Locus of points representing polarized forms referred to major or miner axis
B - Circularly polarized light
AC - Locus of points representing plane polarized light
A
θ = 0°
θ = 5°
θ = 15°
E
θ = 25°
D
θ = 35°
θ = 45°
C
X
B
F
G
ε = 90°
ε = 70°
ε = 50°
ε = 30°
ε = 10°
ε = 0°
α = 0°
α = 5°
α = 15°
α = 25°
α = 35°
α = 45°
ω = 35°
ω = 25°
ω = 15°
ω = 5°
ω = 0°

FIG. 52. THE SECOND GRAPHICAL METHOD.

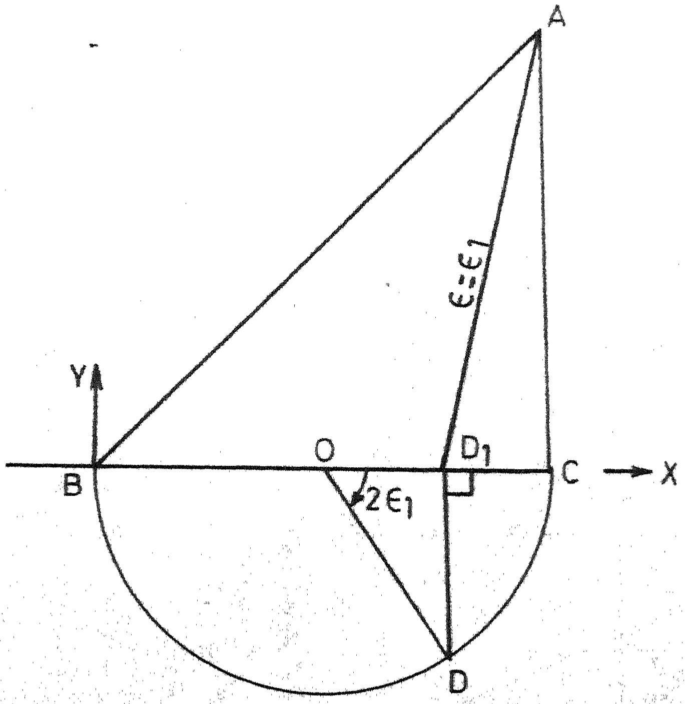

FIG. 53. CONSTRUCTION OF CONSTANT PHASE DIFFERENCE LINCS.

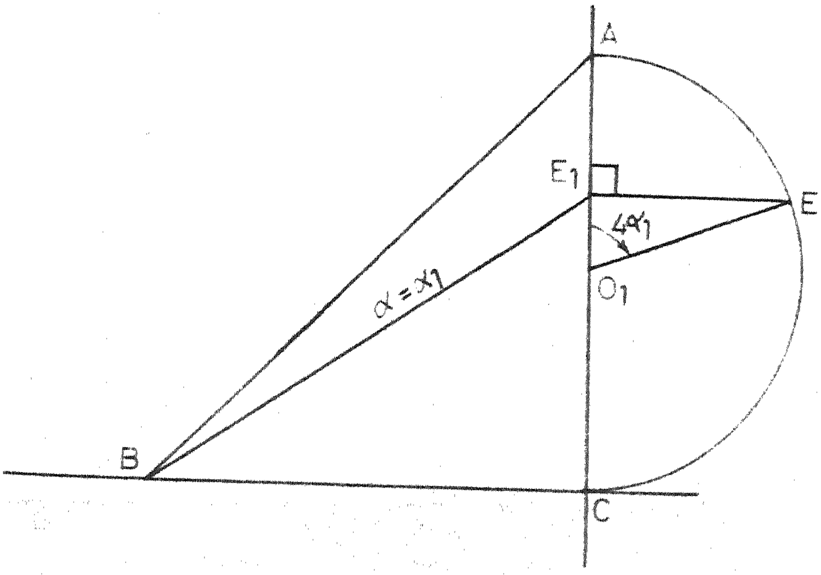

FIG.54. CONSTRUCTION OF CONSTANT AZIMUTH LINES

if $y = 0$

$$x = \cos^2 \epsilon = \cos^2 2\omega$$

$$\text{or } \epsilon = 2\omega$$

Squaring and adding Eqs. (5.42) and (5.43), we obtain

$$\sin^2 2\theta = \cos^2 2\omega \sin^2 2\alpha + \sin^2 2\omega$$

$$\text{or} \quad y = x \cos^2 2\alpha \qquad (5.60)$$

$$\text{If } x = 1,\ y = \cos^2 2\alpha = \cos^2 2\theta$$

$$\text{or } \alpha = \theta$$

The families of straight lines represented by Eqs. (5.59) and (5.60) can be plotted as shown in Fig. 52.

Eq. (5.59) represents straight lines of constant phase difference AC, AG, AF, AB,.... etc. Eq. (5.60) represents straight lines of constant azimuth BA, BE, BD, BC, ..., etc. The ordinates are lines of constant ellipticity and the abscissae are lines of constant amplitude ratio.

Geometrical Construction of $x = \cos^2 2\omega$ And $y = \cos^2 2\theta$ Scales (Figs. 53 And 54)

In Fig. 53. BC = AC = 1 and $\hat{BCA} = 90^\circ$. Draw a semi circle on BC with 0, the mid-point of BC as the center. To construct the constant phase difference line ($\epsilon = \epsilon_1$), take point D on the semicircle such that $\hat{COD} = 2\epsilon_1$. Draw the perpendicular DD_1 to BC. D_1A is the required constant phase difference line with $\epsilon = \epsilon_1$. The proof for this is as follows:

In the graph point B is the origin and line BC is along the x-axis. Also $x = \cos^2 2\omega$ and $y = \cos^2\theta$.

On x-axis,

$$\epsilon = 2\omega$$

as shown above

Now in Fig. 53,

$$BD_1 = BO + OD_1$$

$$= \tfrac{1}{2} + \tfrac{1}{2}\cos 2\epsilon_1$$

$$= \cos^2\epsilon_1$$

If the ellipticity at the point D_1 is tan ω, the phase difference ϵ is given by the relation

$$\epsilon = 2\omega$$

Also, the value of x at D_1 is given by

$$x = \cos^2 2\omega$$

$$= \cos^2 \epsilon_1$$

$$\text{or } 2\omega = \epsilon_1$$

$$\therefore \quad \epsilon = \epsilon_1$$

We know that all constant phase difference lines pass through, the point A (1,1). Therefore the line AD_1 is the constant phase difference line with $\epsilon = \epsilon_1$.

The procedure for construction of constant azimuth lines is exactly similar. In Fig. 54. AEC is the circle on AC with O_1 as center ($AO_1 = O_1C$). To construct the constant azimuth line $\alpha = \alpha_1$, locate the point E on this circle such that $A\hat{O_1}E = 4\alpha_1$. Draw the perpendicular EE_1 on AC from the point E to meet AC in E_1.

For point E_1,

$$x = 1,$$

$$y = \cos^2 2\theta = CO_1 + O_1E$$

$$= \frac{1}{2} + \frac{\cos 4\alpha_1}{2}$$

$$= \cos^2 2\alpha_1$$

$$\therefore \quad \theta = \alpha_1$$

Also $\alpha = \theta$ when $x = 1$ (shown above)

$$\therefore \quad \alpha = \alpha_1$$

So, the azimuth at the point E_1 is α_1.

We know that all the constant azimuth lines pass through the origin B. So BE_1 is the constant azimuth line with $\alpha = \alpha_1$.

To increase the phase difference from ϵ_1 to ϵ_2 we move along the constant amplitude ratio (i.e. parallel to X-axis) and for rotation of the reference axes from azimuth α_1 to α_2 we move along the constant ellipticity line (i.e. parallel to Y-axis).

The same chart can be used for other ranges also i.e. beyond $\pi/2$ but the proper signs are to be taken into account. This is demonstrated at the end of this section.

The striking advantages of this method are that (i) it is very simple and easy to draw since it involves only straight lines and (ii) the nonlinear scales can be easily constructed by using the method described above.

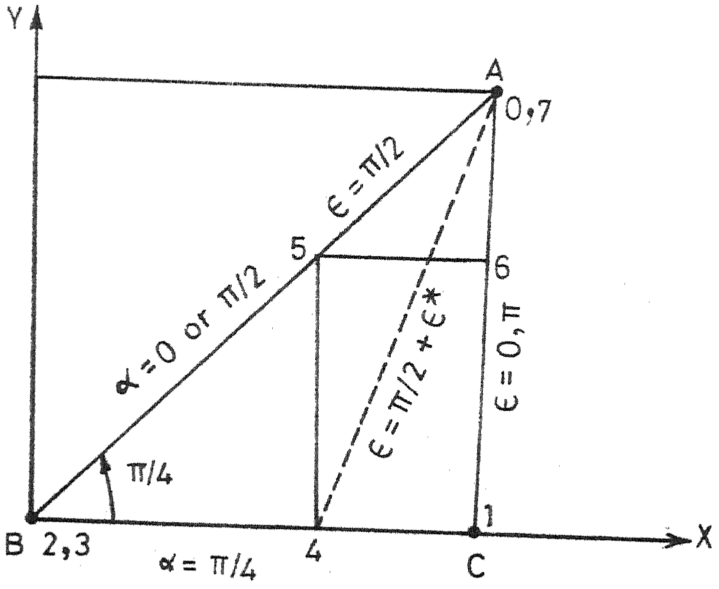

FIG. 55. ANALYSIS OF TARDY'S METHOD USING THE SECOND GRAPHICAL METHOD.

The analysis for plane and circular polariscope using this chart is exactly similar as that described for the first graphical method.

Tardy's Method:

In Fig. 55. the notations are same as those used in Fig. 50. Point O is plane polarized light referred to the axes of polarizer. Point 1 represents light before the first quarter-wave plate referred to its own axes. Addition of a retardation of $\pi/2$ is represented by movement along the constant amplitude ratio line (parallel to X-axis) from $\epsilon = 0$ line (A C) to $\epsilon = \pi/2$ line (A B), that is to the point 2, which represents circularly polarized light. The same vibration, but referred to the principal-stress (inclined at 45° to the first quarter-wave plate axes) is represented by the point 3 (which coincides with point 2). This rotation of the reference axes through 45° is represented on the chart by movement along the constant ellipticity line (i.e. parallel to Y-axis) from $\alpha = 45^\circ$ line (B C) to $\alpha = 90^\circ$ line (A B). Addition of a retardation of ϵ^* in the model is represented by movement from point 3 to point 4 along constant amplitude ratio line till the representative point is on the constant relative phase line with $\epsilon = \pi/2\pi + \epsilon^*$. Light vibration after the model but referred to the axes of the second quarter-wave plate is obtained by moving the representative point from 4 to 5 along the constant ellipticity line. Subtraction of a retardation of $\pi/2$ in the quarter-wave plate is represented by movement along the constant amplitude ratio line from point 5 to point 6. In order to cut off light, the amplitude ratio along the analyser axis must be ∞. This can be achieved by making point 6 come to point 7 along the constant ellipticity line. The orientation of the analyser axis is then $(\alpha_7 - \alpha_6)$ whose value can be found as follows:

From Fig. 55.

$$x_C - x_4 = x_6 - x_5 = y_7 - y_6$$

But $x_C = y_7 = 1$

$\therefore$ $x_4 = y_6$

i.e. $\cos^2 2\omega_4 = \cos^2 2\theta_6$ or $\omega_4 = \theta_6$

Also $\epsilon_C - \epsilon_4 = 2\omega_C - 2\omega_4$

$(\therefore$ when $y = 0, \epsilon = \omega)$

And $\epsilon_C = \omega_C = 0$

$\therefore$ $\epsilon_4 = 2\omega_4$

Also

$\alpha_7 - \alpha_6 = \theta_7 - \theta_6$

$(\because$ when $x = 1, \theta = \alpha)$

But $\alpha_7 = \theta_7 = 0$

$\therefore$ $\alpha_6 = \theta_6$

$\therefore$ $\epsilon_4 = 2\omega_4 = 2\theta_6 = 2\alpha_6$

If the retardation added in the model is ρ then $\rho = \epsilon_4 - \pi/2$. If the angle between the analyser axis and one of the principal-stress axes is β, then

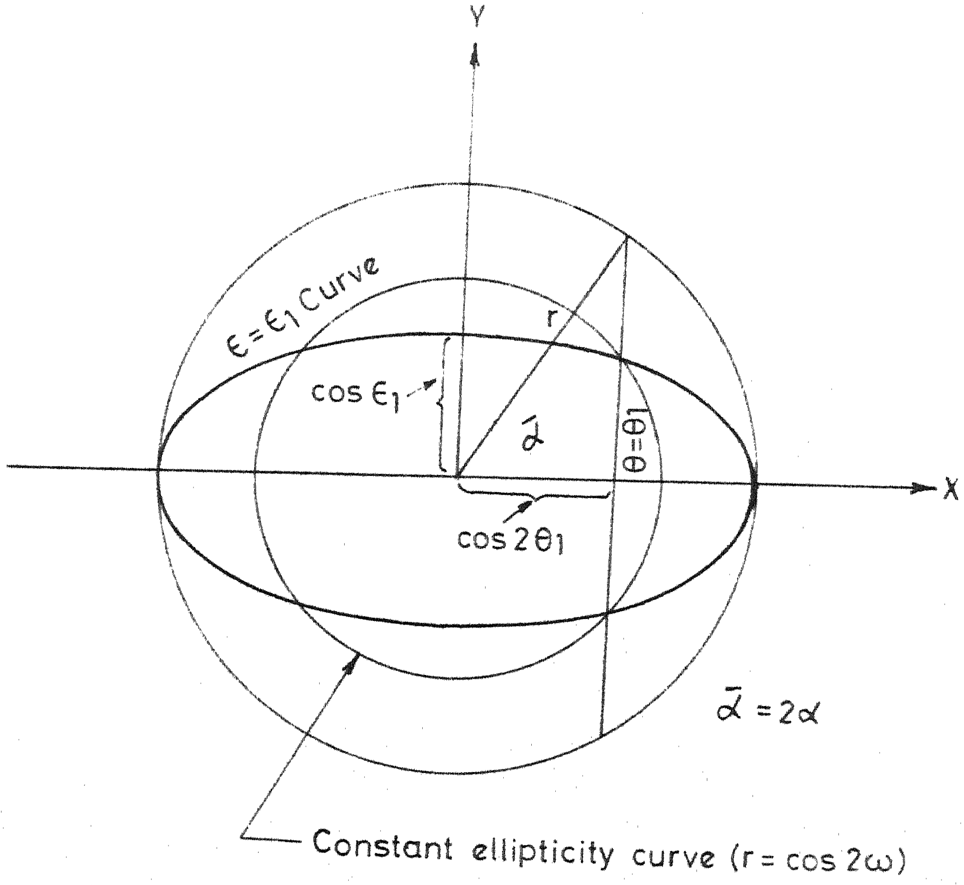

FIG. 56. POLAR CO-ORDINATES FOR J CIRCLE METHOD.

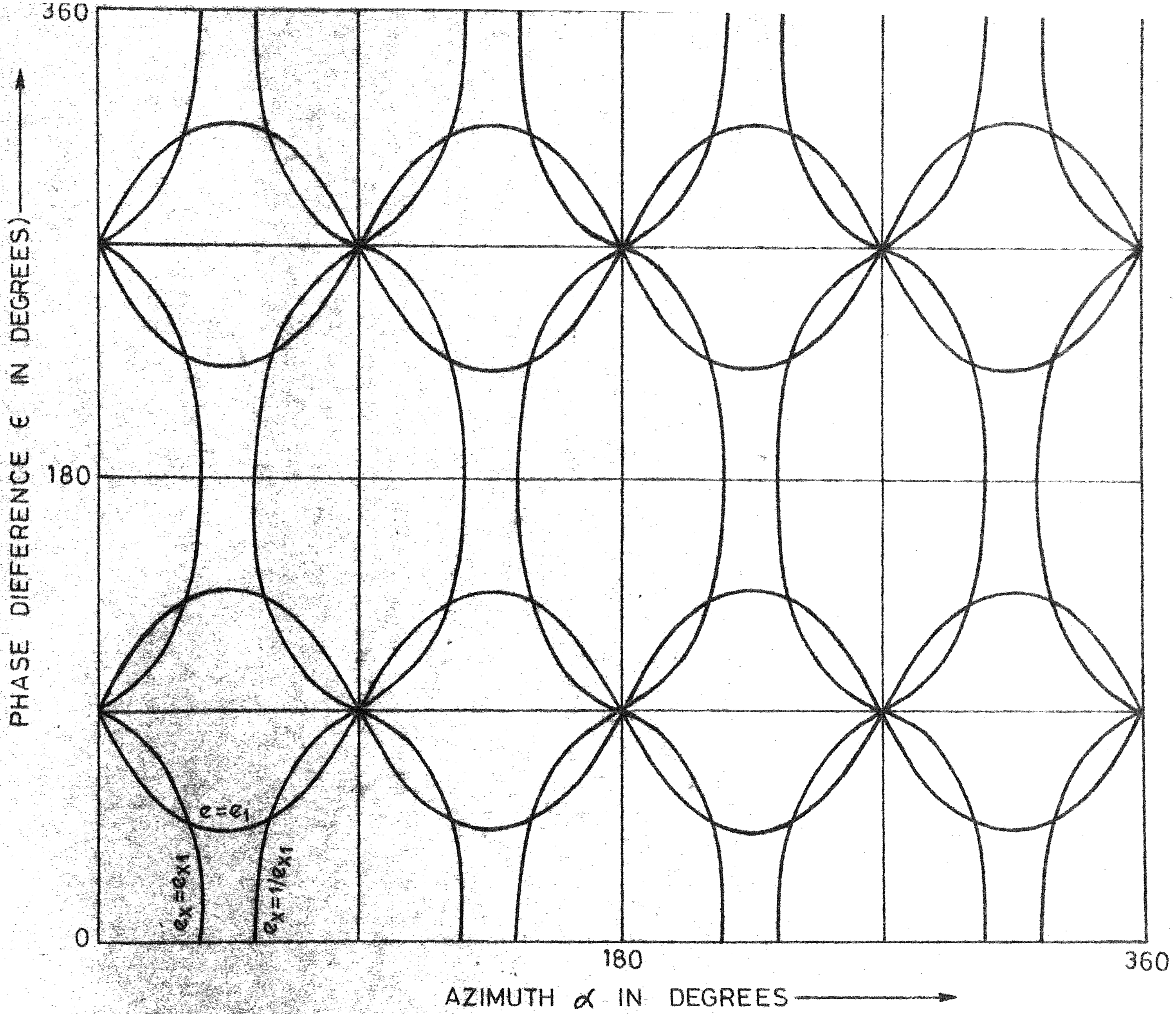

FIG. 57. FIRST GRAPHICAL METHOD $(0<\alpha<2\pi, 0<\epsilon<2\pi)$.

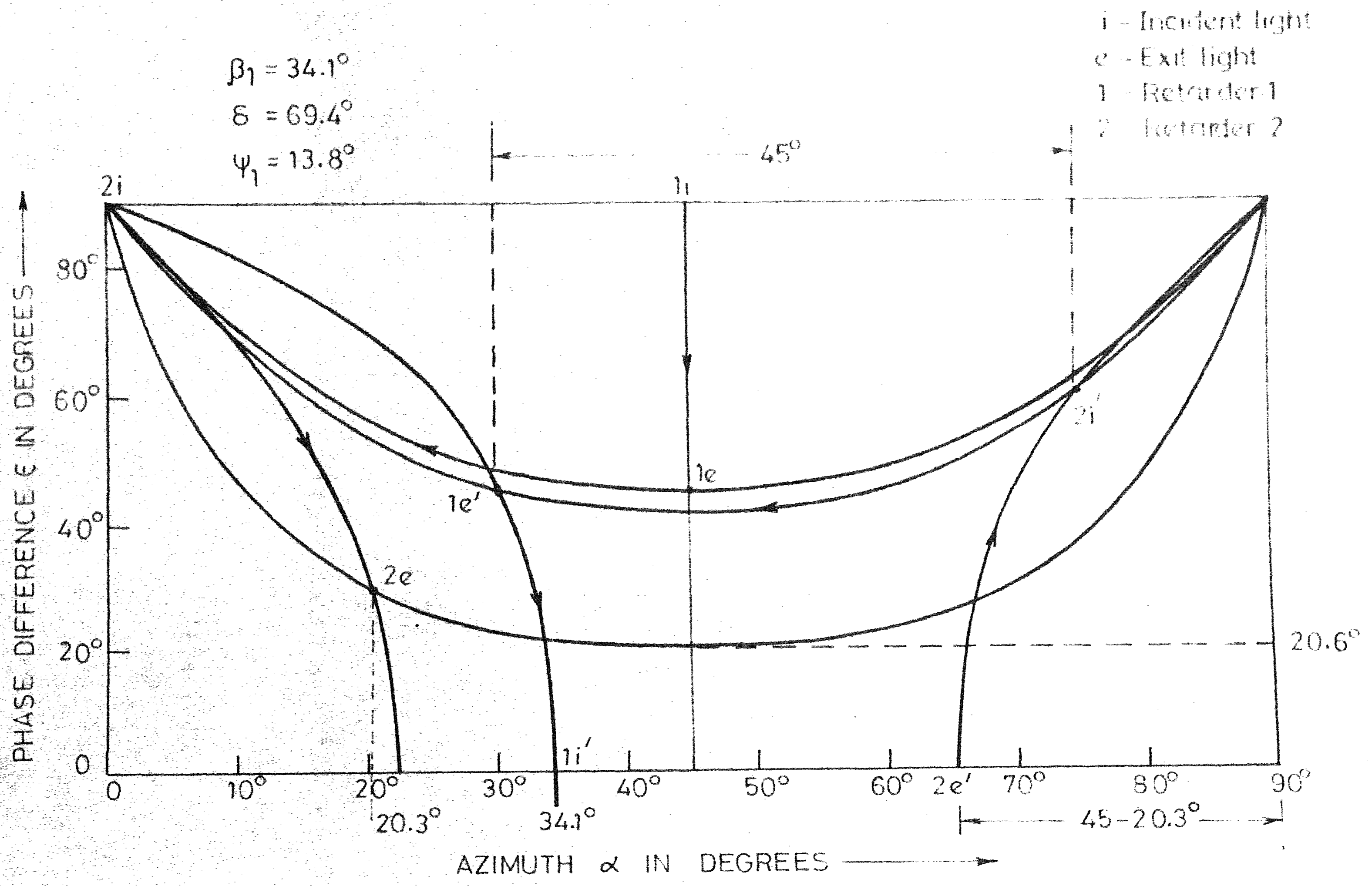

FIG. 58 (a). EXAMPLE (a), FIRST GRAPHICAL METHOD.

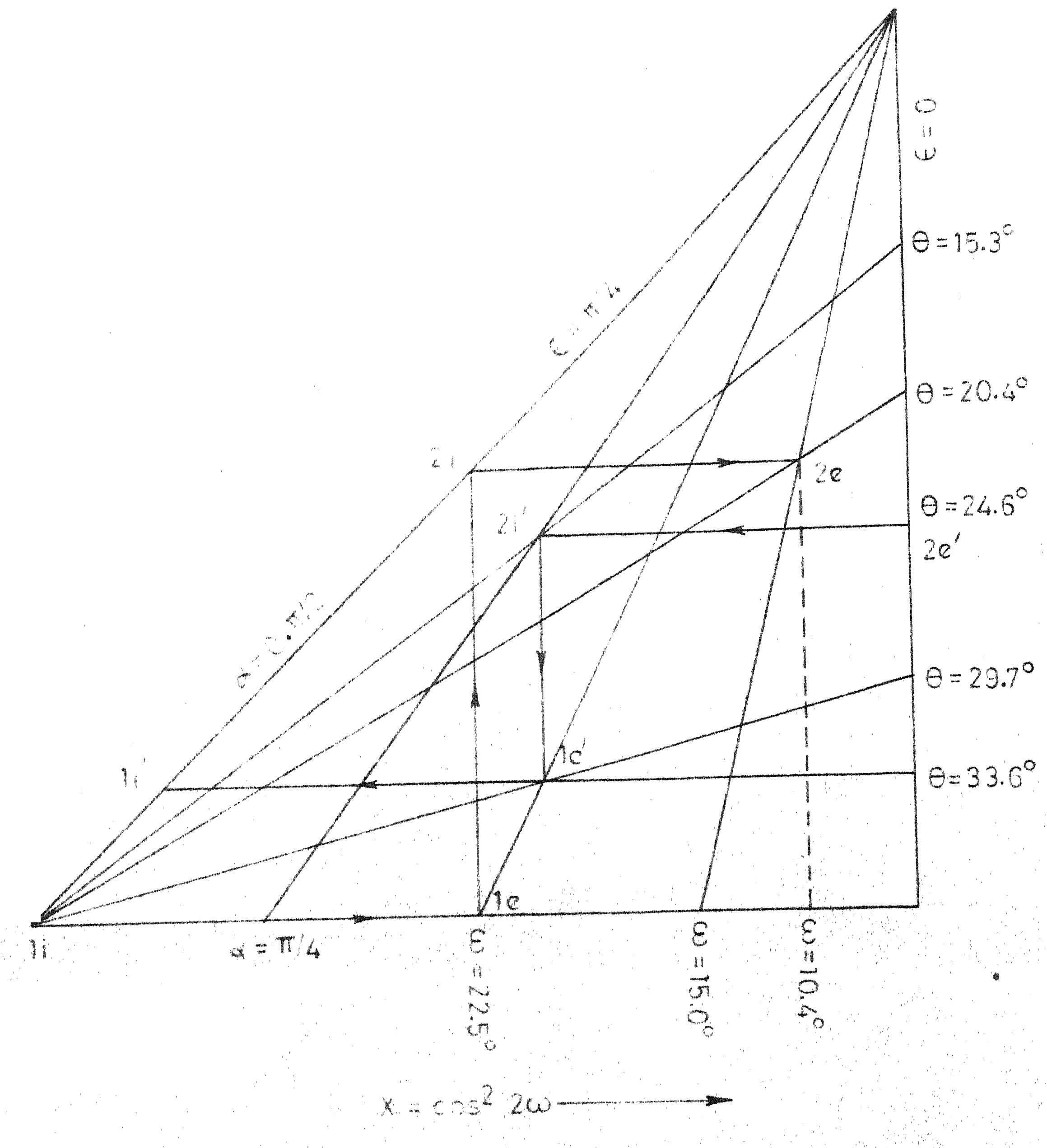

FIG. 58(b). EXAMPLE (a), SECOND GRAPHICAL METHOD

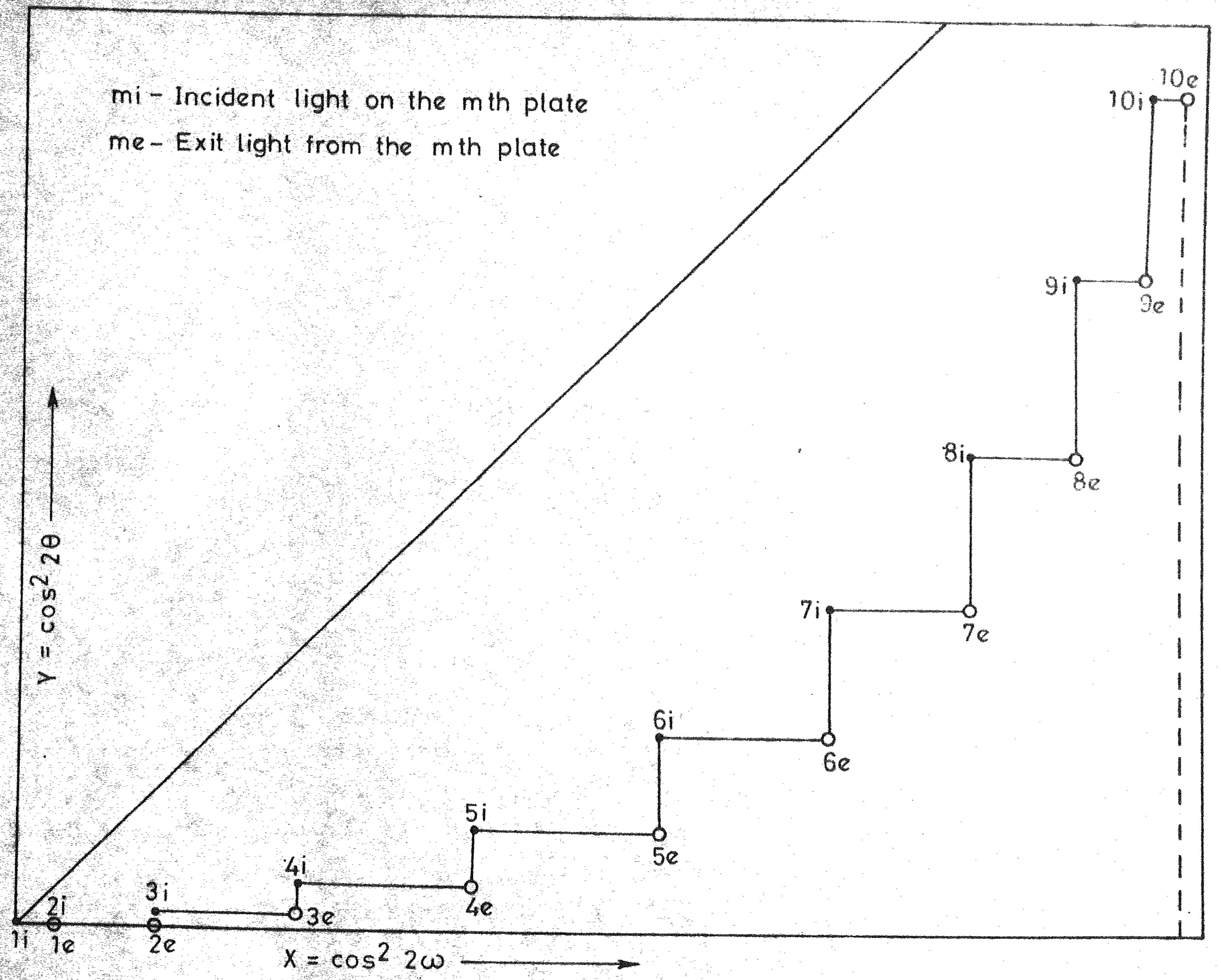
mi - Incident light on the mth plate
me - Exit light from the mth plate
Y = cos² 2θ
X = cos² 2ω
1i
1e
2i
2e
3i
3e
4i
4e
5i
5e
6i
6e
7i
7e
8i
8e
9i
9e
10i
10e

FIG. 59. PROBLEM (b) SECOND GRAPHICAL METHOD.

$$\alpha_6 = \pi/4 - \beta$$

$$\therefore \quad \epsilon = \epsilon_4 - \pi/2$$

$$= 2\alpha_6 - \pi/2$$

$$= -2\beta$$

Derivation of J Circle Method Without Referring To The Poincare' Sphere Representation of Polarized Forms

Consider the polar coordinate system $(r, \bar{\alpha})$, Fig.56.
Let $r = J = (\mathrm{Cos}^2 2\theta + \mathrm{Sin}^2 2\theta \, \mathrm{Cos}^2 \epsilon)^{\frac{1}{2}}$

then $r = \mathrm{Cos}\ 2\omega$ (5.62)

- using Eqs. (5.41) and (5.42)

Therefore, the magnitude of the radius vector r is a measure of the ellipticity. So, the curves of constant ellipticity are concentric circles with center at O, the origin.

Let $\bar{\alpha} = 2\alpha$

where α is the azimuth

then $r\ \mathrm{Cos}\bar{\alpha} = J\ \mathrm{Cos}\ 2\alpha$ (5.63)

But from Eqs. (5.41) and (5.43)

$\mathrm{Cos}\ 2\alpha = \mathrm{Cos}\ 2\theta/J$ (5.64)

so that

$r\mathrm{Cos}\bar{\alpha} = \mathrm{Cos}\ 2\theta$ (5.65)

i.e. the x component $(= r\mathrm{Cos}\bar{\alpha})$ depends on θ only. So, the loci of points of constant amplitude ratio are straight lines perpendicular to the X-axis.

Now,

$$x = r \text{ Cos } \bar{\alpha} = \text{Cos } 2\theta \ .$$

$$y = r \text{ Sin } \bar{\alpha} = \text{Cos } 2\omega \text{ Sin } 2\alpha$$

$$\therefore \quad x^2 + \frac{y^2}{\text{Cos}^2 \epsilon} = \text{Cos}^2 \ 2 \quad + \frac{\text{Cos}^2 2\omega \text{ Sin}^2 2\alpha}{\text{Cos}^2 \epsilon}$$

$$= 1 \qquad \text{- using Eq. (5.42)} \qquad (5.66)$$

Eq. (5.66) represents a family of ellipses with their centers coinciding with the origin and with the lengths of semi-minor and semi-major axes as Cosϵ and unity respectively. So the locus of points of constant phase difference is an ellipse belonging to this family of ellipses. The Wulff's grid (stereographic projection) method can also be derived in a similar way without referring to Poincare' sphere by choosing a proper expression for r, the radius vector.

The graphical methods described can be used for values of phase difference and azimuth beyond the range 0 - π/2. The first graphical method is plotted in Fig. 57. for the ranges $0<\alpha<2\pi$, $0<\epsilon<2\pi$

Some Examples of Using the Graphical Method

We shall now take up the two examples of Schwieger for finding the characteristic parameters.

Example (a)

Consider the combination of two models (linear retarders). Model (1) produces a retardation of $\Delta_1 = 45$ deg. Model (2) produces a retardation of $\Delta_2 = 60$ deg. The angle between the axes of these two models is given by

$$\rho_{12} = 45 \text{ deg.}$$

The characteristic parameters of this system are found by one of the methods described earlier. i.e. the secondary characteristic direction ρ_2 and the characteristic retardation δ are found from the exit light ellipse parameters when the incident light ellipse is circularly polarized. The primary characteristic direction ρ_1 is found by determining the azimuth of light at the entrance which produces plane polarized light along one of the secondary principal-stress axes at the exit of the system. This is found by tracing back from the exit point to entrance point of the system. This is demonstrated in Figs. 58(a) and 58(b). From these graphical methods,

$$\delta = 69.4 \text{ deg.}$$

$$\psi_1 \text{ (rotatory power)} = 13.8 \text{ deg.}$$

Orientation of primary characteristic directions with respect to the axes of the first model) = $\rho_1 = 34.1$ deg.

Results from the second graphical method:
(The procedure is demonstrated in Fig. 59.)

$\psi_1 = -10.8$ deg.

$\rho_1 = 26.7$ deg.

$\delta = 84$ deg.

Theoretical Values using the analytical solution (Chapter 2) :

$\psi_1 = -9.8$ deg.

$\rho_1 = 27.4$ deg.

$\delta = 78.6$ deg.

In this section we have developed two new graphical methods to trace the passage of polarized light through a series of optical elements. These two methods are compared with a few of the existing graphical methods. Procedures for the use of the new graphical methods are described with application to various polariscope arrangements. The first method traces the transformation of polarized light through the same constant ellipticity and constant amplitude ratio curves. The second method also makes use of the same principles, but involves only straight lines in the graph which are convenient from the construction point of view.

B. THEORY OF COMPENSATION

In this section, we shall first present a brief review of the existing methods of compensation and the methods of measuring the integral fringe orders. Then, we shall describe, the development of a compensator which has certain advantages over the previous ones, and a general method of measuring the integral fringe orders. The theory for these methods makes use of the concept of optically equivalent system and various methods of determining this system for a series of retarders which were described in Chapter 3.

The compensator can be defined as an optical device which introduces a required amount of retardation along a particular set of axes. This is equivalent to a two-dimensional photoelastic model in which the principal-stress difference can be varied at will. Jerrard[45] has given an account of different types of optical compensators in vogue.

One of the commonly used compensators in photoelastic investigations is the Babinet-Soleil compensator. This consists of two quartz wedges of same inclination with their fast axes parallel and a rectangular block of quartz in series with these wedges with its fast axis perpendicular to that of the wedges. The retardation is varied by the lateral movement of the wedges and thus their combined thickness in the optical path. Other types of compensators include Coker[20] compensator which is a tensile strip (preferably made of the same material as that of the model) in which the tension can be varied by a loading frame, a model beam compensator, (Jellyman and Milne[46]), in which the fringes resulting from bending are frozen into the material; mica plate compensator, (Phemister [47]), in which the angle of incidence of light is varied to affect a variation of the retardation introduced; etc. The compensation methods which donot involve the use of any additional optical elements are the Tardy compensation, De Senarmont compensation and the inverse Tardy method (Chapter 2). The underlying principle in all these methods of compensation is to introduce a retardation equal and opposite to that introduced along the principal-stress direction (or the characteristic direction in a three-dimensional case), so that total extinction of light is obtained when observed in the polariscope. The retardation introduced can be related to the (secondary) principal-stress difference in the model.

Some of the desirable characteristics of a compensator can be listed as follows:
(1) the principle of operation should be simple and the relation between the movement (angular or linear) in the compensator and the retardation that it introduces should be linear, (2) it should be inexpensive, (3) be accurate, (4) be useful for all wavelengths of light in the visible region (5) have a large field so that it can be used directly in the diffused light polariscope and (6) its retardation should not vary with time.

The Babinet-Soleil compensator involves a very careful preparation of the wedges and so is expensive.

But, it can be used with white light to find the integral fringe order upto about six fringes. But it does not give correct results when the variation of the material fringe constant of the model with wavelength is not linear (assuming that it is so for the quartz wedges and the rectangular quartz block in the compensator). Its field of view is very small and is about 1 cm. in diameter. Coker's compensator is cumbersome because of the loading frame. Phemister's[47] mica plate compensator has a nonlinear relationship between the angle of light incidence and the retardation introduced in the model. It cannot be used to find the integral fringe order directly. The compensators which involve freezing of stresses into a piece of photoelastic material usually exhibit time dependence of the retardations. The Tardy, De Sénarmont and inverse Tardy methods can not be used with white light to find the total fringe order directly. They involve some errors if the wavelength of light is changed since the quarter-wave plates that are used show some dependence of their retardation with the wavelength of light. It is the objective of this section to develop methods of compensation which involve minimum of the above drawbacks using the theory of characteristic parameters discussed in Chapter 3.

Pancharatnam[28], in his analysis on achromatic circular polarizer and achromatic quarter-wave plate suggested that two quarter-wave plates with a half-wave plate in between will act as a compensator. Tuzi[29] suggested that a combination of two retarder plates of equal retardance can be used as a quarter-wave plate. But this combination will have a rotatory power. Childs [48] used the combination of 3 retarder plates to act as a quarter-wave plate with no rotatory power. The present compensator to be described is essentially based on these principles. The analysis for this will be made using the Stoke's vector.

Combination of Two Linear Retarders of Equal Retardance ρ

Consider two linear retarders each of retardance ρ (with the angle between their axes being $\bar{\theta}$). The transformation of the Stokes vector through this system is given by:

(Let V_0 and V be the Stokes vectors of light at the entrance and exit of the first retarder with respect to its axes)

$$V_0 \equiv \begin{bmatrix} S_{1i} \\ S_{2i} \\ S_{3i} \end{bmatrix} \rightarrow \begin{bmatrix} S_{1i} \\ S_{2i} \operatorname{Cos} \rho - S_{3i} \operatorname{Sin} \rho \\ S_{3i} \operatorname{Cos} \rho + S_{2i} \operatorname{Sin} \rho \end{bmatrix} = \begin{bmatrix} S_1 \\ S_2 \\ S_3 \end{bmatrix} \equiv (V)$$

Let V_1 and V_2 be the Stokes vectors at the exit of the first and second retarders referred to the axes of the second retarder. We then have,

$$V \rightarrow V_1 \equiv \begin{bmatrix} S_1 \operatorname{Cos} 2\bar{\theta} + S_2 \operatorname{Sin} 2\bar{\theta} \\ S_2 \operatorname{Cos} 2\bar{\theta} - S_1 \operatorname{Sin} 2\bar{\theta} \\ S_3 \end{bmatrix} \rightarrow \begin{bmatrix} S_1 \operatorname{Cos} 2\bar{\theta} + S_2 \operatorname{Sin} 2\bar{\theta} \\ (S_2 \operatorname{Cos} 2\bar{\theta} - S_1 \operatorname{Sin} 2\bar{\theta}) \operatorname{Cos} \rho - S_3 \operatorname{Sin} \rho \\ S_3 \operatorname{Cos} \rho + \operatorname{Sin} \rho \, (S_2 \operatorname{Cos} 2\bar{\theta} - S_1 \operatorname{Sin} 2\bar{\theta}) \end{bmatrix}$$

$$\equiv V_2$$

Also,

$$V_2 \rightarrow \begin{bmatrix} (S_1 \operatorname{Cos} 2\overline{\theta} + S_2 \operatorname{Sin} 2\overline{\theta}) \operatorname{Cos} 2\overline{\theta} - \operatorname{Sin} 2\overline{\theta} \; \{ \operatorname{Cos} \rho \\ (S_2 \operatorname{Cos} 2\overline{\theta} - S_1 \operatorname{Sin} 2\overline{\theta}) - S_3 \operatorname{Sin} \rho \} \\ \{ (S_2 \operatorname{Cos} 2\overline{\theta} - S_1 \operatorname{Sin} 2\overline{\theta}) \operatorname{Cos} \rho - S_3 \operatorname{Sin} \rho \} \operatorname{Cos} 2\overline{\theta} \\ + \operatorname{Sin} 2\overline{\theta} \, (S_1 \operatorname{Cos} 2\overline{\theta} + S_2 \operatorname{Sin} 2\overline{\theta}) \\ S_3 \operatorname{Cos} \rho + \operatorname{Sin} \rho \, (S_2 \operatorname{Cos} 2\overline{\theta} - S_1 \operatorname{Sin} 2\overline{\theta}) \end{bmatrix}$$

$$= \begin{bmatrix} \overline{S}_1 \\ \overline{S}_2 \\ \overline{S}_3 \end{bmatrix} \equiv \overline{V} \qquad (5.67)$$

where $\overline{V}$ is the Stokes vector of light at the exit of the second retarder with respect to the axes of the first retarder.

If V_0 and V_1 are the Stokes vectors of incident light referred to the axes of the first retarder (reference axes) and the retarder of the optically equivalent system, we have

$$V_0 \equiv \begin{bmatrix} S_1 \\ S_2 \\ S_3 \end{bmatrix} \rightarrow \begin{bmatrix} S_1 \operatorname{Cos} 2\beta_1 + S_2 \operatorname{Sin} 2\beta_1 \\ S_2 \operatorname{Cos} 2\beta_1 - S_1 \operatorname{Sin} 2\beta_1 \\ S_3 \end{bmatrix} \equiv (V_1)$$

$$\rightarrow \begin{bmatrix} S_1 \operatorname{Cos} 2\beta_1 + S_2 \operatorname{Sin} 2\beta_1 \\ (S_2 \operatorname{Cos} 2\beta_1 - S_1 \operatorname{Sin} 2\beta_1) \operatorname{Cos} \delta - S_3 \operatorname{Sin} \delta \\ S_3 \operatorname{Cos} \delta + \operatorname{Sin} \delta \, (S_2 \operatorname{Cos} 2\beta_1 - S_1 \operatorname{Sin} 2\beta_1) \end{bmatrix} \equiv V_2$$

where V_2 is the Stokes vector of light at the exit of the retarder of the optically equivalent system referred to its axes.

This system is equivalent to an optically equivalent system with a single retarder (retardation δ, aximuth β_1 with respect to the axes of the first plate) and a rotator with a rotatory power of ψ_1. The transformation of the Stokes vector through the optically equivalent system is given by Also,

$$V_2 \rightarrow \begin{bmatrix} \text{Cos } 2\psi \, (S_1 \text{ Cos } 2\beta_{11} + S_2 \text{ Sin } 2\beta_1) - \text{Sin } 2\psi \left\{ \text{Cos } \delta \right. \\ \left. (S_2 \text{ Cos } 2\beta_1 - S_1 \text{ Sin } 2\beta_1) - S_3 \text{ Sin } \delta \right\} \\ \text{Cos } 2\psi \left\{ (S_2 \text{ Cos } 2\beta_1 - S_1 \text{ Sin } 2\beta_1) \text{ Cos } \delta - S_3 \text{ Sin } \delta \right\} \\ + \text{Sin } 2\psi \, (S_1 \text{ Cos } 2\beta_1 + S_2 \text{ Sin } 2\beta_1) \\ S_3 \text{ Cos } \delta + \text{Sin } \delta \, (S_2 \text{ Cos } 2\beta_1 - S_1 \text{ Sin } 2\beta_1) \end{bmatrix}$$

$$= \equiv \begin{bmatrix} \bar{S}_1 \\ \bar{S}_2 \\ \bar{S}_3 \end{bmatrix} \equiv \bar{V} \qquad (5.68)$$

where $\psi = \beta_1 + \epsilon_1$ and $\bar{V}$ is the Stokes vector of the light at the exit of the optically equivalent system (after the pure rotator) with respect to the reference axes.

We shall now find the parameters β_1, δ and ψ_1 of the optically equivalent system in terms of ρ and $\bar{\theta}$ using Eqs. (5.67) and (5.68).

Let the incident light be circularly polarized for the original system and the equivalent system. The Stokes vector of this incident light will be (0,0,1). Equating the Stokes vectors at the exit of both the systems and substituting for the incident Stokes vector, the vector (0,0,1), we obtain

$$\overline{S}_3 = \mathrm{Cos}^2\rho - \mathrm{Sin}^2\rho\,\mathrm{Cos}\,2\overline{\theta} = \mathrm{Cos}\,\delta \qquad (5.69)$$

$$\begin{aligned}\overline{S}_1 &= -\,\mathrm{Sin}\,\rho\,\mathrm{Sin}\,2\overline{\theta}\,\mathrm{Cos}\,2\overline{\theta} + \mathrm{Sin}\,\rho\,\mathrm{Cos}\,\rho\,\mathrm{Cos}\,2\overline{\theta}\,\mathrm{Sin}\,2\overline{\theta} \\ &\qquad + \mathrm{Cos}\,\rho\,\mathrm{Sin}\,\rho\,\mathrm{Sin}\,2\overline{\theta} \\ &= \mathrm{Sin}\,\delta\,\mathrm{Sin}\,2\psi \qquad (5.70)\end{aligned}$$

Now, let the incident light be plane polarized along one of the reference axes (i.e. the axes of the first retarder), such that V_0 is (1,0,0) for both the original and optically equivalent systems. Then, by equating the Stokes parameters of light at the exit of the two systems, we obtain

$$\overline{S}_3 = -\,\mathrm{Sin}\,2\overline{\theta}\,\mathrm{Sin}\,\rho = -\,\mathrm{Sin}\,2\beta_1\,\mathrm{Sin}\,\delta \qquad (5.71)$$

If δ is $\pi/2$ and the value of ρ is given, the value of $\overline{\theta}$ can be calculated, i.e., the value of $\overline{\theta}$ for which the system acts as a quarter-wave plate. From Eq. (5.69), for $\delta = \pi/2$, we have

$$\tan^2\rho = \mathrm{Sec}\,2\overline{\theta} \qquad (5.72)$$

Since Sec 2 $\geq$ 1 > $\pi/4$

$$\mathrm{Tan}^2\rho \geq 1 \text{ or } \rho \geq \pi/4 \qquad (5.73)$$

Also, from Eq. (5.71), the value of β_1 can be found as

$$\mathrm{Sin}\,2\overline{\theta}\,\mathrm{Sin}\,\rho = \mathrm{Sin}\,2\beta_1 \qquad (5.74)$$

From Eq. (5.70)

$$\sin 2\psi = \sin\rho \sin 2\overline{\theta}(-\cos 2\overline{\theta} + \cos\rho \cos 2\overline{\theta} + \cos\rho) \tag{5.75}$$

from which the values of ψ and ψ_1 can be calculated.

Combination of Two Quarter-wave Plates

We shall now investigate the behaviour of a combination of two quarter-wave plates and its use as a compensator. Substituting $\rho = \pi/2$ in Eqs. (5.69) and (5.71), we obtain

$$-\cos 2\overline{\theta} = \cos\delta$$

$$\text{or } \theta = \pi - 2\overline{\theta} \tag{5.76}$$

i.e. the characteristic retardation is linearly related to $\overline{\theta}$, the angle between the axes of the quarter-wave plates.

From Eq. (5.71)

$$2\beta_1 = \rho = \pi/2$$

$$\text{or } \beta_1 = \pi/4 \tag{5.77}$$

From Eq. (5.70)

$$-\cos 2\overline{\theta} = \sin 2\psi$$

$$\text{or } \psi = \overline{\theta} - \pi/4$$

$$= \beta_1 + \psi_1$$

$$= \pi/4 + \psi_1$$

$$\text{or } \psi_1 = \overline{\theta} - \pi/2 \tag{5.78}$$

i.e. the rotatory power is also related to $\overline{\theta}$, the angle between the axes of the two quarter-wave plates.

Hence, two quarter-wave plates with angle $\overline{\theta}$ between their axes are equivalent to a retarder (aximuth $\beta = \pi/4$

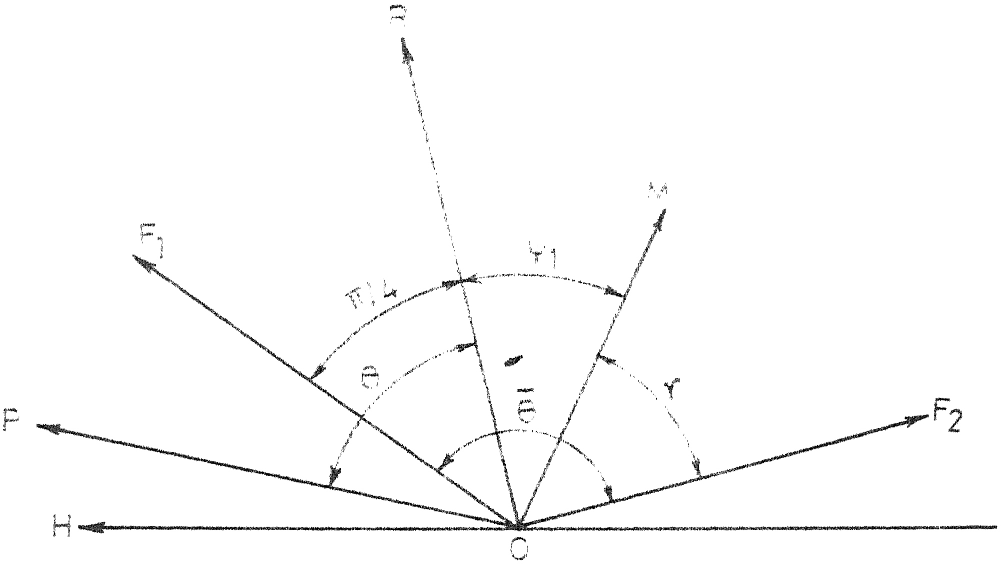

FIG. 60 (a). ORIENTATION OF AXES OF VARIOUS ELEMENTS.

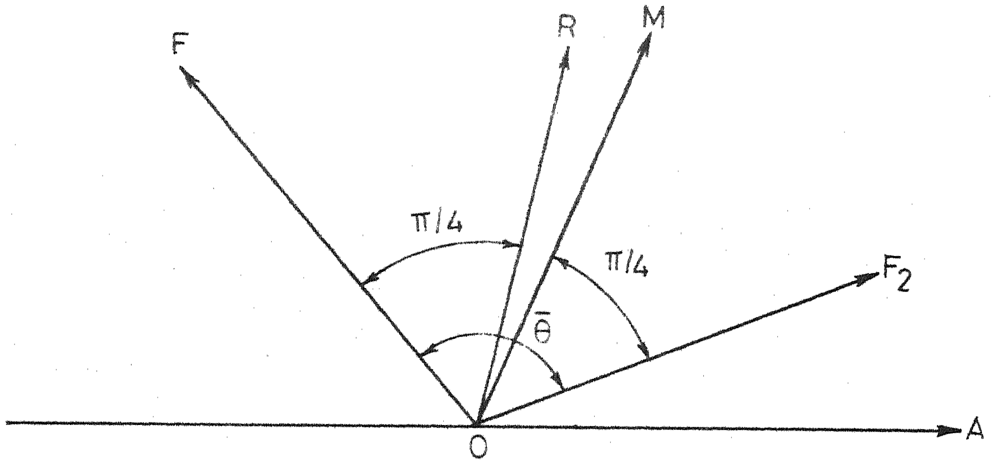

FIG. 60 (b). ORIENTATION OF AXES OF THE TWO QUARTER-WAVE PLATES AND ANALYSER.

with respect to the axes of the first quarter-wave plate, retardation $\delta = \pi - 2\bar{\theta}$) and a pure rotator of rotatory power $\psi_1 = (\bar{\theta} - \pi/2)$.

So this combination can be used as a compensator if this rotatory power is nullified. This can be done in the following way. Consider the system of a light source (unpolarized), a polarizer and two quarter-wave plates, Fig. 60. In Fig. 60(a) -

OP - Axis of the polarizer

OF_1 - Fast axis of the first quarter-wave plate OR - one of the axes of the retarder of the optically equivalent system (one of the primary characteristic directions)

OF_2 - Fast axis of the second quarter-wave plate

OM - One of the secondary characteristic directions

Also,

$$\gamma = \bar{\theta} - \frac{\pi}{4} - \psi_1 = \bar{\theta} - \frac{\pi}{4} - \bar{\theta} + \frac{\pi}{2} = \frac{\pi}{4}$$

i.e. the angle between the secondary characteristic directions and the axes of the second quarter-wave plate is $\pi/4$ which is a constant. So, with this combination of polarizer and quarter-wave plate, we can produce the required amplitude ratio and phase difference along the secondary characteristic directions (say OM and ON). Along these directions, the amplitude ratio will be $\tan\theta$ and the phase difference will be $(\pi - 2\bar{\theta})$. If the amplitude ratio is to remain constant, but the phase difference is to vary, we rotate the polarizer and the first quarter-wave plate together by the

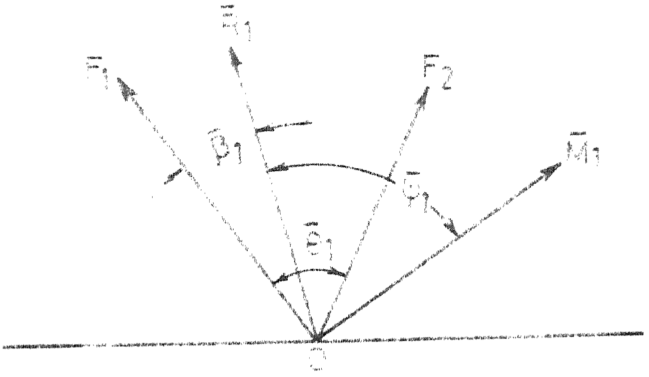

FIG. 61(a)

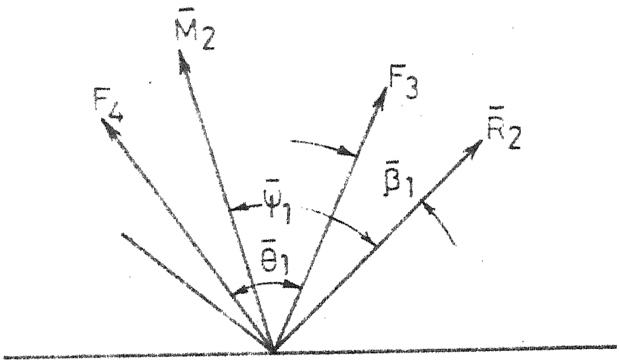

FIG. 61(b)

Orientations of the axes of the four retarders

F_1, F_2, F_3, F_4 are the fast axes of the first, second, third and fourth retarders respectively.

$\bar{R}_1, \bar{R}_2$ are the primary characteristic directions of the first and second systems.

$\bar{M}_1, \bar{M}_2$ are the corresponding secondary characteristic directions.

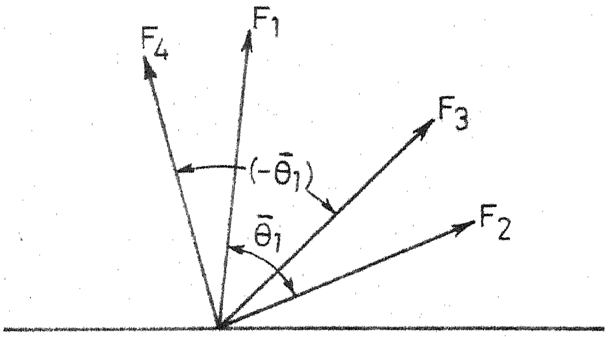

FIG. 61 (c)

required amount. If the phase difference is to be increased by $\bar{\rho}$ we rotate the polarizer first quarter-wave plate combination through an angle $-\bar{\rho}/2$, keeping the second quarter-wave plate fixed.

Similarly, the combination of two quarter-wave plates and analyser can be used as a compensator, Fig. 60(b). In this case, the second quarter-wave plate and analyser are to be rotated together so that retardation is varied along the fixed direction OR (the primary characteristic directions remain fixed in space if the first quarter-wave plate axes are fixed). The retardation added along the primary characteristic directions will again be $(\pi - 2\bar{\theta})$. By altering the value of $\bar{\theta}$, we can obtain the required amount of retardation. Rotation of the analyser is necessary to compensate for the rotation of the secondary characteristic directions with the second quarter-wave plate. A quarter-wave plate will have the same effect when it is rotated through π radians. Its effect will continuously vary as it is rotated through $0 - \pi$ radians. So, the angle $\bar{\theta}$ can take values from 0 to π i.e. We can introduce retardations from π to $-\pi$ (Eq. (5.76)) radians by these compensation techniques.

Now, consider two pairs of retarders, each pair consisting of two retarders of equal retardation ρ. The axes of these retarders and the primary and secondary characteristic directions of the corresponding optically equivalent systems are shown in Figs. 61(a) and 61(b).

F_1 , F_2 , F_3 , F_4 are the fast axes of the first, second, third and fourth retarders respectively.

$\overline{R}_1$, $\overline{R}_2$ are the primary characteristic directions of the first and second systems

$\overline{M}_1$, $\overline{M}_2$ are the corresponding secondary characteristic directions.

Now examine Eqs. (5.72), (5.73) and (5.74). In these equations if $\overline{\theta}_1$ is replaced by $-\overline{\theta}_1$, we obtain $-\overline{\beta}_1$ for $\overline{\beta}_1$, $-\overline{\psi}$ for $\overline{\psi}$ and $-\overline{\psi}_1$ for $\overline{\psi}_1$ ($\because$ $\overline{\psi}_1 = \overline{\psi} - \overline{\beta}_1$ from Eq. (5.68). i.e. if the angle between F_1 and F_2 is $\overline{\theta}_1$ and the angle between F_3 and F_4 is $-\overline{\theta}_1$, the rotatory powers of the equivalent systems for the pairs F_1, F_2 and F_3, F_4 will be equal but in opposite directions. Also, the optically equivalent system can be either a retarder and a rotator or a rotator and a retarder. In both cases, the rotatory powers and characteristic directions will be equal. But the retarder axes will be along the primary characteristic directions in the first case and along the secondary characteristic directions in the second case (Chapter 3). Let the axes of the four retarders be oriented as shown in Fig. 61(c).

Let the combination of the first two retarders be equivalent to a retarder (azimuth $\overline{\beta}_1$ with respect to the axes of the first retarder of retardation $\pi/2$) and a pure rotator of rotatory power $\overline{\psi}_1$. Then the combination of the third and fourth retarders will be equivalent to a system with a retarder (azimuth $-\overline{\beta}_1$ with respect to the axes of the third retarder of retardation $\pi/2$) and pure rotator of rotatory power $-\bar{\psi}_1$, or a system with a pure rotator of rotatory power $-\bar{\psi}_1$ and a retarder (azimuth $-\bar{\beta}_1 - \bar{\psi}_1$ with respect to the axes of the third retarder of retardation $\pi/2$). So, when the four retarders are arranged in sequence as shown in Fig. 61. the rotatory power of the first two retarders will be cancelled by the rotatory power of the combination of the third and fourth retarders. And the combination of the four retarders acts like two quarter-wave plates. The orientation of the axes of these quarter-wave plates will be along the primary characteristic directions for the first two retarders and the secondary characteristic directions of the combination of third and fourth retarders respectively. The orientations of these directions are found from Eq. (5.74) and these are fixed relative to the axes of the retarders once the values of $\bar{\theta}$ and ρ are fixed ($\bar{\rho}$ is the retardation of each of the retarders). Thus the combination of four retarders each of retardation ($\bar{\rho} \geq \pi/4$ from Eq. (5.73)) can be used as a combination of two quarter--wave plates. This in turn can be used as a compensator as described above. By varying the value of $\bar{\theta}_1$, the angle between the retarders, this combination can be used as a compensator for any wavelength of light. The range of wavelength is however limited by the value of $\bar{\rho}$ and the dispersion characteristics, (i.e. the variation of the retardation with wavelength) of the material of the retarders.

In the above discussion, we have shown that the combination of two quarter-wave plates can be used as a compensator provided the rotatory power introduced by the system is nullified by rotating the polarizer or analyser as the case may be. To develop a compensator which does not introduce any rotatory power i.e. to make it act as a single retarder, let us consider the case of a half-wave plate placed between two quarter-wave plates.

A Half-Wave Plate Between Two Quarter-Wave Plates

It will now be shown that a system consisting of a quarter-wave plate, a half-wave plate and a quarter-wave plate in that order, can be used as a compensator. The axes of the two quarter-wave plates are parallel. The angle between these axes and the axes of the half-wave plate is $\overline{e}$. The transformations of Stokes vector through such a system are given below

Let V_0 and V_1 be the Stokes vectors of light at the entrance and exit of the first quarter-wave plate referred to its axes. Then, we have,

$$V_0 = \begin{bmatrix} S_1 \\ S_2 \\ S_3 \end{bmatrix} \rightarrow \begin{bmatrix} S_1 \\ -S_3 \\ S_2 \end{bmatrix} = V_1$$

If V_2 and V_3 are the Stokes vectors of light at the entrance and exit of the half-wave plate referred to its axes

$$V_2 \equiv \begin{bmatrix} S_1 \text{ Cos } 2\bar{\theta} - S_3 \text{ Sin } 2\bar{\theta} \\ -S_3 \text{ Cos } 2\bar{\theta} - S_1 \text{ Sin } 2\bar{\theta} \\ S_2 \end{bmatrix} \quad \begin{bmatrix} S_1 \text{ Cos } 2\bar{\theta} - S_3 \text{ Sin } 2\bar{\theta} \\ S_3 \text{ Cos } 2\bar{\theta} + S_1 \text{ Sin } 2\bar{\theta} \\ -S_2 \end{bmatrix}$$

$$\equiv \quad V_3$$

Also,

$$V_4 \equiv \begin{bmatrix} \text{Cos } 2\bar{\theta}\, (S_1 \text{ Cos } 2\bar{\theta} - S_3 \text{ Sin } 2\bar{\theta}\,) - \text{Sin } 2\bar{\theta}\, (S_3 \text{ Cos } 2\bar{\theta} \\ + S_1 \text{ Sin } 2\bar{\theta} \\ \text{Cos } 2\bar{\theta}\, (S_3 \text{ Cos } 2\bar{\theta} + S_1 \text{ Sin } 2\bar{\theta}) + \text{Sin } 2\bar{\theta}\, (S_1 \text{ Cos } 2\bar{\theta} \\ - S_3 \text{ Sin } 2\bar{\theta}) \\ - S_2 \end{bmatrix}$$

$$\longrightarrow \begin{bmatrix} \text{Cos } 2\bar{\theta}\, (S_1 \text{ Cos } 2\bar{\theta} - S_3 \text{ Sin } 2\bar{\theta}) - \text{Sin } 2\bar{\theta}\, (S_3 \text{ Cos } 2\bar{\theta} \\ + S_1 \text{ Sin } 2\bar{\theta}\,) \\ S_2 \\ \text{Cos } 2\bar{\theta}\, (S_3 \text{ Cos } 2\bar{\theta} + S_1 \text{ Sin } 2\bar{\theta}\,) + \text{Sin } 2\bar{\theta}(S_1 \text{ Cos } 2\bar{\theta} \\ - S_3 \text{ Sin } 2\bar{\theta}) \end{bmatrix}$$

$$\equiv \begin{bmatrix} \bar{S}_1 \\ \bar{S}_2 \\ \bar{S}_3 \end{bmatrix} \equiv (V_5 \qquad (5.79)$$

where, V_4: Stokes vector of light incident on the second quarter-wave plate with respect to its axes.

V_5: Stokes vector of light emerging from the second quarter-wave plate with respect to its axes.

The Stokes vector at the exit of the optically equivalent system is given by Eq. (5.68). Comparing this equation with Eq. (5.79) for $S_1 = S_2 = 0$, $S_3 = 1$, we obtain

$$\overline{S}_3 = \text{Cos}\,\delta = \text{Cos}\,4\overline{\theta} \quad \text{or} \quad \delta = 4\overline{\theta} \tag{5.80}$$

$$\overline{S}_1 = \text{Sin}\,\delta \ \text{Sin}\,2\psi = -\ \text{Sin}\,4\overline{\theta}$$

$$\text{or Sin}\,2\psi = -1$$

$$\because \ \delta = 4\overline{\theta}$$

$$\text{i.e.} \quad \psi = \pi/4 \tag{5.81}$$

for $S_1 = 1$, $S_2 = S_3 = 0$

$$\overline{S}_3 = -\ \text{Sin}\,2\rho_1 \ \text{Sin}\,\delta = \text{Sin}\,4\overline{\theta}$$

$$(\because \ \delta = 4\overline{\theta})$$

$$\text{or} \quad \rho_1 = -\ \pi/4 \tag{5.82}$$

$\therefore$ The rotatory power of the combination $= \psi_1 = \psi - \rho_1 = 0.$

So, this system acts as a single retarder with retardation $4\overline{\theta}$ and azimuth $-\pi/4$ with respect to the axes of the first quarter-wave plate. The retardation introduced can be varied by varying the angle $\overline{\theta}$. Thus, this system can be used as a compensator.

The whole system, i.e. a quarter-wave plate, a half-wave plate and a quarter-wave plate, can be constructed

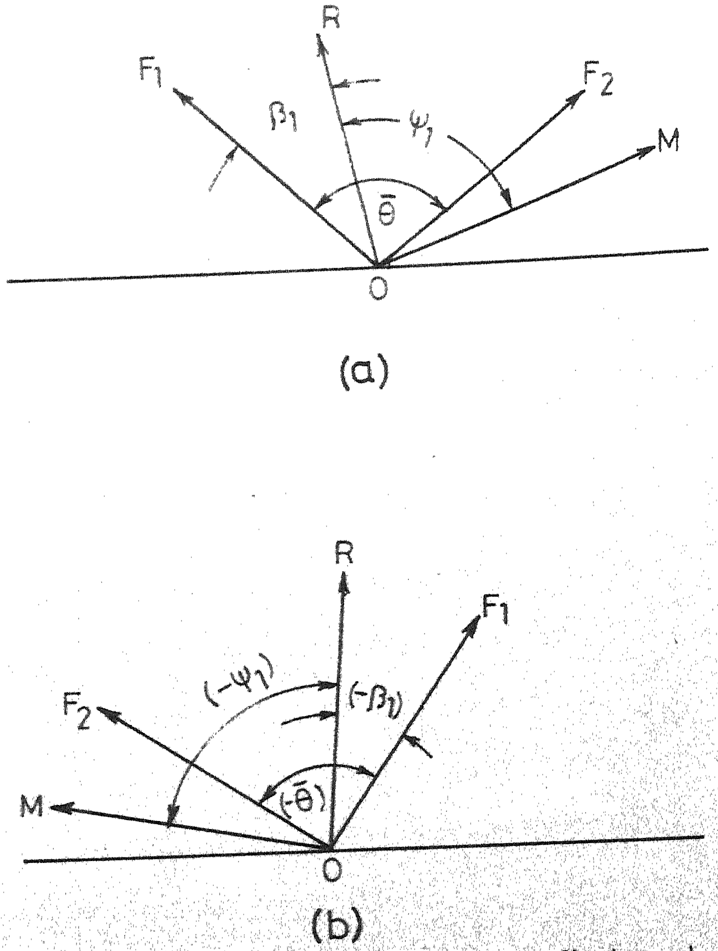

F_1, F_2 - Fast axes of the first and second retarders.

R , M - Primary and secondary characteristic directions.

FIG.62. ORIENTATIONS OF THE RETARDERS IN TWO TYPES OF COMBINATIONS SO AS TO FORM QUARTER-WAVE PLATES.

with eight retarders each of retardation ρ, when tan $\rho \geq 1$ (for the particular wavelength of light under consideration). This can be done as follows.

Consider two types of quarter-wave plates (a) and (b) each of which is a combination of two retarders. The orientations of the axes of these retarders are shown in Fig. 62. In the (a)-type combination, the rotatory power is clockwise where as in the (b) type it is anticlockwise. The difference between these two types of combinations is in that the angles between the axes of the two retarders in types (a) and (b) is $\bar{\theta}$ and $-\bar{\theta}$ respectively. If the type-(b) combination is placed after the type-(a) combination, the rotatory powers of the combinations cancel each other so that the two combinations behave as two quarter-wave plates. So, to construct a compensator we can use four such combinations (combination of two retarders each of retardation ρ) with the first and third combinations of the type (a) and the second and fourth combinations of the type (b). Then the rotatory powers of the first and third combinations are nullified by the rotatory powers of the second and fourth combinations respectively. Thus, the whole system of these eight retarders acts as a series of four quarter-wave plates which in turn can be used as a compensator as described above. By varying the angle $\bar{\theta}$, the angle between the axes of the two retarders in a two retarder combination, according to Eq. (5.72) i.e. $\tan^2 \rho = \text{Sec } 2\bar{\theta}$, we can use the compensator for any wavelength of light for which the condition tan $\rho \geq 1$ is satisfied. (This, in practice is not a severe restriction since the retardation ρ does not vary appreciably within the visible region of the electromagnetic spectrum for most of the photoelastic materials). Using this method large field compensators can be made using large sheet type retarders (ex. frozen-stress sheets). The angle $\bar{\theta}$ can be found experimentally for different wavelengths of light without any calculations. It is advisable to cut all the eight retarders from a single large retarder of uniform retardation. The use of a large field compensator in a lens polariscope eliminates refocussing of the lenses when the compensator is introduced into or removed out of the field of view of polariscope, which is necessary with a Babinet-Soleil compensator because of its small field. The compensator described in this section thus has some additional advantages like large field, cheapness etc. However, the integral fringe order cannot be determined directly with this compensator as can be done with Babinet-Soleil compensator (upto a certain number of fringes, usually about 6). However, the integral fringe orders upto virtually any number can be determined by an altogether different method. We shall now develop this method in the following section.

C. DETERMINATION OF INTEGRAL FRINGE ORDERS IN PHOTOELASTICITY

In analysing a photoelastic specimen having no stress-free corner or, in which the formation of fringes during the loading process cannot be observed, it is desirable to have some means of determining the integral fringe order at a point when the fractional fringe order at that point has been determined by the Tardy or other method. A Babinet-Soleil or a similar compensator can be used to determine the integral fringe order upto a certain value. However, there is a serious point which needs attention when a Babinet-Soleil compensator is used. In practice, to determine the integral fringe order at a point by the help of a Babinet-Soleil compensator, a white light source is used and retardations are added or subtracted until a zero-order fringe (a black fringe) appears on the screen. This process assumes that the compensator acts as a continuation of the model and its behaviour is similar to that of the model. This implies that the model and the compensator introduce retardations which are equal in magnitude but opposite in sign for all colours contained in white light. This is true only if the material of the model and that of the compensator exhibit same type of dispersion characteristics (variation of retardation with wavelength of light). This is not the case in general. Most of the compensators are supplied with a calibration chart which shows the dependence of the compensator on the wavelength of light. Further, experience has shown that using a Babinet-Soleil compensator and a photometer, instances occur where the reading on the photometer is almost zero for two consecutive fringe orders, making it difficult to identify which one corresponds to the zero fringe order. This experience is quite noticeable with a urethane rubber model.

In 1963, Pant[30] showed that by determining the fractional fringe orders with two wavelengths λ_1 and λ_2, one can determine the fractional fringe order obtained by using a third wavelength λ. His analysis ignores the dependence of the stress-optic coefficient λ and also is restricted to the case where the difference between the fringe orders associated with λ_1 and λ_2 is only a fraction, i.e., the integral fringe orders associated with λ_1 and λ_2 are equal.

We shall now show, how by using two wavelengths, one can determine the integral values (and their multiples) for both wavelengths, associated with the fractional fringe orders observed at any point. The solution can be obtained by using a nomogram or constructing a ready reckoner for any two wavelengths λ_1, and λ_2 as shown in this analysis. Further, the usual assumption that the stress-optic coefficient is independent of wavelength, is not used. Its dependence on λ is explicitly shown by experimental results.

Stress-Optic Law

The stress-optic law can be expressed as

$$\rho = \frac{Ch}{\lambda} (p - q) = \frac{1}{f} (p - q) \qquad (5.83)$$

where ρ : retardation

h : thickness of the model or length of light path inside the model

$(p - q)$: principal or secondary (for frozen stress slices) principal-stress difference

λ : wavelength of light used

C : Stress-optic coefficient

f : Model fringe constant in tension

In practice, the stress-optic coefficient C is considered to be independent of wavelength. However more careful observations have shown[20,49] that C is influenced to some extent by the wavelength. For our present analysis, we shall assume that C depends on λ and hence, f is a function of λ . If, in any experiment, C is found to be independent of λ , the analysis remains unchanged.

Let λ_1 and λ_2 be the wavelengths of the light used and ρ_1 , ρ_2 the corresponding retardations. In general, these retardations will consist of an integral value and a fractional value. Let $\rho_1 = (n_1 + \delta_1)$ and $\rho_2 = (n_2 + \delta_2)$, where n_1 , n_2 are positive integers and δ_1 , δ_2 are positive fractions less than unity. Without loss of generality, let f_1 be greater than f_2, so that their ratio $z = \frac{f_1}{f_2} > 1$

From Eq. (5.83)

$$(n_1 + \delta_1) = \frac{1}{f_1}(p - q)$$

$$(n_2 + \delta_2) = \frac{1}{f_2}(p - q)$$

$$\frac{n_2 + \delta_2}{n_1 + \delta_1} = \frac{f_1}{f_2} = z$$

or

$$n_2 - z\,n_1 = z\,\delta_1 - \delta_2 = \epsilon \qquad (5.84)$$

If the stress-optic coefficient happens to be independent of λ, then,

$$z = z^* = \lambda_1/\lambda$$

The experimental investigations will show that using z^* instead of z will lead to erroneous results. In practice, the fractional fringe orders δ_1 and δ_2 are determined and hence ϵ becomes an experimentally determined factor. Eq. (5.84), will then have to be solved for n_1 and n_2 subject to the condition that these are whole numbers.

General Observations:

a) Since $z > 1$ (as experimentally observed), $\rho_2 > \rho_1$. This is obvious when C is independent of λ.

Hence,

$$n_2 + \delta_2 > n_1 + \delta_1$$

and

$$n_2 \geq n_1 \qquad (5.85)$$

b) Since $0 \leq \delta_1 < 1$ and $0 \leq \delta_2 < 1$, for a given z,

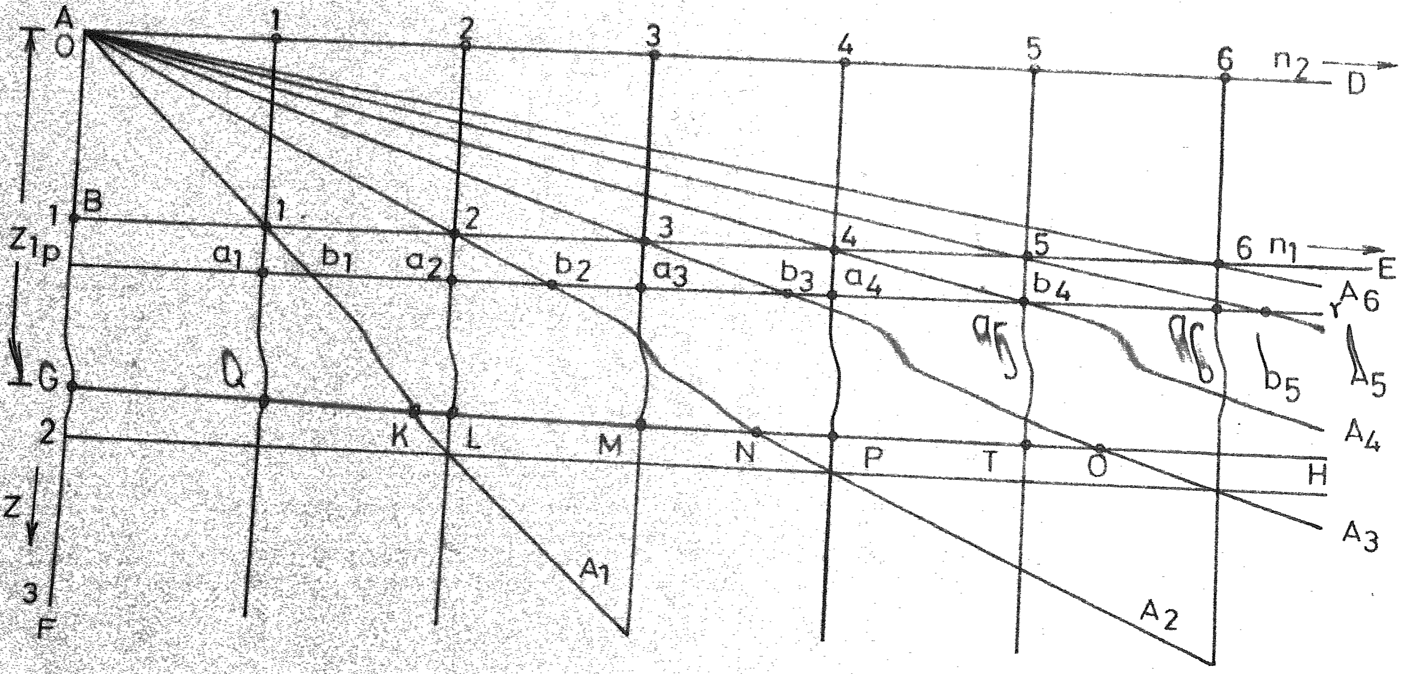
A
O
1
2
3
4
5
6
n₂
D
B
1
Z1p
G
2
Z
3
F
1
2
3
4
5
6
n₁
E
a1
b1
a2
b2
a3
b3
a4
b4
a5
a6
b5
A6
Y
A5
Q
K
L
M
N
P
T
O
H
A4
A3
A1
A2

FIG. 63

$$\epsilon_{max} = (z\ \delta_1)_{max} - (\delta_2)_{min} < z$$

and

$$\epsilon_{min} = (z\ \delta_1)_{min} - (\delta_2)_{max} < -1$$

$$\text{i.e. } z > \epsilon > -1 \tag{5.86}$$

c) In Eq. (5.84), if we add N to n_2 and N/z to n_1 where N and N/z are integers, the equation is still satisfied. Let N be the smallest integer such that N/z is also an integer. Then the solutions **for** n_2 and n_1 are

$$(n_2 + SN) \text{ and } (n_1 + SN/z), \text{ where } S = 0,1,2,\ldots\ldots \tag{5.87}$$

In other words, if we find two basic solutions n_2 and n_1, satisfying Eq. (5.84), then the multiple solutions are given by the above equation.

Construction of Nomogram:

The wavelength in visible spectrum varies from 7700°A (extreme red) to 3900°A (extreme violet) and for this range $z^* = \frac{\lambda_1}{\lambda_2} < 2$. In practice, the usual range is from red (about 7500°A) to blue green (about 5000°A) giving for z a value less than 1.5.

In order to solve Eq. (5.84), one can construct a nomogram as shown in Fig. 63. Line AF represents z, line AD, the integral values of n_2 and line BE, the integral values of n_1. The scales for the values of z, n_2 and n_1 are the same. From A, rays A_1, A_2, A_3, ... etc are drawn passing through the integral values of n_1 = 1,2,3,...etc.

The slopes of these rays are 1,2,3,...etc., by construction.

Let us say that in a particular example, the ratio of the two model fringe constants corresponding to λ_1, λ_2, is $f_1/f_2 = z_1$. In Fig. 63. A G = z_1. A horizontal line G H is drawn cutting the rays AA_1, AA_2, AA_3,....etc. at K,N,G... etc. as shown. As the slopes of these rays are 1,2,3,....etc G K = z_1; G N = 2 z_1, G O = 3 z_1.....,etc. Line G H cuts the vertical lines representing the integral values of n_2 at L, N, P, O,...., etc. Distances L K, M K, P N, T N, etc represent the values of ϵ that one determines experimentally. The procedure for using the nomogram is as follows:

For a given problem, let the measured values of fractional fringe orders be δ_1, δ_2 so that $z \delta_1 - \delta_2 = \epsilon_1$. Identify a point which is the intersection between the line G H and one of the vertical lines representing the values of n_2 (like L, M, P, T,...) such that the distance between this point and the slant ray immediately to the left of it is equal to ϵ_1. Let us say in our case, M is such a point where M K = ϵ_1 where K is a point on the ray immediately to the left of M, i.e. ray A_1. The vertical line on which point M lies gives the value of n_2 (in this case $n_2 = 3$) and the slant ray immediately to the left gives the value of n_1 associated with it (here A_1 has $n_1 = 1$). The proof for this is evident from the figure, since M G - K G = M K, i.e., $n_2 - n_1 z_1 = \epsilon_1$, Eq. (5.84), where n_2 = M G = 3 and $z_1 n_1$ = K G = z_1 with $n_1 = 1$.

Generally for a given value of ϵ_1, there will be more than one point (lying on one side of the vertical lines), such that the distance between this point and the slant ray immediately to its left is equal to ϵ_1. These give multiple values according to Eq. (5.87). This aspect will be discussed later.

One observes from Fig. 63. the values of ϵ can only be discrete. This is evident by the nature of Eq. (5.85). For, we can have a problem where n_2, δ_2 and z are at our command, but n_1 and δ_1 have to satisfy Eq. (5.84) and also that n_1 should be an integer.

In the above procedure, we have assumed that ϵ is positive. If ϵ turns out to be negative say, $\epsilon = -\epsilon_2$, then we measure the distance from the point such as M to the slant ray immediately to the right; i.e. if M is the point such that M N (where N lies on the ray immediately to the right) is equal to $|-\epsilon_2|$, then $n_2 = 3$ and $n_1 = 2$, since the ray on which N lies is A_2 with associated $n_1 = 2$. For negative values of ϵ, the point can also lie on the segment 0 G. Negative values cannot be numerically greater than 1 as shown by our previous analysis.

To make the above procedure clearer, let us take a specific example. Let $z = 1.25$. A horizontal line pr corresponding to this value is drawn as shown in Fig. 63. cutting the vertical lines at a_1, a_2, a_3, ..., etc. Let us assume that we find experimentally $z\,\delta_1 - \delta_2 = 0.25$.

Now we look for a point lying on one of the vertical lines (such as a_1 or a_2 or a_3 or...) such that the distance between this point and the slant ray immediately to its left is 0.25. In our case a_4 is such a point since $a_4\,b_3 = 0.25$. Hence $n_2 = 4$ (point a_4 lies on this) and $n_1 = 3$ (since b_3 lies on ray A_3). We can see that these values of n_1 and n_2 satisfy Eq. (5.84) with $z = 1.25$ and $\varepsilon = 0.25$. On the other hand if ε happens to be -0.5, we select a point such that the distance between this point and the slant ray immediately to the right is equal to 0.5. Hence, we get a point a_2 since $a_2\,b_2 = -0.5$ and b_2 lies to the right of a_2. Then $n_2 = 2$ and $n_1 = 2$.

A value of $\varepsilon = -0.25$ will give us points a_1 and b_1 with $n_2 = 1$ and $n_1 = 1$; a value of $\varepsilon = -0.75$ gives us points a_3 and b_3 with $n_2 = 3$ and $n_1 = 3$; a value of $\varepsilon = 0$ gives us point a_5 (b_4 coincides with it) with $n_2 = 5$ and $n_1 = 4$.

Multiple Values for n_1 and n_2:

From Fig. 63. we notice that for $\varepsilon = -0.25$, we get points a_1 and b_1 as noted above with $n_2 = n_1 = 1$, and also points a_6 and b_6 such that $a_6\,b_5 = |-0.25|$ with associated values $n_2 = 6$ and $n_1 = 5$. These also satisfy Eq. (5.84), since, $6 - 1.25 \times 5 = -0.25$. This is in agreement with Eq. (5.87) which gives all multiple values. For our case, the lowest integer N such that N/z is an integer is 5. The solution for n_2 and n_1 according to Eq. (5.87) are:

$$n_2 + S\,N = 1 + 5\,S = 1,6,11,16,\ldots,\text{etc.}$$

and $$n_1 + \frac{S\,N}{z} = 1 + 4\,S = 1,5,9,13,\ldots,\ \text{etc.}$$

all satisfying Eq. (5.84). This should not cause much of a problem in practice, since the difference between one set of values for n_1, n_2 and the subsequent set is so large that an analysis of the problem can give a clue as to the appropriate value. Further, as will be shown later, one can always choose two appropriate wavelengths such that the difference between two multiple values is so large that there will be little doubt as to the correct value. If ambiguity still exists, one can use the franctional fringe order δ_3 for a third wavelength of light λ_3. That is, one set of multiple solutions are found using the values of δ_1 and δ_2 and a second set is found using the values of δ_2 and δ_3. The value of n_2 common to both these sets gives us the correct solution. For example let these two sets of multiple solutions be given by:

$(n_1, n_2) = (1,2), (6,6), (11,10), (16,14), (21,18), \ldots$etc.

and

$(n_2, n_3) = (0,1), (3,3), (6,5), (9,7), (12,9), \ldots$etc.

then the correct values of the integral fringe orders are given by:

$(n_1, n_2, n_3) = (6,6,5).$

All Possible Values for ε And Associated n_2, n_1 Values:

In practice it is not necessary to use a nomogram. For a given ratio z of the wavelengths, one can write down

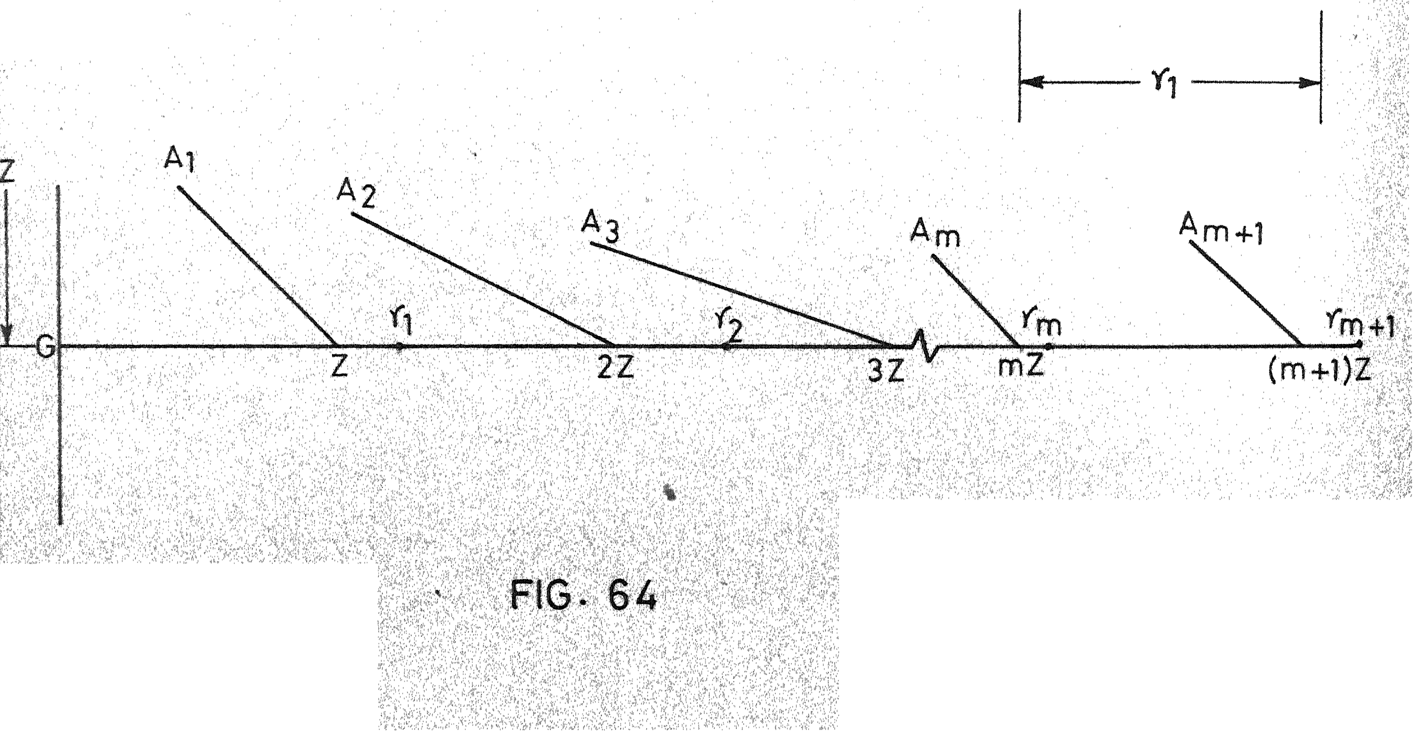

FIG. 64

all the possible values of ϵ that one can determine experimentally and write down the corresponding values of n_1 and n_2. This procedure has several advantages, since one has a sort of a ready-reckoner using which, the associated values of n_2 and n_1 with any given ϵ can be read out. Also, if due to some experimental error, the value of ϵ is not determined exactly, the ready reckoner can immediately tell what should be the correct value of ϵ for any z and a given range of n_2 , n_1. This is so because, for any z, the values of ϵ can only be discrete as was pointed out earlier and as seen in Fig.63. and also for any range of n_2 , n_1 (lying between any two successive rays A_1 A_2 or A_2 A_3 or A_3 A_4,... etc.) the values of ϵ are fixed.

In Fig. 64., a portion of Fig. 63., is shown with G H, the horizontal line cutting the rays A_1 , A_2 , A_3,... etc. at distance of z, 2z, 3z,..., etc. from G. Let γ_1 be the integer next to z, i.e. if $z = a_1 + \mu_1$ where a_1 is the integer part and μ_1 the fractional part less than 1, then $\gamma_1 = a_1 + 1$. If $\mu_1 = 0$, $\gamma_1 = a_1$. Let γ_2 be the integer next to 2z; i.e. if $2z = a_2 + \mu_2$ where μ_2 is the fractional part less than 1, then $\gamma_2 = a_2 + 1$ if $\mu_2 \neq 0$, otherwise, $\gamma_2 = a_2$. This is continued until γ_m, where γ_m is the integer such that $\gamma_m = mz$. The points corresponding to γ_1, γ_2, γ_3,..., γ_m are shown in Fig. 64. Note that the slant ray A_m in Fig. 63. passing through the vertical line $n_2 = m$ will pass through the point γ_m.

From Fig. 6.3. the values of ϵ and the associated values of n_2 and n_1 can be written down. This is shown in Table 5.1. The procedure for constructing this table is as follows:

$$\epsilon = n_2 - n_1 z \qquad (5.84)$$

and

$$z > \epsilon >- 1 \qquad (5.86)$$

Case (i) ϵ is Positive:

Write down the values of ϵ, n_2 for $n_1 = 1$, then for $n_1 = 2$ etc. For $n_1 = 1$, the first possible value for ϵ would be $\gamma_1 - z$ with $n_2 = \gamma_1$. To obtain the other values, the value of n_2 should be increased in steps of 1 so that we obtain $1 + \gamma_1 - z$, $2 + \gamma_1 - z$, $3 + \gamma_1 - z$,....etc. for ϵ and $1 + \gamma_1$, $2 + \gamma_1$, $3 + \gamma_1$,....etc. for n_2. This is continued until the value of ϵ exceeds z. Let the maximum value of ϵ that does not exceed the value of z with $n_1 = 1$ be $\bar{\epsilon}$.

$$\text{i.e. } \bar{\epsilon} < z$$

$$= \bar{n}_2 - \bar{n}_1 z$$

$$= \bar{n}_2 - z$$

($\bar{n}_2$, $\bar{n}_1$ are the corresponding values of n_2 and n_1 respectively so that $\bar{\epsilon} = \bar{n}_2 - \bar{n}_1 z$)

$$\text{i.e. } \bar{n}_2 - z < z$$

$$\bar{n}_2 < 2z$$

The maximum value of $\bar{n}_2$ that satisfies this inequality is $(\gamma_2 - 1)$. Only the maximum value is to be taken since $\bar{\epsilon}$ is to be maximum,

$\therefore \quad \bar{\epsilon} = \gamma_2 - 1 - z$

$\bar{n}_2 = \gamma_2 - 1$ and $n_1 = 1$

Similarly,

for $n_1 = 2$

$\bar{\epsilon} = \bar{n}_2 - 2z$

$\bar{n}_2 - 2z < z$

or $\bar{n}_2 < 3z$

$\bar{n}_2 = \gamma_3 - 1$

for $n_1 = l$

$\bar{\epsilon} = \bar{n}_2 - l\,z < z$

or $\bar{n}_2 < (l + 1)\,z$

$\bar{n}_2 = \gamma_{l+1} - 1$

Case (ii) ϵ is Negative

$\epsilon = n_2 - n_1 z, \; z < \epsilon < -1$

n_1 can not be zero (If it is zero n_2 should be negative to make ϵ negative)

If $n_1 = l$ a positive integer

$\epsilon = n_2 - n_1 z = n_2 - l\,z > -1$

$0 > n_2 - l\,z > -1$

i.e. $n_2 < l\,z$

and $n_2 > l\,z - 1$

i.e. $l\,z > n_2 > l\,z - 1$

$\therefore \quad n_2 = \gamma_l - 1$

The table for negative values of ϵ is constructed using this equation.

TABLE 5.1

Possible Values of ϵ and Associated n_2 and n_1

Positive ϵ :

ϵ	n_1	n_2	ϵ	n_1	n_2
$\gamma_1 - z$	1	γ_1	$\gamma_2 - 2z$	2	γ_2
$1 + \gamma_1 - z$	1	$1 + \gamma_1$	$1 + \gamma_2 - 2z$	2	$1 + \gamma_2$
$2 + \gamma_1 - z$	1	$2 + \gamma_1$	$2 + \gamma_2 - 2z$	2	$2 + \gamma_2$
$3 + \gamma_1 - z$	1	$3 + \gamma_1$	$3 + \gamma_2 - 2z$	2	$3 + \gamma_2$
⋮	⋮	⋮	⋮	⋮	⋮
$\gamma_2 - 1 - z$	1	$\gamma_2 - 1$	$\gamma_3 - 1 - 2z$	2	$\gamma_3 - 1$

	ϵ	n_1	n_2
continue upto	$\gamma_{m-1} -(m - 1) z$	$m - 1$	$\gamma_m - 1$
$n_1 = m$	$1 + \gamma_{m-1} -(m - 1) z$	$(m - 1)$	$1 + \gamma_{m-1}$
where m z is	$2 + \gamma_{m-1} -(m - 1) z$	$(m - 1)$	$2 + \gamma_{m-1}$
an integer	$3 + \gamma_{m-1} -(m - 1) z$	$(m - 1)$	$3 + \gamma_{m-1}$
$= \gamma_m$	⋮	⋮	⋮
	$\gamma_{m-1} -1 - z$	$(m -1)$	$\gamma_{m-1} - 1$

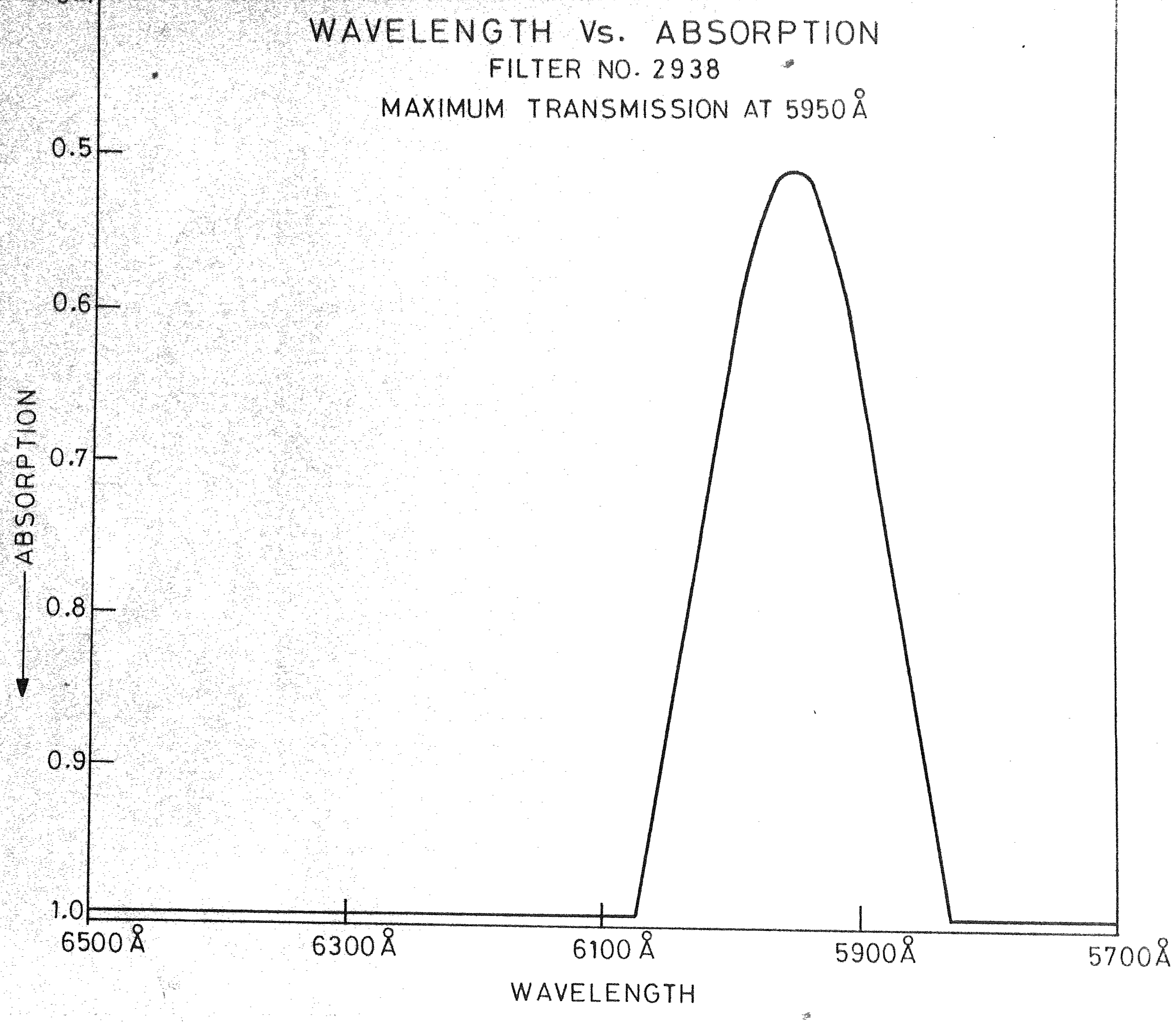
WAVELENGTH Vs. ABSORPTION
FILTER NO. 2938
MAXIMUM TRANSMISSION AT 5950 Å
ABSORPTION
0.5
0.6
0.7
0.8
0.9
1.0
6500 Å
6300 Å
6100 Å
5900 Å
5700 Å
WAVELENGTH

FIG. 65 (a)

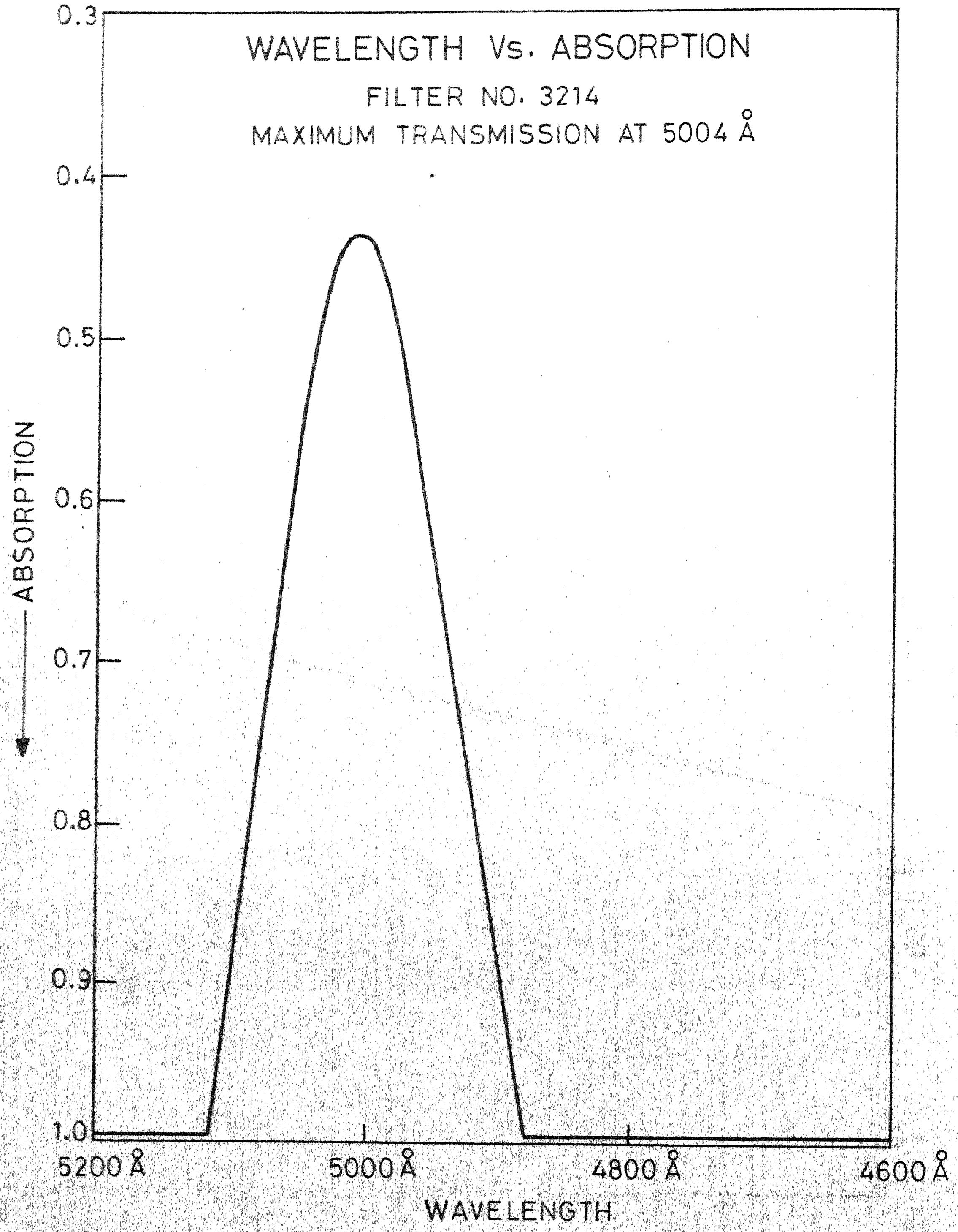
WAVELENGTH Vs. ABSORPTION
FILTER NO. 3214
MAXIMUM TRANSMISSION AT 5004 Å
0.3
0.4
0.5
0.6
0.7
0.8
0.9
1.0
ABSORPTION
5200 Å
5000 Å
4800 Å
4600 Å
WAVELENGTH

FIG. 65 (c)

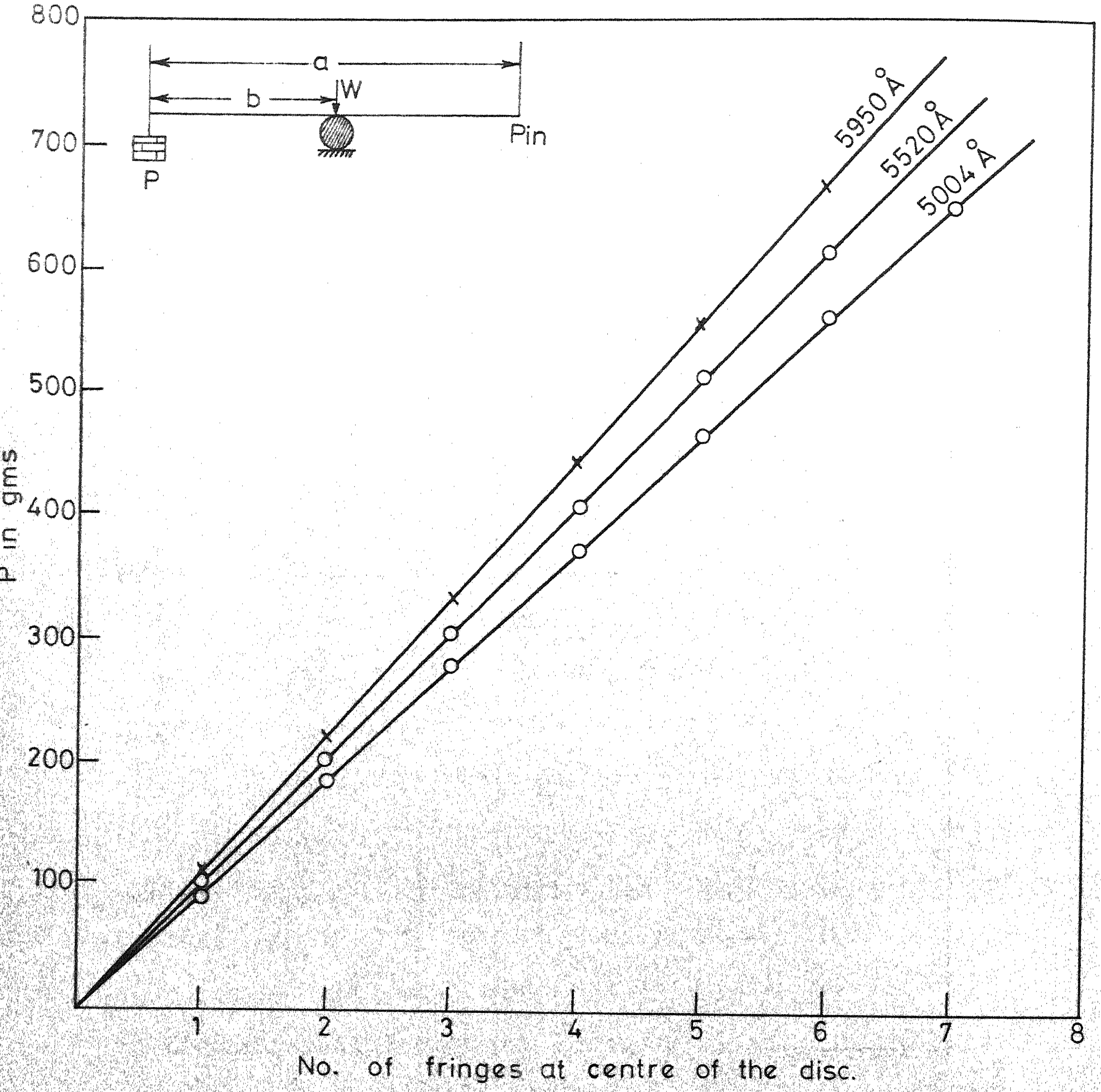
800
700
600
500
400
300
200
100
P in gms
a
b
W
P
Pin
5950 Å
5520 Å
5004 Å
1
2
3
4
5
6
7
8
No. of fringes at centre of the disc.

FIG. 66

Negative ϵ :

ϵ	n_1	n_2
$\gamma_1 - 1 - z$	1	$\gamma_1 - 1$
$\gamma_2 - 1 - 2z$	2	$\gamma_2 - 1$
$\gamma_3 - 1 - 3z$	3	$\gamma_3 - 1$
$\gamma_4 - 1 - 4z$	4	$\gamma_4 - 1$
continue till	.	.
$\gamma_m - 1 - mz$ $= -1$	m	$\gamma_m - 1$
$\therefore \gamma_m = mz$		

Example And Experimental Results:

To show the dependence of the stress-optic coefficient on the wavelength, three filters with wavelengths 5950°A, 5520°A and 5040°A were used to measure the fringe constant. The model was a circular disc of diameter (d) 4.73 cm. with a thickness (h) of 0.648 cm. Figs. 65(a), (b) and (c) show the characteristics of the three filters. Fig. 66. shows the plots of load in gms. vs. fringes at the center of the disc. The geometry of loading is also shown in the figure. Table 5.2 gives the values of the material fringe constant F and the stress-optic coefficient C for each of the filters.

At the center of the disc $(p - q) = 8w/\pi t\, d$

$$C = \lambda/F$$

TABLE 5.2

Wavelength	Material fringe constant (F) gm./cm. fringe	C °A fringe. cm/gm
5950°A	210.1	28.28
5520°A	192.0	28.79
5004°A	172.0	29.11

Though the values of C donot differ very much, still neglecting them can give erroneous results as will be shown subsequently. For the determination of the integral fringe orders from the measured fractional fringe orders, two filters with 5950°A and 5520°A wavelengths were used. The fractional fringe orders were measured by the Tardy method. Table 5.3 gives the values of the experimentally observed fringe orders (integral plus fractional values) and the theoretically calculated values based on the model fringe constant. This table reveals that the fractional fringe orders measured by the Tardy method are quite accurate.

TABLE 5.3

Load P(gm) at end of lever	5950°A filter		5520°A filter	
	Exptal.	Theor.	Exptal.	Theor.
575	5.25	5.23	5.73	5.73
625	5.70	5.68	6.23	6.23
675	6.14	6.14	6.73	6.73
725	6.61	6.59	7.23	7.22
775	7.06	7.04	7.73	7.72
825	7.50	7.50	8.20	8.22

In Fig. 66 $w = \frac{Pa}{(a-b)} = \frac{39.7P}{11.2}$

$$= 3.547P$$

From Table 5.2, we have

$$\lambda_1 = 5950°A, \quad F_1 = 210.1 \text{ gm/cm.fringe}$$

$$\lambda_2 = 5520°A, \quad F_2 = 192.0 \text{ gm/cm.fringe}$$

$$z = \frac{F_1}{F_2} = \frac{f_1}{f_2} = 1.094 \text{ and } z^* = \frac{\lambda_1}{\lambda_2} = 1.078$$

Tables 5.4 and 5.5 give the values of ϵ that one can expect with z and z^*. These are the "ready-reckoner" tables. Table 5.5 which is calculated on the basis of z^* (assuming independence of C on λ) will give erroneous values as shown in Table 5.6.

TABLE 5.4

(Using z)

m z	ε(Positive)	n_1	n_2	ε(Negative)	n_1	n_2
z = 1.094	0.906	1	2	- 0.094	1	1
2z = 2.188	0.812	2	3	- 0.188	2	2
3z = 3.282	0.718	3	4	- 0.282	3	3
4z = 4.376	0.624	4	5	- 0.376	4	4
5z = 5.470	0.530	5	6	- 0.470	5	5
6z = 6.564	0.436	6	7	- 0.564	6	6
7z = 7.658	0.342	7	8	- 0.658	7	7
8z = 8.752	0.248	8	9	- 0.752	8	8
9z = 9.846	0.154	9	10	- 0.846	9	9
10z =10.940	0.060	10	11	- 0.940	10	10
....	1.060	10	12	....		
etc.	etc.			etc.		

TABLE 5.5
(using z^*)

m z	ϵ^*(Positive)	n_1	n_2	ϵ^*(Negative)	n_1	n_2
z = 1.078	0.922	1	2	- 0.078	1	1
2z = 2.156	0.844	2	3	- 0.156	2	2
3z = 3.234	0.766	3	4	- 0.234	3	3
4z = 4.312	0.688	4	5	- 0.312	4	4
5z = 5.390	0.610	5	6	- 0.390	5	5
6z = 6.468	0.532	6	7	- 0.468	6	6
7z = 7.546	0.454	7	8	- 0.546	7	7
8z = 8.624	0.376	8	9	- 0.624	8	8
9z = 9.702	0.298	9	10	- 0.702	9	9
10z =10.780	0.220	10	11	- 0.780	10	10

TABLE 5.6

Load P (gms.)	Fract. Fr. Ord.		$\epsilon = z\delta_1 - \delta_2$	ϵ^*	Exptal.		from ϵ		from ϵ^*	
	δ_1	δ_2		$z^*\delta_1 - \delta_2$	n_1	n_2	n_1	n_2	n_1	n_2
575	0.25	0.73	- 0.46	- 0.46	5	5	5	5	6	6
625	0.70	0.23	+ 0.54	+ 0.53	5	6	5	6	6	7
675	0.14	0.73	- 0.58	- 0.61	6	6	6	6	8	8
725	0.61	0.23	+ 0.44	+ 0.43	6	7	6	7	7	8
775	0.06	0.73	- 0.66	- 0.66	7	7	7	7	8	8
825	0.50	0.22	+ 0.33	+ 0.33	7	8	7	8	9	10

For the wavelengths λ_1 and λ_2, the fractional fringe orders δ_1 and δ_2 are experimentally determined. Using z and z^* the values of ϵ and ϵ^* are then calculated. From Tables 5.4 and 5.5, for the values of ϵ and ϵ^* , the corresponding values of n_1 and n_2 are noted. These values are compared with the experimentally observed values. As pointed out, values based on z^*, i.e., neglecting the dependence of C on λ can lead to wrong values. It is more appropriate to use z (i.e. F_1/F_2). Also, assuming that the values in Table 5.4 are calculated more accurately, the experimentally determined values of ϵ may differ slightly as given in Table 5.6 depending on the method employed to determine the fractional fringe orders.

Conclusions:

Using two wavelengths and knowing the material or model fringe constants for these two wavelengths, one can determine the integral fringe order existing at any point in a plane model by measuring the associated fractional fringe orders. It is shown, that the usual assumption of the stress-optic coefficient being independent of λ may lead to erroneous results. For any two given wavelengths and a model, a 'ready-reckoner' table can be formulated to determine the integral fringe orders based on the measured fractional fringe orders. Alternatively , a nomogram can be constructed.

In this chapter, we have discussed various methods of finding the integrated optical effect in a photoelastic model under three-dimensional state of stress graphically. Two new graphical methods which are derived without referring to Poincaré sphere representation are presented. One of these methods has the advantage that contains only straight lines and so it is easy to construct. In the second section we have presented the construction of a large field compensator using 8 retarders of equal retardance. This is essentially an extension of the works of Pancharatnam and Tuzi. Also presented are a nomogram and a 'ready reckoner table' with which one can find the integral fringe orders using the fractional fringe orders for two wavelengths. This is essentially an extension of Pant's work. Where as with Pant's method or the use of Babinet-Soleil compensator one can find the integral fringe order upto few fringes (about 6), with the nomogram or the ready-reckoner table one can determine the integral fringe order virtually upto any number.

CHAPTER 6

EXPERIMENTAL RESULTS

In the previous chapters, different experimental techniques for the determination of various characteristic parameters were discussed. These were essentially built on the concept of light ellipse. These experimental techniques are very general in nature. In the present chapter, we shall present some experimental results in support of these techniques for completeness. In addition to these, we have already described some experimental results in the previous chapter, connected with the determination of integral fringe orders in photoelasticity.

Test Model:

Tests were conducted on a rectangular bar under combined torsion and tension. Fig. 67 shows the model and the light path under consideration Fig. 68. is the sketch of the loading device. Figs. 69. and 70. show the experimental set up and the loading arrangements, respectively. The model material was paraplex. The experiments were conducted with a 8" - lens type transmission polariscope shown in Fig. 69. Two models with the following dimensions were used:

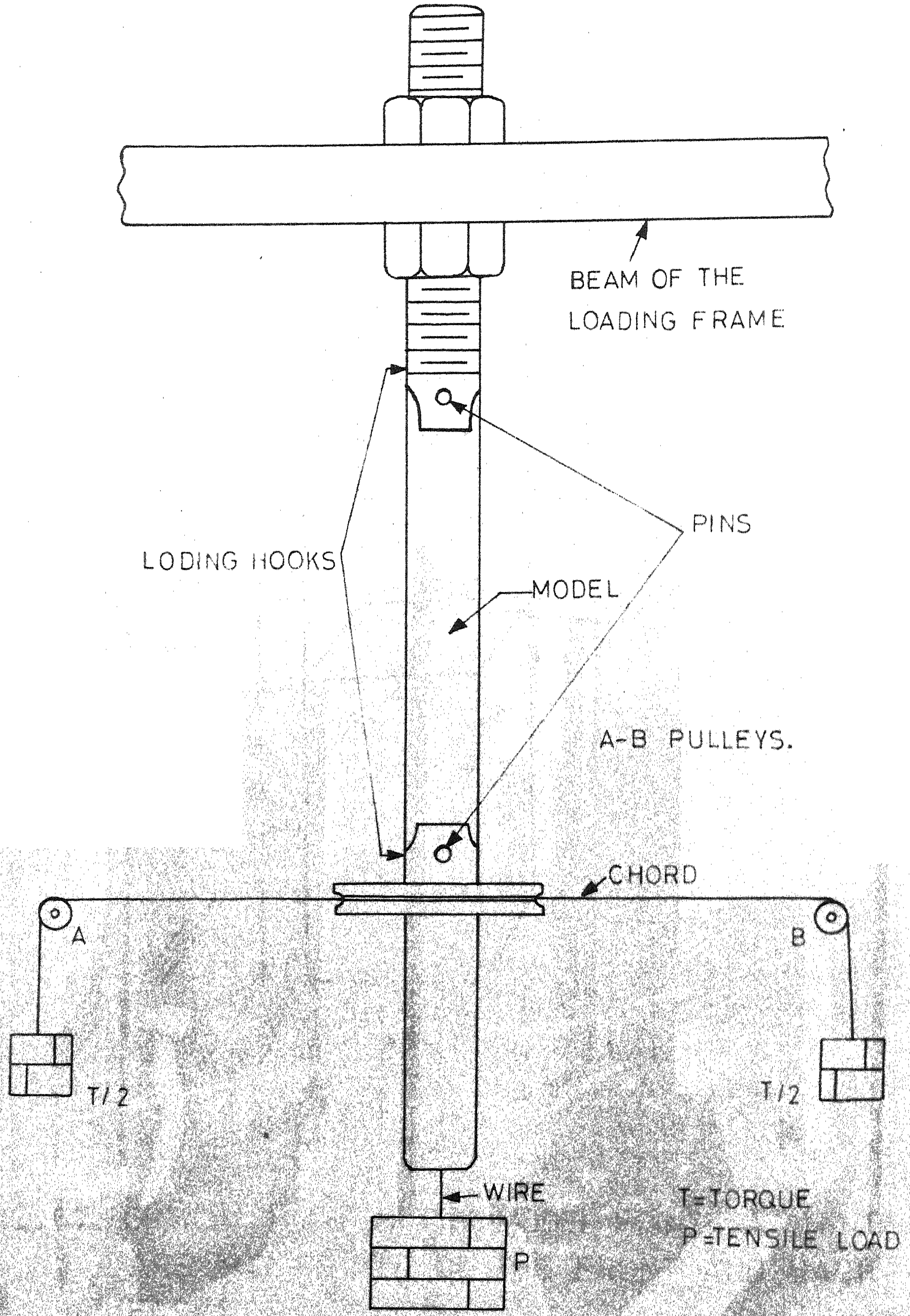

FIG. 68. LOADING DEVICE FOR COMBINED TENSION & TORSION.

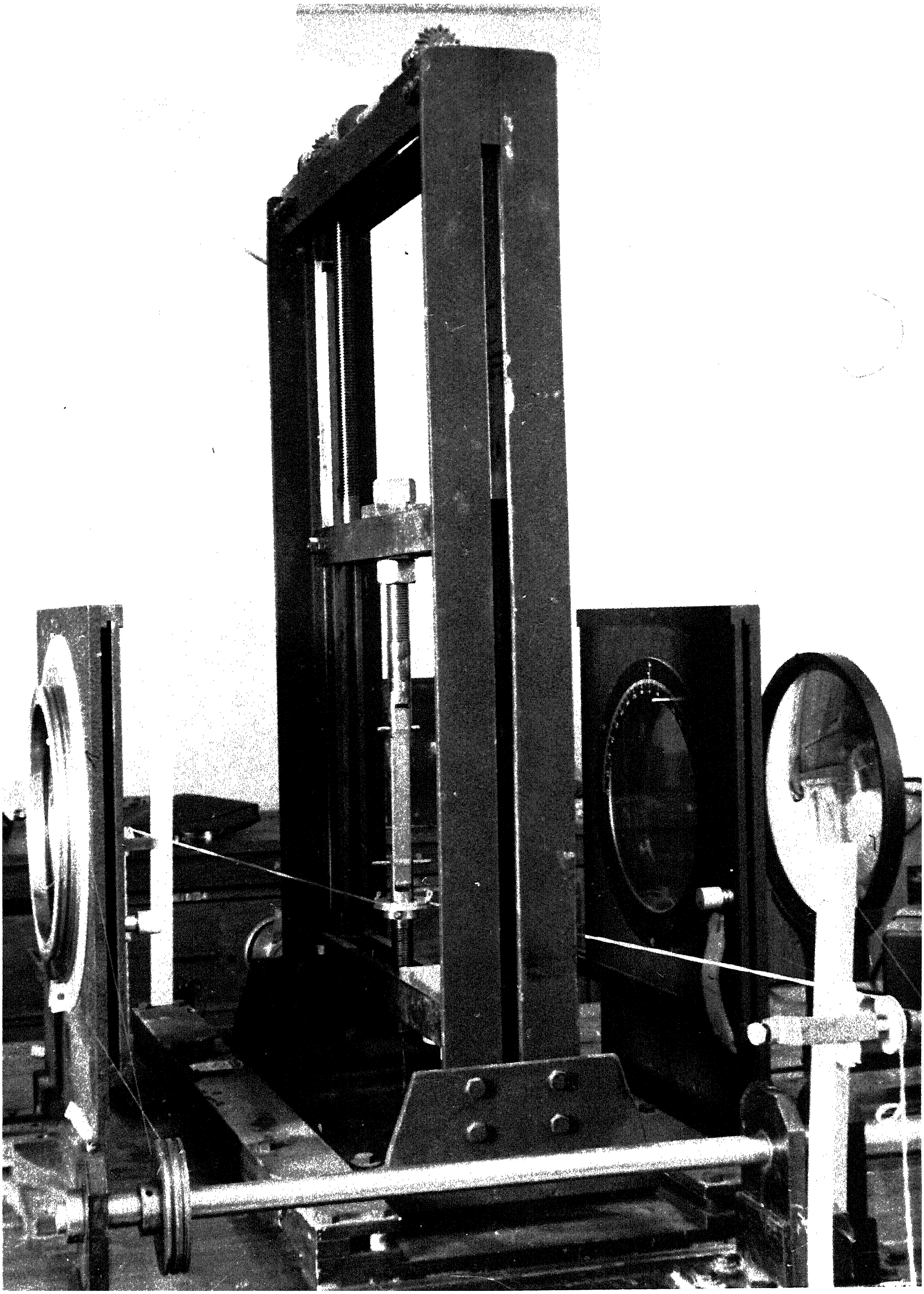

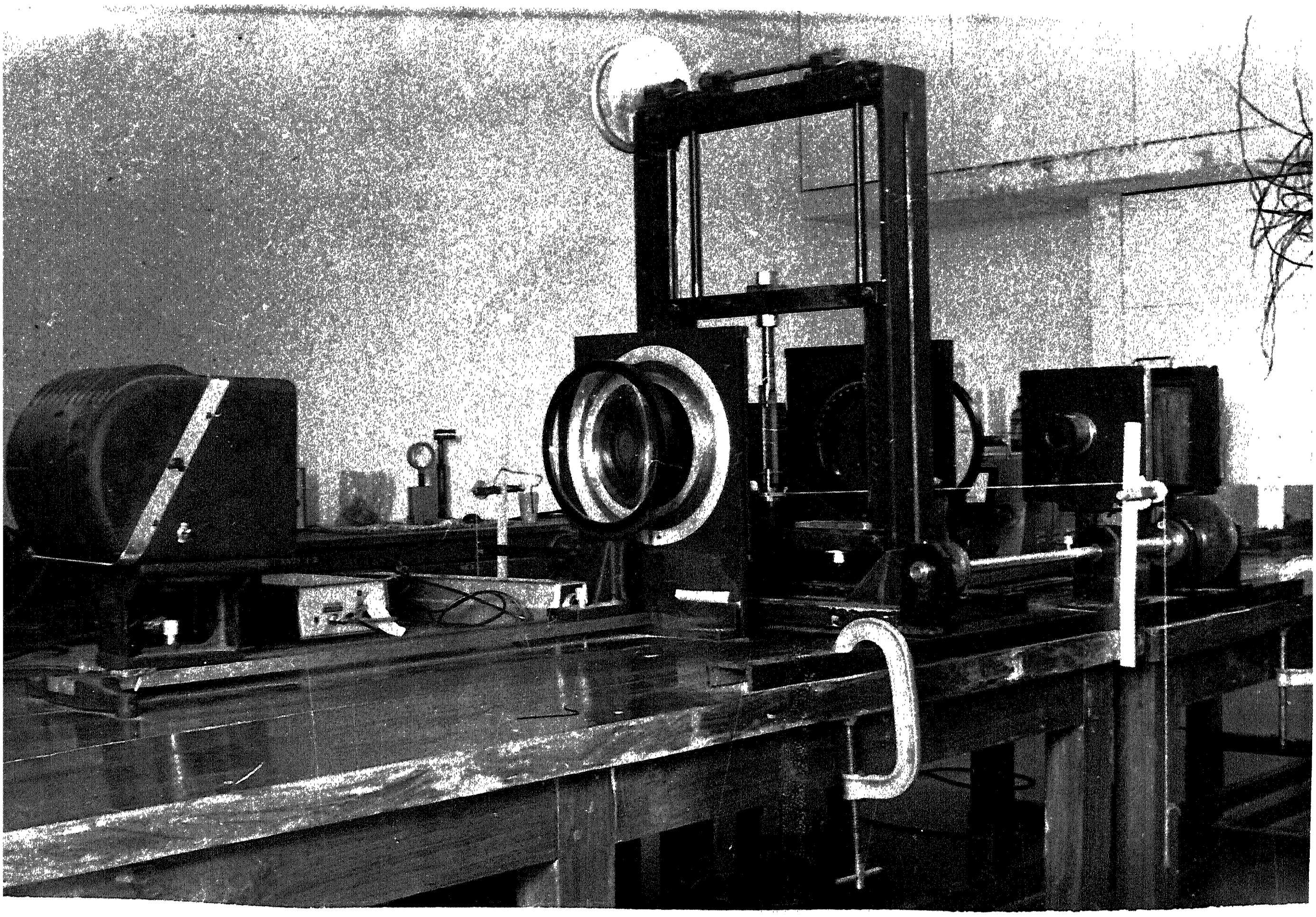

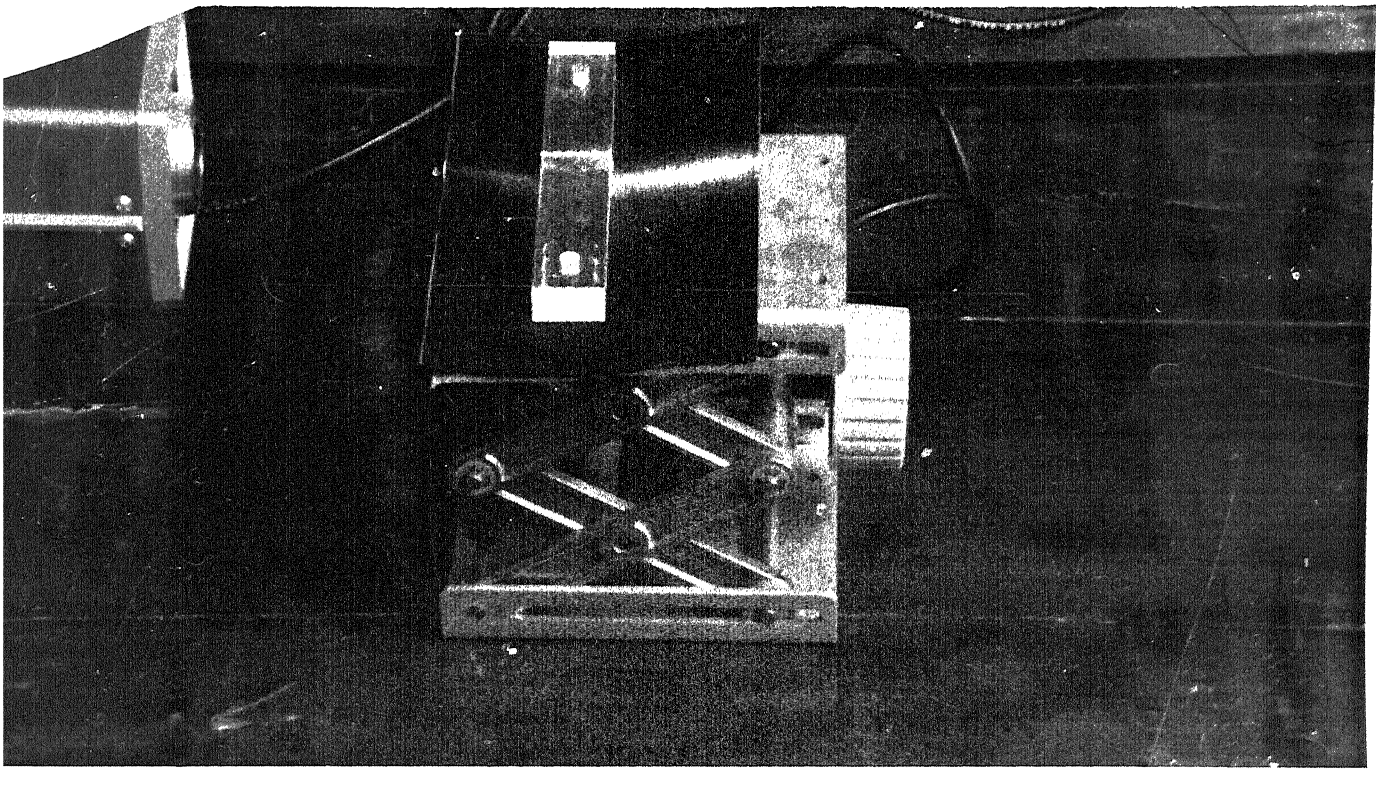

(i) $a = 1''$; $b = 0.528''$; $c = 6\frac{1}{2}''$

(ii) $a = 1''$; $b = 1/2''$; $c = 6\frac{1}{2}''$

The light sources used were mercury and sodium vapour lamps. Three filters of wavelengths 5950°A, 5520°A and 5004°A were also used with white light. The model is checked for residual stresses with a laser (Helium-Neon; 6328°A, 5mw). The scattered light fringe pattern is observed when (i) the laser beam is along the optical path under consideration and (ii) the laser beam is perpendicular to this optical path. No fringes were observed in case (i). The fringe pattern observed in case (ii) is shown in Fig. 71. This shows that for the optical path under consideration no residual stresses exist. Also the residual stresses are normal to the surface of the model (i.e. parallel)to the optical path.

The objects of the various experimental tests are as follows:

(1) Experimental determination of the characteristic parameters for different loadings and checking the validity of the governing optical equations;

(2) Experimental determination of the characteristic parameters for different wavelengths of light and checking the validity of the governing optical equations;

(3) Tests in support of the existence of an optically equivalent system;

(4) Checking the validity of the assumptions involved in the previous scattered light methods[10,11,12] for different loadings.

The details of these tests will be now presented

(1) Experimental Determination of Characteristic Parameters For various Loadings (Refer Chapter 3)

Experimental Procedure:

Method 1: Load the model and keep the first quarter-wave plate axes at 45° to the polarizer axis so that we have a circularly polarized light at entrance to the model. With the second quarter-wave plate out of the field, rotate the analyser for minimum intensity and note this direction D_1. This direction corresponds to the minor axis of the light ellipse. Along the directions $D_1 \pm 45°$, the amplitudes of the components of the light vector are equal and these directions correspond to the secondary characteristic directions.

Now, introduce the second quarter-wave plate so that its axes are parallel to D_1 and $D_1 + 90°$ directions. Rotate the analyser for minimum intensity which will be absolute minimum. Let the minimum intensity position be D_2. Then $2\ (D_2 - D_1) = (90 + \delta)$ where δ is the characteristic retardation. Now remove both quarter-wave plates and keep analyser axes along one of the secondary characteristic directions. Rotate the polarizer for (absolute) minimum intensity. The final orientation of the polarizer axis corresponds to one of the primary characteristic directions.

Method 2: Let the optical set up consist of the polarizer (at arbitrary orientation), the stressed model, the quarter-wave plate (at arbitrary orientation) and the analyser.

Rotate the analyser for minimum intensity thus finding the orientation of the major and minor axes of the light ellipse. Rotate the analyser through 45° in either direction and note the intensity I_{45} with a photometer. All ellipses (of different orientations and ellipticities) will have an intensity equal to I_{45} along directions which make an angle of ± 45° with their major axis. Now keep the angle between the axes of the second quarter-wave plate and analyser equal to 45° and rotate the polarizer until the intensity from the analyser is equal to the previously found value of I_{45}. The final orientation of the axis of the polarizer corresponds to one of the primary characteristic directions. Now remove the second quarter-wave plate and rotate the analyser for absolute minimum intensity. The final orientations of the analyser axes correspond to the secondary characteristic directions. The characteristic retardation can be found as in the first method or by any other method.

The characteristic parameters for various loadings are presented in Table 6.1. Also presented in this table are the theoretical values. All the theoretical values presented in this chapter are found by integrating numerically the governing optical equations in terms of Stokes parameters. The numerical integration is done using the Runge-Kutte-Gill method. The series solution, (Timoshenko[42]), is used to find the values of the shear stress. The computations were done using IBM 7044 computer. Also, the fractional part of the characteristic retardation of the phase difference at the exit along a particular set of axes are found directly by experiment. In most of the cases, the integral fringe order is one. This can be seen by counting the fringe number at the middle point of the model from the edges where the stress is known. (Along the edges, the secondary shear stress is zero). By numerical integration of the optical equations also, the same value for the integral fringe order is obtained.

We shall use the following abbreviations in this chapter.

Th: Theoretical

Ex: Experimental

R: Towards right from the vertical (direction of tensile loading) when looking towards the source

L: Toward left from the vertical when looking towards the source

Ret: Retardation

Pri.ch.dir: Primary characteristic direction

Sec.ch.dir: Secondary characteristic direction

P: Tensile load

T: Torque

Pri.str.dir: Principal-stress direction

TABLE 6.1

Characteristic Parameters For Various Loadings

Model dimensions: a = 1"; b = 1/2"; c = 6½"

Wavelength of light used: 5893°A

Material fringe constant: 139 Psi. in/fringe

Load		Pri.ch.dir.		Sec.ch.dir.		Ch. ret.		Sec.pr. str.dir. at entrance
Tension P lb.	Torsion T lb.in.	Th.	Ex.	Th.	Ex.	Th.	Ex.	Th.
96	8	37°L	31°L	37°R	35°R	338°	332°	27°L
96	12	45°L	41°L	45°R	41°R	401°	394°	32°L
96	16	58°L	52°L	58°R	52°R	444°	445°	35°L
96	24	12°L	8.5°L	12°R	8°R	470°	457°	38°L
90	15	55°L	50°L	55°R	53°R	436°	433°	35°L
100	18	71°L	63°L	71°R	63°R	478°	472°	36°L

In Table 6.1, the agreement between theoretical and experimental values for the characteristic retardation is excellent, the maximum discrepancy being 3%. In Chapter 3, we noted that in anti-symmetric case of stress distribution (like the present case), the primary and secondary characteristic directions will be inclined equally, but in opposite directions to the secondary principal-stress directions at the entrance and exit (of the model) respectively. The values of the characteristic directions in the table, support this statement. The theoretical values for these directions computed numerically are symmetrical about the direction of tensile loading with 1 to 3 degrees difference. This may be due to the effect of round off errors involved in the numerical integration. However in the tables, the average values of these are presented. The values of secondary principal-stresses presented are calculated using the value of shear stress computed from the series solution. However, for some cases, these values are checked using strain gages on the surface of the model. The theoretically computed values for the secondary principal-stress directions exactly coincided with the experimental values. The maximum difference between the theoretical and experimental values of the characteristic directions is 8°. This can be attributed partly due to the errors involved in the numerical integration and partly to the possible errors in the loading alignment. However maximum care was taken to minimise the latter.

The governing optical equations are thus shown to predict the optical phenomena in the presence of the rotation of the secondary principal-stresses fairly accurately. The experimental techniques for the determination of characteristic parameters are successfully employed to determine these parameters. From the values obtained, we note that difference in orientation of the characteristic and secondary principal-stress directions increases as the torsional load is increased.

(2) Experimental Determination of Characteristic Parameters For Various Wavelengths of Light

Experimental Procedure:

The quarter-wave plates of the polariscope are for the green filter (5461°A) attached to the camera of the polariscope. For other wavelengths of light these wave plates cease to be quarter-wave plates. For green light (5461°A) the characteristic parameters are found by the methods described earlier. For other wavelengths of light, the two quarter-wave plates are removed and the compensator is fixed just after the model. The model is taken out of the field, the polarizer and analyser are crossed and the compensator axes are rotated for minimum intensity (with some arbitrary, but nonzero retardation in the compensator). The axes of the compensator are then parallel to the axes of the polarizer. After locating the axes of the compensator thus, its axes are kept at a certain angle to the axes of the polarizer and the retardation in it is varied until the intensity is minimum. The corresponding reading of the compensator corresponds to a zero for that particular wavelength of light. Few other successive readings are found in the same way which correspond to zero retardation or a multiple of 2π retardation. Thus the compensator readings are calibrated for that particular wavelength of light. Now the retardation in the compensator is made 90°. The primary and secondary characteristic directions are found using the method 2. The polarizer axes are kept at 45° to the primary characteristic directions. The ellipticity tan ω of the exit light ellipse is found by Tardy's method. The characteristic retardation $\delta = 2\omega$. The values of characteristic parameters for different wavelengths of light in Table 6.2 are found experimentally in this manner.

TABLE 6.2

Characteristic Parameters For Different Wavelengths of Light.

Load: $P = 109$ lb. $T = 19$ lb. in.

Dimensions: $a = 1''$, $b = 0.528''$, $c = 6\frac{1}{2}''$

Wavelenght of light used	Material Fringe Constant F Psi.in/fringe	Pri. ch. dir.		Sec.ch.dir.		Ch. ret (fractional value)	
		Th.	Ex.	Th.	Ex.	Th.	Ex.
5950	158	34R	36R	34L	38L	89°	75°
5520	147	28R	29R	28L	26L	67°	62°
5004	128	1L	0	1R	2R	50.5°	41°

In Table 6.2 there is excellent agreement between the theoretical and experimental values of the characteristic directions. The discrepancy in the theoretical and experimental values of the characteristic retardation is 4%. (if the integral fringe order of 1 is added to the fractional fringe orders presented in the table. The integral fringe order is found experimentally and by numerical integration to be 1. When the wavelength of light is changed from 5004°A to 5950°A, the orientation of the characteristic directions changed by 34°, which is quite a marked variation. Thus the data (characteristic parameters) for different wavelengths of light can be used to obtain more information about the stress distribution along the optical path. The values in Table 6.2 also show that the governing optical equations can predict the optical phenomena sufficiently accurately. It may be noted that the wavelength and the material fringe constant donot follow any linear relationship. The material fringe constant is found experimentally within an experimental error ± 2 (i.e. about ± 1.5%).

(3) Tests in Support of the Existence of an Optically Equivalent System

It has been proved theoretically, that for a particular wavelength of light, any optical path (or a part of it) in a photoelastic model is equivalent to a system with a single retarder and a pure rotator. The characteristic parameters have also been defined for this optically equivalent system.

So, the following statements hold true:

(i) When a certain amount of retardation is added along the primary characteristic directions at the entrance to the model, it appears as an additional retardation along the secondary characteristic directions at the exit of the model.

(ii) During this process of addition of retardation, the amplitudes of light vector components along the secondary characteristic directions will not vary.

(iii) Using the experimentally determined characteristic parameters, one can predict the exit light ellipse parameters for any type of incident light.

(iv) If the characteristic retardation of the optical path under consideration is nullified with a compensator, the optical path behaves as a pure rotator. If the rotatory power is nullified then the optical path behaves as a single retarder.

Conversely, experimental results which confirm these statements form supporting evidence for the existence of an optically equivalent system.

For a number of cases (of various loadings) the characteristic retardation is nullified with a compensator and then the optical path is then found to be acting as a pure rotator. This confirms that the optical path is equivalent to a single retarder and a pure rotator.

Tables 6.3 and 6.4 show the variation in the intensity and retardation along the secondary characteristic directions when the retardation along the primary characteristic directions is varied. For this the characteristic parameters are found for the particular loading. The axes of the first quarter-wave plate are kept at 45° to the primary characteristic directions. If the angle between the axes of the polarizer and first quarter-wave plate is θ , the retardation along the primary characteristic directions at the entrance to the model is 2θ. The analyser is kept with its axes along the secondary characteristic directions. The polarizer is rotated so that the retardation along the primary characteristic directions is varied and the variation of the photometer reading is noted. To find the retardation along the secondary characteristic directions for a particular value of 2θ, the axes of the second quarter-wave plate are kept at 45°

to the secondary characteristic directions so that we obtain a line ellipse before the analyser. The analyser is then rotated for minimum intensity. If the angle between the axes of the analyser and second quarter-wave plate is ω , the retardation along the secondary characteristic directions is 2ω . Thus the ω values are found experimentally for various values of θ .

In Table 6.5 the parameters of light ellipse at the exit for various types of incident light are presented. Two sets of values are presented in this table. One set corresponds to the values found directly by experiment. The second set of values is computed from the characteristic parameters which are found experimentally. The light ellipse parameters that are tabulated are the phase difference and amplitude ratio along the secondary principal-stress directions at the exit of the model. These directions are computed using the series solution for the shear stress. To find these parameters experimentally, the following procedure is adopted.

Remove the second quarter-wave plate and keep the analyser axes at some inclination to the secondary principal--stress axes at the exit. Introduce a compensator between the model and the analyser with the axes of the compensator along the secondary principal-stress axes. Vary the retardation δ_c of the compensator until the intensity of light from the analyser becomes a minimum. The phase difference along the secondary principal-stress axes at the exit is then - δ_c. Now, we have plane polarized light after the compensator, the direction of which can be found by rotating the analyser for minimum (zero) intensity. If the angle between the axes of the secondary principal-stresses at the exit and the analyser is ω, the amplitude ratio along the secondary principal-stress axes is $\tan\omega$. The proof for this is as follows:

Let the Stokes vector before and after the compensator with respect to its axes be given by V_1 and V_2 which are:

$$V_1 \equiv \begin{bmatrix} S_1 \\ S_2 \\ S_3 \end{bmatrix} \quad \text{and} \quad V_2 \equiv \begin{bmatrix} S_1 \\ S_2 \operatorname{Cos}\delta_c - S_3 \operatorname{Sin}\delta_c \\ S_3 \operatorname{Cos}\delta_c + S_2 \operatorname{Sin}\delta_c \end{bmatrix}$$

when V_2 is referred to the axes of the analyser it becomes

$$\begin{bmatrix} S_1 \operatorname{Cos} 2\bar{\theta} + \operatorname{Sin} 2\bar{\theta}\,(S_2 \operatorname{Cos}\delta_c - S_3 \operatorname{Sin}\delta_c) \\ (S_2 \operatorname{Cos}\delta_c - S_3 \operatorname{Sin}\delta_c) \operatorname{Cos} 2\bar{\theta} - S_1 \operatorname{Sin} 2\bar{\theta} \\ S_3 \operatorname{Cos}\delta_c + S_2 \operatorname{Sin}\delta_c \end{bmatrix} \equiv \begin{bmatrix} \bar{S}_1 \\ \bar{S}_2 \\ \bar{S}_3 \end{bmatrix} \equiv V_3$$

where $\bar{\theta}$ is the angle between the axes of the compensator and the analyser.

$$\frac{\partial \bar{S}_1}{\partial \delta_c} = \operatorname{Sin} 2\bar{\theta}\,(- S_2 \operatorname{Sin}\delta_c - S_3 \operatorname{Cos}\delta_c) = 0$$

if $\operatorname{Sin} 2\bar{\theta} = 0$ or $\tan\delta_c = \frac{-S_3}{S_2} = \tan\epsilon$ i.e. $\delta_c = -\epsilon$

where ϵ is the phase difference along the secondary principal-stresses of the light ellipse from the model.

Also $\operatorname{Sin} 2\bar{\theta} \neq 0$.

TABLE 6.3

Variation of Intensity and Retardation Along the Secondary Characteristic Directions When the Retardation Along the Primary Characteristic Directions is Varied

Dimensions: a = 1", b = 0.528", c = 6½"

Load: P = 109 lb. T = 19 lb.in.

Wavelength of light used: 5461°A

Material fringe constant: 147 Psi.in./fringe

Characteristic Parameters:

	Ex.	Th.
Pri. Ch. Dir.	63°L	62°L
Sec. ch. dir.	60°R	62°R
ch. ret. (fractional value).	56°	67°

The intensity variation along one of the secondary characteristic directions when the retardation along the primary characteristic directions is varied is 2 divisions on 100 scale of photometer.

Ret.along pri.ch.dir. (deg.)	Ret.observed along sec. ch.dir. (deg.)	difference (deg.)	Ret.along pri.ch.dir. (deg.)	Ret.observed sec. ch.dir. (deg.)	difference (deg.)
					24
0	56		100	162	
		18			18
20	74		120	184	
		20			18
40	94		140	202	
		21			18
60	115		160	220	
		23			20
80	138		180	240	

TABLE 6.4

Variation of Intensity and Retardation Along the Secondary Characteristic Directions When the Retardation Along the Primary Characteristic Directions is Varied

Dimensions: a = 1", b = 0.528", c = $6\frac{1}{2}$"

Material fringe constant: 158 Psi.in./fringe

Wavelength of light used: 5893°A

Load: P = 96 lb. T = 16 lb.in.

Characteristic Parameters:

	Ex.	Th.
Pri.ch.dir.	38.5°R	38.5°R
Sec.ch.dir.	36°L	38.5°R
Ch. ret.(fractional value)	-44°	-44°

Ret.along pri.ch. dir. (deg.)	Ret.along sec.ch.dir. (deg.)	difference (deg.)	Ret.added along pri. ch.dir.	Ret. observed along sec. ch.dir.	difference
					19
0	-44		100	56	
		22			21
20	-22		120	77	
		18			19
40	-4		140	96	
		20			20
60	16		160	116	
		21			20
80	37		180	136	

With analyser axis along one of the secondary principal-stress directions at the exit, the intensity reading on 100 scale of photometer varied from 21 to 23, when retardation along the primary characteristic directions was varied.

TABLE 6.5

Parameters of Light Ellipse At Exit Using the Optically Equivalent Model

Load: P = 100 lb.   T = 18 lb. in.

Wavelength of light used: 5461 °A

Dimensions: a = 1", b = 0.528", c = $6\frac{1}{2}$"

Material fringe constant: 147 Psi.in./fringe

Characteristic Parameters:

	Th.	Ex.
Pri. ch. dir.	-116°	-100°
Sec. ch. dir.	65°L	61.5°L
Ch. ret.	65°R	62°R

Sec. pr.str.dir. at entrance : 35°L

Sec.pr.str.dir. at exit. : 35°R

Ret.at entrance along sec. pr.str.dir. (deg.)	Ret.along sec. pr.str.dir.at exit		Amplitude ratio along sec. pr.str. dir. at exit	
	Ex. (deg.)	calculated from ch.par (deg.)	Ex.	calculated from ch.par.
0	42	40	1.54	1.50
15	53	49	2.05	1.93
30	68	62	2.41	2.54
45	91	81	3.08	3.34
60	114	108	4.01	4.00
75	142	140	4.01	3.78
90	162	163	2.75	2.97
105	181	179	2.14	2.25
120	198	190	1.73	1.73
135	202	198	1.28	1.35
150	204	205	1.00	1.07
165	216	212	0.78	0.85
180	227	220	0.63	0.67

From Tables 6.3 and 6.4, we note that the intensity variation along the secondary characteristic directions when the retardation along the primary characteristic directions is varied is 2 divisions on the 100 scale of photometer. Since the photometer pointer by itself shows a fluctuation of 2 divisions on 100 scale, this can be taken to mean that the amplitudes along the secondary characteristic directions remain constant. When the retardation along the primary characteristic directions is varied in steps of 20°, the retardation along the secondary characteristic directions varied in steps of 18° to 24°. The error involved in the measurement of phase difference is 5° in the present experimentation. i.e. the experimental error involved can be as high as 5° with the present experimental set up. So, whatever retardation is added along the primary characteristic direction the same appears as an additional retardation along the secondary characteristic directions. In Table 6.5 the two sets of values of the phase difference ϵ and the amplitude ratio e_x are compared. One set of values is obtained directly by experiment and the other set of values is calculated from the (experimentally determined) characteristic parameters. The agreement between the two sets of values is good. Thus all these experimental results confirm the statements made earlier regarding the optically equivalent system. These form a supporting evidence for the existence of an optically equivalent system for an optical path in a three-dimensional photoelastic system for a particular wavelength of light.

(4) Experimental Check for the Validity of Assumptions Involved in the Previous Scattered Light Methods:

We note that the assumptions involved in the previous scattered light methods[10,11,12] are satisfied when the secondary principal-stress axes at the entrance and exit coincide with the primary and secondary characteristic directions.

Tables 6.6 - 6.10 show the amplitude ratio e_x and the phase difference ϵ along the secondary principal-stress axes at the exit when the retardation is varied along the secondary principal-stress axes at the entrance. Also shown are the values of e_x and ϵ which are computed from the (experimentally determined) characteristic parameters. These sets of values are presented for 5 loadings.

To vary the phase difference along the secondary principal-stress axes at the entrance the axes of the first quarter-wave plate are kept at 45° to these secondary principal-stress axes. The polarizer is then rotated to vary the retardation along these axes. If the angle between the axes of the polarizer and the first quarter-wave plate is α, the retardation introduced along the secondary principal-stresses at the entrance is 2α. The azimuth of the light ellipse at the exit is found with the analyser. The axes of the second quarter-wave plate are kept parallel to the axes of this light ellipse so that it reduces to a line ellipse. The orientation of this line ellipse is found with the analyser. From this orientation the ellipticity and the azimuth of the light ellipse from the model are found, The values of e_x and ϵ are calculated from the parameters of this light ellipse. The characteristic parameters are found experimentally by the methods described earlier. The values of ϵ and e_x for various types of incident light are also computed using these parameters. Sodium vapour lamp (5893°A) was used as the source of light. Only the quarter-wave plates of the polariscope were used for the measurement of ellipticity etc. These introduce only 85° of retardation for wavelength 5893°A and not 90°.

Wavelength of light used: 5893°A

Material fringe constant: 139 Psi.in./fringe

In the tables to foolow, the following abbreviations are used:

Ret. ent. : Retardation added along secondary principal-stress axes at entrance.

Intensity : Intensity of light along one of the secondary principal-stress axes at exit as given by the reading on 1000 scale of photometer.

Initial azimuth : Azimuth of the outcoming light ellipse with respect to the vertical (line of tensile loading)

Q.w.p. : Second quarter-wave plate position

Final azimuth: Final azimuth of the outcoming line ellipse after the introduction of the second quarter-wave plate.

Ph.diff. (Ex.) : Phase difference along the secondary principal - stress axes at exit calculated from the exit light ellipse parameters which are found experimentally.

Ph. diff. (Calc.) : Phase difference along the secondary principal-stress axes at exit calculated from characteristic parameters which are found experimentally.

Ellipticity (Ex) : Ellipticity of the outcoming light ellipse found directly by experiment.

Ellipticity (Calc.) : Ellipticity of the outcoming light ellipse calculated from the characteristic parameters which are found experimentally.

Ampl. ratio (Ex.) : Amplitude ratio along the secondary principal-stress directions calculated from the exit light ellipse parameters which are found experimentally.

Ampl. ratio (Calc.) : Amplitude ratio along the secondary principal-stress directions calculated from the characteristic parameters which are found experimentally.

TABLE 6.6

P = 90 lb. T = 15 lb. in.

Ret. ent.	Initial azimuth	Q.w.p	Final azimuth
0	40°R	50°L	7°R
45°	72°R	27°R	46°R
60°	91°R	46°R	72°R
90°	79°L	56°R	90°L
120°	76°L	59°R	72°L
135°	71°L	64°R	58°L
150°	65°L	70°R	44°L
180°	55°L	80°R	23°R

TABLE 6.7

P = 96 lb. T = 12 lb.in.

Ret. ent.	Initial azimuth.	Q.w.p.	Final azimuth
0	76°L	59°R	52°L
30°	67°L	68°R	35°L
45°	55°L	80°R	17°L
60°	40°L	85°R	1°L
90°	93°R	48°R	71°L
120°	3°L	48°L	11°R
135°	3°R	42°L	10°R
150°	2°R	44°L	4°L
180°	5°R	40°L	8°L

TABLE 6.8

P = 96 lb. T = 8 lb. in.

Ret. ent.	Initial azimuth	Q.w.p.	Final azimuth
0°	85°R	40°R	71°R
30°	85°R	40°R	95°L
45°	86°R	41°R	87°L
60°	83°R	38°R	81°L
90°	84°R	39°R	63°L
120°	12°R	33°L	56°R
135°	9°L	54°L	24°R
150°	8°L	53°L	20°R
180°	7°L	52°L	4°R

TABLE 6.9

P = 96 lb. T = 16 lb. in.

Ret.ent.	Initial azimuth	Q.w.p.	Final azimuth
0	38°L	83°L	10°R
30°	17°L	62°L	5°R
60°	5°L	50°L	7°R
90°	4°R	41°L	4°R
120°	16°R	29°L	3°R
135°	17°R	28°L	0
150°	28°R	18°L	3°R
180°	56°R	11°R	28°R

TABLE 6.10

P = 96 lb. T = 24 lb.in.

Ret. ent.	Initial azimuth	Q.w.p.	Final azimuth
0	4°R	41°L	12°L
30°	22°R	24°L	5°R
45°	28°R	17°L	14°R
60°	38°R	7°L	27°R
90°	48°R	3°R	45°R
120°	66°R	21°R	73°R
150°	72°R	27°R	84°R
180°	84°L	51°R	65°L

TABLE 6.11

P = 90 lb. T = 15 lb.in.

Ret. ent.	Ph. diff.		Ellipticity	
	Ex.	Calc.	Ex.	Calc.
0	77°	84°	0.65	0.53
45°	66°	52°	0.49	0.49
60°	39°	3°	0.34	0.38
90°	22°	21°	0.19	0.15
120°	8°	14°	+0.07	+0.07
135°	28°	38°	+0.24	+0.20
150°	46°	62°	+0.38	+0.31
180°	73°	84°	+0.63	+0.53

TABLE 6.12

P = 96 lb. T = 12 lb.in.

Ret. ent.	Ph.diff.		Ellipticity	
	Ex.	calc.	Ex.	Calc.
0	48°	39°	0.45	0.29
30°	65°	71°	0.63	0.59
45°	80°	85°	0.78	0.76
60°	87°	82°	0.81	0.84
90°	34°	57°	0.29	0.53
120°	-32°	+29°	0.25	0.24
135°	15°	+14°	0.12	0.11
150°	11°	3°	0.09	0.02
180°	27°	39°	0.23	0.29

TABLE 6.13

P = 96 lb. T = 8 lb.in.

Ret. ent.	Ph. diff.		Ellipticity	
	Ex.	Calc.	Ex.	Calc.
0	37°	30°	0.25	0.25
30°	2°	2°	0.00	0.02
45°	22°	19°	0.14	0.15
60°	46°	34°	0.30	0.29
90°	74°	63°	0.66	0.60
120°	88°	89°	0.97	0.93
135°	74°	75°	0.64	0.73
150°	67°	61°	0.53	0.55
180°	31°	30°	0.19	0.25

TABLE 6.16

P = 90 lb.   T = 15 lb.in.

Ret. ent.	Intensity	Ampl. Ex.	ratio. Calc.
0	23	1.44	1.87
45°	13	1.76	0.99
60°	11	1.28	0.81
90°	6	0.97	0.53
120°	4	0.87	0.37
135°	3	0.75	0.34
150°	5	0.68	0.37
180°	8	0.71	0.54

TABLE 6.17

P = 96 lb.   T = 12 lb. in.

Ret. ent.	Intensity	Ampl. Ex.	ratio. Calc.
0	8	0.98	1.82
30°	10	0.86	1.49
45°	12	0.84	1.30
60°	14	0.82	? 1.13
90°	20	1.35	0.84
120°	23	0.60	0.64
135°	23	0.71	0.58
150°	25	0.67	0.54
180°	28	0.78	0.55

TABLE 6.18

P = 96 lb.   T = 8 lb.in.

Ret. ent.	Intensity	Ampl. ratio	
		Ex.	Calc.
0	11	2.11	1.48
30°	11	2.53	1.51
45°	11	2.29	1.45
60°	13	2.18	1.36
90°	17	1.36	1.14
120°	24	0.99	0.93
135°	27	0.70	0.84
150°	29	0.62	0.77
180°	32	0.41	0.67

TABLE 6.19

P = 96 lb.   T = 16 lb. in.

Ret.ent.	Intensity	Ampl. ratio	
		Ex.	Calc.
0	8	0.55	0.57
30°	14	0.51	0.41
60°	20	0.61	0.39
90°	25	0.81	0.53
120°	28	1.20	0.79
135°	27	1.22	0.96
150°	27	1.47	1.17
180°	23	1.38	1.74

TABLE 6.20

P = 96 lb. T = 24 lb. in.

Ret. ent.	Intensity	Ampl. ratio	
		Ex.	Calc.
0	26	0.92	1.53
30°	32	1.54	2.76
45°	34	1.97	3.94
60°	35	3.17	5.23
90°	33	10.76	3.40
120°	28	3.65	1.80
150°	19	2.38	1.08
180°	12	1.03	0.65

In Tables 6.6 - 6.10, the experimental values of the azimuth of the light ellipse at the exit and its orientation after it is reduced to a line ellipse are presented. From these values, the ellipticity, the amplitude ratio and phase difference along the secondary principal-stress directions at the exit are calculated. In Tables 6.11 -6.15, these values of amplitude ratio and phase difference are compared with the values calculated from the characteristic parameters (which are found experimentally). In Tables 6.16 - 6.20, the intensity along the secondary principal-stress directions (as given by the photometer reading) and the amplitude ratio along the secondary principal-stress directions at the exit-(i) calculated from the light ellipse parameters at the exit and (ii) calculated from characteristic parameters, are presented. From these tables we note that both the sets of values of the ellipticities match very well, whereas for phase difference and amplitude ratio, the matching is not good. The reasons for the discrepancy in the later case are: (i) the wave plates used introduce only 85° of retardation for wavelength of light 5893°A (ii) errors in measurement of the orientation of light ellipse severely affect the values obtained for phase difference and amplitude ratio since the constant ellipticity curves are very steep for azimuth values near 0 and 90°, Fig. 44 . (iii) errors in measurement of orientation of light ellipse do not have a significant effect on the values of ellipticity obtained.

Also, we note from these tables that the assumptions of the previous scattered light methods[10,11,12] are not valid for the loadings considered. When the retardation along the sec. pr. str. directions at the entrance is varied, at the exit, the intensity along the secondary principal--stress directions does vary and the phase difference along these directions does not increase by the same amount as the retardation added at the entrance.

In this chapter, we have presented experimental evidence for a number of cases in support of the following statements:

(1) The total light path in a three-dimensional photoelastic model for a particular wavelength of light is equivalent to a system with a retarder and a pure rotator. The three parameters of this equivalent system called the characteristic parameters can be found by the techniques described earlier.

(2) The governing optical equations (derived in Chapter 2) describe the optical phenomena in three-dimensional cases where rotation of the secondary principal-stress axes along the optical path is present.

(3) The variation of the characteristic parameters with wavelength of light can be quite marked in some cases. In the case considered, the characteristic directions varied by 34° when the wavelength of light is varied by 946°A.

(4) The assumptions involved in the previous scattered light methods are not valid when the rotation of the secondary axes is large. These assumptions lead to large errors in such cases.

CHAPTER 7

CONCLUSION

This thesis which consists of six chapters in addition to the present one deals with the problems of stress-induced optical activity and determination of the optically equivalent model in three-dimensional photoelasticity. Chapter 1, the introduction, describes the general problem when the secondary principal-stress axes and their magnitude continuously vary along the light path in a stressed photoelastic model. It gives a brief review of the stress-optic laws in two - and three-dimensions and attempts to modify these in the presence of optical activity. It also discusses briefly some of the scattered light techniques with specific relevance to the effects of optical activity. Finally, the objectives of the present investigation are stated along the methods of approach.

In Chapter 2, the concept of light ellipse is introduced. It is shown that studying the properties and transformations of light ellipse and then using this information in photoelastic analysis has a definite advantage over the usual procedure of resolving the light vector into its components trigonometrically along various directions.

The former method is simpler and presents the physical aspects of the problem involved readily. The light ellipse is described in terms of Stokes vector and throughout this investigation the concept of light ellipse and Stokes vector have been used.

A brief survey of various previous derivations of the governing optical equations in the presence of the rotation of secondary principal-stress axes is presented to show that the kinematically derived equations predict the optical phenomena sufficiently accurately. The optical equations are then derived kinematically in terms of Stokes parameters. These turn out to be a set of three simultaneous first order linear differential equations with variable coefficients. These are very convenient for analysis and application. Using these equations the analytical solution for the case where ratio R of the rate of rotation ϕ' (this can be any arbitrary function) to the rate of retardation ζ' is a constant. The case discussed by Drucker and Mindlin where both ϕ' and ζ' are constants is a particular case of this.

In Chapter 3, the detailed proof for the equivalence of a series of retarders to a system containing a retarder and a pure rotator is presented. Use of Poincare' sphere representation of polarized forms for this proof is also demonstrated. The proof is then extended to any length of optical path in a three-dimensional photoelastic model, that is, any length of optical path in a three-dimensional photoelastic model is again equivalent to a system containing a single retarder and a pure rotator. A discussion of some special cases (case of a pure rotator, anti-symmetric case, axi-symmetric case, reversal of optical path, reflection polariscope) in which there exists a relation between the three characteristic parameters, is presented.

Two simple and direct methods of determining experimentally the characteristics parameters are presented. It is to be noted that there donot exist any such methods to find the characteristic parameters directly in a simple way. However Kent and Lawson[36] suggested an ingeneous device to measure the ellipticity directy. This has been used by Robert and Guillemet[14,15,16] to find the characteristic parameters. But this method requires the rotation of the analyser at a particular speed and some additional instrumentation.

In Chapter 4, a review of some of the previous scattered light techniques, the assumptions involved and the analysis, is made. A critical analysis of these methods is made making use of the analytical solution (obtained in Chapter 2) for the case where $R = \phi'/\rho'$ is a constant (ϕ' can be any arbitrary function) and numerical solutions (of the governing optical equations) for some cases. The limitations of the previous methods are discussed.

The scattered light techniques essentially involve the following steps: (1) measurement of scattered light intensity along different directions taking into account, the variation of the lengths of light path involved, (2) finding the parameters of the light ellipse and the characteristic parameters at the point under consideration (3) evaluating the functions ϕ and ρ using these values and the governing optical equations. Some new scattered light techniques are presented which donot involve any assumptions or the rotation of the analyser at a particular speed.

Chapter 5 deals with 3 main problems, (i) graphical methods in photoelasticity, (ii) theory of compensation and (iii) determination of integral fringe order in photoelasticity. Graphical methods are very convenient to find the integrated optical effect in the presence of the rotation of the secondary principal-stress axes. A review of the earlier graphical methods is made. Of these the stereographic and parallel projections are derived from Poincare' sphere representation of polarized forms. The methods using quaternions needs geometrical construction for each problem. In our discussion a new approach to the graphical methods is described which doesnot involve the use of Poincare' sphere. The light ellipse has essentially four parameters the phase difference, ellipticity, amplitude ratio and azimuth. These are connected by specific relations which can be used to plot two of these four parameters keeping a third parameter constant. Based on these, two graphical methods are presented. One of these is very useful in finding the effect of errors in various polariscopes.

The second method is very simple to construct since it involves only straight lines. Procedures are described to determine the integrated optical effect and the characteristic parameters using these graphical methods.

The second problem deals with the theory of compensation. Use of (a) a system of four retarders each having the same retardation with a polarizer or an analyser and (b) a system of eight retarders each having the same retardation, as a large field compensator is described. The concept of an optically equivalent system is made use of in deriving this. The angles between the axes of different retarders in either system (a) or in (b) are to be adjusted such that the rotatory power of the equivalent system for this system of retarders becomes zero. The principle involved is essentially an extension of the work by Pancharatnam [28] and Tuzi[29].

The third problem deals with the determination of integral fringe orders in two-dimensional photoelastic models under load. The drawbacks of the present methods are discussed. Construction of a nomogram and a ready reckoner table with which one can determine the integral fringe orders virtually upto any number. This procedure doesnot have the limitations of the previous methods. This is essentially an extension of Pant's [30] work in which the integral fringe orders are determined from the fractional fringe orders for two wavelengths of light when the two total fringe orders donot differ by more than unity.

Experimental results are presented in Chapter 6 as supporting evidence to the theory developed in the previous chapters. The experiments were conducted with a rectangular model under combined tension and torsion in a transmission polariscope. These form the supporting evidence for the following statements:

(1) The governing optical equations in terms of Stokes parameters derived in Chapter 2 predict the optical phenomena in the presence of rotation of secondary principal-stress axes (along the optical path) sufficiently accurately.

(2) The techniques described in Chapter 3 can be successfully used to determine the characteristic parameters.

(3) The change in the characteristic directions is found to be 34° when the wavelength is changed from 5004°A to 5950°A (the corresponding change in the material fringe constant is from 128 -158 Psi. in./fringe). This is quite a significant variation and in cases such as this, the data for different wavelengths of light can be used to obtain more information about the state of stress along the optical path.

(4) Any part of optical path in a three-dimensional photoelastic model is equivalent to a system containing a retarder and a pure rotator.

(5) The assumptions on which the existing scattered light techniques are based, are not valid in a general case.

APPENDIX A

(i) Determination of the Characteristic Parameters When the Direction of Observation is Fixed

From Eqs. (4.42)

$$\bar{S}_1 = S_1 \operatorname{Cos} 2\psi + (S_2 \operatorname{Cos} \rho_1 - S_3 \operatorname{Sin} \rho_1) \operatorname{Sin} 2\psi$$

If $S_1 = \operatorname{Cos} 2\theta$, $S_2 = \operatorname{Sin} 2\theta \operatorname{Cos} \epsilon$, $S_3 = \operatorname{Sin} 2\theta \operatorname{Sin} \epsilon$

$$\bar{S}_1 = \operatorname{Cos} 2\theta \operatorname{Cos} 2\psi + \operatorname{Sin} 2\psi (\operatorname{Sin} 2\theta \operatorname{Cos}\epsilon \operatorname{Cos} \rho_1 - \operatorname{Sin} 2\theta \operatorname{Sin}\epsilon \operatorname{Sin} \rho_1)$$

$$\frac{d \bar{S}_1}{d \epsilon} = - \operatorname{Sin} 2\psi (\operatorname{Sin} 2\theta \operatorname{Cos} \rho_1 \operatorname{Sin}\epsilon + \operatorname{Sin} 2\theta \operatorname{Cos}\epsilon \operatorname{Sin} \rho_1)$$

The above expression is equal to zero when

$$\tan\epsilon = - \tan\rho_1$$

$$\text{or } \epsilon = - \rho_1$$

This means that if the retardation ϵ is varied along the primary characteristic direction, the intensity along any arbitrary direction at the exit of the optically equivalent system becomes extremum when $\epsilon = - \rho_1$ where ρ_1 is the characteristic retardation of the equivalent optical system. Let the angle between the axes of the polarizer and the quarter-wave plate be α. Note the intensity I_1. Now rotate the polarizer through 90° and note the intensity I_2.

Change α, the angle between the axes of the polarizer and quarter-wave plate (keeping the quarter-wave plate fixed) and repeat this procedure until $I_1 = I_2$. In this position, the major axis of thelight ellipse at the point under consideration makes an angle of 45° with the direction of observation. (i) One possibility is that this light is circularly polarized. If it is so, the amplitudes along the secondary characteristic directions are equal and the amplitudes along the primary characteristic directions are equal. But the light ellipse after the quarter-wave plate will have its major axis along the quarter-wave plate axes so that along directions making 45° with these axes, the amplitudes will be equal. That is, the quarter-wave plate axes make 45° with the primary characteristic directions. The phase angle along these primary characteristic directions after the quarter-wave plate, is 2α. So, we have $2\alpha + \rho_1 = \pi/2$. All these statements will be true only if the light at the point under consideration is circularly polarized. (ii) The second possibility is that the direction of observation is along one of the secondary characteristic directions. (iii) Neither of the cases (i) and (ii) is true.

To check these, rotate the polarizer and note the intensity I. (i) If I doesnot change when the polarizer is rotated this falls into the second case so that the direction of observation corresponds to one of the secondary characteristic directions. The axes of the quarter-wave plate are at 45° to the primary characteristic directions.

The characteristic retardation cannot be found unless the direction of observation is changed. (ii) If I changes when the polarizer is rotated, find that position of the polarizer for which the condition $I_1 = I_2$ is satisfied. In this position let the angle between the axes of the polarizer and the quarter-wave plate be α_1. Rotate the polarizer for minimum intensity and let this angle be α_2. When the angle between the axes of the polarizer and quarter-wave plate is α_1 for obtaining $I_1 = I_2$ and if the light is circularly polarized at the point under consideration $2\alpha_1 + \rho_1 = \pi/2$. When the polarizer is rotated for minimum intensity $2\alpha_2 + \rho_1 = 0$ so that $(\alpha_1 - \alpha_2) = \frac{\pi}{4}$. Change the orientation of the quarter-wate plate until this condition is satisfied. When this is satisfied, the axes of the quarter-wave plate coincide with the primary characteristic directions and $\rho_1 = \pi/2 - 2\alpha_1 = -2\alpha_2$. To find the rotatory power, nullify the characteristic retardation with a compensator and rotate the polarizer for minimum intensity. The angle between the axes of the polarizer and the direction of observation will give the rotatory power.

(ii) The Whole Field Method

Consider the governing optical equations Eqs. (2.42) - (2.44) referred to some fixed axes

$$S_1' = S_3 \rho' \text{ Sin } 2\phi \qquad (2.42)$$

$$S_2' = -S_3 \rho' \text{ Cos } 2\phi \qquad (2.43)$$

and $S_3' = - S_2 \rho' \text{Cos}2\phi - S_1 \rho' \text{Sin}2\phi$ (2.44)

where ϕ is the orientation of the secondary principal-stress directions with respect to the fixed axes. From Eqs. (2.42) and (2.43)

$S_1' = 0$

when $S_3 = 0$ or $\rho' = 0$ or $\text{Sin}2\phi = 0$ (i.e. $\phi = 0$ or $\pi/2$)

Also

$S_1 = \text{Cos}2\omega \, \text{Cos}2\alpha$

Similarly,

$S_2' = 0$

when $S_3 = 0$ or $\rho' = 0$ or $\text{Cos}2\phi = 0$ (i.e. $\phi = \pi/4$ or $3\pi/4$)

and

$S_2 = \text{Cos}2\omega \, \text{Sin}2\alpha$

S_1 becomes S_2 when α is replaced by $(\alpha - \pi/4)$ (when ω remains constant)

$\therefore$ S_1' becomes S_2' when α is replaced by $(\alpha - \pi/4)$ (when ω remains constant)

For all points where the intensity is extremum along the Z-axis (i.e. along the optical path) for a particular direction of observation

$$S_1' = \frac{dS_1}{dZ} = 0$$

If at a point on the optical path in the model, $S_1' = S_2' = 0$, either $\rho' = 0$ or $S_3 = 0$ or both ρ' and S_3 are zero. To eliminate the case where $S_3 = 0$, the incident light is to be modified. If $S_1' = S_2' = 0$ for any type of incident light we can conclude that at the point under consideration $\rho' = 0$. At this point the directions of the secondary principal-stress axes can not be found since no retardation is being added at this point. If $S_1' = 0$, but $S_2' \neq 0$, the direction of observation is along one of the secondary principal-stress axes. (Because $S_3 \neq 0$, $\rho' \neq 0$ otherwise $S_1' = S_2' = 0$. But $\phi = 0$). This suggests a method of finding the directions of the secondary principal-stresses directly from the scattered light fringe pattern.

The scattered light fringe pattern shows the intensities of scattered light along different directions at different points on the optical path, Swinson et al[13]. At each point find the directions of observation α_1, α_2, α_3 etc. along which $S_1' = 0$. Find the value of S_1' along directions $\bar{\alpha}_1$, $\bar{\alpha}_2$, $\bar{\alpha}_3$ etc. inclined at an angle of 45° to the directions α_1, α_2, α_3 etc. at the corresponding points on the optical path. Let the value of S_1' be nonzero corresponding to the direction $\bar{\alpha}_n$ say. Then the direction α_n is along one of the secondary principal-stress directions. A laser beam of a very small diameter will be an ideal source for obtaining the required scattered light fringe pattern. The effects of varying lengths of (scattered or transmitted) light path can be eliminated in the following way. For this take two scattered light fringe photographs one with right and the other with left circularly polarized light at the entrance. At any point and along a particular direction, the intensities in the two patterns are I_1 and I_2, then the required intensity I (in which the effect of varying light paths is eliminated) in the first pattern is

$$\frac{I_1}{I_1+I_2} \qquad \text{Because,}$$

$$I_1 = \bar{K}\, a_X^2$$

$$I_2 = \bar{K}\, a_Y^2$$

$$I_1+I_2 = \bar{K}$$

$$\therefore \quad a_X^2 = \frac{I_1}{\bar{K}} = \frac{I_1}{I_1+I_2}$$

After knowing the value of ϕ (one of the secondary principal-stress orientation) at each point, the value of ρ' can be calculated by using the relation

$$\rho' = \frac{S_1'}{S_3 \operatorname{Sin} 2\phi}$$

The value of S_3 at any point can be found in the following way.

At a point on the optical path and along a particular set of reference axes X and Y,

$$S_1 = a_X^2 - a_Y^2$$

$$\text{So} \qquad S_1 = \frac{I_1 - I_2}{I_1 + I_2}$$

where I_1 and I_2 are the intensities of the scattered light when the incident light is right and left circularly polarized respectively.

Find the value of S_1 along a-direction 45° to the X direction. This will be equal to S_2 along the X-Direction. Knowing S_1 and S_2, the value of S_3 can be found from the relation

$$S_3 = (1 - S_1^2 - S_2^2)^{\frac{1}{2}}$$

REFERENCES

1. Frocht, M.M., Photoelasticity, Vol.I, John Wiley & Sons, Inc. New York (1965).

2. Srinath, L.S. and Mehrotra, C.L. "On the Interferometric Method of Stress Analysis", Experimental Mechanics, 10(4), pp. 170-171 (1970).

3. Frocht, M.M. "The Growth and Present State of Photoelasticity", Selected papers of M.M. Frocht on Photoelasticity, Pergamon Press, London, pp. 1-23 (1969).

4. Drucker, D.C. "Photoelastic Separation of Principal Stresses by Oblique Incidence", J. Appl. Mech., Vol. 10, No.3 Sept.(1943).

5. Nisida, M. and Saito,H."A New Interferometric Method of Two-Dimensional Stress Analysis", Experimental Mechanics, 4(12), pp. 366-376 (1964).

6. Post,D."On the Interferometric Method of Stress Analysis in Three-Dimensional Photoelasticity", 10(4), pp. 172-174(1970).

7. Dally, J.W. and Riley, W.F., Experimental Stress Analysis, McGraw-Hill Book Company, New York(1965).

8. Frocht, M.M., Photoelasticity, Vol.II, John Wiley & Sons, Inc. New York(1967).

9. Frocht, M.M. and Guernsey, Jr.R."A Special Investigation to Develop a General Method for Three-Dimensional Photoelastic Stress Analysis", Selected Papers of M.M. Frocht on Photoelasticity, Pergamon Press, London, pp. 233-269(1969).

10. Frocht, M.M. and Srinath, L.S. "A Non-destructive Method for Three-Dimensional Photoelasticity", Third U.S. National Congress of Appl. Mech. June (1958).

11. Frocht, M.M. and Srinath, L.S. "Scattered Light in Photoelasticity-Basic Equipment and Techniques", Proc. Fourth U.S. National Congress of Appl. Mech.(1962).

12. Srinath, L.S. and Frocht, M.M. "Potentialities of the Method of Scattered Light", Proceedings International Symposium on Photoelasticity, Pergamon Press, Inc., New York, (1962).

13. Aderholdt, R.W., Mckinney, J.M., Ranson, W.F., and Swinson, W.F. "Effect of Rotating Secondary Principal Stress Axes in Scattered Light Photoelasticity", Experimental Mechanics, pp. 160-165, April(1970).

14. Robert, A.J. and Guillemet, E. "New Scattered Light Method in Three-Dimensional Photoelasticity", Brit. J.Appl.Phys. Vol.15.pp.567-578(1964).

15. Robert, A.J. "New Methods in Photoelasticity", Experimental Mechanics, pp. 224-232, May(1967).

16. Robert, A.J. "The Application of Poincare's Sphere to Photoelasticity, Int. J.Solids and Structures, 6(4) pp. 423-432(1970).

17. Weller, R., J.Appl. Phys. Vol. 10, No. 4(1939).

18. Drucker, D.C. and Mindlin, R.D. "Stress Analysis by Three-Dimensional Photoelastic Methods", J.Appl. Phys., Vol.11(11),(1940).

19. Mindlin, R.D. and Goodman, L.E. "The Optical Equations of Three-Dimensional Photoelasticity", J.Appl.Phys., Vol.20 Jan(1949).

20. Coker, L.N.G. and Filon, E.G., A Treatise on Photoelasticity, 2nd ed. Cambridge University Press p.256(1957).

21. Ginsburg, V.L. "On the Influence of the Terrestial Magnetic Field on the Reflection of Radio Waves from the Ionosphere", Jnl.Phys., 7(6),pp. 289-304(1943).

22. Aben, H.K. "Optical Phenomena in Photoelastic Models by the Rotation of Principal Stress Axes," Experimental Mechanics, 6(1), pp. 137-146 (1966).

23. Ramachandran, G.N. and Ramaseshan, S. Crystal Optics, Handbuch Der Physik, ed. Fluegge, S. Springer-Verlag, Berlin(1961).

24. Jerrard, H.G., J. "Transmission of Light Through [illegible] Birefringent and Optically Active Media: the Poincare'Sphere" J. Opt. Soc. Am.44, pp.634-640(1954).

25. Kuske, A. "The J Circle Method", Experimental Mechanics, p.218,April(1966).

26. Schwieger, H."Graphical Methods for Determining the Resulting Photoelastic Effect of Compound States of Stress", Experimental Mechanics Feb(1969).

27. Cernosek, J. "Simple Geometrical Method for Analysis of Elliptic Polarization", J. Opt. Soc. America, pp. 324-327, Vol.61, No.3, Mar(1971).

28. Pancharatnam, S. "Achromatic Combinations of Birefringent Plates", Part I & II pp. 130-144, Proc. Ind. Academy. Sci. Sec.A, Vol XLI (1955).

29. Tuzi, Z. "Recent Activity in Photoelasticity in Japan", Proc. Intn. Symp. on Photoelasticity, Ed. M.M. Frocht, Oct(1961).

30. Pant, B. "A Method of Determining Integral Fringe Orders in Photoelastic Analysis," Experimental Mechanics, pp.173-171, July(1963).

31. Srinath,L.S. and Sarma, A.V.S.S.S.R. "Role of Light Ellipse in Photoelasticity and New Methods for Isoclinic-Parameter Determination", Experimental Mechanics, pp.271-275,June(1971).

32. Shurchiff, W.A. Polarized Light, Production and Use, Cambridge, Harward University Press,(1962).

33. Born, M. and Wolf, E. Principles of Optics, Pergamon Press, London, (1959).

34. Reira, J.D. and Mark, R. "The Optical - rotation Effect in Photoelastic Shell Analysis", Experimental Mechanics, pp. 9-16, Jan(1969).

35. Hurwitz Jr.H. and Jones, R.C. "A New Calculus for Optical Systems II Proof of Three General Equivalence Theorems.J.Opt.Soc. Am.31, pp.493-499(1941).

36. Hurwitz, Jr. H. and Jones, R.C. "A New Calculus for Optical Systems, II Proof of Three General Equivalence Theorems", J. Opt.Soc.Am.31, pp. 493-499(1941).

37. Salame, E.M. "3-Dimensional Photoelastic Analysis by Scattered Light", Proc. SESA, Vol.5,No.2. pp. 49-52, 1948.

38. Jessop, H.T. "The Scattered Light Method of Exploration of Stresses in 2 - and 3-Dimensional Models, Brit. J. Appl. Phys., Vol. 2 pp. 249-60. Sept.(1951).

39. Menges, J.M. Zeits. & Angewandte Math and Mech., Vol. 20, No. 4(1940). pp. 210-217

40. Cheng, Y.F. "Some New Techniques for Scattered Light Photoelasticity", Experimental Mechanics, 3,(11), pp.275-278(1963).

41. Srinath, L.S."Analysis of Scattered Light Methods in Photoelasticity", Experimental Mechanics, 463-468, Oct.(1969).

42. Timoshenko, S. and Goodier, J.N. Theory of Elasticity, Kogakusha Company Ltd., Tokyo, 1951.

43. Cheng, Y.F. "A Dual Observation Method for Determining Photoelastic Parameters in Scattered Light", Experimental Mechanics, 7(4), pp. 140-144(1967).

44. Nielsen, K.L. and Vanlonkhuyzen, J.H. Plane and Spherical Trigonometry Barnes & Noble, Inc. New York 1958.

45. Jerrard, H.G. "Optical Compensators for the Measurement of Elliptical Polarization", J.Opt. Soc. Am. 38, p.55(1948).

46. Jellyman, P.E. and Milne, A.J. A Large Field Compensator for the Measurement of Birefringence, Nature 161, p 477,(1948).

47. Phemister, T.C. See Photoelastic Analysis by Hendry, A.W. Pergamon Press, 1966 London.

48. Childs, W.H.J. "Composite Quarter and Half-Wave Plates", 33, pp. 298-301, J.Sci.Inst.(1956).

49. Durelli, A.J. and Riley, W.F., Introduction to Photomechanics, Prentice Hall, Inc. / Englewood Cliffs, N.J. 1965.

50. Heywood, R.B. Photoelasticity for Designers Pergamon Press, London (1969).

LIST OF PUBLICATIONS

1) L.S. Srinath and A.V.S.S.S.R.Sarma, "Role of Light Ellipse in Photoelasticity and New Methods for Isoclinic Parameter Determination," Experimental Mechanics, pp. 271-275, June (1971).

2) A.V.S.S.S.R.Sarma and L.S.Srinath, "Photoelastic Analysis with Stokes Vector and New Methods for the Determination of Characteristic Parameters in Three--Dimensional Photoelasticity, Jnl. Aero. Soc. Ind. pp. 299-306, May (1972) - paper presented at 23rd Annual Meeting of Aer. Soc. Ind., held at Kanpur during Feb. 26-28 (1971).

3) A.V.S.S.S.R.Sarma and L.S. Srinath, "Determination of the Optically Equivalent Model in Three-Dimensional Photoelasticity," paper presented at 16th Congress of Th. and Appl. Mech. held at Allahabad during March 29- April 1 (1972).

4) L.S. Srinath and A.V.S.S.S.R.Sarma, "Effects of Stress-Induced Optical Activity in Photoelasticity", Jnl. of Phy. D. (Appl. Phy.), Vol. 5. No.5 pp.883-895, May (1972).

5) L.S. Srinath and A.V.S.S.S.R.Sarma, "Determination of Integral Fringe Orders in Photoelasticity," to appear in Experimental Mechanics.

6) L.S.Srinath and A.V.S.S.S.R.Sarma, "Characteristic Methods in General Three-Dimensional Photoelasticity," to be presented at 13th Int. Congress on Theo. & Appl. Mech. Moscow, Aug. (1972).